Dynamics and Cargo Selectivity of Endocytic Adaptor Proteins

by

Peter Andrew Keyel

Bachelor of Science, University of Minnesota, 2001

Submitted to the Graduate Faculty of

the School of Medicine in partial fulfillment

of the requirements for the degree of

Doctor of Philosophy

University of Pittsburgh

2006

UNIVERSITY OF PITTSBURGH

SCHOOL OF MEDICINE

This dissertation was presented

by

Peter Andrew Keyel

It was defended on

21 August 2006

and approved by

Meir Aridor, Ph.D. Assistant Professor, Department of Cell Biology and Molecular Physiology

Simon Watkins, Ph.D., Professor, Department of Cell Biology and Molecular Physiology

Peter Drain, Ph.D., Assistant Professor, Department of Cell Biology and Molecular Physiology

Adam Linstedt, Associate Professor, Department of Biological Sciences, Carnegie Mellon University

Dissertation Advisor: Linton M. Traub, Ph.D., Associate Professor, Department of Cell Biology and Molecular Physiology

DYNAMICS AND CARGO SELECTIVITY OF ENDOCYTIC ADAPTOR PROTEINS

Peter Keyel

University of Pittsburgh, 2006

Clathrin-mediated endocytosis is a critical process through which a wide variety of extracellular material is internalized. The primary component, clathrin, forms a cargo-selective lattice at the plasma membrane, as well as on endosomes and the TGN, though the cargo-selective components are incompletely defined. An ideal tool for understanding the spatio-temporal dynamics of both the clathrin coat and the cargo selected is total internal reflection fluorescence microscopy (TIR-FM), which permits selective imaging of events closely apposed to the ventral plasma membrane. Previously, observation of the clathrin coat has shown both static and dynamic populations, with some dynamic structures undergoing microtubule-dependent motion; the 70-110 nm decay constant of the TIR-FM field has led to the assumption that these are all representative of coated pits. Here, I demonstrate that the dynamic population of clathrin is primarily endosomal, as it lacks colocalization with the plasma membrane-specific endocytic adaptor AP-2, but colocalizes with large, internalized low density lipoprotein (LDL) and transferrin positive structures. Other clathrin-associated sorting proteins (CLASPs) remain in relatively static structures as well. One such CLASP, autosomal recessive hypercholesterolemia (ARH) protein, is the defective protein in ARH, which is typified by the failure of hepatic LDL receptor internalization, despite no LDL receptor mutations. ARH interacts with AP-2 via the novel, helical FXX[FL]XXXR motif present in its C-terminus. Here, I demonstrate the importance of this motif for targeting ARH to coated pits in cells and LDL uptake. As knockdown of ARH is insufficient to block LDL receptor endocytosis in fibroblasts, I show that the CLASP Disabled-2 (Dab2) works with ARH to sort the LDL receptor. Ablation of these two components using RNAi halts LDL receptor endocytosis, and either exogenous ARH or Dab2 rescue this phenotype. The endocytic defect in the liver of ARH patients is due to the lack of Dab2 expression in hepatocytes, making this cell type sensitive to ARH levels for LDL uptake. This work formally validates the CLASP hypothesis, and demonstrates that these CLASPs are general components of the clathrin-coated pit that are regulated in a tissue-specific fashion.

TABLE OF CONTENTS

LIST OF FIGURES

PREFACE

1.0   INTRODUCTION

1.1   CLASSICAL CLATHRIN-MEDIATED ENDOCYTOSIS

1.1.1   General Overview

Endocytosis is the process through which eukaryotic cells internalize extracellular material. Cells utilize a variety of methods to do this, ranging from phagocytosis, to macropinocytosis and micropinocytosis. Phagocytosis, or "cell eating," is used by a specialized subset of cells, primarily macrophages and neutrophils, to clear dead cells, pathogens and other large debris. Once these cells encounter their target, they send actin-driven extensions out to engulf it. Pinocytosis, or "cell drinking," is performed by most cells and is subdivided into macro- and micropinocytosis. Macropinocytosis is the uptake of fluid from actin-dependent cell ruffling. This ruffling is induced by a large variety of signaling molecules and results in the formation of cup-shaped structures, which close upon themselves to form macropinosomes. Micropinocytosis is the internalization of limited, specific regions of the plasma membrane and small liquid volumes. It is further subdivided by the mediators of internalization, which range from the well-known clathrin coat to the less well understood caveolar structures to poorly understood clathrin- and caveolin-independent mechanisms (Conner and Schmid, 2003b).

1

The clathrin-mediated endocytic pathway is required for a wide variety of vital cellular activities. In addition to the internalization of essential nutrients, like iron, a number of signaling receptors, including epidermal growth factor (EGF), transforming growth factor β (TGF-β), fibroblast growth factor (FGF), platelet-derived growth factor (PDGF) and G-protein coupled (GPCR) receptors, are rapidly cleared from the cell surface via clathrin-mediated endocytosis after activation (Le Roy and Wrana, 2005; Mukherjee et al., 2006). Failure to clear these signaling molecules can have a broad range of consequences, from cell death to carcinogenesis. Neurons also require clathrin-mediated endocytosis at the nerve terminal to regenerate the pool of synaptic vesicles needed for neurotransmitter release (Royle and Lagnado, 2003). Depletion of this pool prevents a neuron from transmitting an action potential across a synapse, leading to paralysis and death. Furthermore, several immune processes hinge on clathrin-mediated endocytosis; many receptors, including the neonatal Fc receptor, Toll-like receptors, and both T cell and B cell receptors, traffic via clathrin-coated vesicles (Husebye et al., 2006; Monjas et al., 2004; Stoddart et al., 2002; Wu and Simister, 2001). Finally, viruses and bacteria, including varicella zoster virus, papillomavirus, rhinovirus, West Nile virus, hepatitis C virus, Dengue virus, and *Listeria monocytogenes*, can hijack clathrin-mediated endocytosis to gain entry into cells or remove immune receptors from the surface (Blanchard et al., 2006; Bousarghin et al., 2003; Chu and Ng, 2004; Codran et al., 2006; Day et al., 2003; Hilgard and Stockert, 2000; Marsh and Helenius, 2006; Pasieka et al., 2003; Snyers et al., 2003; Veiga and Cossart, 2005). Thus, it is critical to understand the molecular mechanisms through which clathrin-mediated endocytosis occurs as well as the fate of internalized cargo.

The general trafficking itinerary of cargo is known. Extracellular materials, such as transferrin (Tfn) or low density lipoprotein (LDL) particles, are rapidly internalized via clathrin-coated vesicles and delivered to early endosomes. Here, sorting occurs between cargo and receptors that will be recycled, including Tfn, the Tfn receptor (TfR) and the LDL receptor, and those which will be degraded, including LDL and the EGF receptor (Maxfield and McGraw, 2004). Recycled cargo is generally sorted into a recycling compartment prior to its return to the surface, while cargo destined for degradation moves into surface-inaccessible late endosomes, which ultimately fuse with the lysosomal compartment (Bonifacino and Traub, 2003). Following LDL from internalization to degradation shows that it requires at least 30 min to reach the terminal degradative compartment, while the LDL receptor recycles within about 10 min (Basu et al., 1981; Brown and Goldstein, 1986). The focus of this dissertation will be upon the initial steps of this pathway, the formation and internalization of clathrin-coated vesicles.

1.1.2   The Clathrin Coat

The clathrin coat was initially observed as a "bristle" coat in blood-fed mosquito oocytes by electron microscopy (Roth and Porter, 1964). In the initial observations, it was astutely speculated that this coat controls cargo selection and internalization (Roth and Porter, 1964). If viewed from the cytosol, looking down on the membrane, the coat appears as a characteristic hexagonal and pentagonal lattice, formed by the polymerization of the protein termed clathrin (Pearse, 1975). Clathrin exists as a three-legged hexamer known as a triskelion, with each leg comprised of one ~190 kDa clathrin heavy chain and one 25-29 kDa light chain (Ungewickell and Branton, 1981; Ybe et al., 1999) (Figure 1-1). The heavy chain domain architecture makes
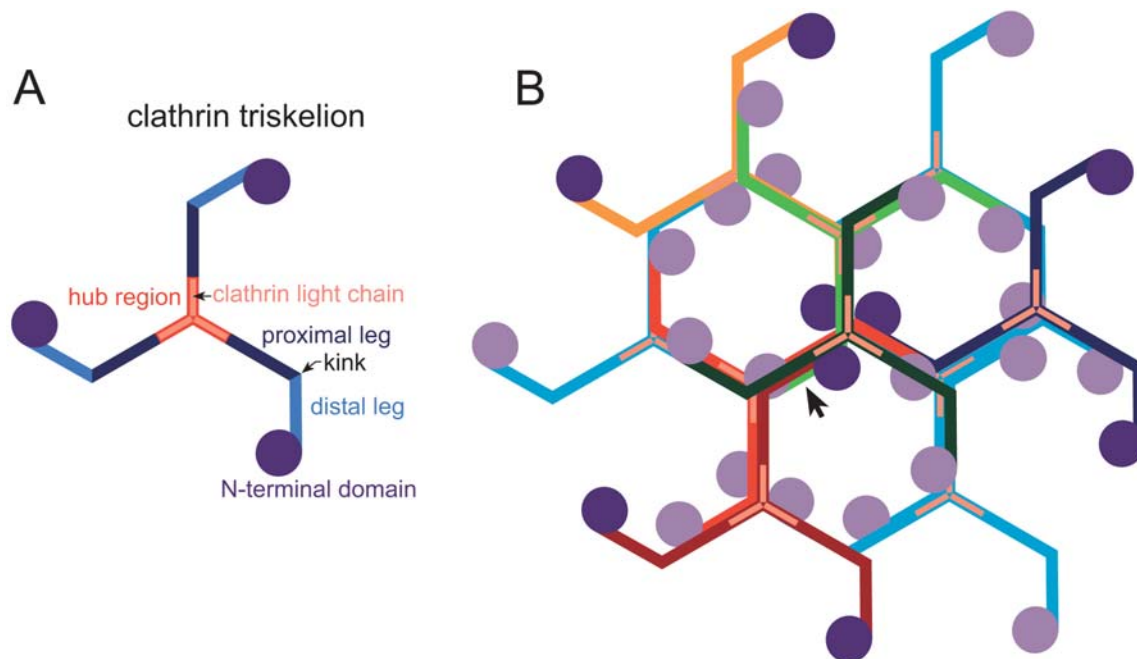
Figure 1-1 Clathrin structure and assembly

(A) A schematic of a clathrin triskelion with light chains and heavy chain domains labeled and colored. (B) A polymerized clathrin lattice demonstrating lattice geometry. The three dark purple N-terminal domains from the dark red, orange and dark blue triskelia cluster below the vertex of the dark green triskelion. The arrow shows a strut containing portions of four distinct heavy chains, colored light or dark green or light or dark red. Clathrin triskelia are slightly offset to show contibutions individual triskelia make to the lattice.

clathrin polymerization possible. The heavy chain contains three general regions, the hub, the leg and the N-terminal domain. The hub is where heavy chains of an individual triskelion join, and contains the binding site for the light chains. The leg consists of a series of stacked α-helices that are divided by a kink into proximal and distal legs (Figure 1-1A). These segments bind to the distal and proximal legs of other triskelia, forming the molecular basis of lattice assembly (Fotin et al., 2004; Smith et al., 1998; ter Haar et al., 1998; Ybe et al., 1999). Projecting from the distal leg is the globular N-terminal domain, which forms a 7-bladed β-propeller (ter Haar et al., 1998). In a polymerized lattice, the light chains are located on the outside surface, while three N-terminal domains are positioned below the vertex of a nearby clathrin triskelion (Figure 1-1B).

Association of N-terminal domains is thought to bring the legs into proximity with each other and initiate clathrin assembly (Greene et al., 2000). In the polymerized lattice, each strut consists of parts of heavy chains from four separate triskelia (Ungewickell and Branton, 1981; Ybe et al., 1999) (Figure 1-1B, arrow).

Clathrin lattices are present on the membrane at several subcellular sorting stations, including plasma membrane, early and recycling endosomes, and *trans*-Golgi network (TGN) (Anderson et al., 1978; Bloom et al., 1980; Raiborg et al., 2001; Stoorvogel et al., 1996). There, these lattices ultimately give rise to the coated vesicles that carry cargo throughout the cell. The initial flat, hexagonal clathrin lattices are remodeled to include pentagons, inducing curvature in the flat clathrin lattice, or curved structures may form at the edges of flat arrays (Heuser, 2000). Once these structures become deeply invaginated, they quickly separate from the membrane to become new clathrin-coated vesicles (Heuser, 2000; Traub, 2005). These vesicles are critical to cell survival, since mutation or targeted gene disruption of clathrin in *Drosophila melanogaster* is lethal (Bazinet et al., 1993).

Formation of empty clathrin lattices in the cytosol is blocked by the light chains. There are two clathrin light chain genes in vertebrates, light chain a (LCa) and light chain b (LCb), which are 60% identical (Jackson et al., 1987; Liu et al., 1995). Binding of the light chains to the heavy chains inhibits the spontaneous polymerization of clathrin at a physiological pH (Ungewickell and Ungewickell, 1991). The light chains contain three N-terminal negatively charged residues that confer pH-sensitivity to clathrin assembly; when bound by the light chains, heavy chains can only polymerize below pH 6.5 (Brodsky et al., 2001). The light chains also

have calcium and calmodulin binding sites. Calcium binding may relieve inhibition by the light chains, as triskelia polymerize *in vitro* at millimolar Ca^{2+} concentrations (Ungewickell and Ungewickell, 1991). Thus, light chains perform a regulatory role, preventing spontaneous polymerization of the triskelia in the cytosol (Ungewickell and Ungewickell, 1991).

Clathrin does polymerize on the membrane, so interactions with membrane bound factors must overcome inhibition by the light chains. These factors also must tether clathrin to the membrane, since clathrin has no intrinsic membrane-binding capabilities. To these ends, clathrin interacts with a variety of membrane-binding endocytic adaptor proteins, primarily through the N-terminal domain. This domain engages a consensus sequence LΦXΦ[DE] (where X is any amino acid and Φ is a bulky hydrophobic), known as a type I clathrin box, on endocytic adaptor proteins (Bonifacino and Traub, 2003; ter Haar et al., 1998). This clathrin box binds to a shallow groove between blades 1 and 2 of the N-terminal domain β-propeller (ter Haar et al., 2000). Additionally, some endocytic adaptor proteins possess a structurally distinct type II clathrin box, or W box motif, PWXXW (Drake et al., 2000; Miele et al., 2004; Mishra et al., 2002a; Ramjaun and McPherson, 1998). This peptide motif binds to the top surface of the N-terminal domain β-propeller, contacting residues from blades 1, 4, 6 and 7, ~20-25 Å from the type I clathrin box binding site (Miele et al., 2004). Binding two discrete sites on clathrin permits these endocytic adaptor proteins to cluster clathrin N-terminal domains, which greatly enhances the rate of lattice polymerization and explains in part how these proteins could overcome inhibition by the light chains (Brodsky et al., 2001; Drake and Traub, 2001; Ungewickell and Ungewickell, 1991). Thus, clathrin polymerization is coupled to the membrane by endocytic adaptor proteins, and restricted to only the membrane by the clathrin light chains.

1.1.3 Assembly Protein Complexes Coordinate Clathrin Assembly and Cargo Selection

The first endocytic adaptor proteins were identified as major components of purified of clathrin-coated vesicles (Keen et al., 1979). These were the heterotetrameric assembly protein-1 (AP-1) and -2 (AP-2) complexes, which localize to either endosomes and the TGN or the plasma membrane, respectively (Ahle and Ungewickell, 1986; Robinson and Pearse, 1986). The importance of AP-2 for endocytosis is illustrated by the consequences of its deletion. Targeted disruption in *Drosophila*, *C. elegans*, or mice is lethal, demonstrating that along with clathrin, AP-2 is absolutely critical for life (Berdnik et al., 2002; Grant and Hirsh, 1999; Mitsunari et al., 2005). Structurally, AP-2 and AP-1 are very similar, comprising a globular core consisting of a small 17-19 kDa, σ subunit, medium 47-50 kDa μ subunit, and the trunks of both a large ~110 kDa β subunit, and adaptor specific γ- (AP-1) or α- (AP-2) subunits, along with appendages projecting off flexible hinges connected to each large subunit (Collins et al., 2002) (Figure 1-2). The σ subunits are thought to be structural subunits, and selectively form hemidimers with either γ or α subunits, while the β and μ subunits form another hemidimer that associates with the α/γ-σ dimer (Page and Robinson, 1995). The μ subunits couple cargo selection to the clathrin coat by binding to the peptide sequence YXXΦ, found in the cytoplasmic tail of a subset of receptors internalized in a clathrin-dependent fashion, including the TfR (Ohno et al., 1995). The YXXΦ motif is accommodated by a β-sandwich subdomain of the μ2 subunit of AP-2 that is normally buried in the core (Collins et al., 2002; Owen and Evans, 1998). The μ2 subdomain becomes accessible to YXXΦ motifs after phosphorylation of a residue positioned in the flexible linker connecting it to the μ2 core, Thr156, by the Ser/Thr kinase adaptor-associated kinase 1 (AAK1). Phosphorylation of Thr156 increases the affinity of AP-2 for the YXXΦ sequence ~25-fold

(Ricotta et al., 2002). This phosphorylation event is further restricted to the population of AP-2 in coated pits by the requirement of assembled clathrin for the stimulation of AAK1 activity (Conner et al., 2003; Jackson et al., 2003).

Another internalization sequence recognized by AP-2 is the dileucine motif, which has the consensus [DE]XXXL[LI], and is found in proteins such as the CD3 γ chain of the T cell antigen receptor or glucose transporter Glut8 (Augustin et al., 2005; Letourneur and Klausner, 1992). In contrast to the YXXΦ motif, [DE]XXXL[LI] is not thought to use the μ2 subunit (Bonifacino and Traub, 2003). Rather, it has been alternately suggested by UV crosslinking or yeast two-hybrid that it interacts with a surface either on the trunk or on the appendage of the β2 subunit, though cellular confirmation of either interaction is lacking (Rapoport et al., 1998; Schmidt et al., 2006). Since this sequence binds to the γ-/σ1-hemicomplex of AP-1 and the δ-/σ3-hemicomplex of the related AP-3 heterotetramer (Janvier et al., 2003), it is more likely that the dileucine motif may bind instead to the α-/σ2-hemicomplex of AP-2.

In addition to likely binding to the dileucine motif, the α subunit contains a phosphatidylinositol 4,5-bisphosphate (PtdIns(4,5)P_2) binding site in the trunk. Similarly, the μ2 subunit also recognizes PtdIns(4,5)P_2. In fact, μ2-mediated PtdIns(4,5)P_2 binding is enhanced when the μ2 subunit simultaneously engages the YXXΦ motif (Honing et al., 2005). Finally, the bilobal α and β2 appendages contain protein scaffolding sites and two clathrin binding sites on the β2 subunit (Gaidarov et al., 1996; Owen and Luzio, 2000; Slepnev and De Camilli, 2000).

These two clathrin binding sites allow AP-2 to cluster N-terminal domains and drive the rapid assembly of clathrin into lattices (Keen et al., 1979). Thus, AP-2 couples cargo and clathrin together at the plasma membrane in a tightly regulated manner.

1.1.4 Classical Model

The detailed knowledge of the clathrin-clathrin and clathrin-AP-2 interactions and the evidence that AP-2 directly recognizes peptide sequences known to be important for internalization is all consistent with the classical model of clathrin-mediated endocytosis (Figure 1-2). In this model, soluble AP-2 binds to random PtdIns(4,5)P_2-rich regions of the plasma membrane. On the membrane, AP-2 recruits clathrin and clusters the N-terminal domains. The clustering of N-terminal domains on the membrane overcomes inhibition of clathrin self-assembly by the light chains, allowing the polymerization of clathrin into a lattice. Clathrin polymerization activates AAK1, enabling AP-2 to rapidly recognize peptide internalization motifs and retain cargo in the assembling lattice. The lattice progressively invaginates the membrane, until the coated pit separates from the rest of the membrane, forming a coated vesicle, and travels deeper into the cell.

1.1.5 Vesicle Scission and Uncoating

Although clathrin and AP-2 cooperate to generate coated pits, they are not sufficient to reconstitute clathrin-mediated endocytosis. Evidence for another protein came from early EM
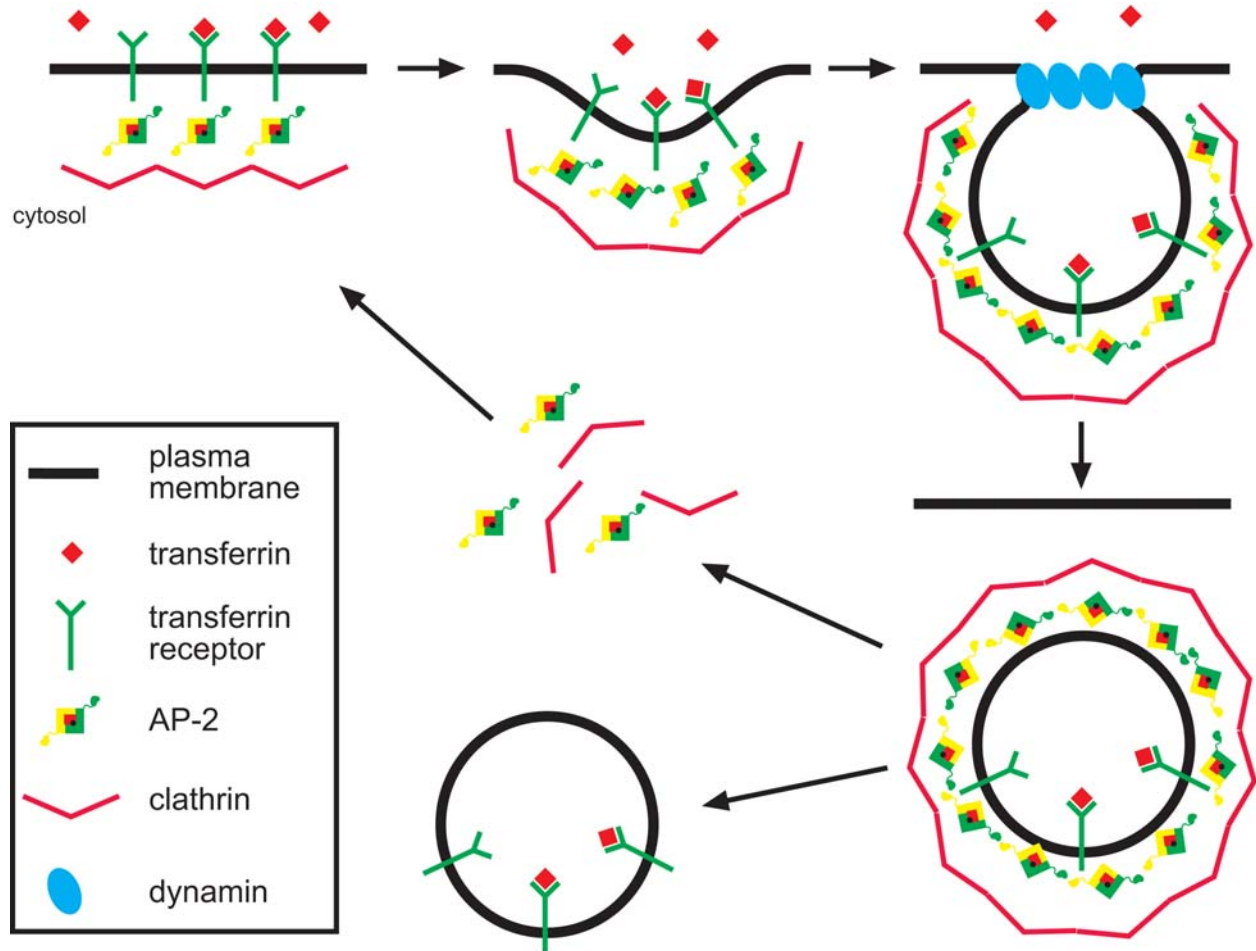
Figure 1-2 Classical model for clathrin-mediated endocytosis

Clathrin is recruited to the plasma membrane by AP-2, which recognizes a cytoplasmic YXXΦ motif present in a receptor independent of ligand binding. As AP-2 polymerizes the clathrin coat, the membrane invaginates until it becomes a deeply invaginated bud. Dynamin is recruited to the neck of these deeply invaginated buds and separates the nascent bud from the plasma membrane. The coated vesicle is rapidly uncoated prior to fusion with an endosome, while the coat components are released into the cytosol to sustain another round of endocytosis.

studies of shibire flies. At a non-permissive temperature, these flies become rapidly paralyzed due to synaptic vesicle depletion (Poodry and Edgar, 1979). Interestingly, the EM studies demonstrated an increase in the number of deeply invaginated clathrin-coated pits (Koenig and Ikeda, 1983; Poodry and Edgar, 1979). The temperature sensitive mutant protein in these flies is dynamin. Dynamin has a GTPase domain, a PtdIns(4,5)P_2 binding pleckstrin-homology (PH) domain, a GTPase effector domain and a proline rich domain (PRD) (Konopka et al., 2006). Dynamin readily deforms liposomes into tubules through oligomerization into a helix that constricts the liposome (Sweitzer and Hinshaw, 1998; Takei et al., 1998; Tuma and Collins, 1995). The distance between turns of a helix changes in a GTP dependent manner, which combined with the placement of dynamin at the elongated necks corresponding to those observed by EM in shibire flies, points to a role in vesicle scission, though the exact mechanism of scission remains controversial (Sever et al., 2000). Despite this controversy, ablation of dynamin is lethal, illustrating its critical role in endocytosis (Conner and Schmid, 2003b).

Interestingly, dynamin has no direct coated pit binding information, and, in fact, plays roles at other intracellular sites. This suggests that it must be recruited to clathrin-coated structures either via binding to PtdIns(4,5)P_2, which is enriched near clathrin-coated pits, and/or via an endocytic adaptor protein present in the clathrin lattice, such as amphiphysin, which binds to the dynamin PRD via an SH3 domain (David et al., 1996; Shupliakov et al., 1997; Takei et al., 1999). In addition to the SH3 domain, amphiphysin possesses a Bin1, Amphiphysin, Rvs161/167p homology (BAR) domain that binds to the membrane, and clathrin boxes and peptide motifs that bind to clathrin and AP-2 (Bauerfeind et al., 1997; Shupliakov et al., 1997;

Wigge et al., 1997). Like dynamin, the amphiphysin BAR domain tubulates lipids, suggesting that amphiphysin may either deform the membrane itself, or sense deformed membranes to correctly position dynamin at the necks of deeply invaginated pits (Ren et al., 2006). However, amphiphysin knock-out mice still sustain endocytosis, despite synaptic vesicle recycling and cognitive defects, indicating that dynamin can be recruited to coated pits in the absence of amphiphysin. (Di Paolo et al., 2002). Thus, there is a redundancy in dynamin recruitment to coated pits (Conner and Schmid, 2003b; Di Paolo et al., 2002).

In addition to dynamin, the actin cytoskeleton may play a role in vesicle scission. Actin is thought to provide mechanical force to separate the nascent vesicle from the plasma membrane. In *Saccharomyces cerevisiae*, clathrin-associated endocytosis is absolutely dependent on actin (Engqvist-Goldstein and Drubin, 2003). In mammalian systems, actin is absolutely required only for clathrin-mediated endocytosis from the apical surface of polarized epithelial cells (Qualmann et al., 2000). It is thought to be involved in endocytosis in other cells, though the precise role actin plays remains controversial (Fujimoto et al., 2000; Qualmann et al., 2000; Yarar et al., 2005). Once the clathrin-coated vesicle has departed from the membrane, it is rapidly uncoated, enabling the clathrin and AP-2 to start a new round of coated pit formation. Uncoating is ATP-dependent, and is mediated by recruitment of cyclin G-associated kinase (GAK)/auxilin. This protein binds directly to clathrin cages and AP-2 and targets the uncoating ATPase Hsc70 to coated vesicles via its J-domain (Ungewickell et al., 1995).

The detailed knowledge of the action of dynamin, actin and uncoating components augments the classical model to explain vesicle scission and uncoating (Figure 1-2). Thus, once clathrin and AP-2 have captured cargo and formed a deeply invaginated coated pit, dynamin and actin are recruited to the vesicle neck, possibly supported by multiple, redundant accessory proteins. This stimulates dynamin GTPase activity and leads to vesicle scission. The coated vesicle is rapidly uncoated in the cytosol by GAK/auxilin and Hsc70 prior to its fusion with other internalized vesicles and early endosomes. Clathrin, AP-2 and the other cytosolic components return to the soluble pool to initiate another round of endocytosis.

1.2 BEYOND THE CLASSICAL MODEL

1.2.1 Failings of the Classical Model

Although the classical model assigns roles to each of the major endocytic players, clathrin, AP-2, dynamin, actin, GAK/auxilin and Hsc70, it does not fully explain clathrin-mediated endocytosis. It does not explain why overexpression of distinct cargo types does not saturate other cargo types (Warren et al., 1997; Warren et al., 1998), nor how all of these cargo types are accommodated by AP-2. Third, this model fails to fully account for the >20 identified endocytic accessory factors identified to date, which may play crucial roles in endocytosis. Finally, recent work shows that depletion of AP-2 using siRNA duplexes targeted against either the α- or μ2 subunits selectively

blocks internalization of TfR and other cargoes utilizing a YXXΦ motif, without impairing the internalization of cargo that utilize neither YXXΦ nor dileucine internalization motifs (Harasaki et al., 2005; Hinrichsen et al., 2003; Motley et al., 2003). Furthermore, the EGF receptor, which bears multiple internalization motifs, is internalized in the absence of AP-2 (Hinrichsen et al., 2003; Huang et al., 2004; Motley et al., 2003). This demonstrates that clathrin-mediated endocytosis can be sustained in the absence of AP-2. Therefore, the classical model, which presumes AP-2 to be the sole cargo selective determinant, is insufficient to completely explain clathrin-mediated endocytosis.

1.2.2 Cargo Internalization Determinants

The first failing of the classical model is to account for internalization determinants apart from the YXXΦ and dileucine motifs. In fact, the first identified internalization motif was neither the common YXXΦ nor dileucine signals, but rather the peptide motif FXNPXY. FDNPVY is present as the only internalization determinant in the LDL receptor tail (Chen et al., 1990). The FXNPXY consensus is also present in other receptors, including LDL receptor family members (Hussain, 2001). In familial hypercholesterolemia patients, inherited mutation of the tyrosine residue in this motif within the LDL receptor tail to cysteine (Y807C) is known as the J. D. mutation, and results in an approximately five-fold decrease in the rate of LDL receptor endocytosis (Chen et al., 1990; Davis et al., 1986). The FXNPXY sequence adopts a tight β-turn that is structurally incompatible with the YXXΦ binding surface of the AP-2 μ2 subunit (Collins et al., 2002). Surface plasmon resonance and UV crosslinking has suggested that the FXNPXY

motif might be directly recognized by another region of the AP-2 μ2 subunit, but this binding was too weak to permit accurate measurements of the K_D (Boll et al., 2002), and probably too weak to drive internalization under physiological conditions.

In addition to peptide-based signals, reversible modifications such as phosphorylation can target proteins for internalization. The seven-membrane spanning GPCRs, the largest family of signaling receptors, are specifically targeted for internalization upon activation (Hausdorff et al., 1990). Along with the propagation of other signals, activation triggers the rapid hyperphosphorylation of the receptor C-terminus by GPCR kinases (GRKs) (Hausdorff et al., 1990). These multiple phosphates on the receptor are directly recognized by the endocytic adaptor protein β-arrestin, which couples GPCRs with AP-2 and clathrin to potentiate GPCR internalization.

A final post-translationally appended internalization determinant is ubiquitin. In *S. cerevisiae*, ubiquitination drives internalization of the α-factor receptor Ste2p, a-factor receptor Ste3p, ABC peptide transporter Ste6p, multidrug transporter Sts1p, general amino acid permease Gap1p, galactose permease Gal2p, uracil permease Fur4p and maltose permease Mal61p, among others (Egner and Kuchler, 1996; Galan et al., 1996; Hicke, 1999; Hicke and Riezman, 1996; Horak and Wolf, 1997; Kolling and Hollenberg, 1994; Medintz et al., 1998; Roth and Davis, 1996; Springael and Andre, 1998). Interestingly, in *S. cerevisiae* endocytosis can proceed in the absence of clathrin, and AP-2 disruption has no discernable effect upon endocytosis, likely because it cannot engage yeast clathrin (Boehm and Bonifacino, 2002). This demonstrates that in yeast, AP-2 is not the cargo-selective determinant and that ubiquitin is the principle endocytic

signal. Ubiquitination as an endocytic signal is conserved in mammalian cells, as it is thought that this is a critical internalization determinant for the EGF receptor, the leptin receptor OB-Ra, the GPCR CXCR4, and the epithelial sodium channel, among others (Belouzard and Rouille, 2006; Jiang et al., 2003; Marchese et al., 2003; Wang et al., 2006). Furthermore, a number of viruses target MHC for internalization and subsequent downregulation by expressing viral E3 ligases that polyubiquitinate MHC (Bartee et al., 2004; Coscoy et al., 2001; Hewitt et al., 2002). The role AP-2 plays in the endocytosis of these transmembrane proteins is unclear, as no direct binding of AP-2 to ubiquitin has been reported. Thus, to account for the efficient clathrin-dependent internalization of these signals, cargo subtypes that display these signals require interactions with other endocytic adaptor proteins.

Perhaps the best example of non-heterotetrameric endocytic adaptor proteins are the β-arrestins, which sort multiply phosphorylated GPCRs into coated pits for internalization. Structurally, β-arrestins consist of two folded lobes held in a "closed" conformation by salt bridges. Upon encountering the multiple receptor-attached phosphates present on an activated GPCR, the salt bridges holding the two folded lobes of β-arrestin are disrupted, inducing β-arrestin activation (Gurevich and Gurevich, 2004; Milano et al., 2002). β-arrestin binds to the AP-2 β2 subunit via a noncanonical endocytic interaction motif that is liberated from the arrestin core by the aforementioned charge-driven activation (Gaidarov et al., 1999a; Kim and Benovic, 2002; Oakley et al., 1999). This interaction motif, along with the type I clathrin box present on a solvent-accessible flexible loop, targets activated β-arrestin/GPCR complexes to coated pits, where they are internalized (Han et al., 2001; Kim and Benovic, 2002; Laporte et al., 2002; Milano et al., 2002). Thus, β-arrestins specifically bridge AP-2 and activated GPCRs.

1.2.3 AP-2 Appendage Interaction Motifs

The presence of endocytic interaction motifs analogous to those present in the β-arrestins is a common feature of many endocytic adaptor proteins. These motifs generally bind to AP-2 via either a platform subdomain on the top surface of each appendage, or a sandwich subdomain located on the side of the second lobe of the appendage (Owen et al., 1999; Owen et al., 2000; Traub et al., 1999) (Figure 1-3). The α subunit platform binds to the short, often tandemly arrayed, peptide motifs DP[FW] or FXDXF found in endocytic adaptor proteins like epsin, Dab2, amphiphysin and AP180/CALM, while the sandwich site binds to the WXXF motif found in regulatory proteins like AAK1, GAK/auxilin and the polyphosphatase synaptojanin (Jha et al., 2004; Ritter et al., 2003; Traub et al., 1999; Walther et al., 2004). The β2-appendage platform binds to a poorly delineated peptide sequence found in the endocytic adaptor proteins β-arrestin and the autosomal recessive hypercholesterolemia (ARH) protein, while an additional site binds both to DPF motifs, present in endocytic adaptor proteins like eps15, and to clathrin (He et al., 2002; Kim and Benovic, 2002; Lundmark and Carlsson, 2002; Mishra et al., 2002b). The capacity for multiple modes of adaptor protein engagement permits AP-2 to temporally scaffold coated pit formation and permit simultaneous engagement by multiple, different cargo-selective endocytic adaptor proteins. The hierarchical binding affinities of the adaptor proteins also ensure that they are recruited to and released from AP-2 in the correct order needed for coated vesicle formation (Mishra et al., 2004).
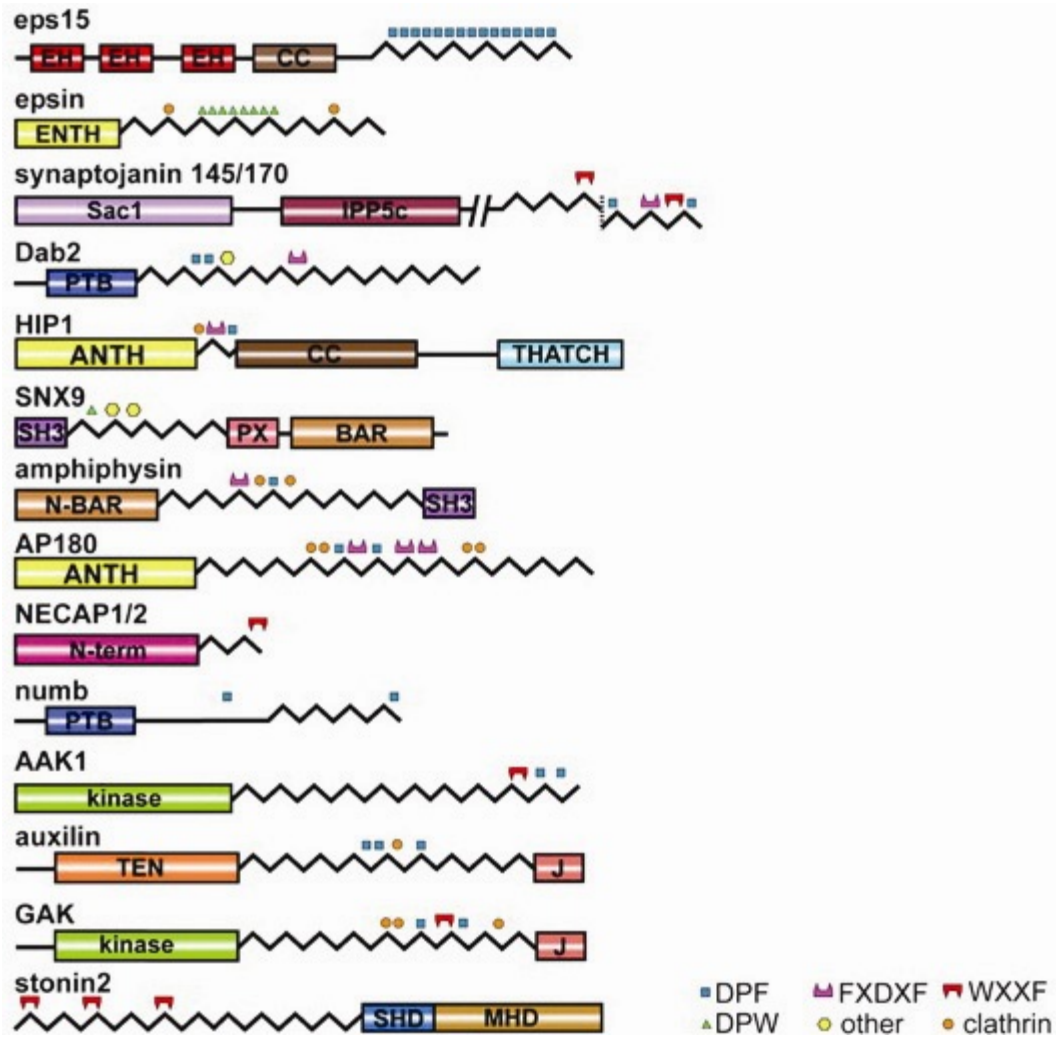
Figure 1-3 Schematic illustration of α appendage-binding motifs in endocytic accessory proteins[*]

Regions not corresponding to known domains are symbolized by straight lines, whereas similar regions for which secondary structure cannot be predicted (Jpred2) are indicated by zigzag lines. Note that α appendage- and clathrin-binding motifs occur in regions for which secondary structure cannot be predicted. ANTH, AP180 N-terminal homology; BAR, BIN-amphiphysin-RVS; CC, coiled coil; EH, Eps15 homology; ENTH, epsin N-terminal homology; IPP5c, inositol 5-phosphatase catalytic domain; J, DNA J domain; MHD, μ subunit homology domain; PTB, phosphotyrosine-binding domain; PX, Phox domain; Sac1, suppressor of actin 1; SH3, Src homology 3; SHD, stonin homology domain; TEN, tensin homology; THATCH, talin-HIP1/1R actin-tethering C-terminal homology.

1.2.4   Endocytic Adaptor Proteins

Many of the endocytic adaptor proteins that interface with the AP-2 appendages also interact with a specific cargo internalization determinant, similar to β-arrestin. Thus, these could account for the full cargo sorting capability of clathrin coats at the plasma membrane. One endocytic adaptor protein that interacts with the FXNPXY internalization motif is ARH. ARH was first identified as the defective protein in patients that carried a milder phenocopy of familial hypercholesterolemia (Garcia et al., 2001). In these patients, LDL receptor endocytosis in the liver is impaired, despite normal LDL receptors, leading to elevated blood LDL levels, tuberous xanthomas, and coronary artery disease (Soutar et al., 2003). Structurally, ARH is a ~35 kDa protein containing a phosphotyrosine binding (PTB) domain and an unstructured C-terminus. This PTB domain recognizes the FXNPXY internalization motif, and actually has a greater propensity for non-phosphorylated tyrosines, as found in the LDL receptor C-terminus (Morris and Cooper, 2001; Yun et al., 2003). It can also simultaneously bind to phosphoinositides on the plasma membrane, including PtdIns(4,5)P_2 (Mishra et al., 2002a). Within the disordered ARH C-terminus, there is a type I clathrin box and the β2-appendage binding site, similar to β-arrestin (He et al., 2002; Mishra et al., 2002b). Also like β-arrestin, ARH is crucially involved in endocytosis, though ARH selects LDL receptors, rather than GPCRs. This is demonstrated by the clinical phenotype, and poor uptake of LDL in ARH^{-/-} human (Garcia et al., 2001) and mouse (Jones et al., 2003) livers, and EBV-transformed lymphoblasts (Soutar et al., 2003). Retroviral expression of ARH in EBV-transformed lymphoblasts restores the ability of these cells to internalize LDL, attesting to this protein's role in endocytosis (Eden et al., 2002). Intriguingly, fibroblasts isolated from ARH patients, or even hepatocytes cultured *in vitro* from ARH^{-/-} mice,

show normal LDL internalization (Garcia et al., 2001; Harada-Shiba et al., 2004). Thus, the linear model where ARH couples AP-2 to LDL receptors does not fully explain LDL internalization.

With 22% identity (46% similarity) to the ARH PTB domain, the endocytic adaptor protein Dab2 may account for LDL receptor internalization in these cell types. The PTB domain of Dab2 also binds nonphosphorylated FXNPXY motifs simultaneously with PtdIns(4,5)P$_2$ (Mishra et al., 2002a; Morris and Cooper, 2001; Oleinikov et al., 2000). Like other endocytic accessory proteins, (Dafforn and Smith, 2004) Dab2 has an unstructured C-terminus following its folded domain containing two clathrin binding sites, DPF and FXDXF AP-2 α subunit binding motifs, NPF triplets that bind to eps15-homology (EH) domains present in eps15 and CIN85, a myosin VI binding site and a PRD that recognizes SH3-domains (Kowanetz et al., 2003; Morris et al., 2002a; Morris and Cooper, 2001; Xu et al., 1998). Dab2 robustly binds both clathrin and AP-2, and can polymerize clathrin into cages similar to AP-2, further implicating a role for it in endocytosis (Mishra et al., 2002a). Through binding to CIN85 and myosin VI, Dab2 may couple clathrin-coated vesicles to the actin cytoskeleton (Bruck et al., 2006; Kowanetz et al., 2003; Morris et al., 2002a). CIN85, also known as CD2AP, interacts with both phosphatases and the actin machinery and its disruption impairs endocytosis (Bruck et al., 2006; Kaneko et al., 2005; Kowanetz et al., 2004). Myosin VI is a minus-ended actin motor that associates with clathrin-coated structures in polarized epithelial cells and is thought to provide force to move coated vesicles to the base of microvilli (Buss et al., 2001). Thus, Dab2 binds to actin-associated proteins that may be necessary for later stages of coated vesicle formation. The PRD of Dab2 is

implicated in signaling, as it has been reported to bind to Grb2 and attenuate MAP kinase signaling (Zhou and Hsieh, 2001). The PTB domain may also take part in signaling, through binding to dishevelled to control Wnt signaling (Hocevar et al., 2003). Dab2 has also been reported to bind to TGF-β receptors, thereby linking both the JNK pathway and Smad pathway to TGF-β signaling (Hocevar et al., 2005; Hocevar et al., 2001). These combined activities are thought to explain why Dab2 is downregulated in a number of ovarian carcinomas (Mok et al., 1998). Disruption of Dab2 in mice is lethal, though conditional knockout mice maintaining Dab2 expression in extra-embryonic tissue are viable, attesting to its importance in the visceral endoderm (Morris et al., 2002b). These mice have a mild proteinuria similar to that observed in mice deficient in the LDL receptor family member megalin, though no hypercholesterolemic phenotypes (Morris et al., 2002b). The lethality in unconditional knockout mice arises from the inability of receptors to be endocytosed from the visceral endoderm, depriving the embryo of essential nutrients (Maurer and Cooper, 2005). Therefore, Dab2, in addition to ARH, is implicated in the internalization of cargo bearing FXNPXY motifs.

Finally, ubiquitinated cargo may be recognized by eps15, eps15-related (eps15R) and epsin. All three of these proteins contain eight or more short, tandemly arrayed DPF or DPW motifs, a clathrin box, and multiple ubiquitin-interacting motifs (UIMs) that recognize ubiquitinated proteins (Benmerah et al., 1995; Carbone et al., 1997; Chen et al., 1998; Drake et al., 2000; Fazioli et al., 1993; Hofmann and Falquet, 2001; Rosenthal et al., 1999; Wong et al., 1995). Additionally, epsin contains a folded epsin N-terminal homology (ENTH) domain that binds to PtdIns(4,5)P$_2$, and an additional type II clathrin box, enabling it to polymerize clathrin (Drake et al., 2000; Rosenthal et al., 1999). In mammalian cells, ablation of epsin, eps15 and

eps15R blocks internalization of reporter CD4 receptors in which the C-terminus has been replaced by a synthetic linker and a covalently attached polyubiquitin chain (Barriere et al., 2006). Evidence of epsin, eps15 and eps15R directly sorting physiologically expressed and ubiquitinated cargo, however, is lacking. Despite this, it is clear that these proteins play an important role in the internalization of ubiquitinated cargo.

1.2.5   The CLASP Hypothesis

Given the ability of these endocytic adaptor proteins to interface with specific cargo classes and the clathrin-coat machinery, a new hypothesis has been proposed (Traub, 2003) that expands the classical model by providing an alternate explanation for cargo selection and accounting for the known biological activity of endocytic accessory proteins. This is the clathrin-associated sorting protein (CLASP) hypothesis, which posits that the sorting repertoire of clathrin-coated pits is expanded to include alternate cargoes by the presence of dedicated endocytic sorting proteins, termed CLASPs, which are general components of clathrin-coated pits (Figure 1-4). Furthermore, through engaging dedicated subsets of cargo, these CLASPs permit the differential internalization of each motif, explaining why overexpression of cargo utilizing one internalization motif does not saturate cargo using other motifs. To accomplish these tasks, CLASPs generally have four common attributes: they simultaneously bind to clathrin, AP-2, the plasma membrane and a certain class of cargo (Traub, 2003). Usually cargo and lipid recognition is mediated by a folded domain, while the clathrin and AP-2 binding activities reside in an unstructured region of the protein. β-arrestins are candidate CLASPs that recognize multiply phosphorylated GPCRs, while Dab2 and ARH are potential CLASPs for FXNPXY-bearing

cargo, and eps15, eps15R and epsin are candidate CLASPs for the recognition of ubiquitinated cargo (Traub, 2003). However, experimental demonstration that even one set of these CLASPs, rather than AP-2, can drive the endocytosis of their cognate cargo in living cells —direct proof of the CLASP hypothesis— is lacking. In this dissertation, I have explored the CLASP hypothesis experimentally, and provide direct proof that Dab2 and ARH sort the LDL receptor into clathrin-coated vesicles.

One extreme interpretation of this hypothesis is that distinct CLASPs will populate separate clathrin-coated pits on the cell surface and selectively sort one type of cargo into them. Ultimately, this relies on the hypothesis that each cargo type is responsible for generating and maintaining a distinct class of coated pits that actively excludes other cargo types. Currently, the evidence in support of this model arises from reports of asymmetric distributions of CLASPs and cargo. This has been reported to be the case for β-arrestin (Cao et al., 1998), despite the use of an overexpression system and other reports demonstrating that β-arrestin targets pre-existing coated structures (Santini et al., 2000). It has also been proposed alternatively that LDL (Lakadamyali et al., 2006) or Tfn (Tosoni et al., 2005) are present in a compositionally distinct class of coated pits, along with CLASPs. In this dissertation, I demonstrate that in several non-polarized cell lines, this hypothesis does not appear correct. I show that at steady state multiple cargoes and CLASPs populate a common pool of clathrin-coated pits, and that the generation and maintenance of compositionally distinct subsets of CLASPs and cargo does not occur.
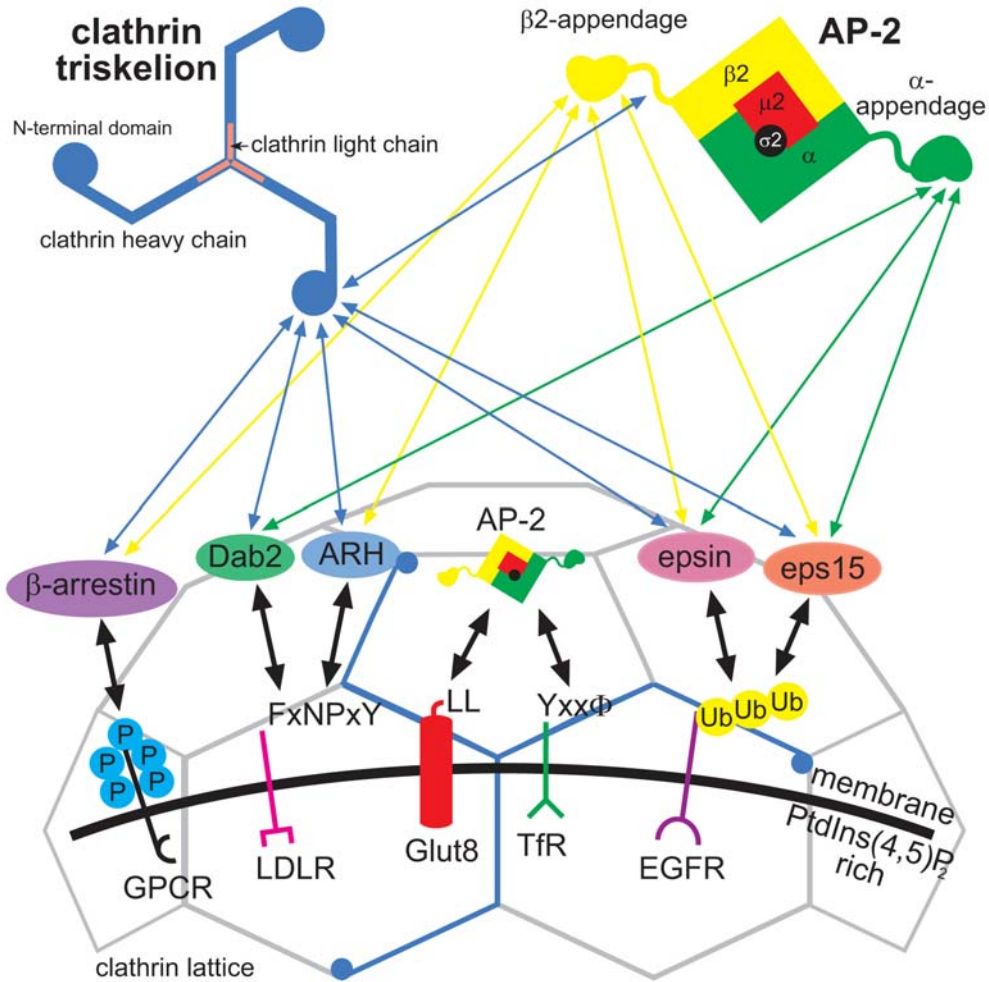
Figure 1-4 The CLASP Hypothesis

Various internalization motifs, including multiple phosphorylations (blue P) or ubiquitination (yellow Ub) or the amino acid sequences FXNPXY, -LL, or YXXΦ, on different receptors are recognized by various endocytic accessory proteins, termed CLASPs. These CLASPs all interact with the α and/or β2-appendage of AP-2, as well as the clathrin heavy chain N-terminal domain, expanding the sorting repertoire of the clathrin-coated pit. GPCR, G-protein coupled receptor; LDLR, low density lipoprotein receptor; TfR, transferrin receptor; EGFR, epidermal growth factor receptor; PtdIns(4,5)P$_2$, phosphatidylinositol-(4,5)-bisphosphate; Dab2, disabled-2; ARH, autosomal recessive hypercholesterolemia.

1.3   DYNAMICS OF ENDOCYTOSIS

1.3.1   Early Determinations of Dynamics

In addition to defining the molecular players and processes in clathrin-mediated endocytosis, the kinetics and spatio-temporal dynamics are of great importance. A 5-fold decrease in the rate of LDL receptor endocytosis results in hypercholesterolemia, underscoring the importance of rate in endocytosis (Chen et al., 1990; Davis et al., 1986). Rates of endocytosis have been measured by radioactively labeling cargo molecules and measuring the relative amounts of radioactivity that could and could not be removed from the cell surface. Using these methods, it was determined that LDL receptors complete a full round of internalization approximately every 10 min (Basu et al., 1981), and transferrin is internalized with a $t_{1/2}$ of 2.5 min (Hopkins and Trowbridge, 1983). However, two major drawbacks exist for this method. First, these assays stage cargo on the surface of cells using the 0-4ºC temperature block, which reversibly blocks endocytosis after lattice polymerization and cargo capture, but before vesicle scission (Sorkin, 2004). Thus, these rates do not account for the kinetics of cargo recognition by their receptors, clustering of the receptors in coated pits, lattice assembly, and possibly even membrane deformation. Furthermore, these are biochemical assays, and do not provide any spatial information about how or where these cargoes are internalized.

To provide spatial information about these ligands, microscopy was used to examine the clathrin coat and follow ligand internalization. Direct observation of the clathrin lattice is possible via EM, where polymerized clathrin appears as either the bristle border or the

characteristic polygonal lattice. Although these static images imply the sequential stages of endocytosis (Roth and Porter, 1964), they do not show the real-time dynamics of cargo internalization. Thus, early work utilized video intensification microscopy to follow fluorescently labeled ligands. In this way, it was demonstrated that EGF, α_2-macroglobulin and insulin entered via a common endocytic route, presumed to be similar to that utilized by the LDL receptor (Maxfield et al., 1978). By taking advantage of the pH sensitivity of fluorescein, it was determined that α_2-macroglobulin, as well as the asialoglycoprotein receptor, rapidly entered an internal acidified compartment prior to lysosomal fusion (Tycko et al., 1983; Tycko and Maxfield, 1982) in fibroblasts and HepG2 cells. Following Tfn and α_2-macroglobulin together in CHO cells showed that they segregate from a common endosomal pool into distinct compartments as early as 5 min after internalization (Yamashiro et al., 1984). This common endosomal pool can receive several successive rounds of endocytosis, ligands only becoming fusion resistant with a $t_{1/2}$ of <3 min for Tfn and 8 min for α_2-macroglobulin (Salzman and Maxfield, 1989). Tfn separates from LDL positive structures with a $t_{1/2}$ of 2.5 min to enter the recycling endosome, while LDL progresses towards late endosomes, which do not accept material from the surface (Ghosh et al., 1994). Thus, the trajectories and kinetics of ligands within the endosomal pathway have been fairly well established. The rapid internalization of ligands from the surface into early endosomes, however, has been more difficult to follow, due to the high speed of internalization and uncertainties over the identity of structures observed by microscopy.

1.3.2   Live cell Imaging of Clathrin-Mediated Endocytosis

Advances in both live cell imaging and fluorescent protein technologies permitted examination of fluorescently-tagged clathrin light chains in living cells, allowing the coat to be directly visualized by light microscopy (Gaidarov et al., 1999b). Examination of COS-7 cells transiently transfected with a GFP-LCa chimera demonstrated that most clathrin structures were static, though some were dynamic, appearing and disappearing with 20-80 s lifetimes, or rapidly traveling laterally (Gaidarov et al., 1999b). Later fluorescence recovery after photobleaching (FRAP) studies demonstrated that these static structures were labile, as both fluorescently labeled clathrin and AP-2 in these punctate structures exchanged rapidly with cytosolic pools, with a $t_{1/2}$ of ~15 s (Wu et al., 2001). Although this provides the general temporal dynamics of coated pit formation and exchange, clathrin present on the TGN, along with endosomal clathrin, complicates analysis of epifluorescent data sets. Confusion with internal structures is also a concern when following fluorescently internalized cargo.

Therefore, total internal reflection microscopy (TIR-FM) was adopted as a technique to measure real-time endocytic dynamics. This technique relies on a laser beam striking an interface of lower refractive index at slightly past the critical angle required for total internal reflection, which results in the generation of an evanescent wave perpendicular to the interface (Axelrod, 1981). This evanescent wave decays exponentially as it travels from the interface, usually with a decay constant of 70-110 nm. Thus, in theory, this technique should eliminate visualization of the majority of endosomal and TGN-associated clathrin. Simultaneous imaging of a structure by both TIR-FM and standard epifluorescence imaging permits one to discriminate between a structure moving out of the TIR-FM field and the disappearance of a structure. Using these

combined techniques, it was demonstrated in 3T3 cells that a burst of dynamin and actin correlated with the disappearance of clathrin from the evanescent field, and that this occurred after approximately 90 s (Merrifield et al., 2002). When examined by TIR-FM in HeLa cells, fluorescently tagged clathrin and AP-2 were largely static, though about 15% appeared and disappeared, and long distance motion was microtubule dependent (Rappoport and Simon, 2003; Rappoport et al., 2003b). While the clathrin positive structures could not be absolutely assigned as the plasma membrane population, it was thought that these structures were generally representative of plasma membrane events and that disappearance from the evanescent field constituted either coated pit invaginations or scission events (Rappoport et al., 2003a; Santini and Keen, 2002). These ideas were based on the 70-110 nm decay constant of the evanescent wave in the TIR-FM systems employed (Rappoport et al., 2003a; Santini and Keen, 2002). However, the idea that only surface-associated structures are visible by TIR-FM is inconsistent with numerous, previous observations of endosomes and lysosomes made by the same investigators (Jaiswal et al., 2002; Kreitzer et al., 2003; Lampson et al., 2001). In this dissertation, I have empirically determined the penetration depth of the TIR-FM and demonstrated that the static population of clathrin structures are coincident with known surface markers, while the dynamic clathrin structures bear the hallmarks of internalized structures, challenging the idea that only surface-associated clathrin structures are apparent in the evanescent field. I have also gone on to use live cell microscopy to probe the properties of Dab2 and ARH.

1.4   SPECIFIC AIMS

The studies presented in this dissertation aimed at understanding the dynamics and the interplay of clathrin, AP-2, CLASPs and cargo. To this end, there were two broad specific aims:

1.4.1   Aim I. Determine the identity of clathrin structures observed by TIR-FM

Initial TIR-FM studies revealed myriad dynamics for clathrin, all of which are generally attributed to plasma membrane clathrin. However, since endosomes and lysosomes are observable by TIR-FM, clathrin on internal structures may also constitute part of the TIR-FM population. Therefore, clathrin dynamics were examined in conjunction with plasma membrane specific CLASPs, and internally-bound cargo. This permitted a determination of what fraction of structures are actually on the plasma membrane, and whether these structures can be segregated by dynamics. This is a vital first step to utilizing TIR-FM and other imaging techniques to capture endocytosis in real-time.

1.4.2   Aim II. Validate the CLASP hypothesis and dissect the roles of ARH and Dab2 in LDL receptor cycling

In addition to understanding the dynamics of endocytosis, the interplay between the components required for selection of cargo not directly recognized by AP-2, such as the LDL receptor, will be examined. AP-2 RNAi does not halt LDL receptor endocytosis. Dab2, however, is a strong candidate as an LDL receptor-selective CLASP, and it, along with ARH, could be the LDL receptor selective CLASPs. The role both of these proteins and their subdomains play in LDL

receptor endocytosis was determined by RNAi knockdown of both proteins and rescue with fluorescently tagged constructs. Further, measurement of the distribution of these CLASPs will dictate whether dedicated coated pits exist for various cargoes, or if CLASPs expand the sorting repertoire of each coated pit. Examination of CLASP dynamics in the course of LDL internalization enabled coated pit dynamics to be correlated with those of cargo. This will validate the CLASP hypothesis and determine if the extreme interpretation of this hypothesis is also valid.

2.0 ENDOCYTIC ADAPTOR MOLECULES REVEAL AN ENDOSOMAL POPULATION OF CLATHRIN BY TOTAL INTERNAL REFLECTION FLUORESCENCE MICRSCOPY[*]

2.1 ABSTRACT

Most eukaryotes utilize a single pool of clathrin to assemble clathrin-coated transport vesicles at different intracellular locations. Coat assembly is a cyclical process. Soluble clathrin triskelia are recruited to the membrane surface by compartment-specific adaptor and/or accessory proteins. Adjacent triskelia then pack together to assemble a polyhedral lattice that progressively invaginates, budding off the membrane surface encasing a nascent transport vesicle that is quickly uncoated. Using total internal reflection fluorescence microscopy to follow clathrin dynamics close to the cell surface, I find that the majority of labeled clathrin structures are relatively static, moving vertically in and out of the evanescent field but with little lateral motion. A small minority shows rapid lateral and directed movement over micrometer distances. Adaptor proteins, including the α subunit of AP-2, ARH, and Dab2 are also relatively static and exhibit virtually no lateral movement. A fluorescently labeled AP-2 β2 subunit, incorporated into both AP-2 and AP-1 adaptor complexes, exhibits both types of behavior. This suggests that the highly

motile clathrin puncta may be distinct from plasma membrane-associated clathrin structures. When endocytosed cargo molecules, such as transferrin or low density lipoprotein, are followed into cells, they exhibit even more lateral motion than clathrin, and gradually concentrate in the perinuclear region, consistent with classical endosomal trafficking. Importantly, clathrin partially colocalizes with internalized transferrin, but diverges as the structures move longitudinally. Thus, highly motile clathrin structures are apparently distinct from the plasma membrane, accompany transferrin, and contain AP-1, revealing an endosomal population of clathrin structures.

2.2   INTRODUCTION

In eukaryotic cells, clathrin coats assemble to transport select cargo molecules from the *trans*-Golgi network (TGN) and the plasma membrane (Brodsky et al., 2001; Conner and Schmid, 2003b; Kirchhausen, 2000; Lafer, 2002), although clathrin has also been detected in association with various endosomal compartments (Futter et al., 1998; Sachse et al., 2002; Stoorvogel et al., 1996; van Dam and Stoorvogel, 2002). A clathrin coat forms upon membranes as a polygonal lattice, which progressively curves to incorporate membrane, cargo, and extracellular fluid into a vesicular transport intermediate (Brodsky et al., 2001; Conner and Schmid, 2003b; Kirchhausen, 2000; Lafer, 2002). Whereas the trafficking itineraries of many cargo molecules sorted into clathrin-coated vesicles are known, the kinetics of clathrin coat assembly, and the mechanics of adaptor protein interaction are not well understood. Transiently transfected, fluorescently-tagged

clathrin, combined with live cell imaging, shows that clathrin-coated structures are extremely dynamic (Gaidarov et al., 1999b). Total internal reflection fluorescence microscopy (TIR-FM) has extended the time-resolved study of clathrin structures by allowing the selective imaging of molecular events very close to the plasma membrane. This permits analysis of the temporal colocalization of clathrin with other proteins (Merrifield et al., 2002; Rappoport and Simon, 2003; Rappoport et al., 2003b). In these studies, four distinct behaviors of clathrin-coated structures have been reported: stasis, disappearance, reappearance, and lateral motility (Gaidarov et al., 1999b; Merrifield et al., 2002; Rappoport and Simon, 2003; Rappoport et al., 2003b).

The evanescent field utilized in TIR-FM has a decay or penetration depth of 70-110 nm, exciting only those fluorophores close to the basal plasma membrane (Axelrod, 1989). Thus, clathrin-coated structures that disappear from the TIR-FM field could be internalized vesicles moving deeper into the cell, the loss of concentrated and hence detectable clathrin because of vesicle uncoating or, finally, because of the physical deformation of the plasma membrane out of the TIR-FM field (Merrifield et al., 2002; Rappoport and Simon, 2003; Rappoport et al., 2003b; Santini and Keen, 2002). These dynamics are coupled, in part, to the activity of dynamin, actin, and tubulin (Gaidarov et al., 1999b; Merrifield et al., 2002; Rappoport et al., 2003b). The selective excitation of TIR-FM also allows imaging of adaptor proteins, which link transmembrane receptors to the clathrin coat. Endocytic adaptor proteins, including AP-2, Disabled-2 (Dab2), and the autosomal recessive hypercholesterolemia (ARH) protein, bind to the plasma membrane via phosphatidylinositol 4,5-bisphosphate, recruit and polymerize clathrin on the membrane, and synchronously bind cargo molecule receptors such as transferrin or low density lipoprotein (LDL) receptors (He et al., 2002; Mishra et al., 2002a; Mishra et al., 2002b;

Morris and Cooper, 2001; Ohno et al., 1995). With the demonstration that AP-2 is not absolutely required for clathrin-mediated endocytosis, understanding the operation of these alternate adaptors is now a priority (Conner and Schmid, 2003a; Hinrichsen et al., 2003; Motley et al., 2003). There is an emerging role for these proteins as part of the endocytic cargo selection machinery, analogous to the role GGA proteins play at the TGN (Doray et al., 2002; Mishra et al., 2002b; Motley et al., 2003).

Here, I describe two other phenomena associated with temporal changes in clathrin-coated structures: coalescence and separation. Examination of the endocytic adaptor proteins AP-2, Dab2, and ARH, along with the cargo molecules transferrin, LDL, and epidermal growth factor (EGF) shows that the previous appearance and disappearance of labeled structures observed using TIR-FM is common to plasma membrane-localized proteins, while proteins and cargo that are associated with endosomes exhibit significant lateral motion within the TIR-FM field. Dual-color TIR-FM defines the relationship between AP-2, transferrin, and clathrin structures, revealing an endosomal clathrin population sensitive to nocodazole treatment. The depth of the evanescent field is also determined empirically, and endosomes are found within this plane. Thus, the highly mobile clathrin structures observed by TIR-FM appear to be endosomal in nature.

2.3   RESULTS

2.3.1   Novel Spatial Clathrin Phenomena

When cells are transiently transfected with the clathrin LCa fused to the carboxyl terminus of GFP (GFP-LCa), the fluorescent clathrin appears as bright puncta that colocalize extensively with endogenous clathrin (data not shown) (Blanpied et al., 2002; Gaidarov et al., 1999b). By epifluorescence, the cytosolic pool of unpolymerized fluorescent clathrin is visible as a diffuse haze, along with bright TGN and surface puncta (Figure 2-1B). When the same fibroblasts are imaged using TIR-FM optics, the signal is restricted to fluorescent structures close to the plasma membrane surface, hence the improved signal-to-noise ratio of the image (Figure 2-1C). In agreement with previous studies examining clathrin dynamics (Gaidarov et al., 1999b; Merrifield et al., 2002; Rappoport and Simon, 2003; Rappoport et al., 2003a; Rappoport et al., 2003b), I observe fluorescent clathrin structures with four different behaviors in living cells (Figure 2-1D-I): appearing (Figure 2-1, open arrows), disappearing (white arrows), moving laterally (arrowheads), and relatively stationary. Importantly, the high signal-to-noise ratio in TIR-FM allows images to be collected using low laser power, restricting the evanescent field and minimizing photobleaching. The lack of photobleaching is evident from the persistence of the fluorescence in non-motile structures immediately adjacent to abruptly disappearing spots (Figure 2-1F).
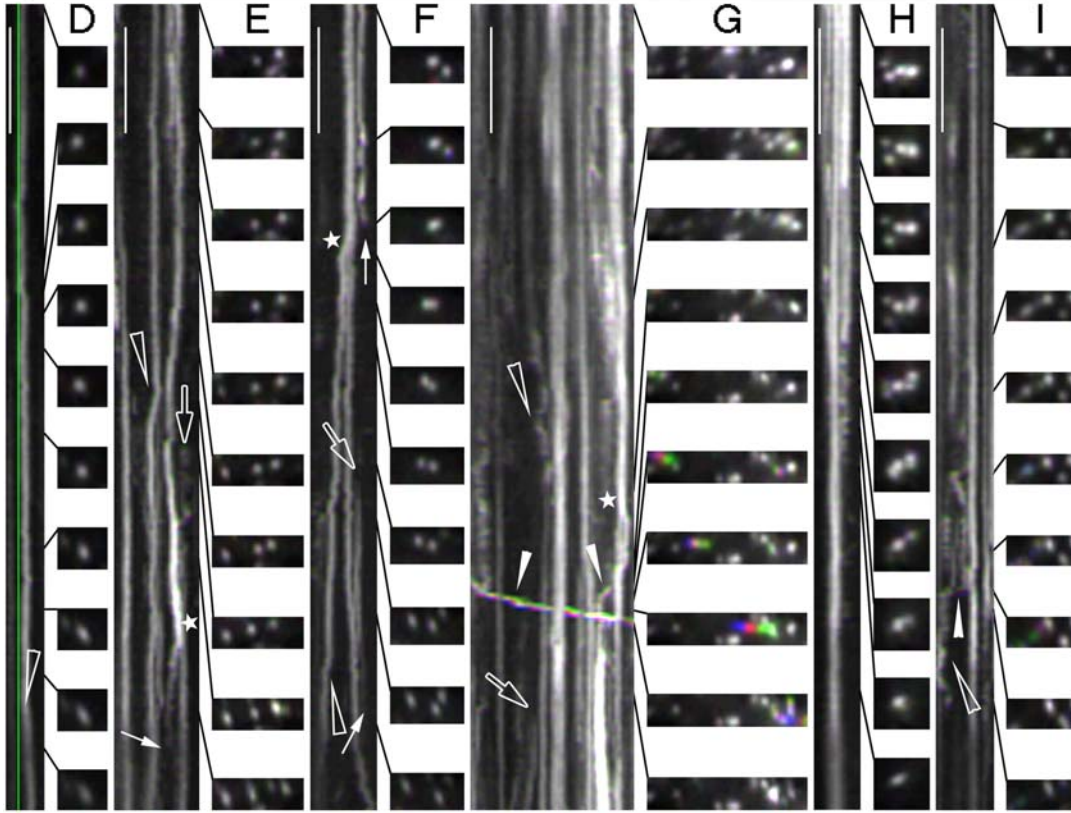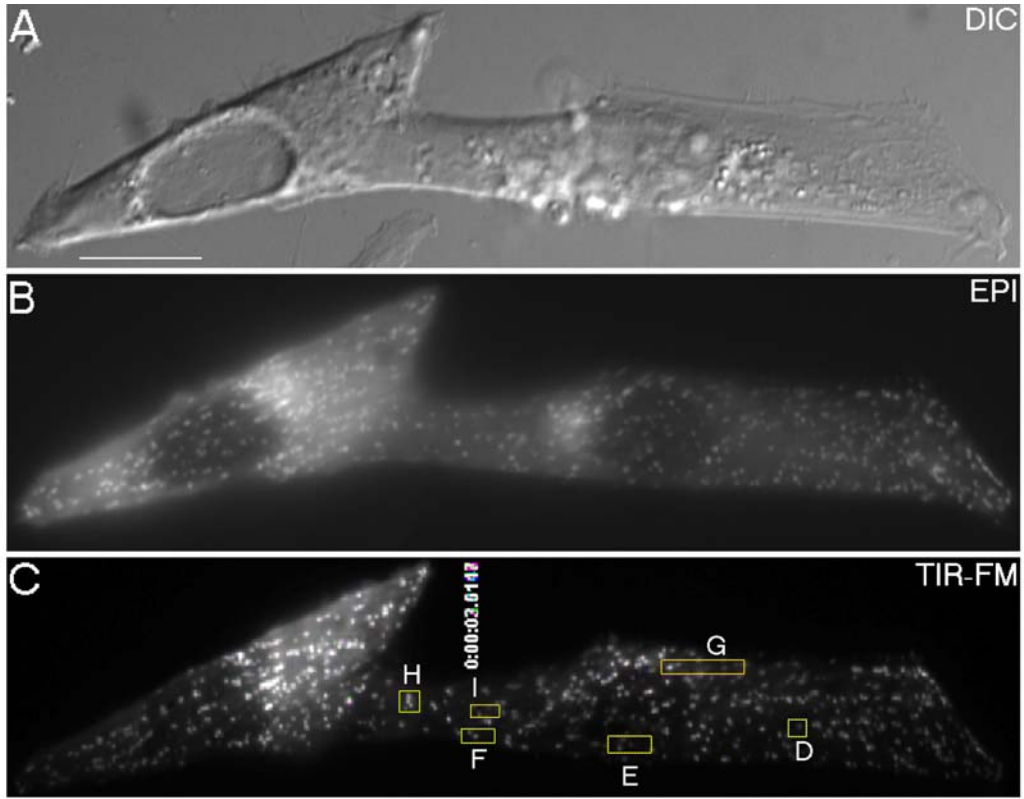
Figure 2-1 Different clathrin dynamics in living cells

Figure 2-1. Different clathrin dynamics in living cells

Normal human fibroblasts were transfected with GFP-LCa 18 h prior to imaging. Two expressing cells, visualized by DIC (A), epifluorescence (B), and TIR-FM (C), show that most of the cytosolic and TGN-associated GFP-LCa is eliminated and the signal-to-noise ratio is improved in the TIR-FM field. To demonstrate appearance (open arrows), disappearance (white arrows), splitting (asterisks), coalescence, long distance (white arrowheads), and local (open arrowheads) motion, kymographs (xt projection) from selected regions of TIR-FM data set are shown (D-I). The accompanying still images show traditional representations from specific time points in the kymographs, indicated by the lines. The vertical green line in D is included to show the degree of local motion. The scale bar is 10 μm for A, and 20 s for D-I.

Two different types of lateral motion are apparent in the data sets. The first is the uncoordinated gyration of a coated structure about a ~1-μm region, which is termed local motion (Figure 2-1, D-F, open arrowheads). The second type of lateral motion is the dynamic (0.5-0.67 μm/s), directed transit of a structure down a roughly linear path (1.5-9 μm travel distance), designated long distance motion (Figure 2-1G, white arrowheads). Others consider this long distance motion to be planar clathrin-coated lattices or invaginated coated pits moving in a microtubule-dependent fashion while still associated with the plasma membrane, although localization to endosomes was not excluded (Rappoport et al., 2003a; Rappoport et al., 2003b). However, Figure 2-1G shows a large (~0.6 μm diameter) clathrin-coated structure moving laterally (white arrowheads, and seen by the green-red-blue transition in the image sequence stills). Along its entire trajectory, this structure travels by several non-motile clathrin-positive structures without evidence of interaction; there is no change in speed, surface area, or collisional activity (see Movie 2-1). Because these objects are larger than the diffraction limit of the optical system being used, and invaginated coated pits are ~100 nm in depth (Santini and Keen, 2002),

37

this suggests that the evanescent wave allows visualization of subcellular structures beyond that indicated by the absolute value of the decay depth (Gaidarov et al., 1999b; Merrifield et al., 2002; Rappoport et al., 2003b).

Because structures with sizes on the order of the depth of the evanescent wave can apparently pass each other within the TIR-FM field, the depth of the excitatory evanescent wave was determined empirically. The intensity of the evanescent wave decreases exponentially with distance,

$$I_z = I_0 e^{-z/d}$$ (Eq. 1)

where I_z is the intensity at depth z, I_0 is the initial intensity, and d is the characteristic decay depth defined as,

$$d = \lambda/(4\pi n_2) \cdot ((\sin^2 \theta / \sin^2 \theta_C) - 1)^{-1/2}$$ (Eq. 2)

where λ is the wavelength of the incident light in a vacuum, θ is the angle of the incident light, θC is the critical angle, defined as sin-1 (n2/n1), and n1 and n2 are the refractive indices of the substrate and liquid medium, respectively (Axelrod, 1989). The refractive indices of the glass coverslip and aqueous culture medium (Figure 2-6B shows Tfn488 in the medium under ~85% of the cell in the TIR-FM field) are 1.518 and 1.33, respectively, making the calculated critical angle 61.2°. Thus, using 69° incident light and a 488-nm excitation wavelength, d is calculated to be 79.4 nm. Empirically, in this system, I measured the critical angle to be 60.2°. Substituting

38

this value for the theoretical value of 61.2° decreases the calculated decay depth for 69° incident light to 73.6 nm. If the refractive index of cytosol (1.36) is used instead of the value for the aqueous medium (1.33) to calculate the critical angle (now 63.6°), then the calculated decay depth becomes 97.5 nm. These values are all within the 70-110 nm range for d quoted in the literature. However, d is only the depth at which the intensity of the evanescent wave is 37% of the initial intensity. To empirically determine the experimental depth at which fluorophores are visible, 1-μm fluorescent beads were imaged in the TIR-FM field. A measured diameter of 786 nm indicates a visible depth of 190 nm (using the Pythagorean theorem), which is over twice the calculated decay depth. Precise determination of the depth of the TIR-FM field is difficult because of the physical limits of the optical system and the diffraction limit of light. Typically, the nucleus of CV-1 cells is ~150 nm from the ventral plasma membrane surface and in some data sets, the nucleus is occasionally observed within the TIR-FM field as an oval, poorly stained region (see Figures 2-5 and 2-6). Therefore, I conclude that in this system, the evanescent wave penetrates deep enough into the cell to excite two vertically aligned clathrin-coated vesicles, and that these structures can be distinct from the plasma membrane.

I also report two other clathrin dynamics seen using TIR-FM: the coalescence and separation/splitting of clathrin-containing structures (Figure 2-1, E-G). The structures that coalesce range in size from diffraction-limited spots to structures 0.8-1.0 μm in diameter. These structures commonly exhibit local motion prior to coalescence. The most common sequence seen is a static structure around which another moves, followed by merging of the two (Figure 2-1H). The reverse dynamic is also seen, where clathrin structures actively separate from others prior to moving laterally or disappearing from the TIR-FM field (Figure 2-1, E-G, asterisks).

The clathrin structures observed by TIR-FM range in diameter from diffraction-limited objects up to 0.6-1 μm. Importantly, the different sized structures distribute unevenly through the cell. Diffraction-limited structures are most abundant in the periphery of the cell (7% large structures), whereas larger objects are prevalent in the perinuclear region (75% large structures; Figure 2-1C). As the TGN lies deep within the cell, this perinuclear clathrin is probably not TGN associated. This is reinforced by epifluorescent images showing that TGN-associated clathrin is localized to a Golgi surface near the top of the perinuclear region (Figure 2-1B). The size and perinuclear clustering of the larger clathrin structures is unusual for coated pits or coated vesicles at the cell surface.

2.3.2 Sucrose Halts All Clathrin Activity

As clathrin movement out of the TIR-FM field is assumed to be because of endocytosis, I tested the validity of this assumption by placing cells transfected with GFP-LCa into 0.45 M sucrose dissolved in culture medium. This treatment is known to block endocytosis by driving the polymerization of clathrin into microcages incapable of participating in vesicle formation (Heuser and Anderson, 1989). Under these conditions, all motion, from appearance and disappearance to local and long distance motion, stops within 30 s following treatment (Figure 2-2). Additionally, there is an increase in the number of clathrin-positive structures to 120% of pre-sucrose levels, consistent with the formation of microcages that deposit on the membrane. These
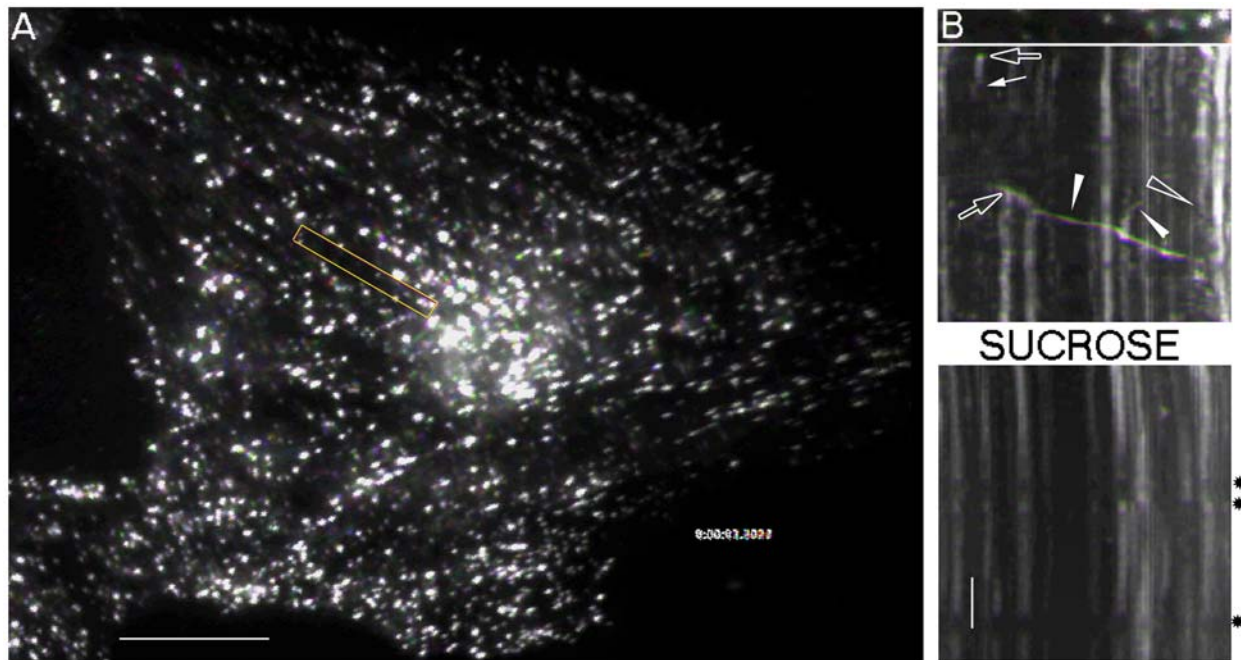
Figure 2-2 Sucrose halts all clathrin dynamics

CV-1 cells were transfected as described in the legend to Figure 2-1 and imaged by TIR-FM, with a ~30-s interval for 0.45 M sucrose addition in the middle of image acquisition. Temporal progression of the boxed region in the TIR-FM image (A) is shown by the kymograph (B). Dynamics are indicated with the same symbols used in Figure 2-1. After sucrose addition, all motion was immediately stopped, and the clathrin bleached faster. The scale bar represents 10 μm in A and 20 s in B.

structures also rapidly bleach ($t_{1/2}$ ~100 s, using laser power that shows minimal bleaching in untreated cells), strongly suggesting that there is no molecular exchange with cytosolic clathrin, as occurs under normal conditions (Wu et al., 2001).

2.3.3   Endocytic Adaptor Proteins Do Not Display Long Distance Motion

Although the dynamics of clathrin in relation to the actin cytoskeleton, dynamin, and, most recently, AP-2 have been examined by TIR-FM (Gaidarov et al., 1999b; Merrifield et al., 2002; Rappoport et al., 2003a; Rappoport et al., 2003b), the spatio-temporal behaviors of alternate endocytic adaptor proteins have not been reported. I expressed and imaged YFP fusions of the α_C and $\beta 2$ subunits of the AP-2 endocytic adaptor (Figure 2-3), as well as the alternate endocytic adaptors ARH, Hip1R, and Dab2, fused to GFP, for comparison (Figure 2-4). These TIR-FM observations are consistent with previous reports on the distribution of the endogenous proteins that, in each case, localizes to punctate structures on the membrane (Engqvist-Goldstein et al., 2001; Laporte et al., 1999; Metzler et al., 2001; Mishra et al., 2002a; Mishra et al., 2002b; Morris and Cooper, 2001; Sorkina et al., 2002). However, in living cells, the motion of these adaptors is quite different from that of clathrin. The AP-2 α_C subunit, ARH, and Hip1R all localize to small, diffraction-limited punctate structures that appear and disappear in common with clathrin puncta (Figure 2-3, A-C and Figure 2-4, A-D and F, arrows), but less than 1% of the structures show any long distance motion. Dab2 also localizes to appearing/disappearing/static structures, but many of these are considerably larger, up to 1 μm in diameter (Figure 2-4E). These tagged proteins do appear and disappear in the same spot, supporting the idea that there are endocytic "hot spots" on the plasma membrane (Santini and Keen, 2002).
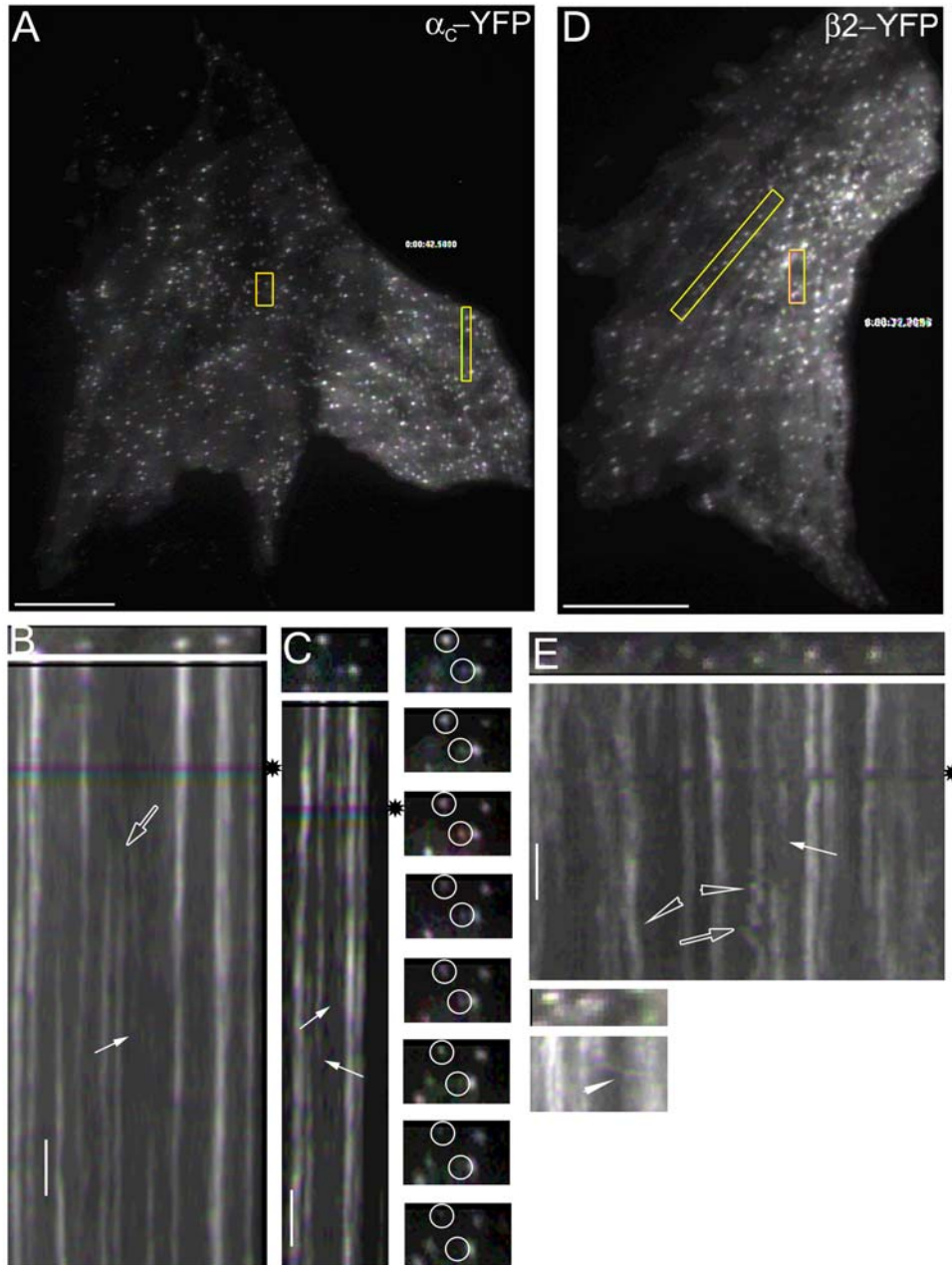
Figure 2-3 Dynamics of the large subunits of the AP-2 adaptor

CV-1 cells were transfected as described in the legend to Figure 2-1 with either AP-2 α_C-YFP (A-C) or $\beta 2$-YFP (D and E) and imaged by TIR-FM. The boxed regions in the TIR-FM images (A and D) are shown by the kymographs (B, C, and E). Dynamics are indicated with the same symbols used in Figure 2-1. The black asterisks denote focal shifts in the data set. Although the AP-2 α subunit shows appearance and disappearance (arrows and circles in still images), it exhibits little to no lateral motion. The $\beta 2$ subunit, however, displays nearly identical dynamics to clathrin. The scale bar represents 10 μm (A and D) or 20 s (B, C, and E).
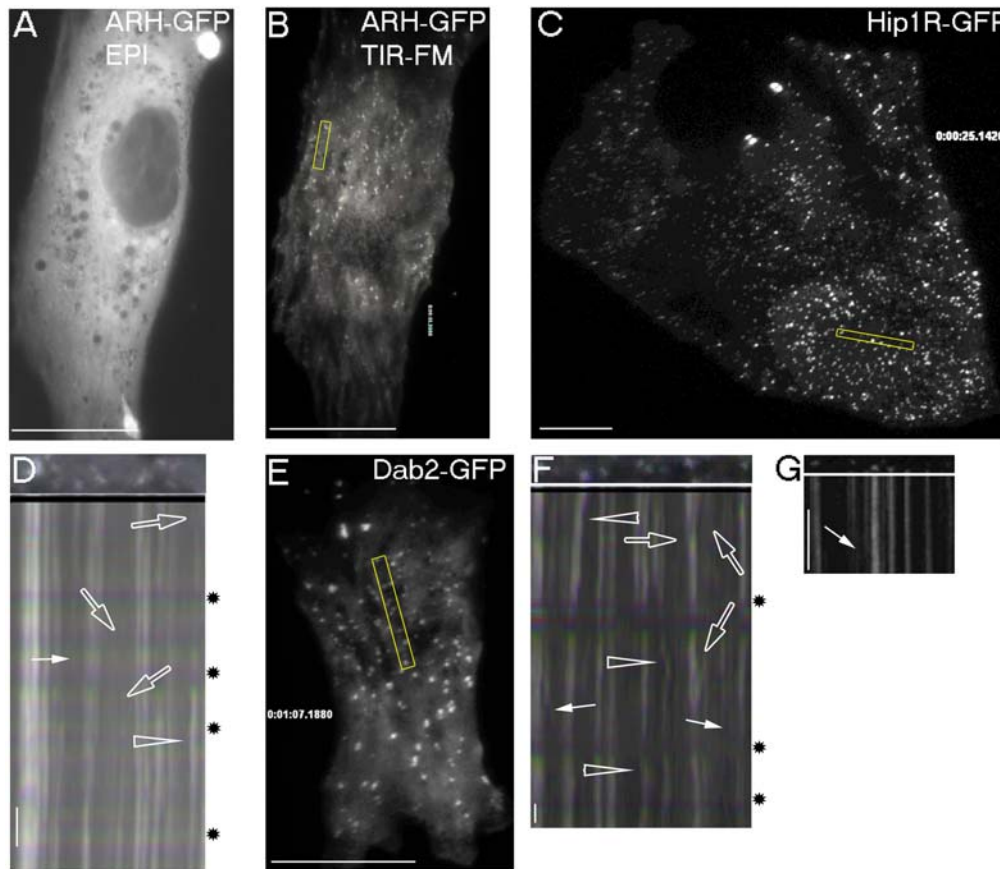
Figure 2-4 Temporal behavior of the endocytic adaptors ARH, Hip1R, and Dab2

CV-1 cells were transfected 6-20 h prior to imaging by TIR-FM. Although epifluorescence images show the cytosolic distribution of the adaptors, as typified by ARH (A), TIR-FM shows that ARH (B), Hip1R (C), and Dab2 (E) each localize to punctate structures. Dynamics are indicated with the same symbols used in Figure 2-1. The scale bar represents 10 μm (A-C), 5 μm (E), or 20 s (D, F, and G).

Standard immunofluorescence microscopy shows that Hip1R localizes to surface clathrin-coated puncta at steady state (Engqvist-Goldstein et al., 2001), as do AP-2 and Dab2 (Mishra et al., 2002a; Morris and Cooper, 2001; Rappoport et al., 2003a; Wu et al., 2003). Rapid freeze/deep etch EM shows that the Hip1R puncta correspond to both planar clathrin structures and coated pits (Engqvist-Goldstein et al., 2001). If either of these structures display lateral motion, the fluorescent Hip1R should also exhibit lateral motion. I find that only ~3% of Hip1R-

positive structures exhibit local motion, compared with 30% for clathrin-positive structures, and they have minimal long distance motion (<0.4% structures) (Figure 2-4, C and F). Similarly, AP-2 and Dab2, both of which colocalize extensively with clathrin at steady state, have fewer puncta exhibiting local motion than GFP-LCa, <1 and 9%, respectively (Figures 2-3, A-C and 2-4). ARH does show some lateral motion (16%), although the protein localizes less well with clathrin-containing structures (Figure 2-4, A and B) (Mishra et al., 2002b). Thus, I conclude that the clathrin-positive structures exhibiting long-range motion are not associated with plasma membrane-associated coat components.

2.3.4   Distinct Dynamic Behavior of the AP-2 α_C and $\beta2$ Subunits

In contrast to the AP-2 α_C subunit, ARH, Dab2, and Hip1R, the AP-2 $\beta2$ subunit exhibits both long distance and local motion (5 and 32%, respectively), in common with clathrin (Figure 2-3, D and E). To better understand this difference in the dynamics of the α_C and $\beta2$ subunits, I correlated the relative motion of clathrin and AP-2 by simultaneous expression of DsRed-LCa and AP-2 α_C- or $\beta2$-YFP fusions in CV-1 cells. When expressed together, clathrin does not show perfect colocalization with the α_C subunit-YFP fusion, a specific marker for AP-2 (Figure 2-5A). In fact, α_C-YFP is only seen in static and disappearing/appearing structures and not in long distance moving structures (Figure 2-5B), in agreement with the single-color experiments. Therefore, the division of clathrin structures into laterally motile or stationary/appearing/disappearing is a classification that appears to discriminate between AP-2 adaptor-positive clathrin, and AP-2 adaptor-negative clathrin.

However, long distance motion is clearly apparent when the β2-YFP fusion protein is expressed alone. When CV-1 cells cotransfected with β2-YFP and DsRed-LCa are examined, cells that express low levels of β2-YFP (Figure 2-6, A-C) show colocalization of β2-YFP with ~10% of long distantly moving clathrin structures (~8% of total clathrin). About 20% of the DsRed-LCa and β2-YFP structures in these cells exhibit disappearing/appearing behavior per min. By contrast, in cells expressing high levels of β2-YFP (Figure 2-6, D and E), all of the long range mobile clathrin structures are now positive for the β2-YFP signal and colocalization between all β2-YFP and DsRed-LCa structures increases from ~75 to 85%. As the primary sequence of the AP-2 β2 subunit shows 85% homology to the β1 subunit of the AP-1 adaptor complex it can act as a functional replacement for the β1 subunit in AP-1 complexes. This is shown experimentally (Page and Robinson, 1995; Sorkin et al., 1995) and the promiscuity is also observed *in vivo*, where native AP-1 complexes purified from brain contain the β2 subunit (Traub et al., 1996). Thus, upon overexpression of the β2-YFP construct, the puncta observed probably represent both AP-1- and AP-2-positive structures. AP-1 localizes to the TGN, which generally cannot be observed by TIR-FM (Schmoranzer and Simon, 2003; Toomre et al., 2000), but is also found on endosomes (Huang et al., 2001; Meyer et al., 2000; Waguri et al., 2003). Because the AP-2 α_C subunit exhibits virtually no long distance and limited local motion, one explanation for the highly mobile clathrin population could be that it contains AP-1 adaptors, which are not present on the plasma membrane. Importantly, the extent of AP-1 labeling will also increase as the expression level of the β2-YFP subunit rises. Therefore, I propose that the clathrin observable by TIR-FM is accounted for by both AP-1 and AP-2 positive structures, the former correlating with the long distance motile structures, and the latter correlating with the static, appearing and disappearing structures.
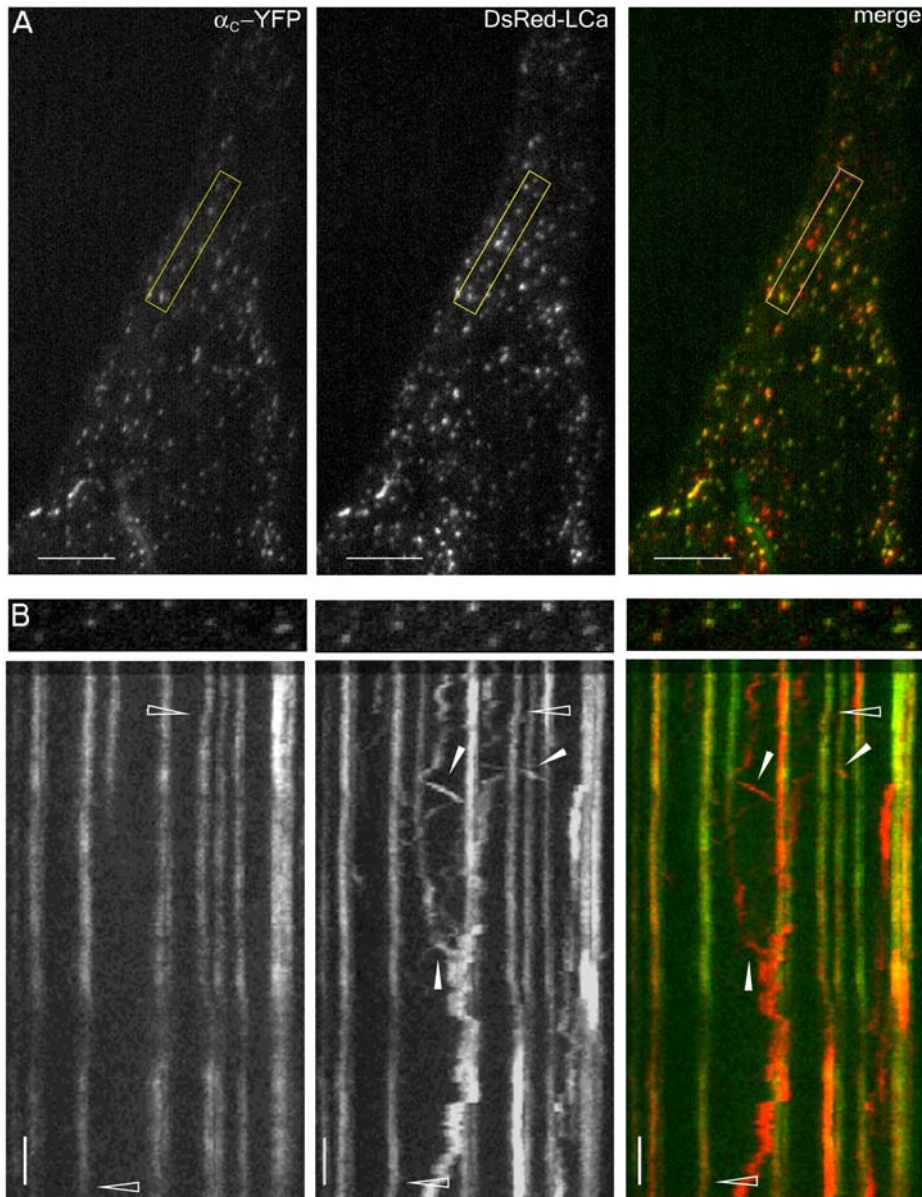
Figure 2-5 The AP-2 α subunit does not colocalize with clathrin structures undergoing long distance motion

CV-1 cells were transfected as described with DsRed-LCa and AP-2 α_C-YFP and imaged by TIR-FM. There are two distinct populations of DsRed-LCa-labeled structures (middle panels, red in merged image) visible in these cells (A), a laterally motile population devoid of AP-2 and a relatively immobile, AP-2-associated population. The kymograph (B) demonstrates that AP-2 (left panels, green in merged image) is present in appearing and disappearing structures, but the adaptor is absent from structures undergoing lateral motion. Dynamics are indicated with the same symbols used in Figure 2-1. The scale bar represents 10 μm (A) or 20 s (B).

Figure 2-6 The AP-2 β2 subunit colocalizes with clathrin structures undergoing long distance motion

48
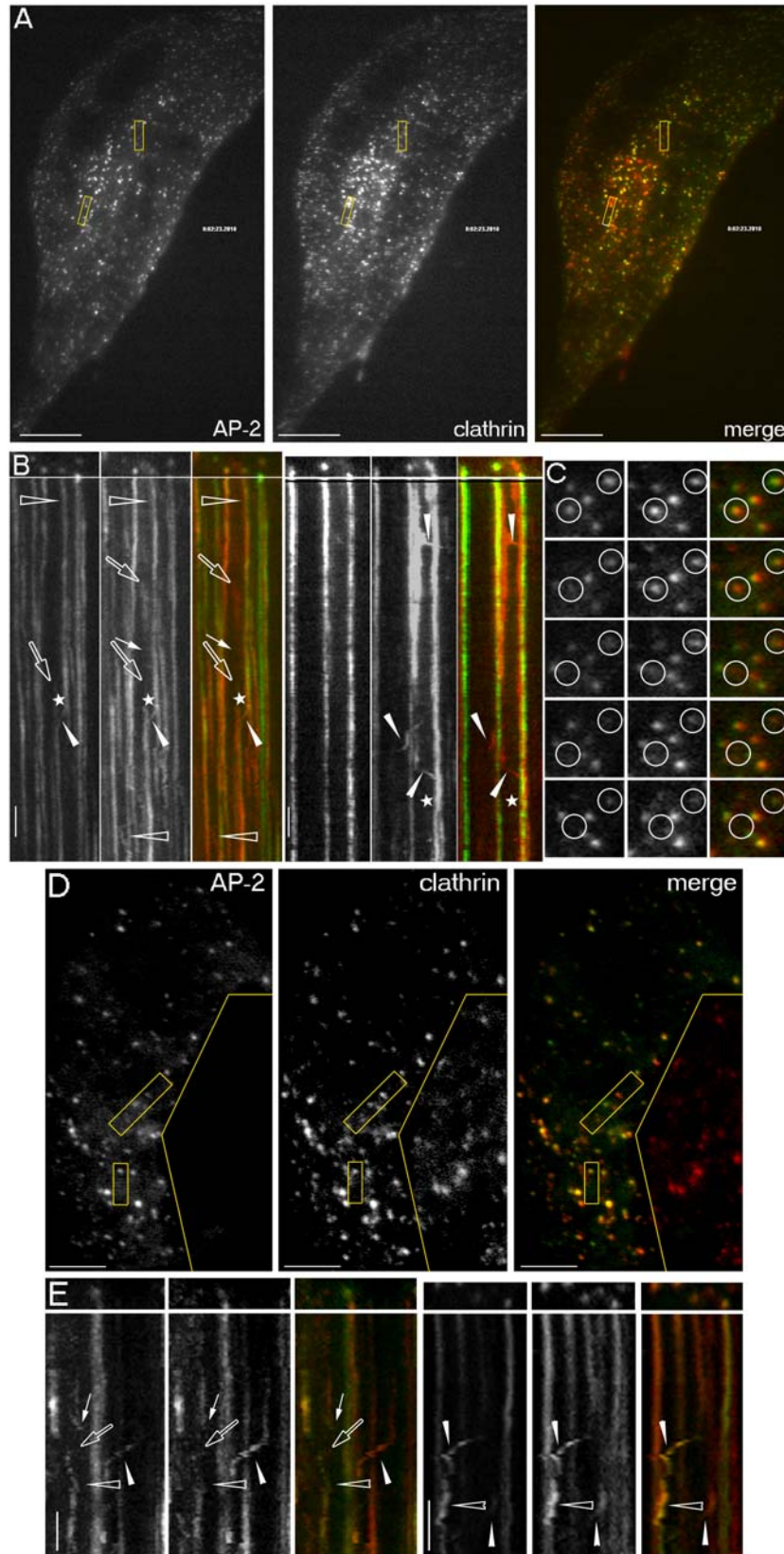
Figure 2-6 The AP-2 β2 subunit colocalizes with clathrin structures undergoing long distance motion
CV-1 cells were transfected as described with DsRed-LCa and AP-2 β2-YFP and imaged by TIR-FM. In a cell expressing relatively low levels of the β2-YFP fusion (A), only some of the laterally moving DsRed-LCa structures are also β2-YFP positive, as shown in the kymograph (B). The AP-2 β2 subunit does colocalize with DsRed-LCa in appearing and disappearing structures as shown by the kymograph, and in the series of still images (C, circles). In a cell expressing greater levels of β2-YFP (D), however, the laterally motile clathrin structures also contain the β2 subunit, as shown in the kymograph (E). In each set, the left panel is the AP-2 β2-YFP (green in merged images), the middle panel is DsRed-LCa (shown in red in merged images), and the right panel is the merged image. Dynamics are indicated with the same symbols used in Figure 2-1. The scale bar represents 10 μm (A and D) or 20 s (B and E).

In general, these data agree with a previous study showing that laterally mobile clathrin structures are devoid of AP-2 (Rappoport et al., 2003a). They differ in two important respects, however. First, the correlation between the β2 subunit-clathrin overlap and the β2 subunit expression level shown here suggests that the long distance mobile population does contain an associated adaptor complex, AP-1. Second, within the static population of fluorescent α_C and β2 subunits, the appearance and disappearance behavior typical of budding clathrin structures is clearly seen. For example, in a selected image sequence from α_C-YFP expressing CV-1 cells (Figure 2-3D, circles), two labeled structures disappear abruptly from the field. Similarly, in dual-color images of DsRed-LCa and β2-YFP, synchronous exit of double-labeled yellow structures is seen (Figure 2-6C, circles). I believe that this demonstrates that AP-2 and clathrin leave the plasma membrane together in the form of a polymerized coat, in contrast to the view that AP-2 positioned on the cell surface is entirely static and not seen in structures during internalization (Rappoport et al., 2003a).

2.3.5 Cargo Molecules followed into the Cell by TIR-FM

There is compelling evidence for the formation of clathrin-coated buds and vesicles upon transferrin-positive early and recycling endosomal elements (Stoorvogel et al., 1996; van Dam and Stoorvogel, 2002). In whole mount EM images, these structures are often in close proximity to the plasma membrane (Stoorvogel et al., 1996; van Dam and Stoorvogel, 2002), probably within the constraints of the evanescent field in TIR-FM. Indeed, the uptake and intracellular trafficking of Tfn488 can be clearly observed by TIR-FM in living cells (Figure 2-7, A-D) (Lampson et al., 2001). The media appears intensely fluorescent because of the presence of unbound Tfn488. The unlabeled regions in the field correspond to focal adhesions (Figure 2-7A, white arrows) where the cell is in tight contact with the coverslip and thus excludes the fluorescent probe. Elsewhere, the cell surface is separated from the glass substrate such that media diffuses freely underneath, accounting for the diffuse background fluorescence observed in these experiments. During Tfn488 uptake, diffraction-limited peripheral structures appear throughout the cell, which then move rapidly (0.5 μm/s) toward the perinuclear region, where they separate and fuse with each other, forming structures up to 1 μm in diameter over time (Figure 2-7B). At the periphery of the cell, the motile properties of the transferrin-positive structures mimic that of the static clathrin and AP-2 populations. Between this region and the larger juxtanuclear recycling endosomes, an intermediate zone is characterized by rapid, bidirectional long distance trajectories (Figure 2-7B). In the continued presence of Tfn488, the larger vesicles are apparent after 15 min of uptake, characteristic of recycling endosomes (Figure 2-7, A and B). Tfn488 exhibits more long distance motion than GFP-LCa (15 versus 7%) with a longer average path length (5 versus 2.5 μm). When CV-1 cells are pulsed with fluorescently
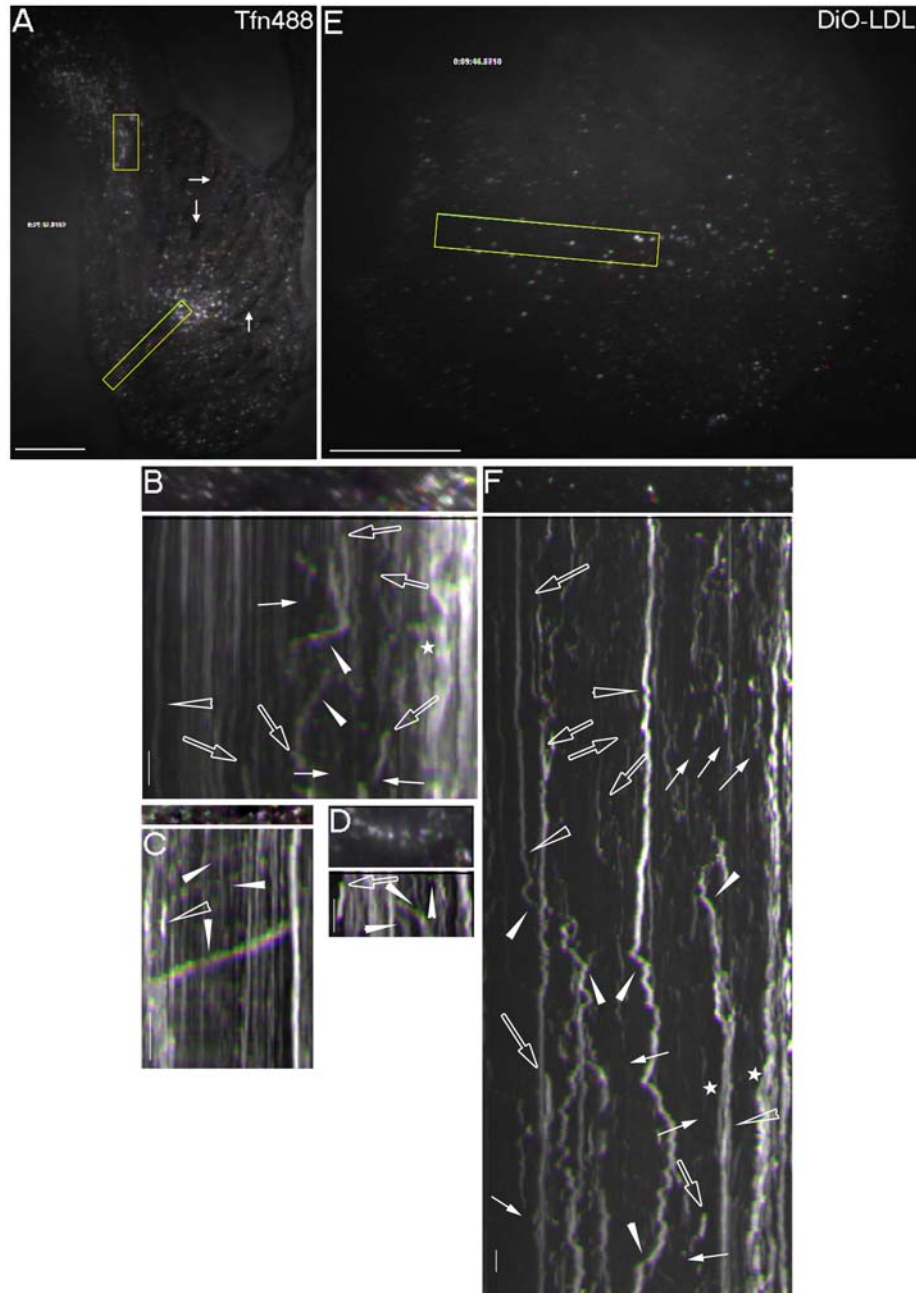
Figure 2-7 Internalization of LDL and transferrin observed by TIR-FM

CV-1 cells were serum-starved for 1 h (transferrin) or grown in lipoprotein-deficient serum overnight (LDL) prior to placement on the microscope. Tfn488 (A-D) or DiO-LDL (E and F) was added and the cells were imaged about 5-15 min later in the continued presence of the fluorescent cargo. The regions boxed in the TIR-FM images (A and E) are shown by the kymographs (B, D, and F). The kymograph in C comes from a different Tfn488 uptake dataset. The various dynamics are marked with the same symbols used in Figure 2-1. Both DiO-LDL and Tfn488 display greater long distance motion than the AP-2 β2 subunit or clathrin, as shown in the kymographs. The scale bar represents 10 μm (A and B) or 20 s (C and D).

labeled LDL particles (DiO-LDL), similar motion is observed with the LDL moving to ~1-μm diameter perinuclear structures, although, in contrast, no recycling is seen (Figure 2-7, E and F). This shows clearly that portions of the endocytic pathway can be observed by TIR-FM.

Occasionally, several independent Tfn488-labeled structures are seen sequentially trafficking several micrometers along a single track within a short time period (Figure 2-7C, white arrowheads). This long distance motion of Tfn488, and of GFP-LCa, is arrested by treating cells with 10 μM nocodazole for 30 min prior to imaging (data not shown), demonstrating that the labeled structures move in a motor-dependent fashion along microtubule tracks, as previously reported (Rappoport et al., 2003b; Sakai et al., 1991). Furthermore, following nocodazole treatment, the larger 0.6-1-μm structures do not accumulate in the perinuclear region. Nocodazole treatment does not alter the appearance/disappearance behavior of either in the TIR-FM field, however, confirming that endocytosis from the plasma membrane is unaffected by microtubule depolymerization. In related experiments, I find that when cells pulsed with Tfn488 are treated with 0.45 M sucrose, most motion halts within 30 s of sucrose treatment, similar to GFP-LCa (2% post-sucrose motion versus 15% pre-sucrose) (data not shown). The only motion remaining after 30 s of sucrose treatment is the continued long distance travel of a few Tfn488 puncta that are moving much slower (0.1 μm/s) than usual. These results suggest that the effect of hyperosmotic stress goes beyond the arrest of clathrin-mediated endocytosis. In fact, incubating cultured cells in hyperosmotic sucrose fragments the Golgi/TGN (Lee and Linstedt, 1999; Wu et al., 2003) and osmotic stress can exert profound effects on ER-Golgi trafficking and COPI coat dynamics within 5 min (Lee and Linstedt, 1999).

2.3.6 Relationship between Dynamic Clathrin and Internalized Transferrin

Although long distance motion is observed with both GFP-LCa and Tfn488, the motile Tfn488-positive structures are more numerous and travel further (Figure 2-7 compared with Figures 2-4 and 2-5). To examine the spatio-temporal relationship between clathrin and Tfn488 structures, I pulsed Tfn488 into DsRed-LCa-transfected cells for 30 min and then removed the transferrin before imaging. Perinuclear accumulation of Tfn488 is found within compact recycling endosomes by epifluorescence (Figure 2-8A), although, as expected, it is not readily seen in the TIR-FM image (Figure 2-8B). Yet TIR-FM does show that both Tfn488- and DsRed-LCa-positive structures are concentrated in the perinuclear region, with significant (36%) colocalization. When TIR-FM is performed in the continued presence of Tfn488, the colocalization is increased to 56%. Interestingly, long distance clathrin motion appears to be aligned, but not exactly coincident with transferrin-positive elements. Upon initiation of long distance motion, the two fluorescent labels are often close, but spatially resolved. For example, while moving rapidly along a similar overall trajectory, a double-labeled structure separates into a DsRed-LCa structure trailing a Tfn488 structure (Figure 2-8C, white arrowhead). These observations may be related to the complex and temporally malleable morphology of transferrin-bearing endosomes as they progress from early to recycling structures. Nevertheless, the data do indicate that at least a portion of the motile transferrin-positive structures have closely apposed clathrin.
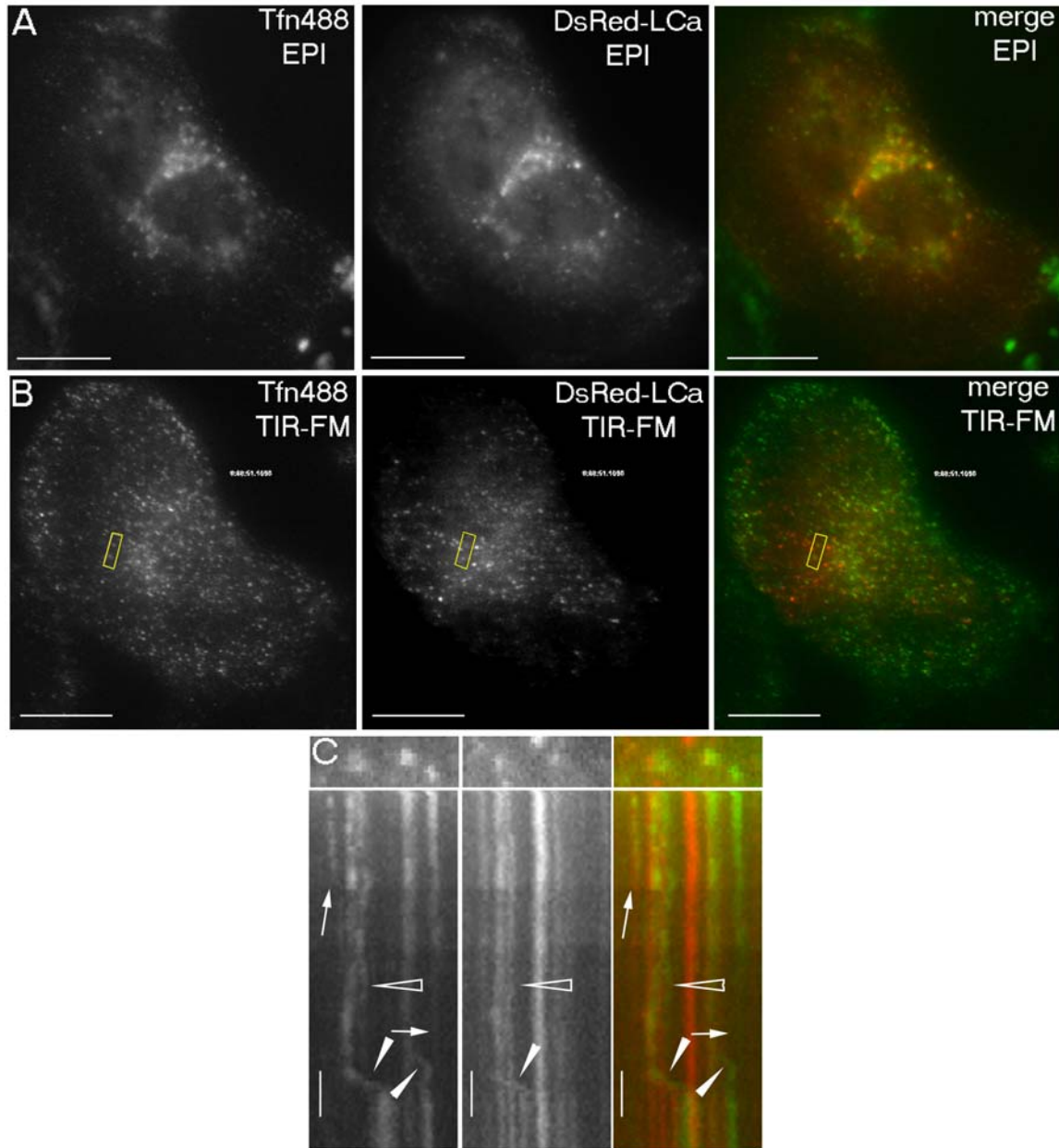
Figure 2-8 Simultaneous visualization of clathrin and Tfn488 containing structures

CV-1 cells transfected with DsRed-LCa (middle panels) and pulsed with Tfn488 (left panels) were imaged by TIR-FM. Epifluorescent images (A) clearly show prominent accumulation of transferrin in juxtanuclear recycling endosomes and clathrin in the TGN region. The TIR-FM images (B) reveal a different population of structures also concentrated in the perinuclear region. The regions shown in the kymographs (C) are boxed in the TIR-FM image. Dynamics are indicated with the same symbols used in Figure 2-1. Notice in C that the structure showing long distance motion is yellow prior to motion and then separates into green and red structures moving along the same tract. The scale bar represents 10 μm (A and B) or 20 s (C).

2.3.7 Long Distance Motion and Enlarged Endosomal Structures in Cuboidal Cells

CV-1 cells and fibroblasts are extremely flat cells. Thin section EM analysis of CV-1 cells reveals a distance of ~150 nm from membrane to membrane at the extreme periphery, with a similar distance between the nucleus and the basal plasma membrane (data not shown). One plausible reason for observing endosomes in these cells by TIR-FM is that these structures cannot be accommodated elsewhere in these cultured cells. Alternatively, a fraction of endosomes may generally traffic within ~200 nm of the plasma membrane. To distinguish between these possibilities, GFP-LCa dynamics and cargo uptake were examined in the cuboidal, epithelial-like A431 carcinoma cell line. GFP-LCa dynamics include the complete range of motion observed in CV-1 cells (Figure 2-9, A and C). Again, the 0.6-1-µm structures are present, although their abundance is similar to the peripheral abundance of these structures in fibroblasts (8% in A431 cells compared with 7% in fibroblasts). This supports the idea that there is a population of endosomes generally within 200 nm of the plasma membrane, although this population is increased because of cytoplasmic space constraints in CV-1 cells and fibroblasts.

A431 cells express millions rather than thousands of EGF receptors, so I examined the uptake of fluorescent EGF (EGF488) in addition to Tfn488 dynamics. Both EGF488 and Tfn488 initially label only the periphery because A431 cells are tightly associated with the basal glass surface and apparently do not freely allow diffusion of these molecules below the cell. As time progresses, Tfn488 and EGF488 are internalized and penetrate deeper into the cell, where they either disappear or merge into larger structures (Figure 2-9, B and D, and data not shown). As in

CV-1 cells, the larger structures form as time progresses. The peripheral fluorescent EGF488 is very dynamic because the plasma membrane undergoes extensive actin-dependent ruffling upon EGF stimulation (Chinkers et al., 1979). Together, these experiments show that the population of surface proximal endosomes is not wholly because of cellular geometry constraints but rather a feature of several morphologically distinct cultured cell types.
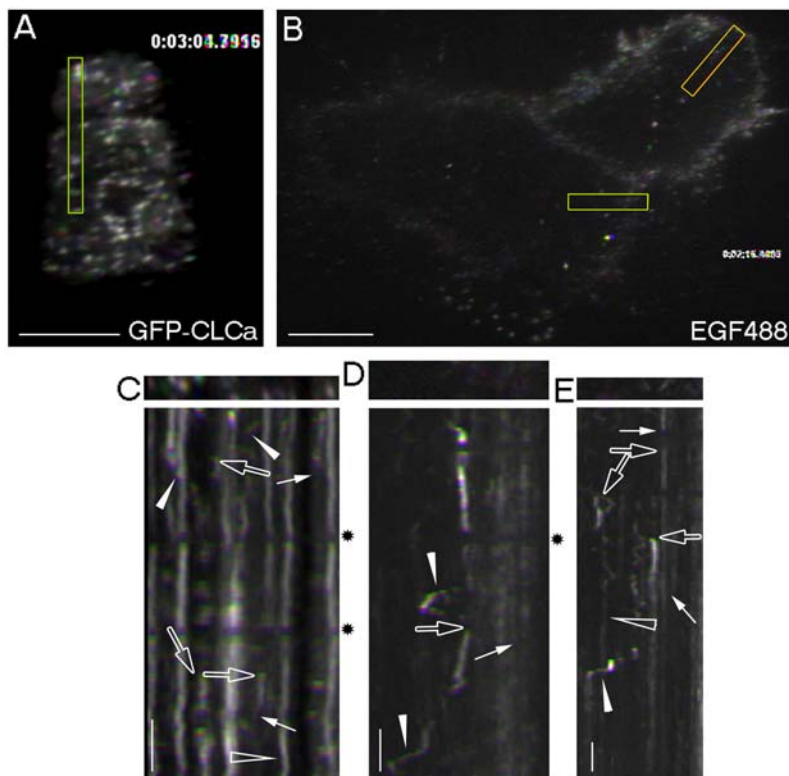
Figure 2-9 Epithelial-like cells also demonstrate long distance motion

A431 cells were transfected with GFP-LCa as described (A and C) or serum starved for 1 h followed by addition of EGF488 (B, D, and E) and imaged by TIR-FM. The boxed regions in the TIR-FM images (A and B) are shown by the kymographs (C-E). In these cuboidal cells, clathrin and endocytic ligands display a similar range of motion to the flatter fibroblast or CV-1 cells. Dynamics are indicated with the same symbols used in Figure 2-1. The scale bar represents 5 µm (A and B) or 20 s (C-E).

2.4   DISCUSSION

The diversity of intracellular clathrin-coated structures now known to exist makes it difficult to definitively assign fluorescent clathrin signals to one particular subcellular site without additional compartmental information. In other studies utilizing TIR-FM, the conclusion that the observed fluorescent structures are confined to the plasma membrane is based upon idealized optical properties of the illumination system, with a typical decay depth of 70-110 nm (Merrifield et al., 2002; Rappoport and Simon, 2003; Rappoport et al., 2003a; Rappoport et al., 2003b). However, at this depth, the evanescent field still maintains 37% of the maximal intensity. At three decay depths from the interface, the signal diminishes to 5% of maximal intensity, so the excitatory field approaches extinction at 200-300 nm into the cell. Empirical measurements here concur and indicate that under these TIR-FM imaging conditions, molecules 150-200 nm from the interface are readily detected. I believe that this expands the number and type of structures that must be considered when interpreting the TIR-FM data sets. In fact, intracellular actin rockets propelling endocytic vesicles (Merrifield et al., 1999), fluorescently tagged secretory vesicles (Han et al., 1999; Steyer et al., 1997; Toomre et al., 2000), labeled endosomes (Lampson et al., 2001), and lysosomes (Jaiswal et al., 2002) have all previously been observed with TIR-FM by others.

The data showing that AP-2 and several alternate adaptors generally do not move in a rapid, directed fashion parallel to the plane of the membrane agree well with an independent, recently published TIR-FM study (Rappoport et al., 2003a). The absence of adaptor subunits

from both the disappearing and motile clathrin populations prompted the suggestion that these coat components dissociate before the internalization phase begins (Rappoport et al., 2003a). Because experiments combining TIR-FM with wide field imaging show that clathrin-positive puncta persist in the epifluorescence images after departing from the TIR-FM field (Merrifield et al., 2002), one possibility is that AP-2 is disassembled/released before the outermost clathrin lattice, which accompanies the transport vesicle (Rappoport et al., 2003a). I find this hypothesis unlikely for a number of reasons. First, there is good evidence for enrichment of adaptor proteins like AP-2, AP180/CALM, and HIP1/Hip1R in preparations of biochemically purified clathrin-coated vesicles. Second, clathrin trimers alone have no affinity for biological membranes and require AP-2, alternate adaptors, or accessory proteins like amphiphysin to be targeted to the cell surface (Ford et al., 2001; Lafer, 2002; Mishra et al., 2001; Mishra et al., 2002a). Third, although it is now known that AP-2 is not absolutely necessary for the endocytic uptake of EGF or LDL (Conner and Schmid, 2003a; Motley et al., 2003), alternate clathrin- and cargo-binding endocytic adaptors like epsin, Dab2, and ARH must promote clathrin coat assembly in the absence of AP-2 (Traub, 2003). Yet I do not find that Dab2, ARH, or the endocytic protein Hip1R display long range lateral mobility, apparently eliminating these proteins as potential linkers for membrane-associated clathrin. Fourth, the available data indicates that the kinesin family microtubule motor KIF13A binds physically to AP-1 (Nakagawa et al., 2000) and there is no evidence currently for binary associations between clathrin and motor proteins that I am aware of. In my TIR-FM data sets, I see abrupt disappearance of both AP-2 subunits and clathrin indicating that AP-2 and clathrin bud from the plasma membrane assembled together in a polyhedral clathrin coat.

I also find that the minor, highly motile clathrin population contains the β2 subunit of AP-2, but the augmented coincidence of this subunit with DsRed-clathrin at higher expression levels suggests that the β2 subunit is being incorporated into the AP-1 heterotetramer. Together with my results showing endosomal movement in the TIR-FM field and the 150-200 nm depth of the excitatory field, my current interpretation of the data is that the fluorescent clathrin population associated with long-range motion represents AP-1-positive structures of endosomal origin. Is there any evidence to support a role for AP-1 and clathrin in endosomal sorting? In polarized Madin-Darby canine kidney cells, AP-1, identified by the unique γ subunit, is found associated with a population of pleiomorphic clathrin-coated endocytic tubules that are responsible for proper sorting of the transferrin receptor to the basolateral surface (Futter et al., 1998). AP-1 is also present on transferrin-positive endosomes in non-polarized Madin-Darby canine kidney cells (Futter et al., 1998), as well as in peripheral structures in HeLa cells expressing a GFP-tagged AP-1 γ subunit and pulsed with fluorescent transferrin (Waguri et al., 2003). Extensively tubulated transferrin-positive endosomes with numerous clathrin-coated buds are also present in A431 and HeLa cells (Stoorvogel et al., 1996; van Dam and Stoorvogel, 2002). The assembly of clathrin on these structures is sensitive to brefeldin A (Futter et al., 1998; van Dam and Stoorvogel, 2002), which hints at AP-1 involvement. In all cases, these coated structures are suggested to play a role in recycling by governing the formation of vesicles returning apo-transferrin·transferrin receptor complexes back to the cell surface. Although I do not observe extensive coincidence between the motile DsRed-LCa and Tfn488 signals in these TIR-FM studies, this may be because the amount of labeled transferrin sorted into individual coated transport intermediates could be below the limit of detection by fluorescence. It is also important to note that because the transferrin receptor recycles at a rate equivalent to lipid probes (Mayor et

al., 1993), receptor recycling is not absolutely dependent on adaptor-based sorting, and parallel routes for return to the plasma membrane exist. Consequently, not all of the endocytosed transferrin is expected to be sorted into clathrin-coated structures. Furthermore, in cells expressing a dominant-negative clathrin hub, normally peripheral early endosomes collapse to a perinuclear location but, nevertheless, the kinetics of transferrin recycling are not altered significantly (Bennett et al., 2001). Endosomal clathrin is thus proposed to regulate the intracellular positioning and organization of the early endosome compartment (Bennett et al., 2001).

Based on my observations, and those of others (Blanpied et al., 2002; Gaidarov et al., 1999b; Merrifield et al., 2002), the appearance and disappearance of clathrin-positive puncta is almost certainly because of the physical formation and release of coated vesicles from the plasma membrane, because both clathrin and adaptors show a parallel behavior. What is surprising is that adaptors appear less motile than might be expected. The majority of the clathrin and AP-2-positive structures at the periphery of the cell appear relatively static and long-lived. The local gyrational motion of these coat components probably reflects the extent of free diffusion of the coated pits along the membrane. Indeed, it has been previously shown that local motion increases in the presence of latrunculin B, an actin depolymerizing agent (Gaidarov et al., 1999b). Many structures persist for several minutes without showing dramatic alterations in either fluorescence intensity or position. These observations are consistent with the published wide field (Gaidarov et al., 1999b) and confocal (Blanpied et al., 2002) data, and with live cell fluorescence recovery after photobleaching experiments with both GFP-tagged LCa and the AP-2 α subunit (Wu et al., 2001; Wu et al., 2003). In these studies, a large fraction of peripheral fluorescent clathrin or AP-2

remains in the same relative position over a 2-min period. The dynamic properties of clathrin LCa-GFP transfected into primary hippocampal neurons after *in vitro* culture for 20-40 days (Blanpied et al., 2002; Blanpied et al., 2003) are also remarkably similar to my observations in non-neuronal cells. The relatively static structures found in the older cultured neurons prompted the designation of a "stable endocytic zone" (Blanpied et al., 2002) that is clearly endocytically active despite the apparently limited clathrin dynamics (Blanpied et al., 2002; Blanpied et al., 2003). In this system, clathrin LCa-GFP overexpressed in younger neurons, cultured for fewer than 10 days, is considerably more dynamic (Blanpied et al., 2002). This significant finding rules out that the observed static behavior is a consequence of the transfection procedure and suggests instead that the dynamic properties of surface clathrin lattices may depend on cell type, culture conditions, and physiology.

The dynamic properties of fluorescent AP-2 and clathrin over time are also similar to the behavior of an assembled, non-clathrin coat, the COPI coatomer coat. In ε-COP-GFP image sequences covering about 60 s, many COPI-coated structures near the Golgi region of the cell remain roughly static with relatively little fluorescent intensity fluctuation (Presley et al., 2002). However, I do find that about 20% of the clathrin structures appear and disappear per min, suggesting that all of the plasma membrane clathrin could turn over in ~5 min, roughly consistent with the time required for receptor internalization. I have considered the possibility that the GFP tag interferes with normal functioning of the fusion proteins, altering the kinetics observed. However, the various tagged proteins I use have the GFP at different positions and the relatively static behavior of the AP-2 α subunit, Dab2, ARH, and Hip1R suggests a common dynamic. The fact that the β2-YFP moves into the highly mobile fraction in higher overexpressors also argues

for two distinct populations of clathrin. Studies on the internalization of fluorescent influenza virus, which is internalized via clathrin-mediated endocytosis, reveal three stages during viral entry and transport (Lakadamyali et al., 2003). The first stage, which corresponds to endocytic uptake and local actin-dependent movement, takes the longest, about 6 of the ~8 min required for viral fusion after initial binding to the cell surface (Lakadamyali et al., 2003). The second stage is rapid, microtubule-dependent transport of the virus to the perinuclear region preceding the third stage fusion event (Lakadamyali et al., 2003). Thus, the overall kinetics and intracellular trajectory of virus internalization mirrors the behavior I observe for clathrin.

3.0   THE AP-2 β2 APPENDAGE SCAFFOLDS ALTERNATE CARGO ENDOCYTOSIS

3.1   ABSTRACT

The independently-folded appendages of the large α and β2 subunits of the endocytic AP-2 adaptor complex coordinate proper assembly of endocytic accessory proteins during clathrin-mediated endocytosis. Structural studies reveal that the appendage domain of the β2 subunit contains a common, privileged binding site for β-arrestin or ARH. To determine the importance of this interaction surface in living cells, I used siRNA-based gene silencing. The effect of extinguishing β2 subunit expression on the internalization of transferrin is considerably weaker than AP-2 α subunit knockdown. I show this mild sorting defect is due to fortuitous substitution of the β2 chain with the closely related endogenous β1 subunit of the AP-1 adaptor complex. Simultaneous silencing of both β1- and β2 subunit transcripts recapitulates the strong α subunit RNAi phenotype, and results in loss of ARH from endocytic clathrin coats. Transient expression of an RNAi-resistant β2-YFP in the β1+β2-silenced background rescues cellular AP-2 levels, robust transferrin internalization, and ARH colocalization with cell surface clathrin. Transfection of truncated β2-YFP, lacking both hinge and appendage, also restores AP-2 levels and surface transferrin clustering, but fails to rescue ARH clathrin coat localization. A β2-YFP with a

disrupted ARH binding surface likewise fails to restore ARH colocalization with clathrin, demonstrating the importance of this contact site for precise deposition of ARH at clathrin assembly zones. Thus, functional rescue of AP-2 with an RNAi-resistant fluorescently-tagged subunit shows that ARH, and likely β-arrestin, depend on the privileged β2 appendage site for proper recruitment to clathrin bud sites.

3.2   INTRODUCTION

Clathrin-mediated endocytosis is a process through which many nutrient receptors, signaling receptors, ion channels, and even pathogens, are internalized from the cell surface and delivered to endosomes. This process requires the fine coordination of cargo selection, membrane invagination, and actin dynamics (Conner and Schmid, 2003b; Edeling et al., 2006; Kaksonen et al., 2006; Robinson, 2004). At the plasma membrane, these diverse processes are managed, in part, by the AP-2 heterotetramer. The brick-like AP-2 core is composed of a small, structural σ2 subunit, the cargo selective μ2 subunit, along with the N-terminal trunks of two large chains, the β2- and (AP-2-specific) α subunits (Collins et al., 2002). Projecting off both α- and β2 subunit trunks, via flexible hinges, are bilobal appendages that contain binding sites for clathrin and numerous other endocytic proteins (Edeling et al., 2006; Robinson, 2004).

The four assembled subunits permit AP-2 to coordinate various aspects of clathrin-coat formation. The plasma membrane-enriched lipid phosphatidylinositol-4,5-bisphosphate (PtdIns(4,5)P$_2$) is engaged via both the α- and μ2 subunits, YXXØ-type sorting signals (as found in the transferrin receptor) are bound directly by the μ2 subunit, and assembly protein and clathrin associations are established through the α- and β2 appendages (Honing et al., 2005; Keen, 1987; Ohno et al., 1995; Traub, 2005). The α appendage has two interaction surfaces, one each upon the platform and sandwich subdomains. The platform site can bind to DPW, DPF and FXDXF motifs (Brett et al., 2002; Praefcke et al., 2004), while the sandwich site engages the WXXF motif (Mishra et al., 2004; Praefcke et al., 2004; Ritter et al., 2004). These short interaction motifs are typically positioned within tracts of intrinsically unstructured polypeptide, and proteins bearing the former class of motifs are typically involved in cargo selection and lattice polymerization. Proteins bearing the latter set generally include regulatory proteins such as adaptor-associated kinase 1 (AAK1), cyclin G-dependent kinase (GAK) and the phosphoinositide polyphosphatase synaptojanin 1 (Jha et al., 2004; Praefcke et al., 2004; Walther et al., 2004). Some of the regulatory proteins, like synaptojanin 1, also contain platform binding sites, potentially allowing them to compete previously bound clathrin-associated sorting proteins (CLASPs) off AP-2 (Mishra et al., 2004; Praefcke et al., 2004). Thus, the α appendage regulates the temporal organization of the developing clathrin lattice through binding sites that permit the recruitment of first lattice assembly and cargo selective factors, followed by regulatory proteins that control bud formation and likely promote release of proteins from AP-2 once their role in endocytosis is complete.

Similar to the α appendage, the β2 appendage also contains two interaction surfaces, one analogous to the β2 appendage-platform site, and one positioned on the opposite side from the cognate α appendage sandwich site (Edeling et al., 2006; Schmid et al., 2006). The contact sites on the β2 appendage do not appear to control accessory proteins in precisely the same manner as the hierarchical α appendage-binding sites. Biochemical studies suggest the β2 appendage-platform site is largely dedicated to CLASPs, such as the β-arrestins, which concentrate G protein-coupled receptors (GPCRs), the autosomal recessive hypercholesterolemia (ARH) protein, which decodes the FXNPXY-type sorting signal, and epsin 1, which recognizes poly/multiubiquitinated cargo (Barriere et al., 2006; Hawryluk et al., 2006; He et al., 2002; Kim and Benovic, 2002; Laporte et al., 2002; Milano et al., 2002; Mishra et al., 2002b). These discrete classes of cargo internalization signal do not bind directly to AP-2. The β2 appendage-sandwich site, along with a type I clathrin box in the β2-hinge, allows AP-2 to polymerize clathrin and regulate eps15 positioning within the assembling lattice (Cupers et al., 1998; Edeling et al., 2006; Owen et al., 2000). Thus, the β2 subunit contains functionally distinct binding sites that simultaneously allow privileged access of certain CLASPs to the lattice along with clathrin recruitment. Overall, AP-2 acts as a master adaptor, binding to the plasma membrane, sorting YXXØ-bearing cargo and coordinating clathrin vesicle formation while simultaneously providing access for alternative types of cargo by scaffolding CLASPs. Accordingly, targeted gene disruption or mutation of AP-2 μ2- or α- subunit genes is homozygous lethal in mice (Mitsunari et al., 2005), *Drosophila* (Gonzalez-Gaitan and Jackle, 1997) and C. elegans (Shim and Lee, 2000).

Inherited deficiency of one CLASP in humans, ARH, results in a pathological hypercholesterolemia similar to, but less severe than, familial hypercholesterolemia (Eden et al., 2001; Garcia et al., 2001). Structurally, ARH contains a phosphotyrosine binding (PTB) domain that binds simultaneously to both FXNPXY peptides and PtdIns(4,5)P$_2$, and an unstructured C-terminus containing a type I clathrin box and the β2 appendage-binding sequence (Eden et al., 2002; He et al., 2002; Mishra et al., 2002b). Functionally, it may play an analogous role to the β-arrestins, which utilize a related, helical FXX[FL]XXXRX$_{1-2}$[DE]$_n$ β2-binding sequence to usher GPCRs to preformed clathrin coats (Edeling et al., 2006; Kim and Benovic, 2002; Laporte et al., 2000; Milano et al., 2002). ARH may likewise use primarily the β2 appendage-binding site, rather than the clathrin box, to shuttle or retain LDL receptors in clathrin structures.

To test ARH dependence on β2-appendage binding, I replaced endogenous AP-2 β2 subunits with various β2-YFP mutants using RNAi, which has not been previously described. When characterizing the β2 subunit knockdown necessary for this approach, I found that simultaneous depletion of the β1 subunit from the related *trans*-Golgi network (TGN)/endosome-localized AP-1 complex is also necessary, because, otherwise, the highly related, endogenous β1 subunit compensates for β2 subunit RNAi. In the context of a β1+β2 subunit knockdown, the β2 subunit trunk is sufficient to rescue known AP-2 knockdown phenotypes (Hinrichsen et al., 2003; Motley et al., 2003), clustering transferrin in clathrin coats and restoring cellular AP-2 levels, though ARH surface localization is clearly disrupted. Rescue of the β1+β2 subunit knockdown with a full length β2-YFP bearing a point mutation in the β2-platform subdomain also fails to rescue ARH localization to clathrin structures, though both wild

type β2-YFP or β2-YFP lacking clathrin binding sites rescued ARH localization to clathrin puncta. This suggests that AP-2 is vital both as the YXXØ-selective CLASP and as a scaffold controlling endocytic protein recruitment to clathrin-coated pits during endocytosis.

3.3   RESULTS

3.3.1   Gene silencing of the AP-2 α subunit

In HeLa SS6 cells, I find transfection of siRNA duplexes targeting the AP-2 α subunit mRNA reduces the protein level of all four adaptor subunits >75% within 48 hours (Figure 3-1A), in very good agreement with previous results (Hinrichsen et al., 2003; Motley et al., 2003). Depletion of AP-2 is also seen morphologically, as a dramatic decrease in the intensity of AP-2-positive puncta compared with the control cells (Figure 3-1B). It is known that AP-2 knockdown reduces the amount of clathrin positioned at the plasma membrane but not that recruited to other structures or total cytoplasmic amounts (Hinrichsen et al., 2003; Motley et al., 2003) so, to selectively visualize clathrin at plasma membrane, I briefly treated cells with brefeldin A to dissociate clathrin from internal membrane structures, and then rapidly permeabilized the cells before fixation (Fig, 3-1C & D). In mock-transfected cells, this treatment effectively eliminates TGN, endosomal and cytosolic clathrin, without perturbing the plasma membrane associated

clathrin pool. No AP-1 γ subunit staining is observed, and the remaining β subunit signal is fully sensitive to α subunit RNAi (Figure 3-1C). Although the total amount of clathrin recruited to the plasma membrane is greatly diminished upon AP-2 α subunit RNAi (Figure 3-1D), in agreement with others (Harasaki et al., 2005), I do not observe that the total number of surface puncta decreases ~10-fold as originally reported (Hinrichsen et al., 2003; Motley et al., 2003), possibly because AP-2 foci are not completely eliminated (Figure 3-1B).

Extinguishing AP-2 also abrogates the clustering of surface receptors bearing a YXXØ internalization signal, exemplified by the transferrin receptor, at clathrin-positive puncta. Unlike the mock-treated cells, transferrin marks a population of diffuse receptors on the surface of AP-2-deficient cells (Figure 3-1E). Other receptors, like the LDL receptor, that bear the FXNPXY-type internalization signal decoded by the CLASPs ARH and Dab2, can internalize in an AP-2-independent manner (Eden et al., 2002; Garuti et al., 2005; Maurer and Cooper, 2006) (see also chapter 4). Nonetheless, because Dab2 and ARH each bind physically to both AP-2 and clathrin, in mock-treated cells, the LDL receptor and transferrin congregate in common surface structures (Figure 3-1E), which contain clathrin and AP-2 (see chapter 4). Yet, when AP-2 complexes are extinguished, only the surface distribution of the transferrin receptor, and not the LDL receptor, alters dramatically (Figure 3-1E). A consequence of this dispersion of the transferrin receptor is that transferrin is very poorly internalized (Figure 3-1F). To verify that the internalization defect is general to proteins bearing the YXXØ signal, I examined the surface distributions of the CI-MPR and LAMP-1. The trafficking trajectory of these transmembrane proteins takes them through the plasma membrane relatively infrequently and normally the proteins are concentrated, at steady state, in multivesicular endosomes/TGN and lysosomes, respectively. If delivered to the cell surface, both are retrieved via clathrin-mediated endocytosis (Dahms and Hancock, 2002). In
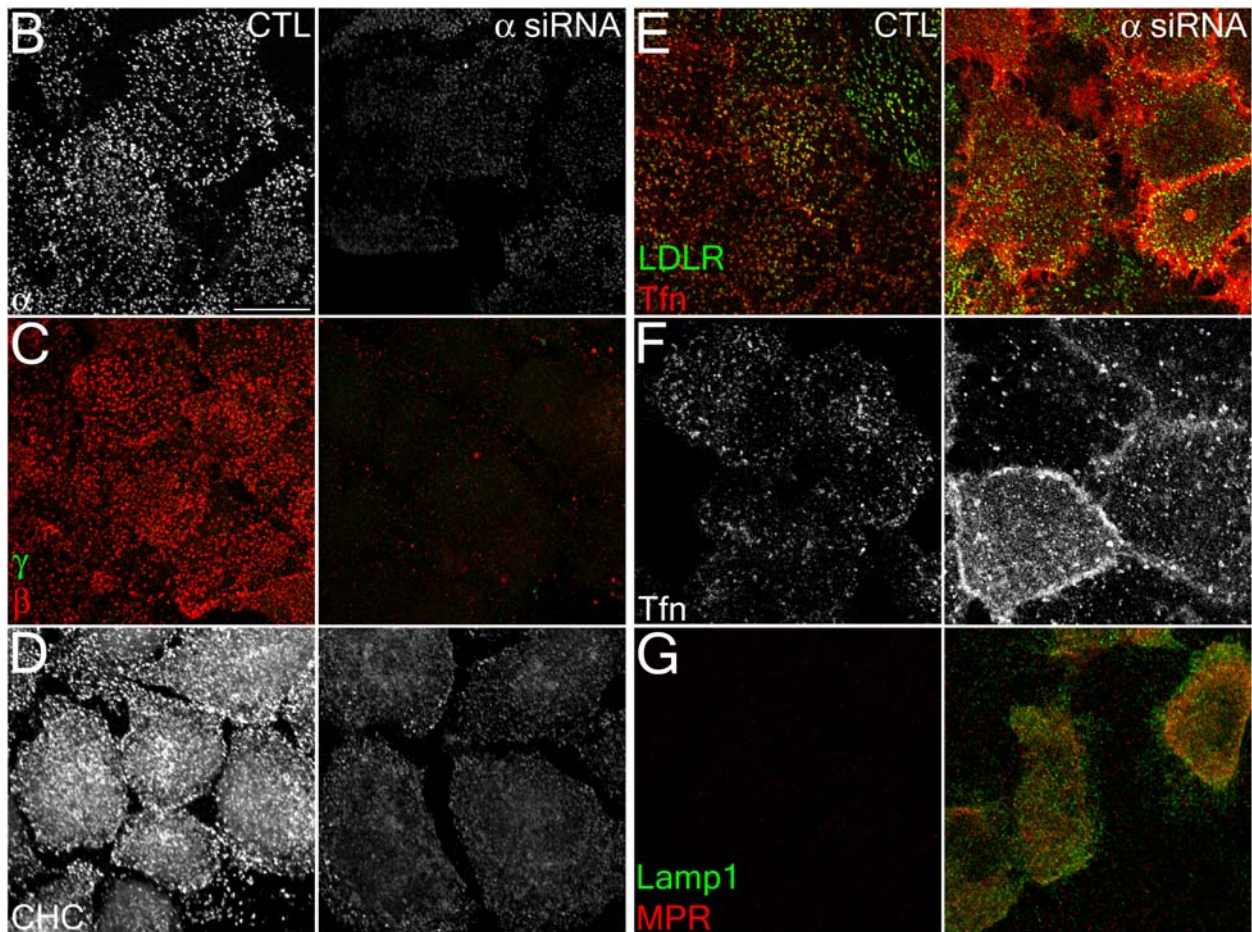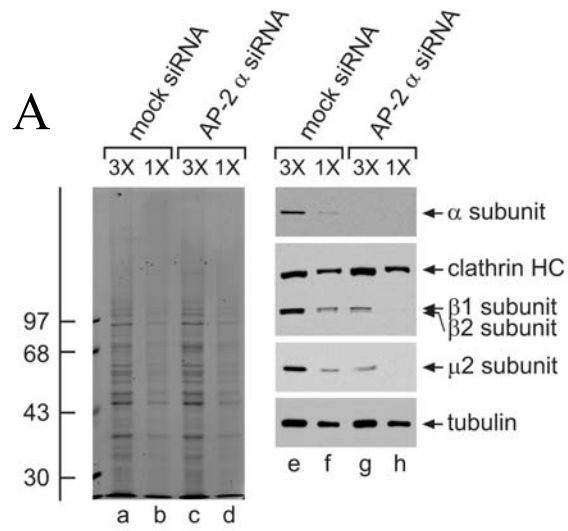
Figure 3-1 siRNA gene silencing of the AP-2 α subunit

Figure 3-1 siRNA gene silencing of the AP-2 α subunit

(A) Lysates of HeLa cells untreated or treated with AP-2 α subunit siRNA were resolved by SDS-PAGE and either Coomassie stained (lanes a-d) or transferred to nitrocellulose (lanes e-g). Sections of the blots were probed with the Transduction Laboratories anti-AP-2 α subunit mAb, anti-β1-/β2 subunit antibody 100/1, anti-clathrin heavy chain antibody TD.1, or anti-AP-2 μ2 antiserum and relevant portions displayed. The position of molecular mass standards (in kDa) are indicated on the left. (B)-(D) HeLa cells untreated (left panel) or treated with AP-2 α subunit siRNA (right panel) were treated with 10 μg/mL brefeldin A for 15 minutes, permeabilized on ice for 1 minute prior to fixation and prepared for immunofluorescence using the anti-AP-2 α subunit mAb AP.6 (B), anti-AP-1 γ subunit mAb (C, green), anti-β1-/β2 subunit antibody GD/2 (C, red), or anti-clathrin heavy chain mAb X22 (D). (E) – (G) HeLa cells untreated (left panel) or treated with AP-2 α subunit siRNA (right panel) were incubated on ice for one hour with either anti-LDL receptor C7 mAb (E, green), Tfn568 (E, red and F), anti-Lamp1 mAb (G, green) or anti-MPR antibody (G, red) and fixed (E and G) or washed and warmed to 37° C for 15 minutes and fixed (F) followed by indirect immunofluorescence. The scale bar represents 10 μm.

the context of α subunit knockdown, and consistent with both the absolute dependence of the YXXØ signal on AP-2 for sorting into clathrin-coated vesicles and previous observations (Harasaki et al., 2005; Janvier and Bonifacino, 2005), a surface population of both the CI-MPR and LAMP-1 becomes readily detectable as they stagnate on the surface (Figure 3-1G).

3.3.2 Gene silencing of the AP-2 β2 subunit does not inactivate AP-2

Next, as a prelude to evaluating the function of the β2 subunit hinge and appendage through rescue of AP-2 RNAi, I selectively knocked down the AP-2 β2 subunit in HeLa cells. Although the β2 subunit polypeptide is very effectively diminished (Huang et al., 2004), in marked contrast to the α RNAi, the abundance of other AP-2 subunits is mildly affected (Figure 3-2A). A comparatively weak effect on AP-2 levels is also apparent by immunofluorescence. The levels of the α and, surprisingly, β subunits of AP-2 in the context of a β2 subunit knockdown are

reduced from normal levels, but clearly not to the extent observed in an α subunit knockdown (Figure 3-2B). Likewise, the other phenotypes characteristic of α subunit knockdown are not as penetrant when using β2 subunit siRNA duplexes (Figure 3-2C-E). The intensity of clathrin within punctate structures is intermediate between control and α subunit knockdown, which is likely due to the presence of functional AP-2 complexes in the cell (Figure 3-2C). Also, AP-2-dependent cargo, the CI-MPR and LAMP-1, do not accumulate appreciably at the cell surface (Figure 3-2D) and, although the transferrin distribution is more diffuse on the surface than in mock-transfected cells, it is also present in numerous puncta on the plasma membrane (Figure 3-2E). I conclude, therefore, that AP-2 β2 subunit knockdown produces a milder variant of the α- or μ2 subunit RNAi phenotypes, due to incomplete ablation of AP-2.

3.3.3   The AP-1 β1 subunit is incorporated into AP-2 in the absence of a β2 subunit

A clue to the biochemical basis for the milder β2 RNAi phenotype comes from the surface β subunit signal in cells lacking the β2 subunit (Figure 3-2B). The β1 and β2 subunits of AP-1 and AP-2 are ~85% identical, in contrast to the other three subunits of the heterotetramers, which display less than 50% identity (Figure 3-3A). In fact, *Drosophila melanogaster* has only a single β subunit that is incorporated into both AP-1 and AP-2 (Camidge and Pearse, 1994). All available antibodies raised against the vertebrate β subunits recognize both β1 and β2 subunits, though these subunits can be resolved by SDS-PAGE (Page and Robinson, 1995; Sorkin et al., 1995; Traub et al., 1996). Thus, the fluorescent signal observed in β2 subunit-knockdown cells may be due to the β1 subunit incorporated into AP-2. To test this hypothesis, I treated HeLa SS6
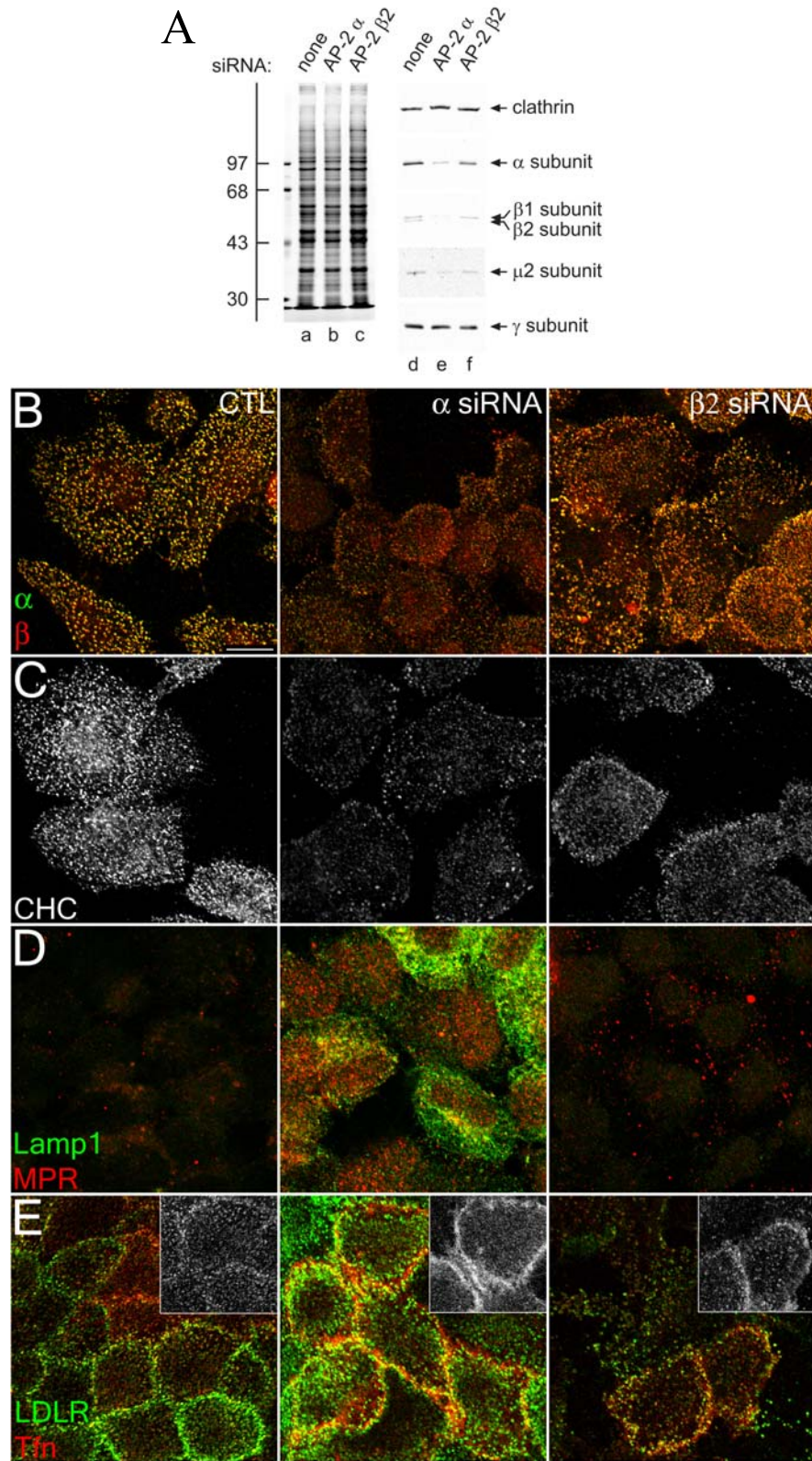
Figure 3-2 Knockdown of AP-2 β2 subunit

Figure 3-2 Knockdown of AP-2 β2 subunit

(A) Lysates of HeLa cells untreated or treated with either AP-2 α or β2 subunit siRNA were resolved by SDS-PAGE and either Coomassie stained (lanes a-c) or transferred to nitrocellulose (lanes d-f). Sections of the blots were probed with the Transduction Laboratories anti-AP-2 α subunit mAb, anti-β1-/β2 subunit antibody 100/1, anti-clathrin heavy chain antibody TD.1, anti-AP-1 μ1 subunit antibody RY1, and anti-AP-2 μ2 antiserum and relevant portions displayed. The position of molecular mass standards (in kDa) are indicated on the left. (B and C) HeLa cells untreated (left panel) or treated with AP-2 α- (center panel) or β2 subunit siRNA (right panel) were treated with 10 μg/mL brefeldin A for 15 minutes, permeabilized on ice for 1 minute prior to fixation and prepared for immunofluorescence using the anti-AP-2 α subunit mAb AP.6 (B, green), anti-β1-/β2 subunit antibody GD/2 (B, red), or anti-clathrin heavy chain mAb X22 (C). (D and E) HeLa cells untreated (left panel) or treated with AP-2 α- (center panel) or β2 subunit siRNA (right panel) were incubated on ice for one hour with either anti-Lamp1 mAb (D, green), anti-MPR antibody (D, red), anti-LDL receptor C7 mAb (E, green), or Tfn568 (E, red), fixed and prepared for indirect immunofluorescence. The inset in (E) shows Tfn568 immunofluorescence from each sample. The scale bar represents 10 μm.
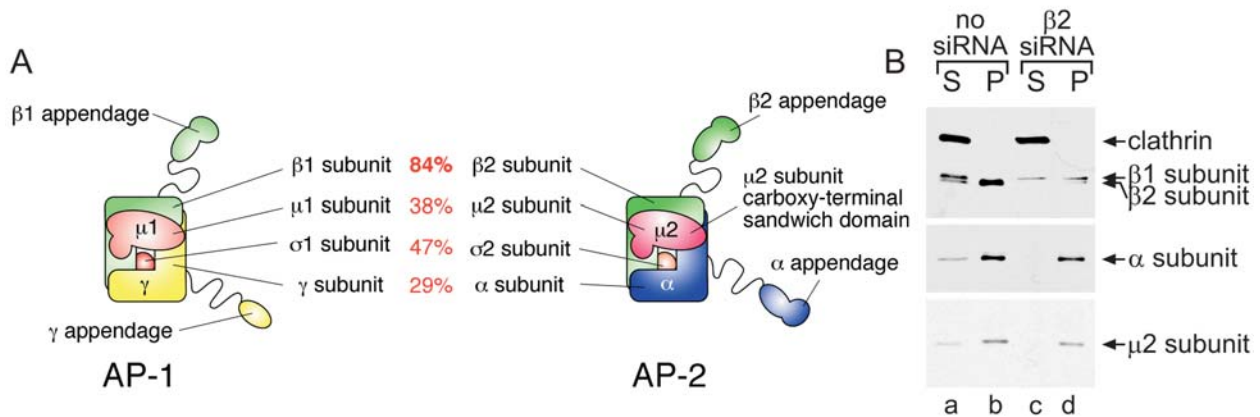
Figure 3-3 β1 subunit rescues β2 subunit knockdown of AP-2

(A) Schematic of AP-1 and AP-2 indicating homology between subunits. (B) β1 subunit rescues β2 subunit knockdown of AP-2. HeLa cell lysates either untreated or treated with β2 siRNA were prepared, immunoprecipitated as described in the methods using the anti-AP-2 α subunit mAb AP.6 and the supernatant and immunoprecipitate for both control and β2 RNAi resolved by SDS-PAGE and transferred to nitrocellulose. The relevant portions of the blots were probed with the Transduction Laboratories anti-AP-2 α subunit mAb, anti-β1-/β2 subunit antibody 100/1, anti-clathrin heavy chain antibody TD.1, anti-AP-2 μ2 antiserum or anti-tubulin mAb E7 as indicated.

cells with or without β2 subunit siRNA, and then immunoprecipitated AP-2 with an α subunit-specific mAb. In mock-transfected cells, the majority of AP-2 is recovered in the immunoprecipitate, and the principal β subunit incorporated into AP-2 is the faster migrating β2 chain (Figure 3-3B). However, when the β2 subunit is depleted, this smaller form disappears almost completely, and the majority of the β subunit now assembled into AP-2 is the larger β1 subunit (Figure 3-3B). Therefore, I conclude that, because of the high degree of homology, the β1 subunit is promiscuously incorporated into AP-2 when cellular β2 subunit levels are low, and that this misassembly preserves the functional AP-2 heterotetramer. Interestingly, this substitution phenomenon occurs naturally to a limited extent, as incorporation of endogenous β2 into AP-1 in brain and β1 into AP-2 in liver has been documented (Sorkin et al., 1995; Traub et al., 1996).

3.3.4 Simultaneous knockdown of β1 and β2 subunits functionally ablates AP-2

Since gene silencing of the β2 subunit alone is insufficient to reduce AP-2 levels and disrupt sorting, an siRNA duplex to extinguish the β1 subunit was designed. Transfection of this duplex selectively targets the β1 subunit, and together the β1+β2 subunit siRNAs silence both AP-1 and AP-2 (Figure 3-4A). Furthermore, the combined β1+β2 RNAi reproduces the α subunit knockdown phenotype (Figure 3-4B-D). Morphologically, the level of the AP-2 α subunit is decreased by β1+β2 subunit RNAi similar to that observed with an α subunit knockdown (Figure 3-4B), and, the amount of clathrin deposited on the plasma membrane is reduced to that observed with the α subunit RNAi (Figure 3-4C). Most important, transferrin receptor

internalization is strongly blocked and fluorescent transferrin accumulates in a diffuse pattern on the cell surface (Figure 3-4D). Thus, simultaneous knockdown of both β1 and β2 subunits functionally incapacitates AP-2 and phenocopies AP-2 α- or μ2 subunit ablation.

3.3.5 Functional rescue of AP-2 with β2-YFP

To begin to probe the function of the β2 subunit *in vivo* then, an siRNA-resistant β2 subunit fused at the carboxyl terminus to YFP (β2-YFP) was ectopically expressed in HeLa SS6 cells also transfected with the β1+β2 subunit-silencing duplexes. The transiently expressed β2 construct clearly rescues AP-2 function successfully, as steady-state protein levels of both the α and μ2 subunits in β2-YFP-transfected cells are stabilized compared with the levels in knocked-down cell populations not transfected with the β2-YFP (Figure 3-5A). β2-YFP targets to α subunit puncta in control cells and restores normal clustering of surface transferrin localization to coated pits in β1+β2 subunit knockdown cells (Figure 3-5B, D). Only the transfected cells have normal AP-2 levels, as seen by immunofluorescence, and permit efficient transferrin internalization (Figure 3-5F). Importantly, these effects are not the result of reduced transfection efficiency due to the simultaneous addition of β2-YFP plasmid DNA during siRNA treatment, as adding similar amounts of control GFP plasmid DNA restores neither AP-2 levels nor the punctate surface transferrin localization (Figure 3-6). Therefore, the β2-YFP appears to functionally rescue AP-2 in β1+β2 subunit knocked-down cells.
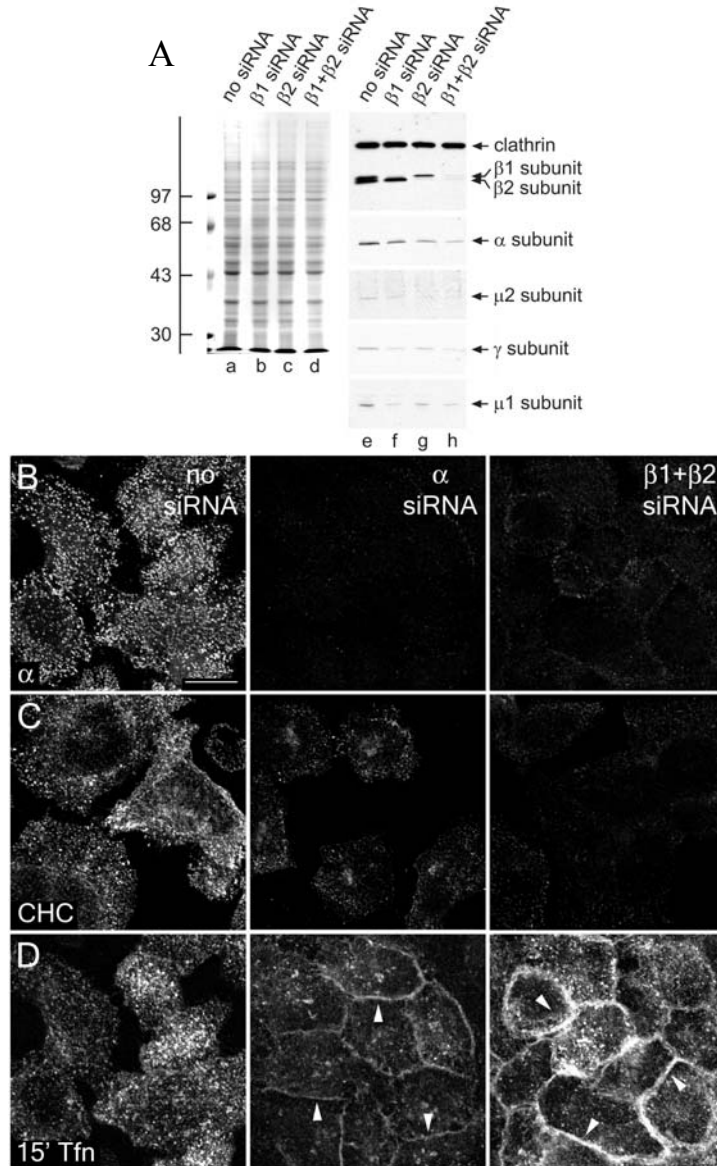
Figure 3-4 β1+β2 subunit RNAi recapitulates α subunit RNAi phenotype

(A) Lysates of HeLa cells untreated (lane a) or treated with either AP-1 β1 (lane b), AP-2 β2 (lane c), or both β1 and β2 subunit siRNA (lane d) were resolved by SDS-PAGE and either Coomassie stained or transferred to nitrocellulose. Sections of the blots were probed with the anti-clathrin heavy chain antibody TD.1, anti-β1/β2 subunit antibody 100/1, Transduction Laboratories anti-AP-2 α subunit mAbs, anti-AP-2 μ2 subunit antiserum, anti-AP-1 γ subunit antibody AE-1, and anti-AP-1 μ1 subunit antibody RY1 polyclonal Abs and relevant portions displayed. The position of molecular mass standards (in kDa) are indicated on the left. (B – E) HeLa cells were either untreated (left panels), or treated with either AP-2 α subunit siRNA (middle panels) or both AP-1 β1 and AP-2 β2 subunit siRNA (right panels), and either fixed and probed with anti-AP-2 α subunit mAb AP.6 (B), brefeldin treated and permeabilized on ice prior to fixation and probed with anti-clathrin HC antibody X22 (C), or serum starved for one hour, given 25 μg/mL Tfn568 continuously for 15 minutes at 37° C and fixed (D). The scale bar represents 10 μm.
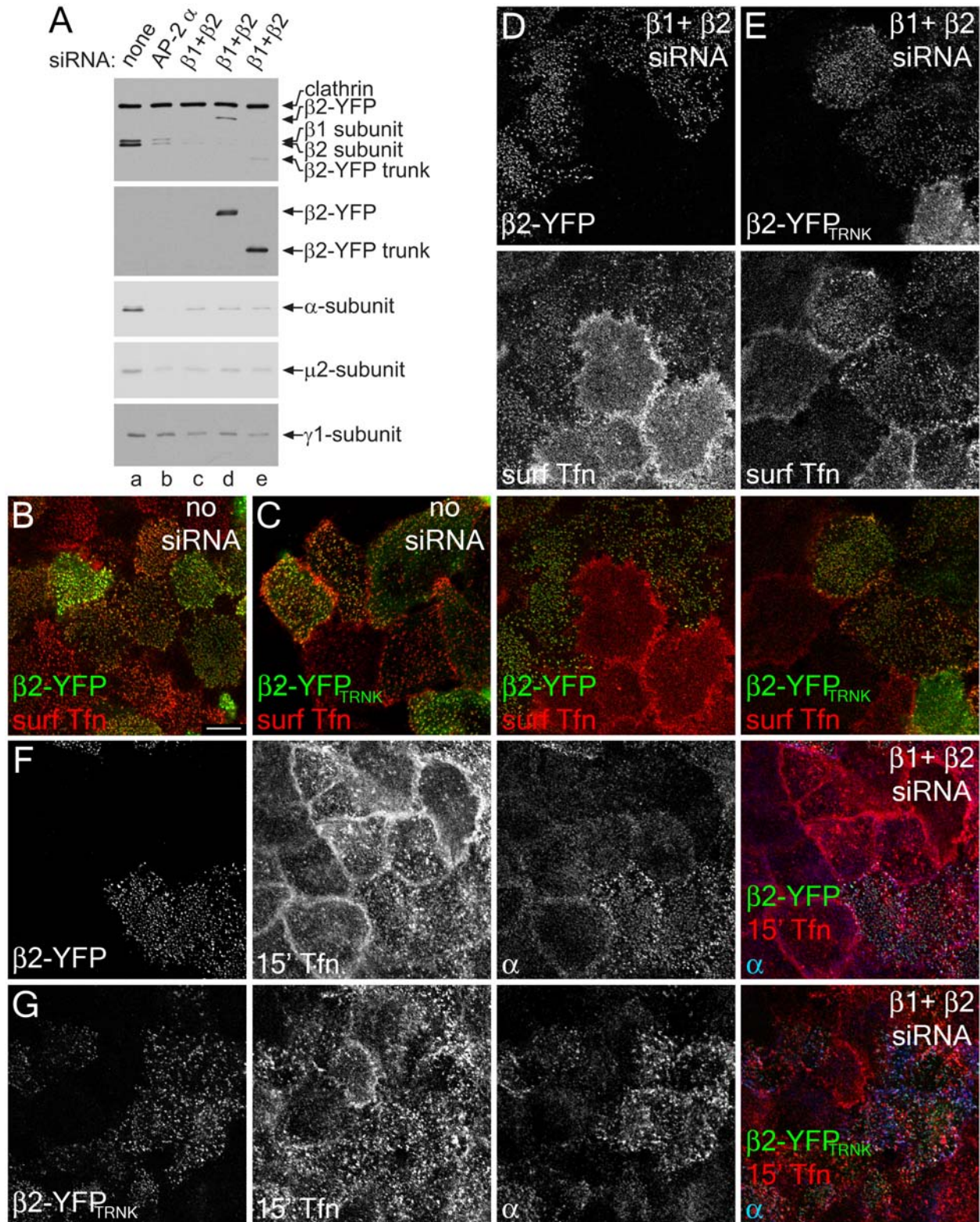
Figure 3-5 Rescue of AP-2 knockdown with β2-YFP

78

Figure 3-5 Rescue of AP-2 knockdown with β2-YFP

(A) Lysates of HeLa cells untreated (lane a) or treated with either AP-2 α subunit, (lane b), or both AP-1 β1 subunit and AP-2 β2-subunit siRNA (lane c) along with β2-YFP (lane d) or β2-YFP$_{TRNK}$ (lane e) were resolved by SDS-PAGE and transferred to nitrocellulose. Sections of the blots were probed with the anti-clathrin heavy chain antibody TD.1, anti-GFP antibody, anti-β1/β2 subunit antibody 100/1, Transduction Laboratories anti-AP-2 α-subunit mAbs, anti-AP-2 μ2 subunit antiserum, or anti-AP-1 μ1 subunit antibody RY1 and relevant portions displayed. (B – G) HeLa cells transiently transfected with mock (B, C) or β1+β2 siRNA duplexes (E – G) and either transfected with β2-YFP (B, D, F) or β2-YFP$_{TRNK}$ (C, E, G) (green in merged images), alternatively surface labeled with Tfn568 (B – E) (red in merged images) and fixed or given Tfn568 continuously for 15 minutes at 37° C (F, G), fixed and probed with anti-AP-2 α subunit mAb AP.6 (D) (blue in merged image). The

3.3.6   The β2 subunit trunk is sufficient to stabilize AP-2 levels and promote transferrin receptor clustering

Next, to probe the role of the unstructured hinge segment and appendage domain of the β2 subunit in endocytosis, a β2-YFP construct lacking these regions (β2-YFP$_{TRNK}$) was expressed in β1+β2 subunit knocked-down HeLa cells. Similarly to the wild type β2-YFP, the β2-YFP$_{TRNK}$ targets to transferrin positive structures and does not interfere with the siRNA efficiency (Figure 3-5A, C). Since YXXØ cargo selectivity is governed by the μ2 subunit, the reconstituted AP-2 is partially functional, as the β2-YFP$_{TRNK}$ reestablishes the localization of surface transferrin to clathrin-containing puncta (Figure 3-5E). Transferrin endocytosis appears to proceed and the AP-2 levels are only stabilized in cells expressing β2-YFP$_{TRNK}$ (Figure 3-5G). I conclude that an intact AP-2 core is necessary for cargo retention in coated pits, and the binding sites present on the β2-hinge and appendage are not absolutely critical for endocytosis.
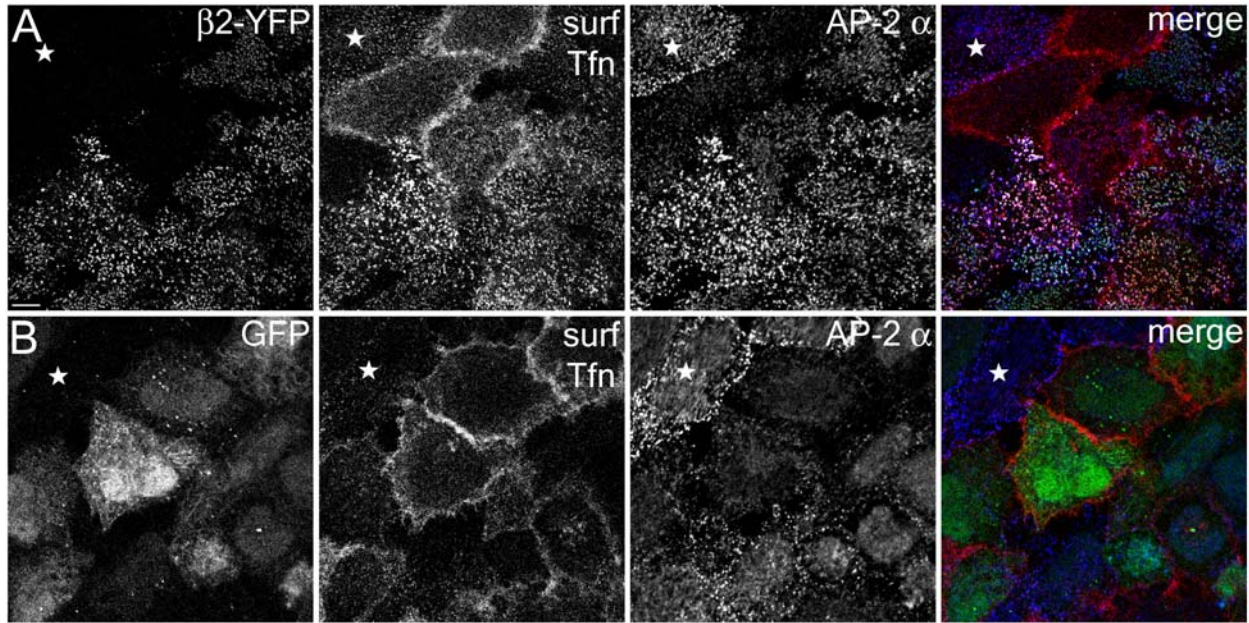
Figure 3-6 Addition of DNA does not compromise RNAi

HeLa cells transfected with β1+β2-subunit siRNAs and either β2-YFP (A) or GFP (B) (green in merge) were surface labeled with Tfn568 (red in merge), fixed and stained with anti-α-subunit mAb AP.6 (blue in merge). The asterisk indicates a cell not transfected with β1+β2 siRNA duplexes. The scale bar represents 10 μm.

3.3.7 ARH requires the β2-appendage for coated pit localization

I then examined the effects the β1+β2 subunit knockdown had on the β2 subunit binding partner ARH. ARH uses a helical FXX[FL]XXXR motif to engage the platform site on the β2-appendage (Edeling et al., 2006). Knockdown of the β1+β2 subunits reduces the amount of ARH localized to coated pits (Fig 3-7A, B). This can be reversed by expression of the β2-YFP, but not β2-YFP$_{TRNK}$ (Fig 3-7C, D). This failure to rescue is due solely to lack of a functional platform binding site, as rescue with β2-YFP bearing the platform site-disrupting Y888V mutation fails to rescue ARH localization, but simultaneous deletion of the clathrin box and introduction of the
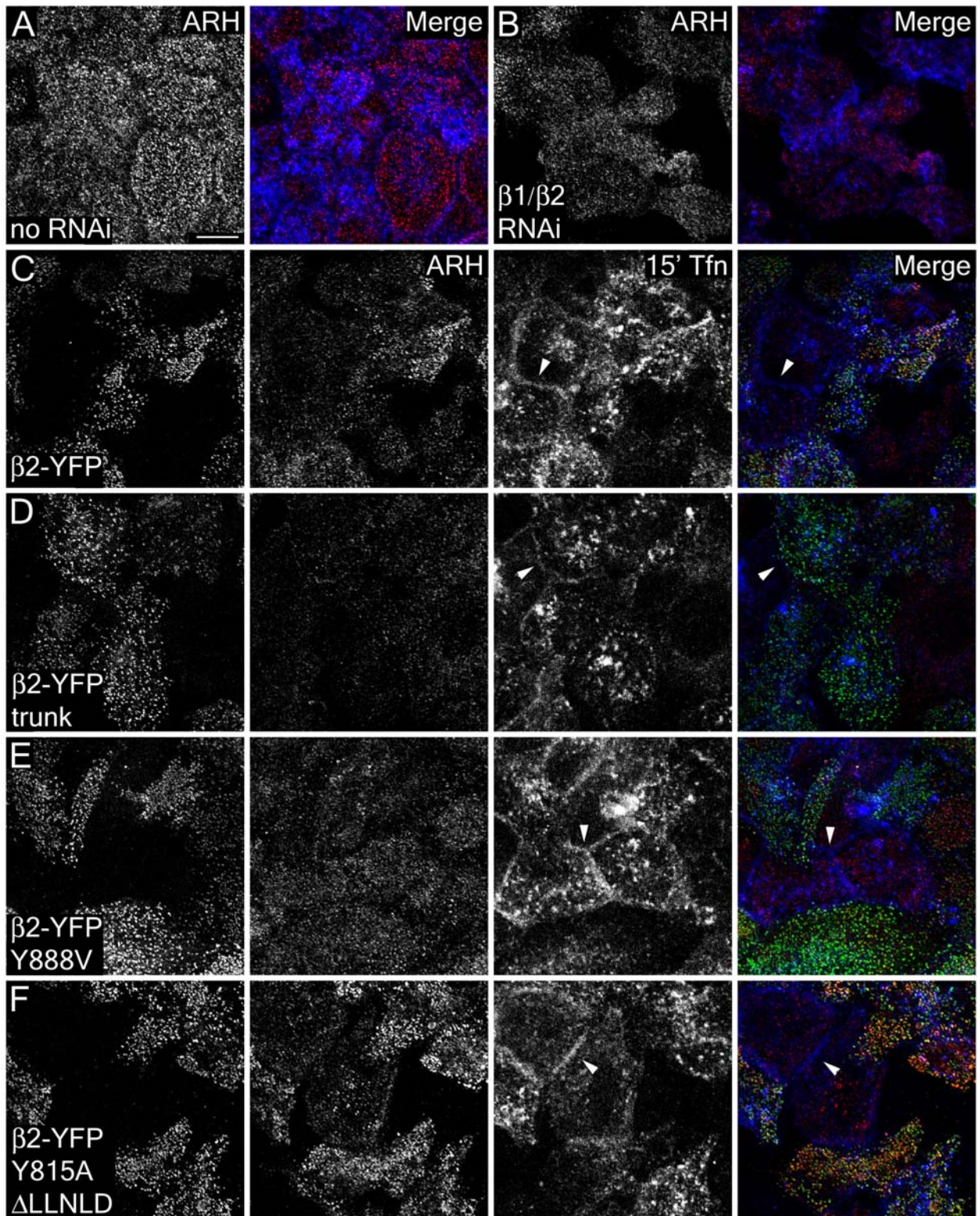
Figure 3-7 ARH requires the β2-appendage platform for plasma membrane localization
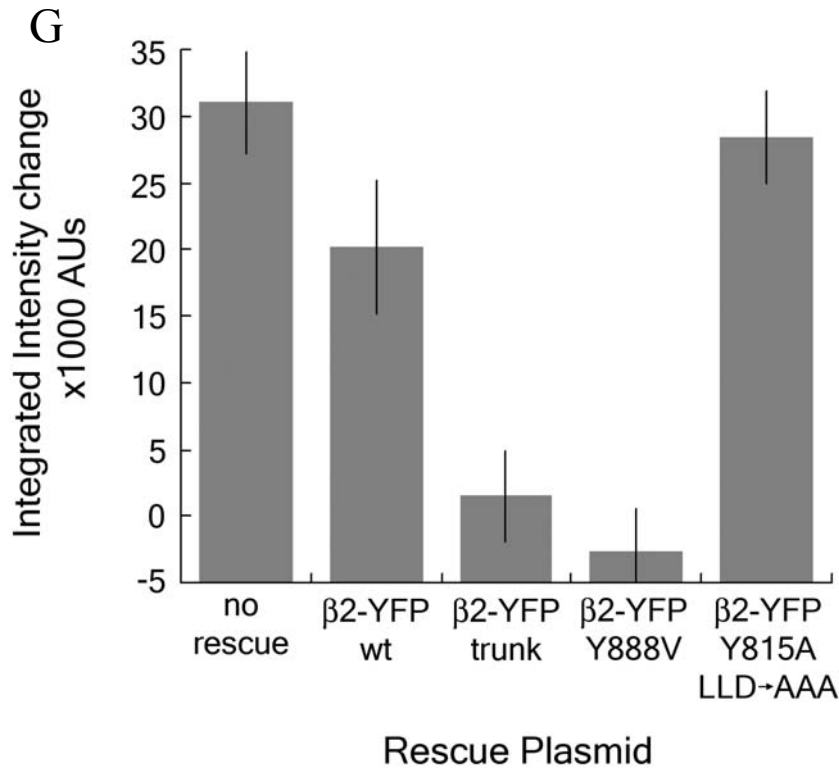
Figure 3-7 ARH requires the β2-appendage platform for plasma membrane localization

HeLa cells either mock transfected (A) or transfected with β1+β2 subunit siRNAs alone (B) or with β2-YFP wild type (C), trunk (D), or bearing Y888V (E), or Y815A and ΔLLNLD (F) mutations (green) were incubated with 50 μg/mL Tfn633 (blue) for 15' at 37º C, permeabilized, fixed and stained with polyclonal anti-ARH antibodies (red). The scale bar represents 10 μm. (G) A comparison of the fluorescence intensity between β2-YFP transfected cells and knockdown cells (as determined by lack of Tfn633 internalization) shows changes between β2-YFP fusions that recruit ARH to the membane and those that do not. The scale bar represents 10 μm.

sandwich site disrupting Y815A mutation into β2-YFP rescues ARH coated pit localization (Figure 3-7E, F). Measurement of the difference in fluorescence intensity between transfected cells and neighboring knockdown cells demonstrates that the AP-2 dependence of ARH coated pit localization is wholly dependent on the β2-appendage platform site (Figure 3-7G). I conclude that ARH requires its β2-appendage binding sequence to efficiently target to coated pits in order to promote efficient sorting of LDL.

3.4   DISCUSSION

Here I have characterized RNAi knockdown of AP-2 via the α and β2 subunits and the first described rescue of AP-2, using an RNAi-resistant β2-YFP. In contrast to α subunit RNAi, RNAi of the β2 subunit results in an incompletely penetrant phenotype. I show that this is due to the promiscuity between β1 and β2subunits, further demonstrating their functional redundancy. One implication of this redundancy is that the β2 subunit is not the limiting component of AP-2, as β1 subunits could substitute for β2 subunits and buffer AP-2 levels. This is likely the only subunit of AP-2 that can be rescued by its AP-1 counterpart, as the σ1 subunit does not interact with the α subunit (Page and Robinson, 1995), and the μ2 subunit RNAi phenocopies the α subunit RNAi (Motley et al., 2003). It has been previously known that β1 subunits can incorporate into AP-2 in vitro and in vivo (Page and Robinson, 1995; Sorkin et al., 1995; Traub et al., 1996), and at moderately high levels, β2-YFP can incorporate into AP-1 (see Figure 2-6).

At even higher levels of β2-YFP overexpression, β2-YFP accumulates in large aggregates not associated with AP-2 (Edeling et al., 2006). However, the localization of β2-YFP to coated pits, restoration of AP-2 levels, localization of Tfn to coated pits in the absence of endogenous β1+β2 subunits, and low expression level suggest that in these experiments β2-YFP is expressed at physiological levels and efficiently incorporated into AP-2 (Figure 3-6, 3-7). This provides a powerful tool for live cell imaging of the AP-2 complex, as the population of unlabeled AP-2 is practically nonexistent compared to the fluorescent population and is known to be functional, since the β2-YFP rescues the RNAi phenotypes. However, the β1 subunit is also knocked down, so the extent of β2-YFP incorporation into AP-1 needs to be more fully investigated before it can be assumed that β2-YFP is present at insufficient levels to label AP-1.

β2-YFP is efficiently incorporated into AP-2, as it restores ARH coated pit localization in β1+β2 subunit RNAi cells, though. This AP-2 dependence of ARH is also evident from data showing that RNAi against Dab2 and AP-2 together blocks LDL receptor endocytosis, though RNAi against either alone does not (see Figure 4-8). As Dab2 has been reported to have signaling properties (He et al., 2002; Hocevar et al., 2003; Hocevar et al., 2001), ARH is likely necessary when those signaling functions are detrimental to the cell type in question. Through binding to a site on AP-2 that is always accessible, ARH may also increase the rate of LDL receptor endocytosis. A high rate of endocytosis is critical in organs that endocytose large mass amounts of LDL receptor family members, such as the liver with LDL receptors in human and mouse (Garcia et al., 2001; Jones et al., 2003), and oocytes with the vitellogenin receptor in *Xenopus* (Zhou et al., 2003).

The failure of ARH to robustly target to coated pits in the absence of AP-2 suggests that this is the primary binding determinant in ARH. This is supported by two lines of evidence. First, overexpression studies show that mutation of the β2-appendage binding region of ARH relieves inhibition of LDL endocytosis to a greater extent than does mutation of the clathrin box (Mishra et al., 2005). Second, the binding affinity of ARH to the β2-appendage is likely greater than its affinity to any other binding partner. ARH binds to the β2-appendage with a K_D of 1-2 μM (Mishra et al., 2005), compared to 22 μM for type I clathrin box LLDLD binding to clathrin (Miele et al., 2004), 10-100 μM for the Shc PTB domain binding to PtdIns(4,5)P_2 (Zhou et al., 1995) and 1-4 μM for various PTB domains binding to NPXY peptides (Howell et al., 1999; Li et al., 1998; Stolt et al., 2003). This is similar to the other CLASP completely dependent on this binding site, β-arrestin, in which the AP-2 binding sequence functions as a molecular switch to promote β-arrestin interactions with coated pits (Edeling et al., 2006; Kim and Benovic, 2002; Laporte et al., 2002). However, there is no evidence of ARH acting as a molecular switch to promote regulated LDL receptor internalization.

The role of the β2-appendage in assisting cargo internalization has been underappreciated. Apart from cargo bearing YXXΦ, dileucine and certain Trp based internalization motifs which bind directly to AP-2, all other known cargo internalization sequences engage proteins that interact with the β2 subunit. GPCR and FXNPXY selective CLASPs interact with the platform subdomain, and the polyubiquitin-selective CLASPs epsin and eps15 bind to the platform and sandwich subdomains of β2-appendage respectively (Edeling et al., 2006). Despite this, redundancies have been built in to the system, such that the elimination of this portion of the system does not compromise endocytosis of these ligands in

most systems. AP-2 reduction via β2 subunit RNAi has been reported to block both EGF receptor and TfR endocytosis to a similar extent as observed for an α or μ2 subunit knockdown (Huang et al., 2004). However, the extent of inhibition of TfR endocytosis, ~50-60%, is much less than the >90% reported by others for α or μ2 subunit RNAi (Hinrichsen et al., 2003; Motley et al., 2003), and consistent with the partial inhibition of Tfn localization observed here. Overall, the β2-appendage of AP-2 is one arm of an intricate web of protein-protein interactions that promote alternate cargo endocytosis. Here I have defined the molecular characteristics of the β2-appendage-CLASP binding platform site, which is important for the localization of these CLASPs to the plasma membrane.

4.0 A SINGLE COMMON PORTAL FOR CLATHRIN-MEDIATED ENDOCYTOSIS OF DISTINCT CARGO GOVERNED BY CARGO-SELECTIVE ADAPTORS[*]

4.1 ABSTRACT

Sorting of transmembrane cargo into clathrin-coated vesicles requires endocytic adaptors, yet RNAi-mediated gene silencing of the AP-2 adaptor complex only disrupts internalization of a subset of clathrin-dependent cargo. This suggests alternate clathrin-associated sorting proteins participate in cargo capture at the cell surface and a provocative recent proposal is that discrete endocytic cargo are sorted into compositionally and functionally distinct clathrin coats. I show here that the FXNPXY-type internalization signal within cytosolic domain of the LDL receptor is recognized redundantly by two phosphotyrosine-binding domain proteins, Dab2 and ARH; diminishing both proteins by RNAi leads to conspicuous LDL receptor accumulation at the cell surface. AP-2-dependent uptake of transferrin ensues relatively normally in the absence of Dab2 and ARH, clearly revealing delegation of sorting operations at the bud site. AP-2, Dab2, ARH, transferrin and LDL receptors are all present within the vast majority of clathrin structures at the surface, challenging the general existence of specialized clathrin coats for segregated internalization of constitutively-internalized cargo. However, Dab2 expression is exceptionally low in hepatocytes, likely accounting for the pathological hypercholesterolemia that accompanies ARH loss.

4.2   INTRODUCTION

When the clathrin coat was first discovered in mosquito oocytes (Roth and Porter, 1964), it was astutely speculated that the 'bristle' coat provided cargo selective properties that govern the process of yolk internalization. Mosquito yolk precursor receptors, the vitellogenin and lipophorin receptors, are members of the low density lipoprotein (LDL) receptor superfamily. The first endocytic sorting signal was identified in this superfamily, when it was discovered that the [802]FDNPVY sequence within the carboxy-terminal cytosolic domain of human LDL receptor promotes rapid clathrin-mediated uptake of LDL (Chen *et al.*, 1990). Other internalization signals have subsequently been identified, including the wide-spread YXXØ motif, found in transferrin and mannose 6-phosphate receptors, the [DE]XXXL[LI]-type dileucine motif, and reversible poly/multiubiquitination (Bonifacino and Traub, 2003).

To link these sorting signals to an assembling clathrin lattice, adaptor proteins are required because clathrin triskelia, the protomers of the characteristic polyhedral coat, contain no direct membrane-binding information. The first endocytic adaptor characterized was AP-2, a multifunctional heterotetramer comprised of a core of small σ2, medium μ2 and large α and β2 subunits. An independently-folded appendage projects off each large subunit, connected to the core by a flexible polypeptide hinge (Owen *et al.*, 2004). The β2 subunit hinge and appendage bind physically to triskelia, allowing AP-2 to couple clathrin to the membrane, since the adaptor core binds phosphatidylinositol 4,5-bisphosphate (PtdIns(4,5)P_2) directly, and also interacts with

YXXØ and [DE]XXXL[LI] motifs (Honing et al., 2005; Ohno et al., 1995; Owen et al., 2004). Accordingly, AP-2 has a well accepted role as the major cargo selective component for endocytic coated vesicles. Nevertheless, distinct internalization signals neither saturate internalization at the same surface density nor compete directly with one another (Marks *et al.*, 1996; Santini *et al.*, 1998; Warren *et al.*, 1998), which is not expected if AP-2 performs all cargo selective steps, and AP-2 does not readily bind to alternative internalization signals, including polyubiquitin and the FXNPXY sequence. Moreover, when small interfering RNA (siRNA) is used to ablate AP-2, transferrin uptake halts but cargo utilizing alternative endocytic signals, like the LDL receptor, still internalize efficiently (Hinrichsen *et al.*, 2003; Motley *et al.*, 2003).

Endocytic clathrin coats must therefore contain alternative sorting adaptors. These clathrin-associated sorting proteins (CLASPs) should synchronously bind clathrin, the plasma membrane, cargo, and other lattice assembly proteins, such as AP-2 (Traub, 2003). Disabled-2 (Dab2) and the autosomal recessive hypercholesterolemia (ARH) protein are potential FXNPXY-signal sorting CLASPs; both contain an amino-terminal phosphotyrosine binding (PTB) domain that simultaneously interacts with non-phosphorylated FXNPXY motifs and PtdIns(4,5)P$_2$, along with an unstructured carboxy-terminal segment that contains tandemly arrayed clathrin- and AP-2-binding information (He et al., 2002; Mishra et al., 2002a; Mishra et al., 2002b; Morris and Cooper, 2001; Yun et al., 2003). Huge overexpression of a tandem Dab2 PTB domain construct selectively disrupts internalization of LDL receptor (Mishra *et al.*, 2002a) and the type-2 apolipoprotein E receptor (Cuitino *et al.*, 2005). However, this does not unambiguously prove the involvement of Dab2 in clathrin-mediated endocytosis; rather it shows a binary interaction between the PTB domain and the FXNPXY sorting signal. That Dab2-

nullizygous mice exhibit a (mild) proteinuria, indicative of megalin (a hepatic scavenger receptor of the LDL receptor superfamily) dysfunction in the renal proximal tubule, supports a role for Dab2 in endocytosis. There are two major splice isoforms of Dab2, so-called p96 (full length) and p67, with the central AP-2 and clathrin binding region spliced out (Xu *et al.*, 1995). The poor ability of the p67 isoform to promote megalin-dependent transferrin uptake in developing embryos (Maurer and Cooper, 2005) also argues for Dab2 coupling cargo selection to clathrin coat assembly. Yet, conditionally-null Dab2$^{-/-}$ mice are surprisingly viable and fertile (Morris et al., 2002b). Conversely, targeted ARH gene disruption in mice, just as in ARH patients (Arca et al., 2002; Garcia et al., 2001; Naoumova et al., 2004; Zuliani et al., 1999), leads to elevated circulating LDL and LDL internalization defects in the liver (Jones *et al.*, 2003), but there is no evidence of proteinuria. These experiments hint at possible functional overlap between Dab2 and ARH activity in decoding FXNPXY sorting signals, but also uncover a seemingly complex interrelationship of the two proteins *in vivo*.

In this chapter, I show that Dab2 and ARH sort the LDL receptor in a functionally redundant manner; knocking down both proteins with siRNA causes extensive accumulation of LDL receptors at the cell surface. Assigning the CLASPs responsible for FXNPXY signal recognition is significant as LDL receptor superfamily members regulate numerous cellular processes; for instance, megalin appears to participate in steroid hormone action by promoting internalization of sex hormone-binding globulin complexes (Hammes *et al.*, 2005). In *Drosophila*, where the FXNPXY signal is conserved, lipoproteins play an important role transporting lipid-linked morphogens like Wingless and Hedgehog, and contribute to establishment of appropriate morphogen gradients during development (Panakova *et al.*, 2005),

and this process might be conserved in chordates. In addition, clear appreciation of how Dab2 and ARH orchestrate FXNPXY sorting allows assessment of whether these CLASPs and cognate cargo are confined to functionally discrete subsets of clathrin structures at the plasma membrane. Despite recent propositions (Cao et al., 1998; Lakadamyali et al., 2006; Tosoni et al., 2005), I do not find evidence of major compositional heterogeneity within clathrin coats at the surface of non-polarized cells, questioning the general existence of specialized vesicles dedicated to internalization of select subsets of cargo.

4.3   RESULTS

4.3.1   Selective LDL receptor internalization by Dab2 and ARH

Cultured fibroblasts derived from ARH patients do not display major defects in LDL uptake, unlike LDL receptor-defective fibroblasts from individuals with familial hypercholesterolemia (Eden et al., 2002; Garcia et al., 2001). As ARH$^{-/-}$ fibroblasts do express Dab2 (Mishra *et al.*, 2002b), the common domain/sequence signatures and functional analogy between ARH and Dab2 suggest that Dab2 might compensate for the absence of ARH in these cells. Indeed, Dab2 is positioned in small puncta scattered apparently randomly over the surface of ARH-null cells, most of which colocalize with both AP-2 and the LDL receptor (Figure 4-1A and B). Transiently

91

diminishing Dab2 levels by transfection with siRNA oligonucleotides (Figure 4-1C) strongly diminishes Dab2 staining, but the AP-2 distribution is unaltered (Figure 4-1D). In ARH^{-/-} cells with depressed Dab2 levels, the LDL receptor diffuses over the cell surface and weak foci of clustered receptor, compared to adjacent non-gene-silenced cells, correspond mostly to clathrin-coated regions harboring residual Dab2 (Figure 4-1E). Fluorescence intensity analysis of these images shows clearly that in ARH^{-/-} fibroblasts, peaks of LDL receptor labeling coincide precisely with a Dab2 signal but that there is negligible correspondence with the more diffuse LDL receptor after diminishing Dab2 protein levels (Figure 4-2). By contrast, the transferrin receptor remains concentrated at bud sites irrespective of the intracellular Dab2 concentration (Figure 4-1F). Internalization of DiI-labeled LDL and subsequent concentration in perinuclear endosomes is also obviously slowed in ARH^{-/-} cells with decreased Dab2 levels (Figure 4-1G and H). Together, these results suggest that Dab2 actively clusters LDL receptors at clathrin bud sites in ARH nullizygous fibroblasts.

In HeLa cells, RNAi-mediated gene silencing of either Dab2 or ARH transcripts (Figure 4-3A) results in only mild impairment of LDL uptake. Compared with control cells, LDL receptors accumulate at the cell surface, although substantial LDL internalization is evident (Figure 4-3C and D). Again, transferrin endocytosis proceeds normally in both control and RNAi-treated cells, and the intracellular transferrin colocalizes, in part, with internalized LDL. Yet, simultaneously knocking down both ARH and Dab2 with siRNA duplexes has a dramatic effect on LDL receptor trafficking (Figure 4-3E). LDL accumulates diffusely over the surface, but transferrin uptake continues relatively unimpeded. Anti-LDL receptor antibody binding shows a surface density increase of at least fivefold after Dab2+ARH RNAi. Time-resolved
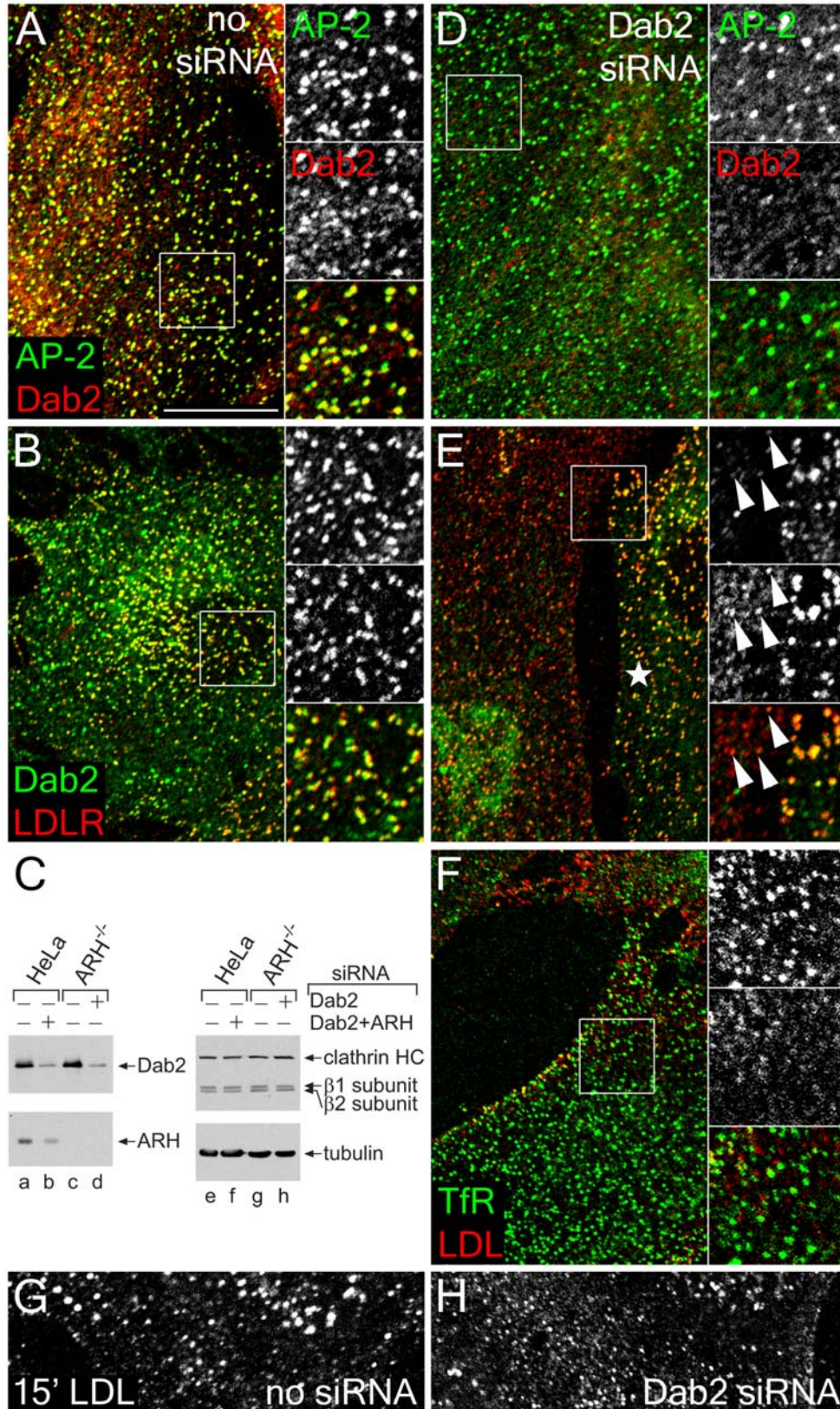
Figure 4-1 Dab2 activity in ARH-null fibroblasts

Figure 4-1 Dab2 activity in ARH-null fibroblasts

GM00697 ARH$^{-/-}$ fibroblasts nucleofected with mock (A, B, and G) or Dab2-specific siRNA duplexes (D-F, and H) were fixed and stained with anti-AP-2 α-subunit mAb AP.6 and/or affinity-purified anti-Dab2 antibodies, or, prior to fixation, were incubated on ice with anti-LDL receptor mAb IgG-C7 (LDLR), or anti-transferrin receptor (TfR) mAb RVS-10 and DiI-LDL on ice for 60 min. Representative single confocal optical sections are shown with color-separated AP-2 (green channel, top) and Dab2 (red channel, middle) and merged magnifications of each boxed region shown on the right. Alternatively, whole cell lysates from HeLa SS6 or ARH$^{-/-}$ fibroblast transfected with mock, Dab2+ARH, or Dab2 siRNA duplexes were prepared, resolved by SDS-PAGE and transferred to nitrocellulose (C). Portions of the blots were probed with anti-Dab2 or ARH polyclonal antibodies, anti-clathrin heavy chain (HC) mAb TD.1 and anti-β1/β2 subunit mAb 100/1, or anti-tubulin mAb E7, and only the relevant region of each blot is shown. Mock (G) or Dab2 siRNA transfected (H) ARH$^{-/-}$ fibroblast cells were also incubated with DiI-LDL at 37°C for 15 min before fixation. In E, an untransfected cell is indicated with an asterisk, and residual Dab2-positive structures containing LDL receptor are shown with arrowheads. The scale bar represents 10 μm
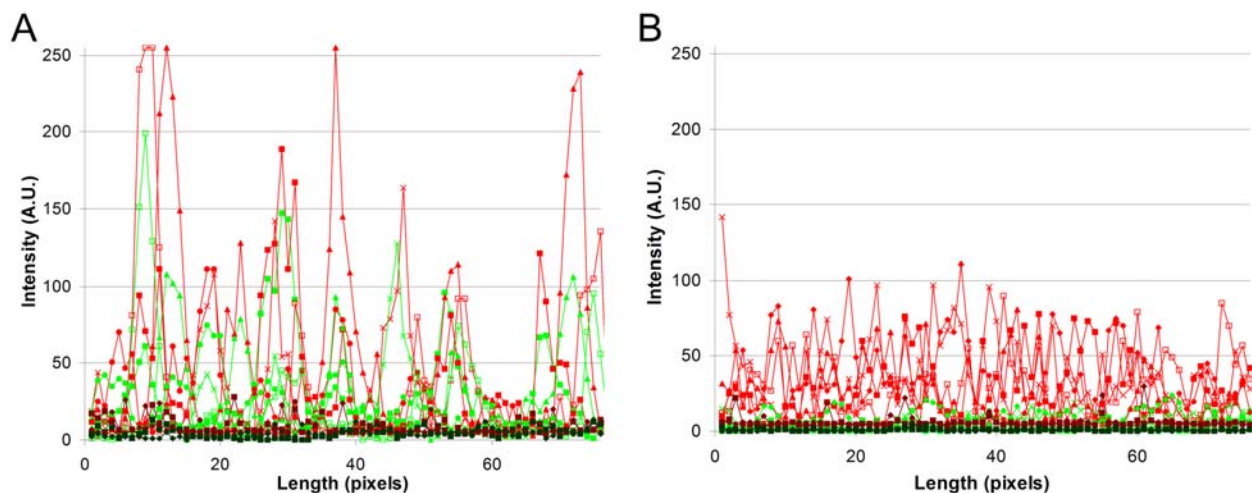
Figure 4-2 Linescan fluorescence intensity analysis in ARH$^{-/-}$ fibroblasts treated with Dab2-specific siRNA duplexes

The intensity (in arbitrary units, A.U.) of Dab2 (green traces) or LDL receptor (red traces) in ARH$^{-/-}$ fibroblasts mock transfected (A) or transfected with Dab2 siRNA (B) was measured along five representative 3-pixel wide lines. For individual lines, the same symbol is used on the green and red traces, so the colocalization of Dab2 and LDL receptors is evident in control cells (A). Dark green and red traces indicate background fluorescence. Note the decreased peak but higher median intensity and loss of Dab2 signal in knockdown compared to control cells.

imaging of cells incubated with fluorescent LDL and transferrin confirms the severe effect of the Dab2+ARH double knockdown. While LDL and transferrin are efficiently internalized and some sorted into common endosomes in the mock-treated HeLa cells, the surface of the siRNA-treated cells is heavily labeled with LDL, also diffusing into filopodia despite normal transport of transferrin to the cell interior (Movie 4-1). Strikingly, these results are the reciprocal of those obtained when AP-2 levels are reduced >75% by RNAi, where transferrin but not LDL accumulates at the cell surface (Hinrichsen *et al.*, 2003; Motley *et al.*, 2003) (see also Figure 4-10A and B).

Since Dab2 has multiple clathrin-binding sites like AP-2 (Mishra *et al.*, 2002a), it is possible that general clathrin lattice assembly is impaired in the Dab2+ARH double knockdowns and this, rather than sorting aberrations, is responsible for the surface LDL accumulation. However, RNAi of epsin 1, an abundant poly/multiubiquitin-selective CLASP with multiple clathrin-binding sites, does not produce a similar affect. Despite >80**%** decrease in epsin levels in siRNA-transfected HeLa cells (Figure 4-4A), LDL uptake is similar in control and epsin depleted cells (Figure 4-4B and F), and in ARH or epsin+ARH knocked-down cells (Figure 4-3C and G). Still, tandem Dab2+ARH knockdown severely blocks LDL internalization, with characteristic accumulation of surface LDL (Figure 4-4E). Clathrin (and dynamin 2; not shown), but not AP-2, ablation likewise inhibits LDL internalization, though the LDL still accumulates in punctate structures on the surface, which, given the presence of LDL-selective CLASPs and the fact that adaptors/CLASPs retain appropriate intracellular positioning in the absence of clathrin (Hinrichsen *et al.*, 2006), is expected (Figure 4-4H and I, arrowheads). In these
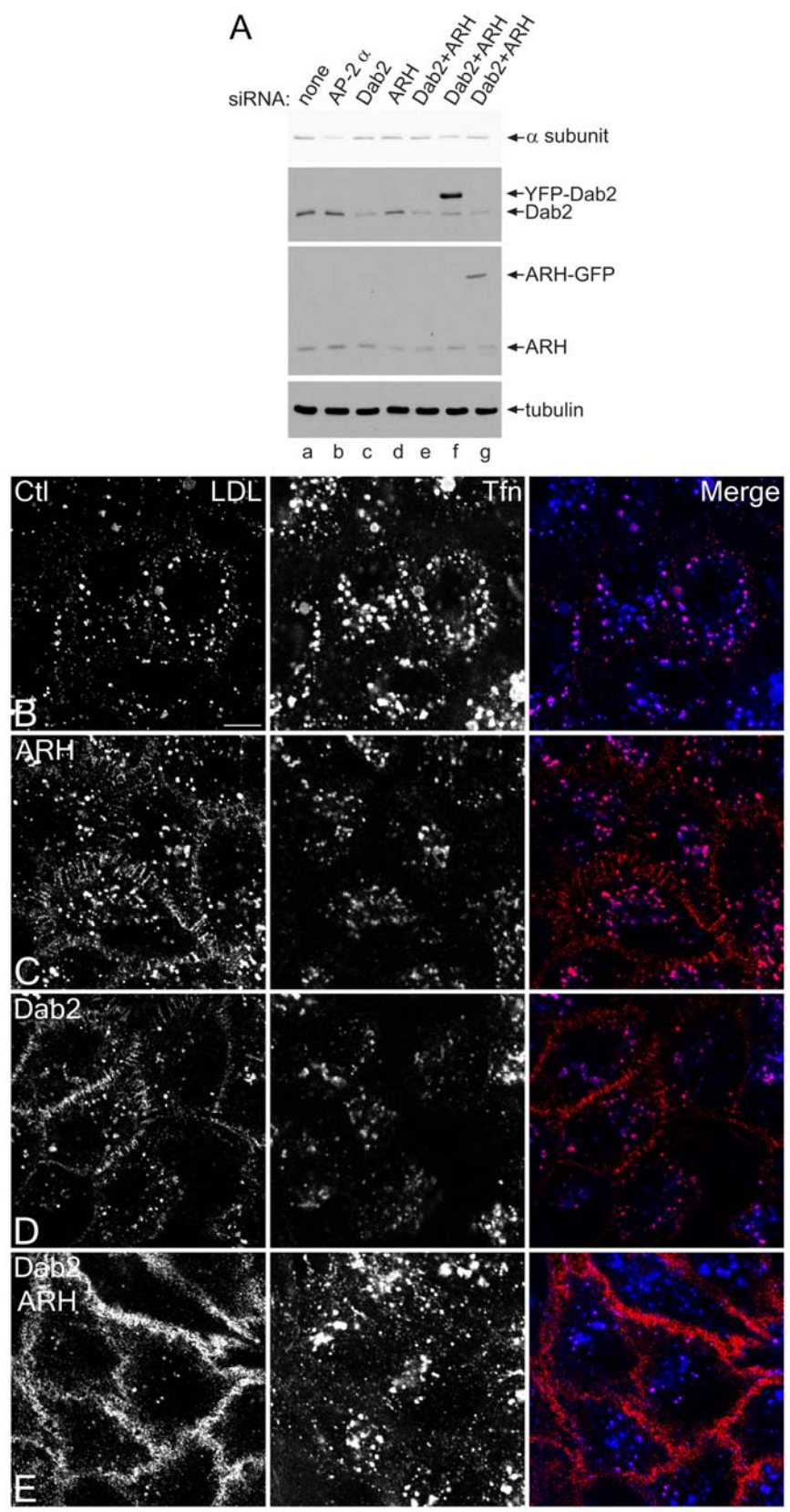
Figure 4-3 Cargo selective effect of Dab2 and ARH silencing

96

Figure 4-3 Cargo selective effect of Dab2 and ARH silencing

HeLa SS6 cells transiently transfected with mock (A, lane a; B) or siRNA duplexes targeting the AP-2 α subunit (A, lane b), Dab2 (A, lane c; D), ARH (A, lane d; C), or Dab2+ARH alone (A, lane e; E), or together with YFP-Dab2 (A, lane f) or ARH-GFP (A, lane g) were lysed, resolved by SDS-PAGE and transferred to nitrocellulose. Portions of the blots were probed with anti-AP-2 α-subunit mAb clone 8, anti-Dab2 or anti-ARH polyclonal antibodies or anti-tubulin mAb E7 (A). Only the relevant portions of the blots are shown. Alternatively, transfected cells on coverslips were incubated together with 4 μg/ml DiI-LDL (left, red in merge) and 50 μg/ml Tfn633 (center, blue in merge) for 15 min at 37ºC and fixed (B-E). Representative single confocal optical sections are shown. Note the pronounced surface accumulation of LDL, but not transferrin, in the Dab2+ARH knockdown and to a much lesser extent in the single knockdowns. The scale bar represents 10 μm.

experiments, the extent of ARH depletion is somewhat variable (compare Figure 4-3A, 4-4A and 4-10A). Nevertheless, no substantial increase in the extent of ARH gene silencing is seen if a multiple siRNA-containing SMARTpool is used instead of the single duplex utilized for the majority of this chapter. In both cases, ~80% decrease in steady-state ARH levels can be achieved (Figure 4-5).

A clear kinetic lag in the uptake of DiI-LDL occurs in Dab2+ARH-silenced cells (Figure 4-6 and Figure 4-7). Both transferrin and LDL populate common peripheral endosomes in control cells incubated for five min in the continuous presence of both ligands (Figure 4-6C and Figure 4-7). Between 20 and 40 min, marked concentration of LDL in juxtanuclear endosomes is apparent (Figure 4-7B and C). A low level of LDL is present at the surface in the control cells between one and five min (Figure 4-6A, C and E, and Figure 4-7A and G), which is in accord
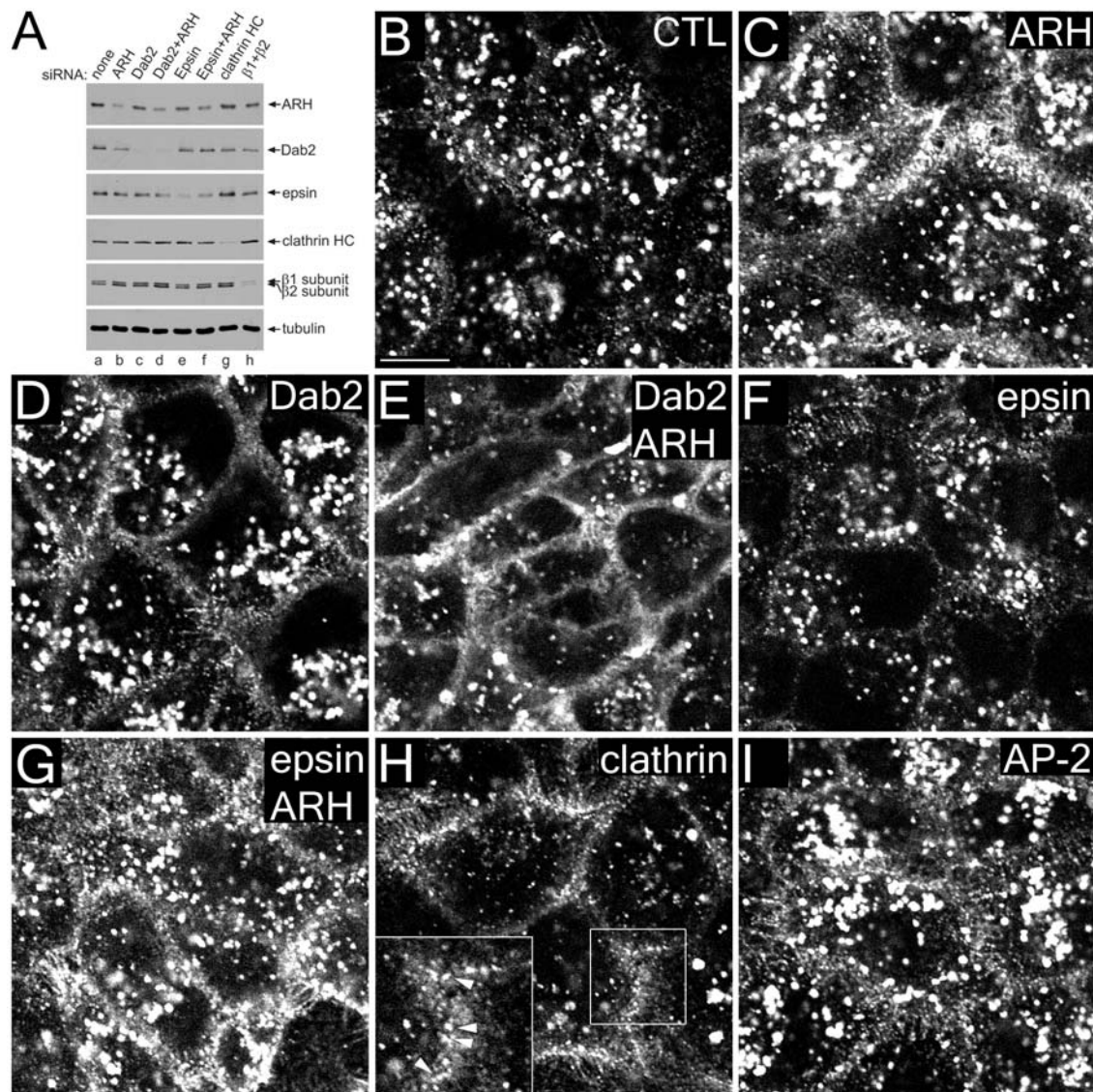
Figure 4-4 Dab2 and ARH are LDL-specific CLASPs

HeLa SS6 cells transiently transfected with mock (A, lane a; B) or with specific siRNA duplexes directed against ARH (A, lane b; C), Dab2 (A, lane c; D), Dab2+ARH (A, lane d; E), epsin 1 (A lane e; F), epsin1+ARH (A, lane f; G), clathrin heavy chain (A, lane g; H) or AP-1 β1 and AP-2 β2 subunits (A, lane h; I) were lysed, resolved by SDS-PAGE and transferred to nitrocellulose. Portions of the blots were probed with either affinity-purified anti-ARH, anti-Dab2, or anti-epsin 1, anti-β1/β2 subunit mAb 100/1 antibodies, anti-clathrin HC mAb TD.1, or anti-tubulin mAb E7. Alternatively, transfected cells on coverslips were incubated with 4 μg/ml DiI-LDL for 15 mins at 37ºC and fixed (B-I). Representative single confocal optical sections are shown with a magnification of the boxed region in H shown on the lower left. Note the dramatic surface accumulation and diminished internalization of LDL in clathrin or Dab2+ARH double knockdowns, but some surface LDL still appears clustered in puncta in the absence of clathrin (H inset, arrowheads). The scale bar represents 10 μm.
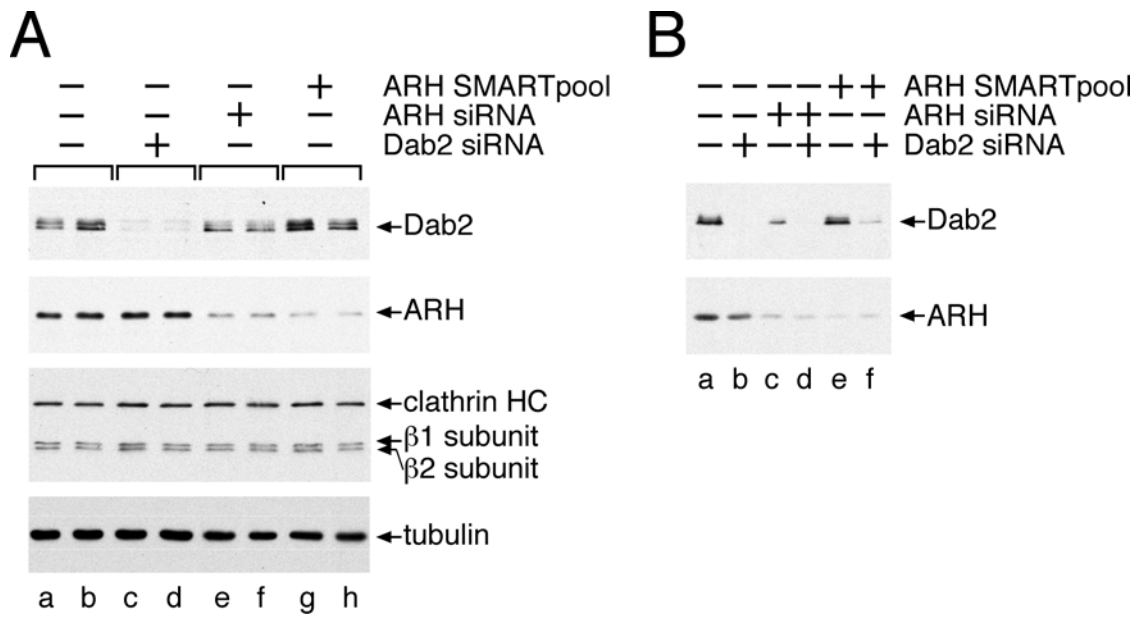
Figure 4-5 Extent of Dab2 and ARH gene silencing with different siRNA duplexes

(A) Equivalent volumes of whole-cell lysates from HeLa SS6 cells transfected in duplicate with mock (lane a and b), Dab2 (lane c and d) or ARH (lane e and f) siRNA duplexes or an ARH-targeting SMARTpool (lane g and h), were prepared, resolved by SDS-PAGE and transferred to nitrocellulose. Portions of the blots were probed with affinity-purified anti-Dab2 or -ARH polyclonal antibodies, anti-clathrin heavy chain (HC) mAb TD.1 and anti-β1/β2 subunit polyclonal GD/1, or anti-tubulin mAb E7. Only the relevant region of each blot is shown. (B) Equivalent volumes of whole cell lysates from HeLa SS6 cells transfected with mock (lane a), Dab2 (lane b), ARH (lane c) or Dab2+ARH siRNA duplexes (lane d), or an ARH-targeting SMARTpool alone (lane e) or ARH SMARTpool+Dab2 (lane f) were prepared, resolved by SDS-PAGE and transferred to nitrocellulose. Portions of the blots were probed with affinity-purified anti-Dab2 or -ARH polyclonal antibodies, and only the relevant region of each blot is shown. Quantitatively similar results are obtained whether ECL or ^{125}I-labeled anti-rabbit IgG is used for detection.

with both the lower absolute rate of internalization and a less abundant rate-limiting component for LDL uptake compared with transferrin (Warren *et al.*, 1998). In the Dab2+ARH-depleted cells, already between one and five min, very prominent appearance of a circumferential band of LDL at the plasma membrane occurs, and is still evident at 40 min (Figure 4-7F). While LDL endocytosis is slowed (compare Figure 4-6F to E), the ligand is nonetheless still internalized and traffics to the transferrin-positive early endosome compartment, but not as efficiently as in mock-treated cells (Figure 4-7G). This overall slowed internalization of LDL in the FXNPXY-selective CLASP-depleted cells is fully consistent with the ~5-fold reduction in internalization index characteristic of LDL receptor FXNPXY mutants devoid of an operational sorting signal (Chen et al., 1990; Davis et al., 1986; Davis et al., 1987).

Importantly, efficient LDL uptake is restored upon transient expression of either an ARH-GFP or an siRNA-resistant YFP-Dab2 fusion protein in Dab2+ARH knockdown cells (Figure 4-8A and E). This demonstrates that either of these proteins can individually restore LDL uptake, and that the appended fluorescent tags do not significantly interfere with LDL endocytosis. I conclude that Dab2 and ARH appear to operate in a functionally redundant manner to drive the efficient internalization of the LDL receptor in non-polarized cells, and that the YXXØ (transferrin receptor) and FXNPXY (LDL receptor) sorting signals are decoded by distinct components of the clathrin coat.
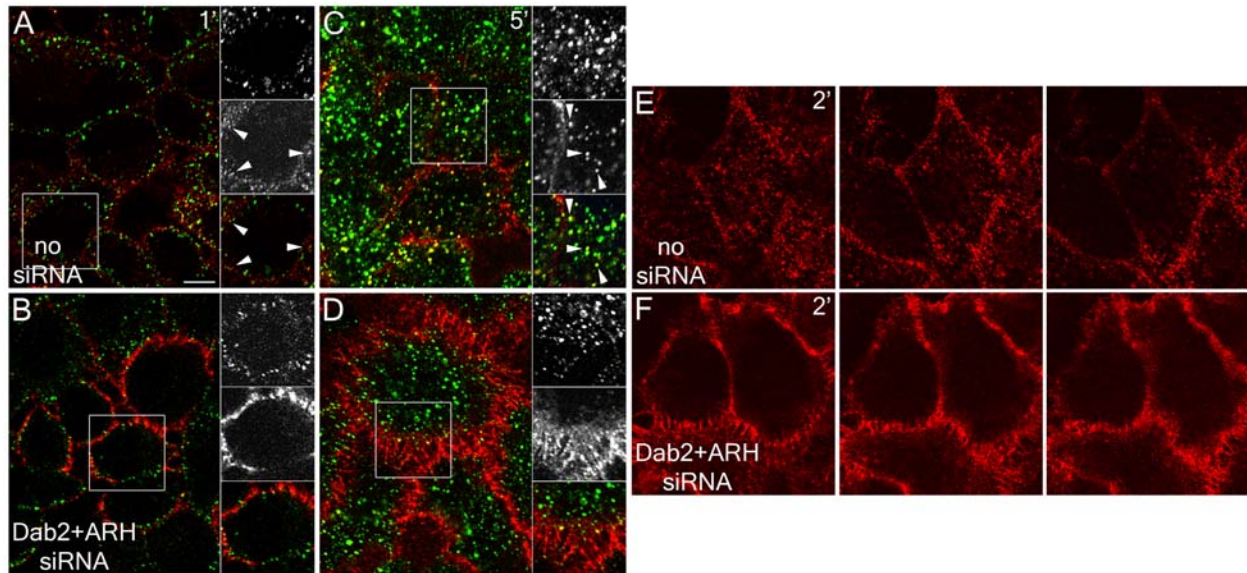
Figure 4-6 Slowed LDL uptake in Dab2- and ARH-depleted HeLa cells

(A-D) HeLa SS6 cells either mock transfected (A, C) or transfected with Dab2+ARH siRNA duplexes (B, D) were incubated at 37ºC in the continuous presence of both 25 μg/mL Tfn488 (green) and 5 μg/mL DiI-LDL (red) either for 1 (A, B) or 5 min (C, D), rapidly washed on ice, and then fixed. The boxed regions are enlarged at the right of each image, with transferrin (green), LDL (red) and merged channels shown. Arrowheads mark punctate endosomal structures. Importantly, the DiI-LDL concentration used is considerably lower than the ~50 μg/ml required to saturate the surface LDL receptor in control cells (Brown and Goldstein, 1986) and, consequently, not all LDL receptors are occupied under these conditions. (E and F) HeLa SS6 cells either mock transfected (E) or transfected with Dab2+ARH siRNA duplexes (F) were incubated at 37ºC with 5 μg/mL DiI-LDL for 2 min, washed on ice and fixed. Representative sequential confocal optical sections are shown to illustrate the general delay in LDL internalization in the Dab2+ARH-depleted cells. The scale bar represents 10 μm.
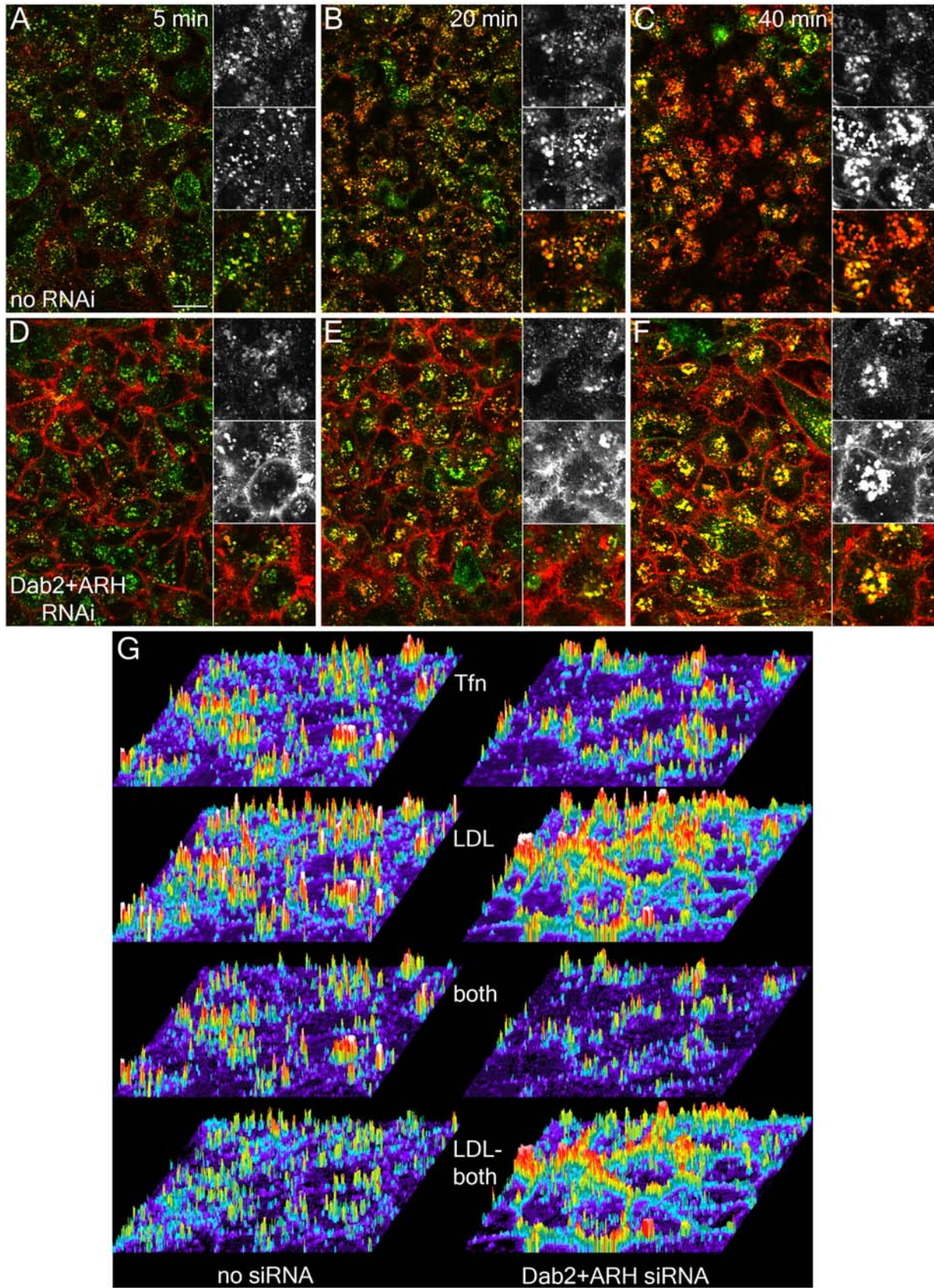
Figure 4-7 Delayed internalization and surface accumulation of LDL in Dab2+ARH-silenced cells

Figure 4-7 Delayed internalization and surface accumulation of LDL in Dab2+ARH-silenced cells

HeLa SS6 cells transiently transfected with mock (A-C, G, left column) or siRNA duplexes targeting Dab2 and ARH (D-F, G, right column) and grown on coverslips were incubated with 4 μg/mL DiI-LDL (red) and 25 μg/mL Tfn488 (green) for 5 min (A, D, G), 20 min (B, E) or 40 min (C, F), washed on ice and fixed. The severe surface accumulation and loss of transferrin/LDL colocalization in Dab2+ARH knockdown is apparent even at 5 min, shown by the intensity profile (G), where color variation and peak height represent intensity of transferrin (Tfn) (top panel), LDL (upper middle panel), transferrin and LDL (lower middle panel) or LDL only (bottom panel, determined as the difference between upper middle and lower middle panels). The scale bar represents 20

4.3.2 Functional modules within ARH and Dab2

Dab2 and ARH each contain cargo- (FXNPXY), PtdIns(4,5)P_2-, AP-2- and clathrin-binding regions, which allow direct coupling of bound cargo to the clathrin coat machinery (Garuti et al., 2005; He et al., 2002; Mishra et al., 2002a; Mishra et al., 2002b; Morris and Cooper, 2001). If either the AP-2 or the clathrin binding information within ARH-GFP is singly compromised by mutation of either F259A or [212]LLD→AAA, respectively, the expressed protein still promotes LDL internalization (Figure 4-8B and C), though quantitation reveals that neither mutant rescues fully (Figure 4-8G) (Garuti *et al.*, 2005). These results are reminiscent of data obtained when the analogous binding sequences for clathrin or AP-2 are singly altered in β-arrestin 2 (Kim and Benovic, 2002; Laporte et al., 2000; Santini et al., 2002). When both these binding sites are disrupted, the ARH-GFP becomes diffusely distributed in the cytoplasm and fails to rescue the Dab2+ARH knockdown phenotype (Figure 4-8D). S122Y, a PTB domain mutation affecting the FXNPXY binding surface of YFP-Dab2 (Stolt *et al.*, 2004), similarly prevents restoration of LDL internalization (Figure 4-8F), even with the expressed Dab2 still residing in puncta that colocalize with clathrin. By contrast, mutations to the phosphoinositide binding region (K51M

and K150E) of the ARH PTB domain are still compatible with LDL internalization (Figure 4-8G), despite strongly interfering with ARH binding to PtdIns(4,5)P$_2$ *in vitro* (Figure 4-9). This affirms that the lipid-binding surface of ARH is juxtaposed to, but functionally separate from, the FXNPXY contact site (Mishra *et al.*, 2002a; Mishra *et al.*, 2002b; Stolt *et al.*, 2004). Thus, Dab2 and ARH (when overexpressed) require engagement of both cargo and core coat components for proper LDL receptor sorting, while additional interactions with PtdIns(4,5)P$_2$ and clathrin likely increase the efficiency of the process.

4.3.3   ARH requires AP-2 to drive LDL uptake

Despite the apparent functional redundancy of Dab2 and ARH, the two CLASPs clearly engage the AP-2 adaptor in molecularly distinct ways. Dab2 has several low affinity (K_D ~50-150 μM), tandemly-arrayed α appendage-binding motifs (Mishra et al., 2002a; Morris and Cooper, 2001) while ARH might function similarly to β-arrestins, not participating directly in clathrin lattice assembly, but rather ushering LDL receptors through pre-existing coated buds. One prediction of this idea is that ARH requires AP-2 for localization to clathrin bud sites. Indeed, in AP-2+Dab2 knocked-down cells, but not with AP-2 or Dab2 knockdown alone, both transferrin and LDL receptor internalization is impaired despite normal ARH levels (Figure 4-10F). In these uptake experiments, fluorescent ligands are added directly to cells at 37°C, and in the AP-2-depleted cells (Figure 4-10B), transferrin, but not LDL, is poorly internalized and accumulates diffusely over the cell surface. Consistent with the ability of Dab2 to polymerize clathrin (Mishra *et al.*, 2002a) and drive LDL receptor internalization (Maurer and Cooper, 2005; Morris et al., 2002b), Dab2 does not exhibit a requirement for AP-2; knockdown of ARH+AP-2 dramatically impairs transferrin but not LDL receptor internalization (Figure 4-10E). Taken altogether, these experiments clearly reveal important
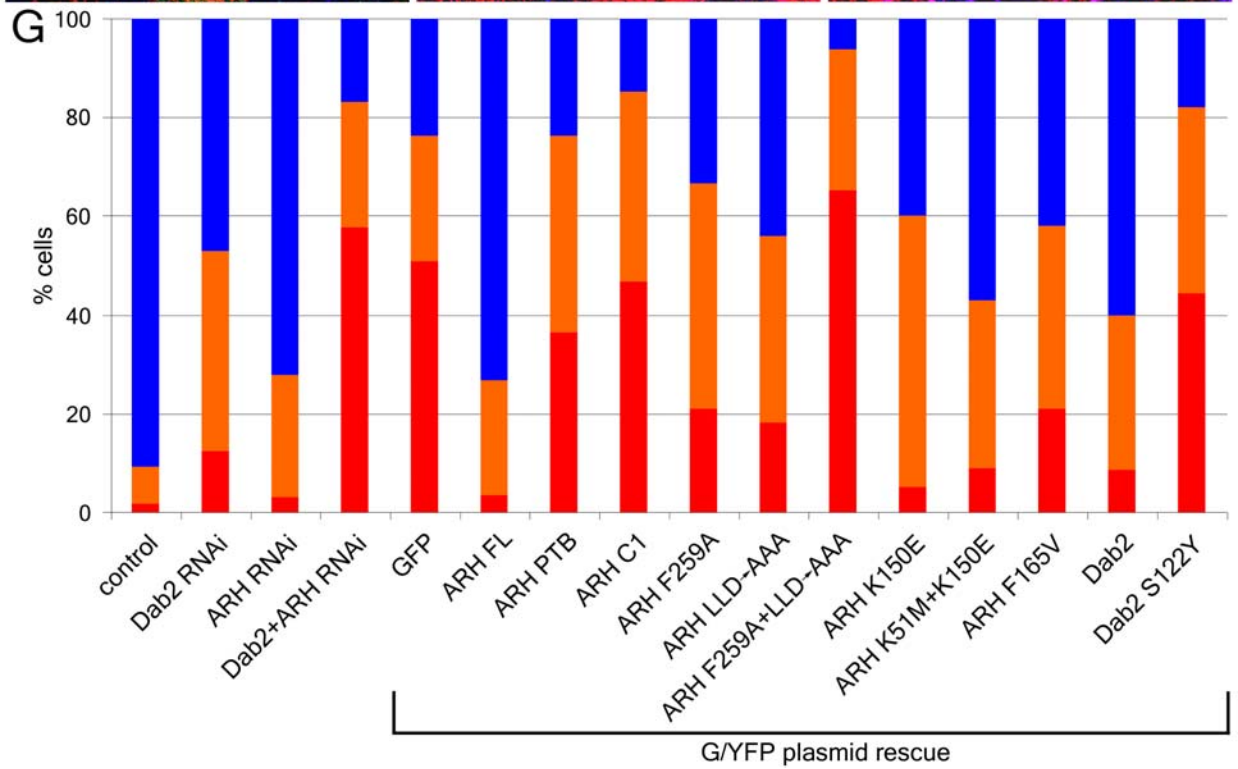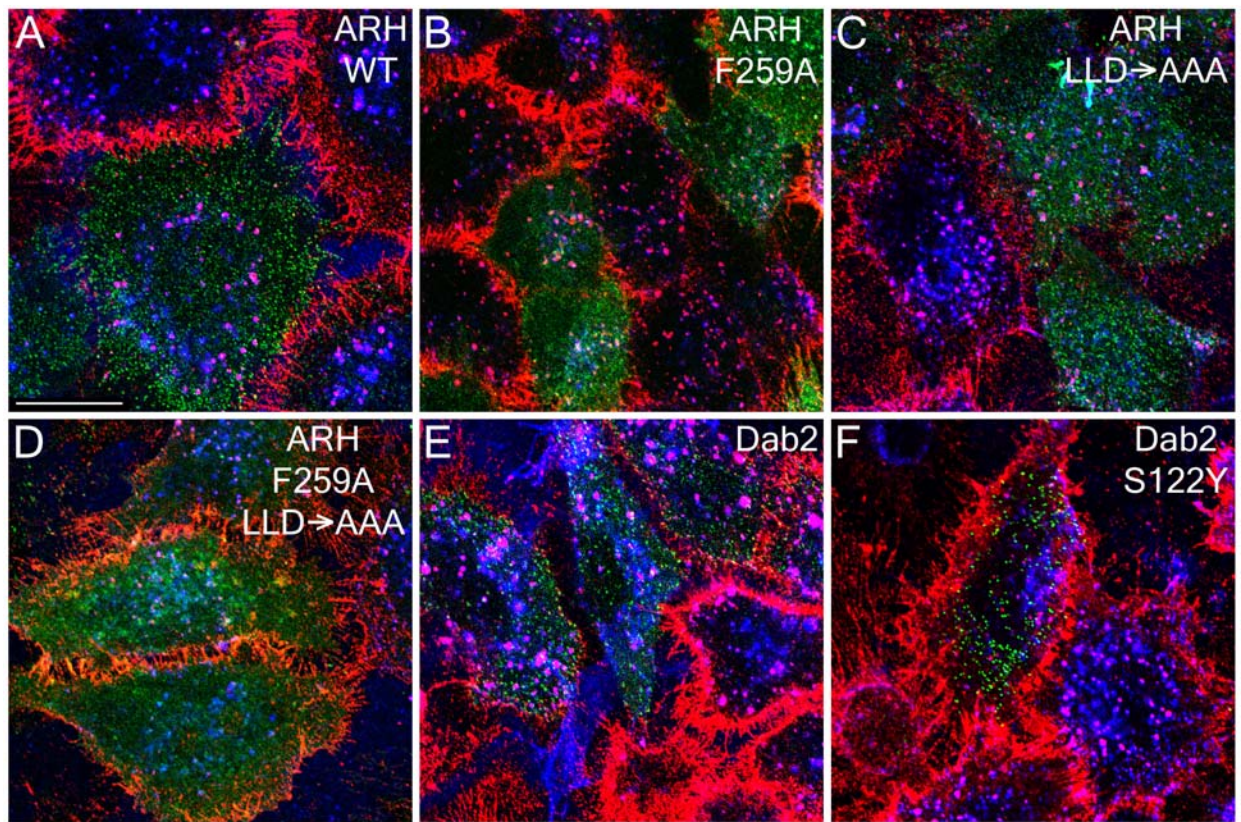
Figure 4-8 Cargo- and AP-2-binding domains of ARH and Dab2 are necessary for LDL sorting

105

Figure 4-8 Cargo- and AP-2-binding domains of ARH and Dab2 are necessary for LDL sorting

HeLa SS6 cells transiently transfected with siRNAs targeting both ARH and Dab2 along with either wild type ARH-GFP (A), or F259A (B), [212]LLD→AAA (C), F259A+[212]LLD→AAA (D) ARH mutations, or wild-type YFP-Dab2 (E) or a S122Y Dab2 mutation (F), were grown in DMEM with LPDS overnight, incubated with 4 μg/mL DiI-LDL (red) and 50 μg/mL Tfn633 (blue) for 15 min at 37ºC and then fixed. The scale bar represents 10 μm. (G) Quantitation of various ARH-GFP or YFP-Dab2 constructs rescuing LDL internalization. The percentage of cells showing normal (blue), impaired (approximating the level of LDL internalization seen in ARH or Dab2 single knockdowns) (orange), or blocked LDL internalization (red) was determined for control (n = 1194 cells), Dab2 (n = 718), ARH (n = 686) or Dab2+ARH (n = 3455) siRNA-treated cells, or for the Dab2+ARH siRNA background with rescue plasmids GFP (n = 412), ARH full length (ARH FL, n = 231), ARH residues 1-179 (ARH PTB, n = 195), ARH residues 180-308 (ARHC1, n = 177), ARH F259A (n = 235), ARH LLD→AAA (n = 93), ARH F259A+LLD→AAA (n = 178), ARH K150E (n = 20), ARH K51M+K150M (n = 91), ARH F156V (n = 110), Dab2 (n = 183) or Dab2 S122Y (n = 45).
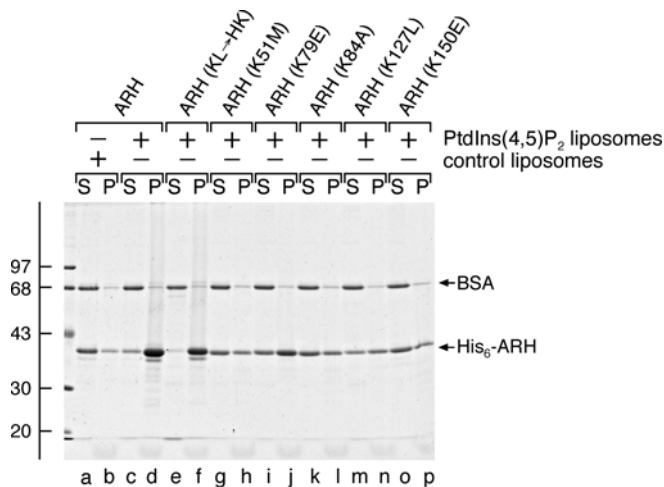
Figure 4-9 Mapping of the phosphoinositide-binding region of the ARH PTB domain

Either His6-tagged ARH (1-308) or the indicated ARH point mutants were added at a concentration 0.1 mg/ml to reactions containing 0.4 mg/ml of either control (lane a and b) or PtdIns(4,5)P2-containing liposomes (lane c-p) in the presence of 0.1 mg/ml BSA and incubated on ice for 60 min. After centrifugation, aliquots of 1/35 of each supernatant (S) or 1/5 of each pellet (P) were analyzed by SDS-PAGE and stained with Coomassie blue. The position of the molecular mass standards (in kDa) is indicated on the left. ARH (KL→HK) represents a double amino acid substitution (K84L and L85H) intended to mimic the positioning of critical Dab2 PTB domain residues involved in PtdIns(4,5)P2 binding. Note that the K51M (lane g and h) and K150E (lane o and p) mutations both severely perturb binding of ARH to the sedimented PtdIns(4,5)P2 liposomes compared with native ARH (lane c and d).

differences in the molecular mode of operation of these two CLASPs: like β-arrestin, ARH operates by directing LDL receptors to pre-existing clathrin-coated structures containing AP-2, while Dab2 can sustain clathrin-dependent LDL internalization independent of AP-2.

4.3.4 Dab2 populates the majority of surface clathrin structures

If Dab2 can maintain LDL endocytosis independent of AP-2, it is possible that this CLASP nucleates discrete clathrin coats, allowing different cargo types to be internalized within different subpopulations of coated vesicles, a possibility already suggested for certain GPCRs (Cao *et al.*, 1998), transferrin (Tosoni *et al.*, 2005), and LDL (Lakadamyali et al., 2006) receptors. In this case, Dab2 should only be present within a select subpopulation of coated structures along with the respective cargo. However, in both normal and ARH$^{-/-}$ fibroblasts at steady state, AP-2 is present in 92% of surface-proximal clathrin structures, Dab2 in 82%, and Dab2 populates 92% of the AP-2-positive structures (Figure 4-1 and Figure 4-11) (Morris and Cooper, 2001). Essentially analogous results are observed with HeLa and CV-1 cells (Figure 4-12A and B, and data not shown), clearly discrepant with the reported distribution of Dab2 in BS-C-1 cells (Lakadamyali et al., 2006), which, like CV-1 cells, are derived from the African green monkey (see below). Freeze-etch EM reveals Dab2 positioned within the majority of clathrin structures at the plasma membrane. Frequently, the CLASP appears positioned near the edges of the lattice (Figure 4-13), like eps15 (Edeling et al., 2006; Tebar et al., 1996), a Dab2 binding partner, although immunogold Dab2 labeling is also seen within regions of assembled lattice and on
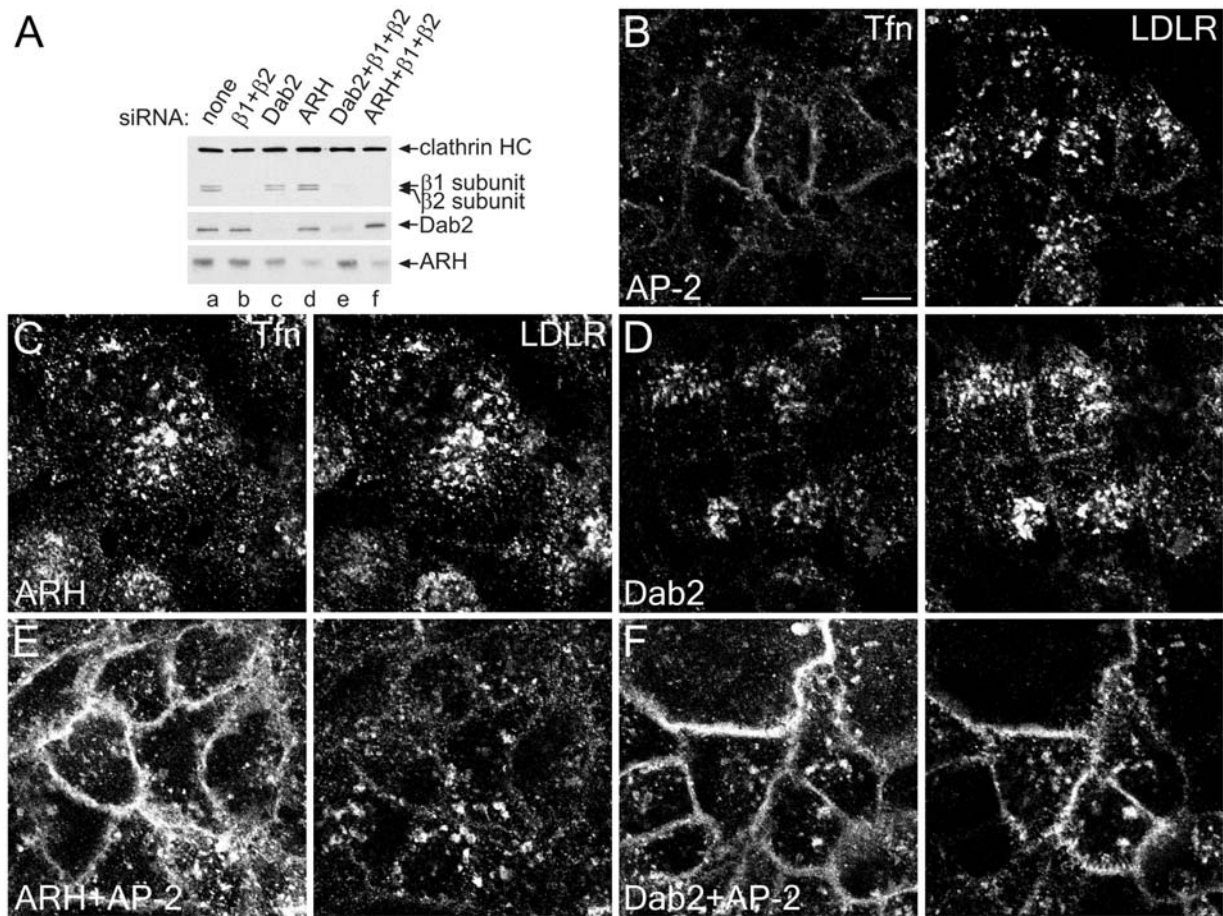
Figure 4-10 ARH requires AP-2 for LDL sorting function

HeLa SS6 cells mock transfected (A, lane a) or transfected with AP-2 (β1+β2 subunits; A, lane b; B), Dab2 (A, lane c; D), ARH (A, lane d; C), or Dab2+β1+β2 (A, lane e; F) or ARH+β1+β2 (A lane f, E) specific siRNA duplexes grown overnight in DMEM with 10% LPDS were lysed, resolved by SDS-PAGE and transferred to nitrocellulose. Portions of replicate blots were probed with anti-clathrin heavy chain mAb TD.1, anti-β1/β2 subunit mAb 100/1, or polyclonal anti-Dab2 or anti-ARH antibodies (A). Alternatively, transfected cells on coverslips were incubated for 15 min at 37ºC with 25 μg/mL Tfn568 (Tfn) and anti-LDL receptor mAb IgG-C7 (LDLR) before fixing (B-F). Representative single confocal optical sections are shown. The scale bar represents 10 μm.

buds, particularly in HeLa cells. The predominantly coat-associated distribution of Dab2 is similar to the near-perfect colocalization observed for either eps15 or epsin in HeLa, CHO and A431 cells (Chen et al., 1998; Hawryluk et al., 2006; Yim et al., 2005).

Moreover, the distribution of Dab2 is paralleled by the LDL receptor; the vast majority (84-89%) of surface LDL (and transferrin; 89-93%) is found in Dab2-positive puncta (Figures 4-11 and 4-12). In fibroblasts, 77% of ARH positive puncta are positive for the LDL receptor and, at steady state, LDL, transferrin and clathrin signals are also highly coincident in both HeLa cells and fibroblasts; 88% of clathrin light-chain positive structures contain transferrin, 81% contain LDL, and 56% have both transferrin and LDL signals when fibroblasts are labeled simultaneously with both ligands on ice (Figures 4-11 and 4-12). Upon adding LDL to cells at 37°C, YFP-Dab2 and endogenous ARH colocalize with LDL receptors during the initial period of LDL uptake, but diverge within 5 min (Figure 4-12G and H). Also, in HeLa cells, 95% of eps15 positive structures contain LDL receptors (Figure 4-12C), again attesting to the occurrence of numerous CLASPs within a single assembling coat. EM views of replicas of the external surface of fibroblasts show oval, ~25 nm LDL particles clustered around and within invaginations (coated buds; Figure 4-13E) (Heuser, 1980; Heuser and Anderson, 1989; Sanan et al., 1987). HeLa cells, too, have LDL massed at presumptive bud site invaginations (Figure 4-13F). I also note that the extent of LDL receptor upregulation upon culture in lipoprotein deficient serum is not uniform in all cells, so adjacent cells often display different LDL receptor densities at the surface (Figure 4-12B and 4-15D). Dab2 is nevertheless distributed throughout surface clathrin structures and, indeed, there is little difference in the subcellular distribution of Dab2 between cells grown in whole or lipoprotein deficient serum (Figure 4-11). In sum, at least for constitutively endocytosed receptors, I find little evidence of obvious compartmentalization
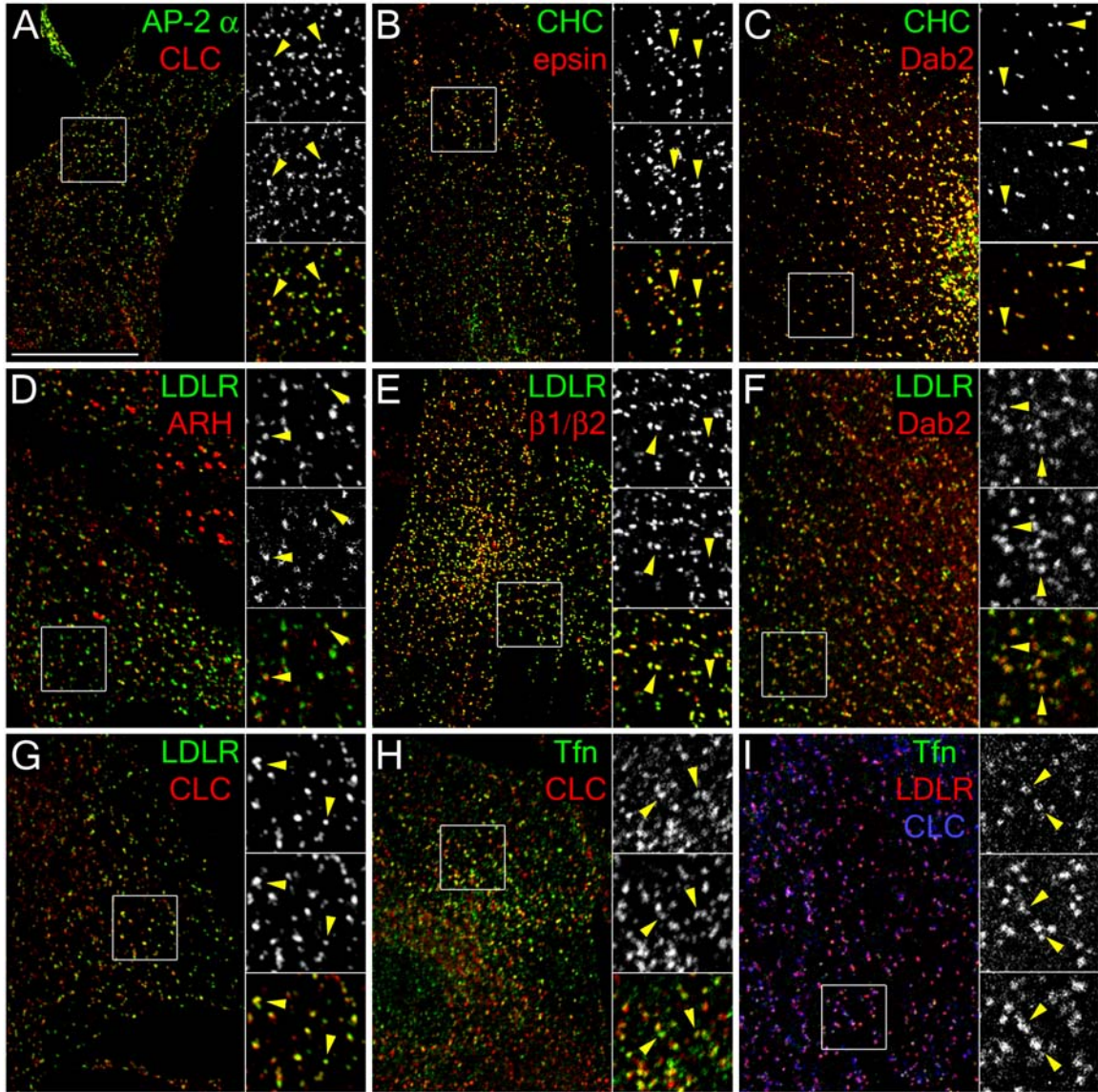
Figure 4-11 CLASPs and surface LDL receptors localize to the majority of endocytic clathrin coats in fibroblasts

Control GM01386 fibroblasts grown in 10% normal FCS (A-C) or 10% LPDS (D-I) overnight were either fixed and stained with anti-AP-2 α-subunit mAb AP.6 and anti-clathrin light chain antibody R461 (A), anti-clathrin HC mAb X22 and either anti-epsin antibody (B), or anti-Dab2 antibody (C), or surface labeled with anti-LDL receptor mAb IgG-C7 on ice, fixed and stained with either anti-ARH antibody (D), anti-AP-1/2 β1/β2-subunit antibody GD/1 (E), or anti-Dab2 antibody (E), or anti-clathrin light chain antibody R461 (G), or surface labeled with Tfn488, fixed and stained with anti-clathrin light chain antibody R461 (H). Alternatively, cells were surface labeled with both Tfn488 and anti-LDL receptor mAb IgG-C7 on ice, fixed and stained with anti-clathrin light chain antibody R461 (I). Representative single confocal optical sections of fixed cells are shown with color-separated and merged magnifications of each boxed region shown on the right. The scale bar represents 10 μm.
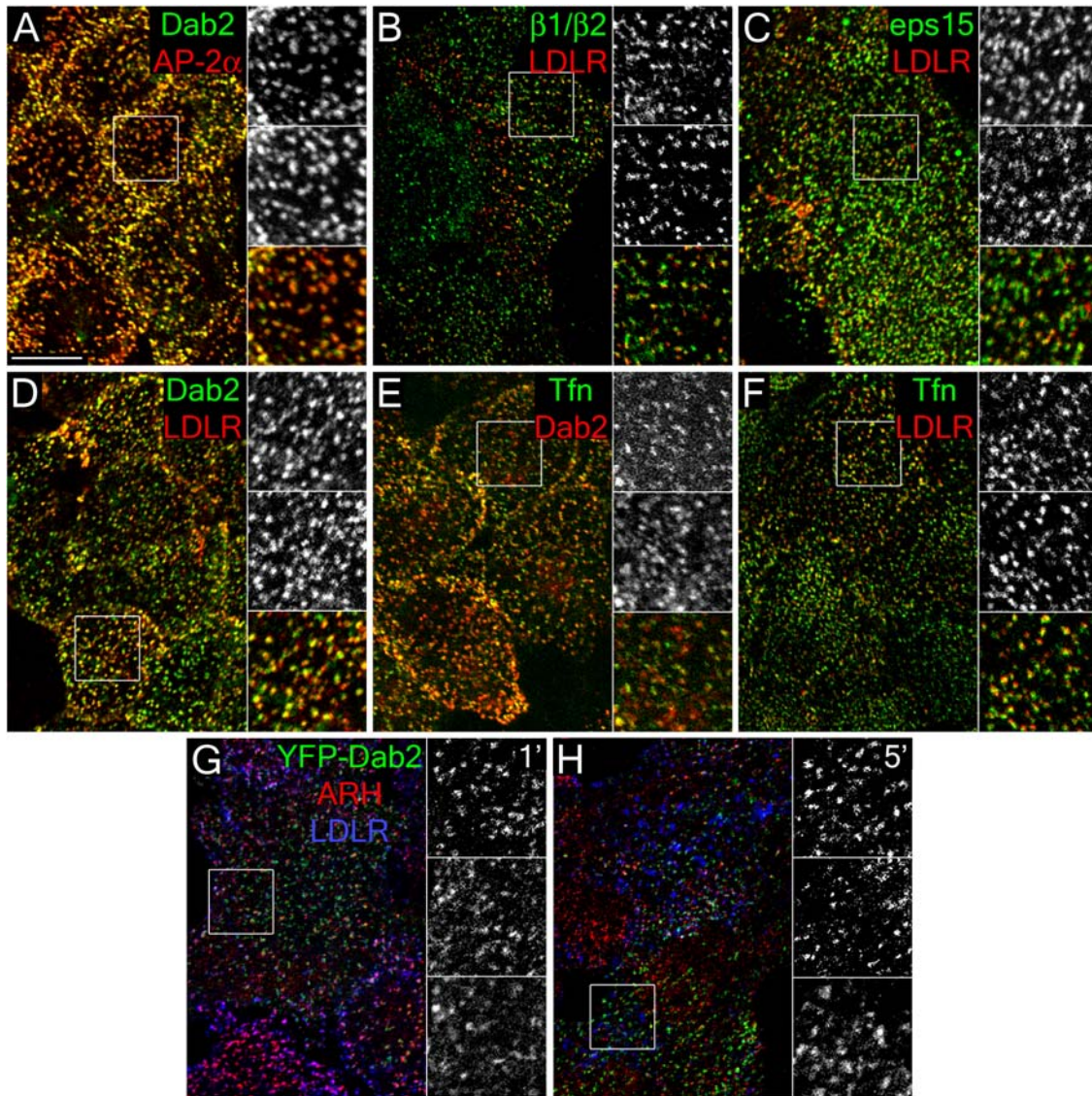
Figure 4-12 General localization of CLASPs and LDL receptors to endocytic coated structures at steady state

HeLa SS6 cells cultured in DMEM containing 10% LPDS overnight were either fixed and stained with anti-Dab2 antibody and anti-AP-2 α-subunit mAb AP.6 (A), or surface labeled with anti-LDL receptor mAb IgG-C7 (LDLR), fixed and stained with either affinity-purified anti-AP-1/2 β1/β2-subunit GD/1 (B), anti-eps15 (C), or anti-Dab2 (D) antibodies, or surface labeled with Tfn488 (Tfn), fixed and stained with anti-Dab2 antibody (E), or surface labeled with both Tfn488 and anti-LDL receptor mAb IgG-C7 (F). Representative single confocal optical sections are shown with color-separated and merged magnifications of each boxed region shown on the right. Alternatively, HeLa SS6 cells transfected with YFP-Dab2 were incubated with anti-LDL receptor mAb IgG-C7 for 1 (G) or 5 min (H) at 37°C, fixed, and stained with anti-ARH antibody. The scale bar represents 10 μm.
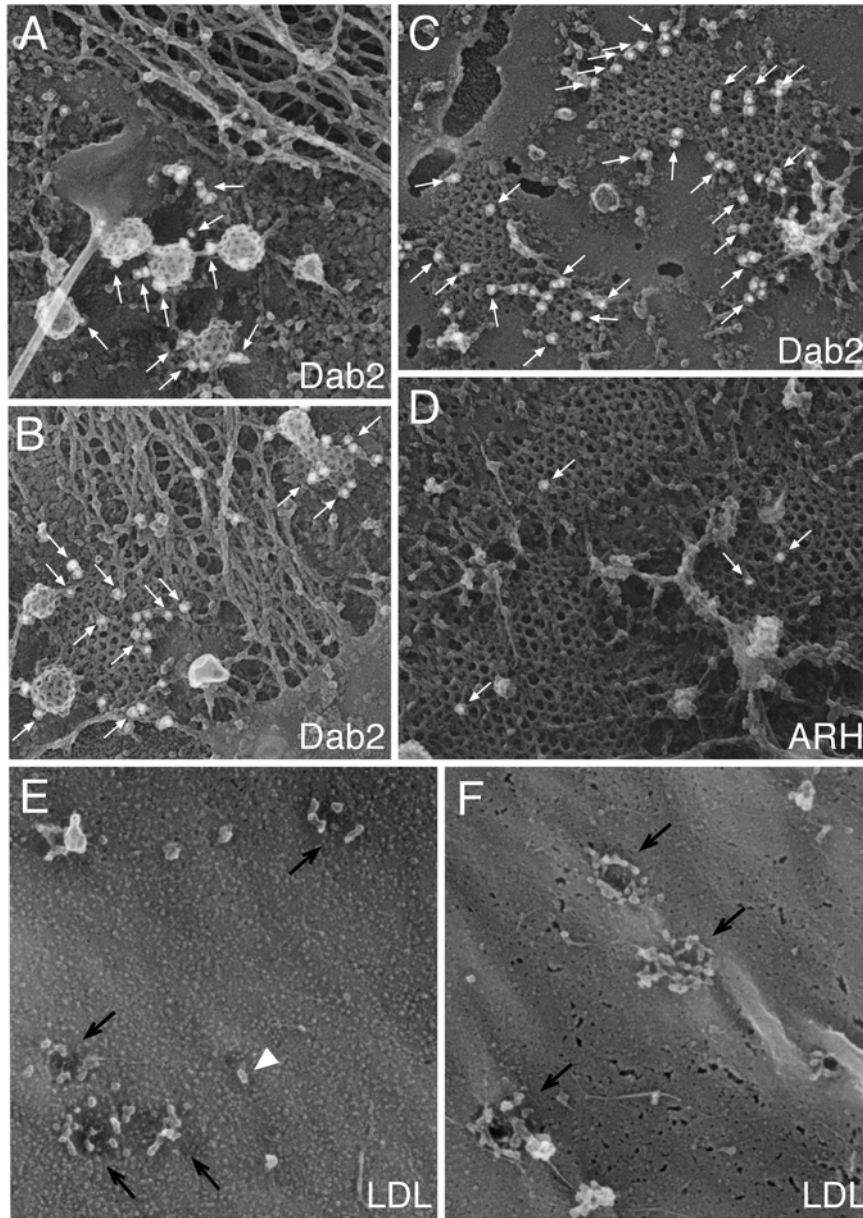
Figure 4-13 Ultrastructural localization of Dab2, ARH and LDL in clathrin coats

(A-F) Fixed plasma membrane sheets prepared from control GM01836 fibroblasts (A , D, and E) or HeLa cells (B, C, and F) were labeled with either affinity-purified anti-Dab2 or ARH antibodies and then secondary antibodies conjugated to 15-nm colloidal-gold particles. Individual gold particles appear as white spheres (arrows) and representative freeze-etch images show the spatial distribution of endogenous Dab2 and ARH. (E and F) Control fibroblasts (GM01386, E) or HeLa cells (F) incubated in 10% LPDS for 24 h were incubated with 50 μg/ml LDL at either 0°C (F) or 37°C (E) and fixed before preparation of replicas of the external cell surface. Individual LDL particles (arrowheads) and invaginated pits (arrows) are indicated.

112

of incoming cargo within functionally distinct surface clathrin-coated structures, and the localization of FXNPXY-recognizing CLASPs to endocytic coats appears independent of receptor level fluctuations.

4.3.5 Spatio-temporal analysis of CLASPs during LDL internalization

The small dispersed surface puncta that transiently overexpressed YFP-Dab2 and ARH-GFP both localize to in HeLa cells (Figure 4-8 and 4-12) contain AP-2 and clathrin (not shown). In these structures, the recovery of Y/GFP fluorescence following photobleaching reinforces the adaptor-like properties of these CLASPs (Figure 4-14A and B). YFP-Dab2 repopulates bleached puncta with a $t_{1/2}$ of ~15 s, analogous to clathrin and AP-2 (Wu *et al.*, 2001; Wu *et al.*, 2003), while ARH-GFP recovers slightly quicker ($t_{1/2}$ = ~9 s) (Figure 4-14C). Typically, >85% of the pre-bleach puncta rapidly reacquire up to ~70% of the initial fluorescence in these experiments, consistent with both Dab2 and ARH cycling between soluble and membrane-bound states. Yet, despite dynamic oscillation of Dab2 and ARH at bud sites, many surface structures appear comparatively immobile over time, a behavior typically observed for tagged clathrin, AP-2, and other endocytic components (Bellve et al., 2006; Gaidarov et al., 1999b; Keyel et al., 2004; Merrifield et al., 2005; Rappoport et al., 2003a) but which, nonetheless, correlates with endocytic uptake (Bellve et al., 2006). In time-resolved images of transiently transfected HeLa cells, added DiI-LDL initially clusters at YFP-Dab2-positive surface puncta while, 5-20 min later, internalized LDL within larger, mobile endosomes is not colocalized with Dab2 (Figure 4-14E, Movie 4-2); instead, rapid lateral LDL translocations indicative of directed endosome movement are apparent (Movie 4-2 and Figure 4-14E, kymograph). Consequently, I judge the small

113
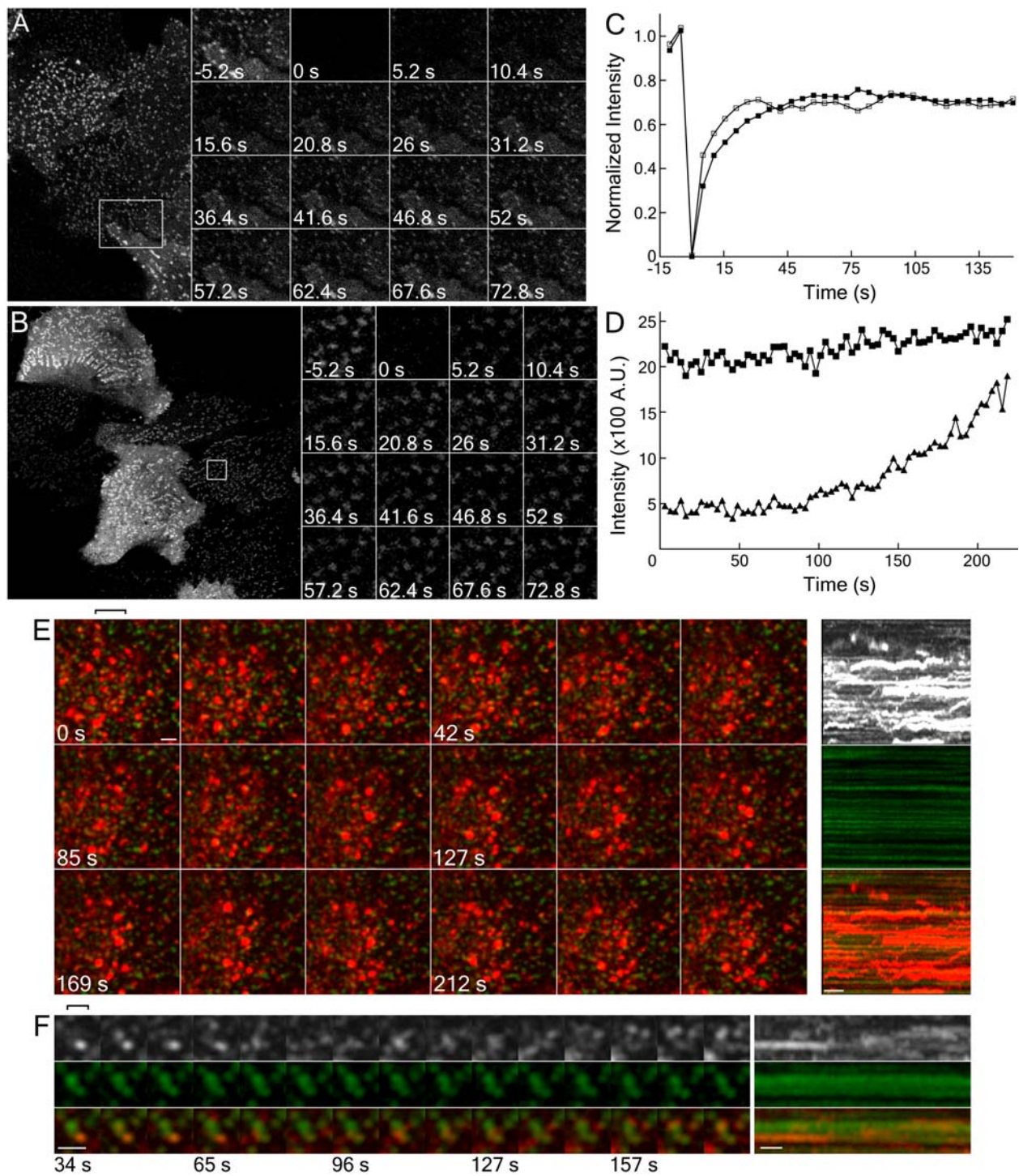
Figure 4-14 Live cell dynamics of Dab2 and ARH

Figure 4-14 Live cell dynamics of Dab2 and ARH

HeLa cells transiently transfected with either YFP-Dab2 (A) or ARH-GFP (B) were photobleached (boxed region) with a 405 nm laser at time 0 and imaged every 5.2 s to follow recovery of the fluorescent signal. Magnified views of the bleached region at the indicated times are shown in the insets. (C) Normalized fluorescence intensity of YFP-Dab2 (14 separate cells, filled squares) and ARH-GFP (29 separate cells, open squares) within the bleached regions. (D-F) YFP-Dab2 (middle panels, green) transfected HeLa cells were grown in LPDS overnight, incubated with 4 μg/mL DiI-LDL (top panels, red) and imaged every 3.3 (D) or 3.4 (E, F) s either during LDL addition (D) or 21 min later (E, F). (D) Quantitation of the fluorescence intensity of 17 structures during early time points shows that the intensity of LDL (filled triangles) accumulates in these Dab2-positive structures (filled squares). The averaged intensity for Dab2 and LDL in all these structures is shown. (E and F) At later time points, the internalized DiI-LDL has moved to larger, brighter YFP-Dab2-negative endosomal compartments, though LDL still accumulates and internalizes from surface Dab2-positive structures. Importantly, the concentration of LDL used in these experiments is ~10-fold below the saturating concentration at 37°C (>50 μg/ml (Brown and Goldstein, 1986)), so only a subset of surface LDL receptors are marked with fluorescent ligand. A cluster of selected surface YFP-Dab2 structures containing LDL, indicated with the rectangle in E, is magnified in F. Separation of the DiI-LDL signal from the Dab2-YFP and local movement of the internalized vesicle are evident. E and F are from Movie 2. The brackets indicate the vertical position from each image set used to generate the kymograph. The scale bar represents 10 μm in A, B, 1 μm in E, and 500 nm in F and the kymograph scale bar represents 20 s. Note the striking differences in the dynamics of the Dab2-YFP and DiI-LDL structures seen in the kymographs.

relatively immobile spots to be coats assembling at the plasma membrane. Similar DiI-LDL-containing clusters are seen in HeLa cells expressing ARH-GFP, GFP-epsin 1, or GFP-clathrin light chain (LCa) (not shown), verifying the surface positioning these structures and, again, showing LDL concentrates in clathrin regions containing various CLASPs. At these small peripheral structures, LDL can be seen to accumulate within a min or two following addition of DiI-LDL (Figure 4-14D and E) and, in general, LDL concentrates in these puncta (Figure 4-14D).

The temporal relationship between Dab2 and LDL in these data sets can be categorized into what appear to be distinct types of budding events. For example, occasions where both Dab2 and LDL signals disappear from the optical section simultaneously occur. More frequently, overlapping Dab2- and LDL-positive puncta separate and the Dab2 signal is lost rapidly revealing an LDL positive endocytic vesicle (Figure 4-14F), which moves locally and often fuses with an adjacent vesicle. Also noticeable are larger LDL-rich endosomes moving close to the plasma membrane surface that consume local cargo emerging from assembled Dab2 zones (Movie 4-2). The behavior of these structures is strikingly reminiscent of the consumption of just internalized endocytic vesicles by actin-dependent directed-movement of cargo-laden endosomal vesicles recently reported in *S. cerevisiae* (Toshima et al., 2006). Altogether, my imaging studies confirm that the spatio-temporal behavior of Dab2 and ARH is consistent with a proposed role as FXNPXY-selective CLASPs. Further, the data reveal a dense subsurface population of dynamic, LDL-positive transport vesicles and a substantial degree of rapid homogenization/intermingling of the internalized ligand within early sorting endosomes.

4.3.6 Regulated Dab2 expression in hepatocytes

Finally, if Dab2 and ARH are both generally present in surface coated buds and can operate analogously to promote LDL receptor internalization, why is ARH so crucial for maintaining normal plasma levels of LDL *in vivo*? One potential explanation is tissue-specific expression patterns of Dab2 and ARH. Comparisons of rat liver homogenate, purified Golgi membranes and isolated plasma membrane sheets show dramatically different overall protein compositions (Figure 4-15A, lane a-c) and the expected enrichment of AP-1 at the Golgi and AP-2 on the

plasma membrane (Figure 4-15A, lane g-i). However, both Dab2 and ARH are similarly enriched within the isolated plasma membrane preparation. These sheets are purified from whole liver homogenates (Hubbard *et al.*, 1983) but when separated hepatocyte and non-hepatocyte fractions are compared, Dab2 is strikingly absent from asialoglycoprotein receptor-positive hepatocytes, although the CLASP is well expressed in the nonparenchymal (Kupffer and sinusoidal endothelial, and hepatic stellate cells) fraction (Figure 4-15B). By contrast, ARH and epsin 1 are present in both populations. Purified rat hepatocytes express less Dab2 protein at steady state than previously characterized cultured cell lines with downregulated Dab2 (MDA-MB-231 and MCF-7) (Fazili *et al.*, 1999) although, again, ARH levels are roughly comparable. Also of note, HepG2, a human hepatoma line and BS-C-1 cells also contain low relative levels of Dab2 (Figure 4-15B). Yet, in my experiments, BS-C-1 cells still cluster LDL receptors at the majority AP-2 (σ2-GFP) containing structures (Figure 4-14C), and at many surface clathrin (LCa-GFP) puncta (Figure 4-15D). These results again reinforce the redundancy between ARH and Dab2, and differ from a recent report showing only ~30% of surface clathrin structures associated with labeled LDL in BS-C-1 cells (Lakadamyali et al., 2006). I conclude that since the vast majority of plasma LDL is cleared/degraded by hepatocytes *in vivo* (Osono *et al.*, 1995), the exceedingly low level of Dab2 present in this cell type is fully consistent with the phenotype that results from inheritance of two mutant ARH alleles; although nonparenchymal cells may be able to internalize LDL in an ARH^{-/-} background, hepatocytes are clearly unlikely to internalize FXNPXY signals normally.
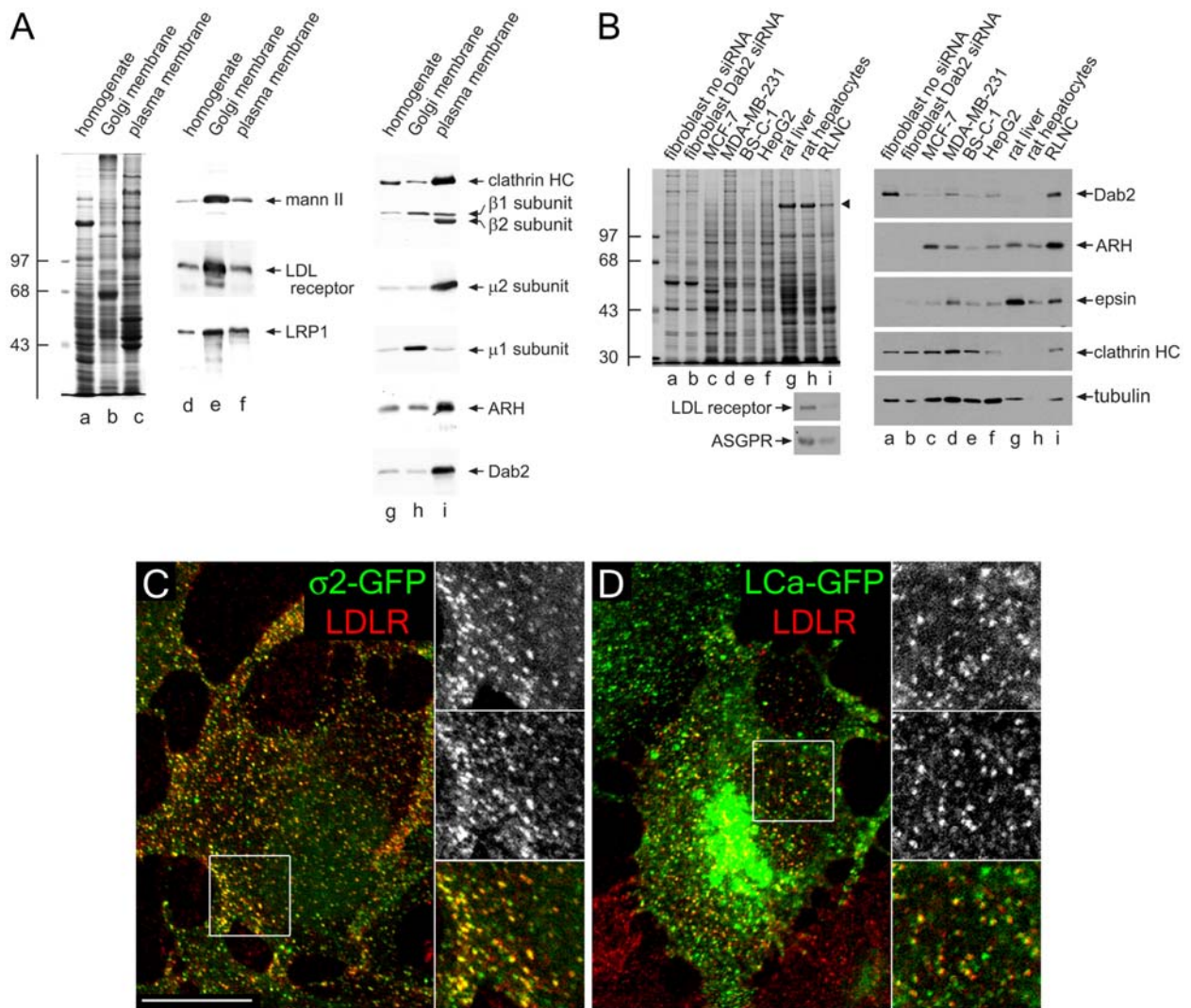
Figure 4-15 Cell-type-specific expression of Dab2 in the liver

Figure 4-15 Cell-type-specific expression of Dab2 in the liver

(A) Samples of 25 μg of rat liver homogenate (lane a, d and g), purified rat liver Golgi membranes (lane b, e and h) or rat liver plasma membrane sheets (lane c, f and i) were resolved by SDS-PAGE and either stained with Coomassie blue (lane a-c) or transferred to nitrocellulose (lane d-i). Portions of replicate blots were probed with antibodies directed against α-mannosidase II (mann II), the LDL receptor, LRP1, clathrin heavy chain (HC), AP-1/2 β1/β2 subunits, AP-2 μ2 subunit, AP-1 μ1 subunit, ARH, or Dab2. The position of the molecular mass standards (in kDa) is indicated on the left. (B) Lysates from ARH-/- fibroblasts either mock (lane a) transfected or transfected with Dab2 siRNA (lane b), MCF-7 (lane c), MDA-MB-231 (lane d), BS-C-1 (lane e), or HepG2 (lane f) cultured cell lines, rat liver homogenate (lane g), rat hepatocyte (lane h), or rat liver non-hepatocyte cell (RLNC, lane i) lysates were resolved by SDS-PAGE under reducing (top left, right panels) or non-reducing (bottom left panels) conditions and stained with Coomassie blue (top left) or transferred to nitrocellulose. A major 180-kDa hepatic polypeptide that prevents efficient transfer of the clathrin heavy chain onto nitrocellulose is indicated on the stained gel (arrowhead). Relevant portions of the blots were probed with affinity-purified anti-Dab2, anti-ARH, anti-epsin or rat-specific anti-LDL receptor polyclonal antibodies, or anti-clathrin HC mAb TD.1, anti-tubulin mAb E7, or anti-asialoglycoprotein receptor mAb 8D7. Analogous results are obtained using an independent goat anti-Dab2 antibody (not shown). (C-D) BS-C-1 cells stably expressing either AP-2 σ2-GFP (C, green) or clathrin LCa-GFP (D, green) were grown overnight in DMEM containing LPDS, surface labeled with anti-LDL receptor mAb C7 (LDLR, red) on ice. Representative single confocal optical sections of fixed cells are shown with color-separated and merged magnifications of each boxed region shown on the right. The scale bar represents 10 μm.

4.4   DISCUSSION

Clathrin-coated vesicles are high-capacity carriers that efficiently shuttle numerous cargo types into the cell interior in a generally non-competitive manner (Marks *et al.*, 1996; Santini *et al.*, 1998; Warren *et al.*, 1998). While it is well accepted that cargo selection depends upon adaptors, here I provide functional evidence that efficient internalization of the LDL receptor is only indirectly dependent upon the AP-2 adaptor, and can, if driven by Dab2, occur in the absence of the heterotetramer. Thus, these experiments formally validate the CLASP hypothesis (Robinson, 2004; Sorkin, 2004; Traub, 2003) and lead to three major conclusions. First, the FXNPXY-selective CLASPs ARH and Dab2 operate in a functionally redundant fashion, despite engaging the clathrin coat machinery in molecularly distinct ways; these proteins operate analogously to, and in parallel with, AP-2-dependent sequestration of transferrin receptors (Hinrichsen *et al.*, 2003; Motley *et al.*, 2003) and epsin/eps15/eps15R-mediated sorting of poly/multiubiquitinated proteins (Barriere et al., 2006; Duncan et al., 2006a; Hawryluk et al., 2006; Wang et al., 2006). Very similar results revealing both the cargo selectivity and functional redundance of ARH and Dab2 have been obtained in two independent studies (Jonathan Cooper and Anne Soutar, personal communication). Second, when Dab2 is present at 'normal' cellular levels, the CLASP generally populates most clathrin-coated structures along with AP-2, epsin, and eps15,

independent of LDL receptor expression levels. Third, Dab2 expression is cell-type specific and, consequently, appears to underlie the hypercholesterolemic phenotype observed in both ARH-nullizygous patients and mice.

Given the selectivity and ability of certain CLASPs to sustain clathrin-mediated endocytosis in the absence of AP-2, refined models positing biased sorting of different cargo classes into discrete subpopulations of surface clathrin coats have been proposed (Lakadamyali et al., 2006; Tosoni et al., 2005). In one model, the protein SH3BP4, newly-christened transferrin receptor trafficking protein (TTP), restricts TfR to a distinct, but partially overlapping, subset of coated pits from the LDL and EGF receptors in HeLa cells (Tosoni et al., 2005). TTP contains an SH3 domain that interacts with both the PRD of dynamin and an unconventional SH3 domain binding site on the TfR, along with clathrin and AP-2 binding determinants, likely responsible for TTP enrichment in coated pits and colocalization with TfR. (Tosoni et al., 2005). Either ablation or overexpression of TTP are reported to selectively block TfR, but not EGF receptor, internalization (Tosoni et al., 2005). This suggests that TTP is a TfR-specific sorting adaptor. Furthermore, TTP does not colocalize with EGF receptors, and the general colocalization reported between EGF, LDL and Tfn receptors in HeLa cells did not exceed 30% (Tosoni et al., 2005). This distinct population of TfR positive coated pits is thought to be generated by the interaction of TTP with non-tyrosine phosphorylated dynamin (Tosoni et al., 2005). Dynamin can become tyrosine phosphorylated by activated receptor tyrosine kinases such as the EGF receptor (Tosoni et al., 2005). Similarly, dynamin is thought to be phosphorylated in the presence of LDL receptors in coated pits (Tosoni et al., 2005). Thus, TTP only localizes to coated pits lacking activated EGF receptors, or LDL receptors, and hence, tyrosine-phosphorylated

dynamin, and driving TfR into only these coated pits. In summary, this model suggests that TfR is only present in a subpopulation of coated pits, that this asymmetry is generated after dynamin recruitment to the coated pit, and that any AP-2 present in EGF or LDL receptor positive pits cannot sort TfR without TTP.

Another model proposing the biased sorting of cargo proposes that cargo destined for lysosomal degradation is preferentially sorted into a subset of coated pits, while recycled cargo generally targets all coated pits. This model arose out of studies of endosomal dynamics. About 35% of early endosomes, defined as Rab5 positive structures, rapidly acquire the late endosomal marker Rab7, and become highly dynamic (Lakadamyali et al., 2006). It was observed that cargo destined for the lysosome, such as LDL or EGF, was preferentially enriched in this dynamic subset, with ~80% of each ligand present in this subset, while Tfn was generally delivered to all Rab5 positive endosomes (Lakadamyali et al., 2006). Investigations into the origin of this segregation suggested that it occurred at the surface for three reasons. First, there was insufficient time between clathrin uncoating and acquisition of Rab5 for segregation of cargo (Lakadamyali et al., 2006). Secondly, in the context of AP-2 siRNA, there was an 8-fold decrease in the number of static Rab5 structures, suggesting that the majority of static Rab5 structures arise from AP-2 positive coated pits (Lakadamyali et al., 2006). Finally, when the BS-C-1 cells were either labeled with subsaturating concentrations of LDL, or stained for Dab2, only 15-30% of coated pits contained either LDL or Dab2, suggesting that coated pits with alternate adaptors give rise to the dynamic pool of endosomes that rapidly acquire Rab7 (Lakadamyali et al., 2006). In contrast to the previous model, this model posits that recycled cargo like Tfn is

nonspecifically targeted to all coated pits, while it is cargo destined for the lysosome that is restricted to a specialized subset of coated pits, possibly via the asymmetric localization of Dab2 or other CLASPs.

I believe that CLASPs are unlikely to target/generate distinct populations of clathrin-coats for several reasons. First, classic EM studies document the colocalization of various cargo within single budding profiles at the plasma membrane: for example, LDL and α_2-macroglobulin (LRP1) (Via *et al.*, 1982), transferrin and asialoglycoprotein (Neutra *et al.*, 1985; Stoorvogel *et al.*, 1987), lysosomal hydrolases (mannose 6-phosphate receptor) and α_2-macroglobulin (Willingham *et al.*, 1981), LDL and EGF (Carpentier *et al.*, 1982), EGF and transferrin (Hanover *et al.*, 1984), and EGF and α_2-macroglobulin or adenovirus (Willingham *et al.*, 1983). Further, active segregation of CLASPs and cargo would certainly require energy but, as most cargo sorted by clathrin-mediated events converge in a common early endosome population (Ajioka and Kaplan, 1987; Dunn *et al.*, 1989; Maxfield and McGraw, 2004), any advantage of presorting various cargo would evidently be eliminated. In non-polarized cells, peripheral Rab5-positive LDL-containing early endosomes mature by fusing with other Rab5- and transferrin/LDL-positive structures; homotypic fusion is estimated to occur once or twice per min as early endosomes expand in size over ~10-15 min, mingling incoming endocytic vesicle contents (Rink *et al.*, 2005). Rab4-containing tubules emanate from these early endosomes, allowing transferrin to exit while LDL (and other molecules destined for degradation) concentrates within the vacuolar portion of the sorting endosome. There is a replete literature showing LDL,

asialoglycoprotein and transferrin initially enter common sorting endosomes and segregate with a $t_{1/2}$ of ~2.5 min (Dunn et al., 1989; Ghosh et al., 1994; Maxfield and McGraw, 2004; Stoorvogel et al., 1987), and the combined data have been synthesized into a general model for the iterative processing of cargo types that accompanies endosome maturation (Maxfield and McGraw, 2004). The enlarged LDL-positive late endosomes that ensue (Figure 4-4 and 4-14, Movie 2) must mean that LDL-carrying structures fuse together as the endosome transits toward the lysosome and converts to a Rab7-positive stage. The time frame of this transition from small Rab5-positive to large Rab7-positive endosomes is about 20-40 min (Ghosh *et al.*, 1994; Rink *et al.*, 2005), in excellent agreement with classic data showing that detection of LDL degradation products requires >30 min following initial internalization (Brown and Goldstein, 1986). With this general and extensively substantiated model for endosome maturation along the degradative pathway, the teleological benefit of targeting a population of LDL-laden coated vesicles to a Rab7 positive status within only a few min (Lakadamyali et al., 2006) is not at all obvious to me. In this regard, it is also worth noting that although LDL moves to the late endosome for catabolism, the LDL receptor has a long biological life (~20 h) and follows a different trajectory, recycling back to the surface roughly five/six times per hour in fibroblasts (Brown and Goldstein, 1986), similar to the transferrin receptor. Furthermore, the slowed progression of LDL toward the late endosome reported after EGF stimulation (Rink *et al.*, 2005) tends again to argue against compositionally-distinct partitioning of LDL into a subset of clathrin structures at the cell surface.

Perhaps a more serious concern with the general idea of cargo-specific coats at the plasma membrane is that I believe there is currently no plausible mechanistic basis for their formation. Cargo-selective CLASPs, including β-arrestins, epsin, ARH and Dab2, bind with relatively high affinity to clathrin and PtdIns(4,5)P$_2$, general components of all surface clathrin structures, as well as to AP-2. The membrane and cytosolic pools of these adaptors exchange rapidly, with a t$_{1/2}$ of ~15 s (Figure 4-14) (Wu *et al.*, 2003; Yim *et al.*, 2005), permitting soluble adaptors to interchange repeatedly at each clathrin bud during its 20-90 s lifetime (Gaidarov et al., 1999b; Merrifield et al., 2002; Wu et al., 2003). Therefore, an ongoing and efficient segregation mechanism would be necessary to ensure the conversion of random CLASP encounters with assembling lattices into differential patterning of CLASPs within only a subset of coats, rather than in all of them. Yet, several time-resolved imaging studies demonstrate that fluorescently tagged β-arrestins populate virtually all detectable clathrin structures at the surface following ligand activation of a suitable GPCR (Santini *et al.*, 2002; Scott *et al.*, 2002). ARH accesses clathrin coats in a manner strictly analogous to β-arrestins, by binding to the AP-2 β2 appendage platform and the clathrin heavy chain terminal domain. Indeed, ectopically expressed ARH-GFP is found in the majority of clathrin structures on the surface (Figure 4-14B). Thus, my current understanding of the dynamics and points of contact between CLASPs and the core clathrin machinery makes the assembly and maintenance of compositionally distinct buds improbable, and is clearly inconsistent with the steady-state distribution of Dab2 (Morris and Cooper, 2001), ARH, surface LDL receptors (Anderson *et al.*, 1978; Heuser and Anderson, 1989; Sanan and Anderson, 1991) and epsin 1 (Chen et al., 1998; Hawryluk et al., 2006; Yim et al., 2005) in several cell types.

Instead, my data show specifically that Dab2 is present in the majority of clathrin structures at the surface, consequently allowing clustering of LDL. I cannot, however, rule out that under some circumstances, regulation of CLASP cargo-engagement properties, perhaps by phosphorylation as occurs with AP-2 (Honing et al., 2005; Olusanya et al., 2001), limits the composition of single clathrin buds by focally disabling certain CLASPs within the assembled coat. However, regulation by dynamin tyrosine phosphorylation is unlikely for several reasons. Dynamin is thought to be one of the later factors recruited to the coated pit, limiting the amount of time the coated pit would have for cargo selection. Dynamin is also thought to be tethered to coated pits by accessory proteins which require the TfR-binding AP-2. Thus, some mechanism would need to exist to couple either AP-2 displacement or dephosphorylation to dynamin tyrosine phosphorylation to prevent AP-2 mediated TfR recruitment to EGF or LDL receptor positive coated pits. Furthermore, any TfR recruited prior to dynamin phosphorylation would need sufficient time between dynamin tyrosine phosphorylation and vesicle scission to diffuse out of the coated pit.

It is also conceivable that massed cargo could stabilize CLASPs in the assembly zone to generate cargo-selective buds, but this would apparently require preferential entry of transmembrane cargo into specific, but not all, coat-forming regions on the plasma membrane. Yet, LDL receptors are seemingly dispersed randomly over the surface membrane upon reinsertion from recycling endocytic vesicles, as are internalization-defective LDL receptors (Sanan *et al.*, 1987). The deep-etch images reveal that Dab2 is frequently positioned around the rims of the clathrin lattice. This may be due, in part, to association of Dab2 with eps15, which is

almost exclusively positioned at lattice edges (Edeling et al., 2006; Tebar et al., 1996). Similar visualization of LDL particles on the extracellular plasma membrane surface (Heuser, 1980; Heuser and Anderson, 1989; Sanan and Anderson, 1991; Sanan et al., 1987), as well as thin section analysis (Handley et al., 1981; Orci et al., 1978; Paavola et al., 1985), often shows clustered peripheral LDL particles, positioned circumferentially around the involuting bud (Figure 4-13). While epitope masking that reduces detection of Dab2 within the lattice interior cannot be ruled out, it is probable this peripheral clustering of LDL is due to deposition of Dab2 near the edges. My live cell data show some YFP-Dab2 does, on occasion, accompany LDL on a budding vesicle, and I also do observe some Dab2 labeling within the lattice, on invaginating buds, and in coated vesicle preparations (Hawryluk *et al.*, 2006). ARH, on the other hand, appears to be found predominantly in the interior of clathrin lattices, occasionally on invaginating regions. Although the density of ARH labeling is low, this finding is consistent with ARH and β-arrestin playing similar roles and β-arrestin being enriched in preparations of purified coated vesicles (Blondeau *et al.*, 2004). In time-resolved studies, the majority of the YFP-Dab2 signal at surface puncta is relatively immobile, in accord with other endocytic proteins (Bellve et al., 2006; Keyel et al., 2004; Rappoport et al., 2003a) and recent work in primary adipocytes (Bellve et al., 2006). Indeed extensive arrays of flat hexagonal clathrin lattice are not only found on the ventral surface of normal human fibroblasts (Heuser, 1980; Heuser and Anderson, 1989), but on the dorsal surface as well (Damke *et al.*, 1994), where LDL is similarly enriched around the circumference of the clathrin assemblies (Sanan and Anderson, 1991). Thus, in cells where extensive arrays of clathrin occur, Dab2 may locally concentrate FXNPXY cargo molecules, like the LDL receptor, for packaging into buds that form within or at the periphery these extended

There are at least two mammalian tissues where functional redundancy between Dab2 and ARH appears to have been selected against. Hepatocytes do not express Dab2 in sufficient quantity to bypass ARH loss and, reciprocally, during embryonic development the visceral endoderm does not appear to express ARH (Maurer and Cooper, 2005) and, consequently, targeted gene disruption of Dab2 is homozygous lethal (Morris et al., 2002b). Hepatocytes characteristically respond to liver damage or partial hepatectomy with rapid proliferation and remodeling to restore the functional capability and mass of the liver. Because Dab2 acts downstream of TGF-β receptors to promote SMAD activation (Hocevar *et al.*, 2001), and hepatocyte DNA synthesis and proliferation is potently suppressed by TGF-β (Wollenberg *et al.*, 1987), perhaps the very low level of Dab2 in parenchymal cells is functionally related to the intrinsic proliferative capacity of hepatocytes.

5.0   SUMMARY AND CONCLUSIONS

In this dissertation, I have outlined several contributions to the understanding of clathrin-mediated endocytosis. First of all, I have demonstrated that clathrin dynamics are more complex than initially thought, as endosomal populations of assembled clathrin complicate analysis, even using TIR-FM. However, through simultaneous imaging of CLASPs, I define the static structures as those most likely to represent plasma membrane associated clathrin. Through analysis of the CLASP responsible for autosomal recessive hypercholesterolemia, ARH, I demonstrated the importance of the novel FXX[FL]XXXR motif present in the C-terminus for ARH targeting to coated pits in cells. However, knockout of ARH is insufficient to block LDL receptor endocytosis in fibroblasts. I demonstrated that this is due to the functionally redundant CLASP Dab2, which works with ARH to sort the LDL receptor, as ablation of these two components halts LDL receptor endocytosis. The endocytic defect in the liver of autosomal recessive hypercholesterolemic patients is most likely due to the lack of Dab2 in hepatocytes, requiring this cell type to rely solely on the absent ARH for LDL uptake. The implications of these data will be considered sequentially.

5.1 CLATHRIN DYNAMICS *IN VIVO*

The development of TIR-FM has allowed the selective excitation of fluorophores near the ventral plasma membrane, making it an ideal tool with which to study clathrin-mediated endocytosis, as deeper structures will not impede analysis. However, misconceptions about the meaning of the characteristic decay depth, *d*, lead many to presume that the TIR-FM field only measures surface events, and that the evanescent wave can only excite fluorophores within 110 nm of the cell surface (Merrifield et al., 2002; Rappoport et al., 2003a; Santini and Keen, 2002; Yarar et al., 2005). Here I demonstrate that this is clearly not the case, as measurement of fluorescent beads indicate that the penetration depth is close to 200 nm, and dynamic structures indicative of endosomes can be readily imaged in the TIR-FM field (Figure 2-1) (Lampson et al., 2001). Furthermore, many flat cells are preferred for imaging because a larger region of plasma membrane is available in a single focal plane. I show that these cells, however, can be only ~150 nm deep in their periphery, so any endosomes in the periphery should be visible by TIR-FM. Indeed, in my hands, and others', the flat BS-C-1 cells stably transfected with the LCa-GFP show an even larger number of the highly dynamic clathrin structures than do HeLa or CV-1 cells (data not shown) (Ehrlich et al., 2004). Thus, it is necessary to distinguish between the internal and surface structures observed by TIR-FM.

When one couples examination of clathrin to that of surface-associated CLASPs, it becomes easier to discriminate between surface and internal populations. Based upon the colocalization of AP-2 and clathrin, it appears that the static structures are predominantly surface structures, while the laterally mobile structures are internal. This is further supported by cargo dynamics, as internalized cargo is highly dynamic (Figure 2-5) (Lakadamyali et al., 2003;

Rappoport et al., 2003a). Although all laterally dynamic structures appear to be endosomes, they occasionally halt, making it difficult to positively ascribe all stationary structures to the surface. This demonstrates that a large proportion of the observed clathrin structures are not surface-associated, and identifying structures as surface-associated requires the coordinate use of an appropriate surface marker.

Pinpointing the precise internalization event, however, is extremely difficult. CLASPs are present on coated vesicles, preventing their use to discriminate between coated pit and coated vesicle. Other methods exist to define uptake from the plasma membrane, but each has difficulties when combined with live cell imaging. Pharmacological treatments that specifically perturb clathrin-mediated endocytosis either also affect clathrin in other subcellular locations (i.e., sucrose treatment), or are irreversible, preventing absolute determination of which subset are coated pits. Clathrin-mediated endocytosis is also blocked at 0-4ºC, but I have found that thermally induced focal drifts during the change to a permissive temperature prevent capture of the rapid internalization event by TIR-FM. Furthermore, this temperature block occurs after cargo capture and lattice assembly, so using it would not provide any information on receptor clustering or lattice assembly, even if the focal drift could be overcome (Sorkin, 2004). Thus, it is difficult to determine when the internalization event occurs.

Because it is extremely difficult to capture the internalization event, many studies focus on the departure of cargo from the early, sorting endosome, where elegant work following endocytosed ligands has clearly documented this step (Cheng et al., 1980; Dunn and Maxfield, 1992; Ghosh et al., 1994; Lippincott-Schwartz and Fambrough, 1986; Rink et al., 2005; Salzman

and Maxfield, 1989; Sorkin et al., 1991; Tabas et al., 1990; Yamashiro et al., 1984). Some determinations have also been made of the extent to which coated vesicles fuse with other vesicles, or with pre-existing early endosomes. It is generally thought that early endosomes can receive cargo for up to 5-10 min, simultaneous with translocation along microtubules and acidification as they mature into surface inaccessible late endosomes (Maxfield and McGraw, 2004). However, my examination of endocytosed LDL, and others' measurement of endosomal dynamics in yeast (Toshima et al., 2006), show that endosomes are highly mobile structures, and appear to scavenge newly endocytosed cargo from coated structures. This assigns a more active role to the early endosomes, since they move about surface structures collecting newly endocytosed cargo rather than passively awaiting fusion with coated vesicles. Unfortunately, this complicates simple analysis of surface events, as it is possible that early endosomes temporarily dock within the 200 nm diffraction limit of visible light to receive cargo from coated pits and then depart. In image sequences, this transient docking may be confused for cargo accumulation and subsequent scission from the plasma membrane, especially if the endosome came from an extra-focal plane. This would rationalize the results of Rappoport et al., who observe clathrin departing without AP-2 from AP-2 positive structures without their insistence that AP-2 is not incorporated into coated vesicles (Rappoport et al., 2003a).

To circumvent some of the uncertainties just mentioned, two modifications to the TIR-FM techniques have recently been used. The first is the sequential imaging of structures using both epifluorescent and TIR-FM optics; structures that disappear from the TIR-FM field without leaving the epifluorescent field are considered endocytic events. Given the correlation of actin and dynamin bursts observed with the departure from the TIR-FM field, these may well

represent internalization events (Merrifield et al., 2002). However, Merrifield et al. restricted their analysis to an undisclosed percentage of coated structures, making it unclear what fraction of the total endocytic events, or even what fraction of clathrin positive structures, possess this burst of actin or dynamin. (Merrifield et al., 2002). Another modification pioneered by Merrifield et al. relies on the pH sensitivity of the GFP-derivative pHlourin, and the ability to cycle extracellular pH between quenching and non-quenching conditions (Merrifield et al., 2005). Using this technique, it was demonstrated that the static clathrin structures are indeed endocytically active, consistent with others' results (Bellve et al., 2006) and those presented here (Figure 4-14). However, this study, along with certain earlier studies, (Merrifield et al., 2002; Merrifield et al., 2005; Yarar et al., 2005) have used the clathrin LCa coupled to DsRed to visualize cellular clathrin. DsRed must tetramerize in order to fluoresce (Yarbrough et al., 2001), and this artificial tetramerization of clathrin light chains could severely alter endocytic dynamics. Indeed, ultrastructural examination of the 3T3 cells stably expressing the DsRed-LCa reveals that the clathrin has extensive inter-triskelion crosslinking, even to the extent of tethering endosomes to coated pits by the DsRed tetramers (J. Heuser, personal communication). Thus, the dynamics of these different compartments may be altered depending on how the DsRed-LCa is crosslinked in the cell. This is observed in experiments I have done in HeLa and MDA-MB-231 cells, where there are more motile YFP-Dab2 structures in cells co-expressing DsRed-LCa and YFP-Dab2 than in cells only expressing YFP-Dab2 (data not shown). This could be indicative of clathrin crosslinked between surface structures and internal structures, since the YFP-Dab2 is a marker of surface structures, and motility is indicative of internal structures. The severity of this crosslinking may vary by cell type or expression level, since the DsRed-LCa dynamics in

experiments described here in CV-1 cells did not show altered dynamics of the AP-2 α subunit (Figure 2-5). Future studies will greatly benefit from red fluorophores that do not require tetramerization, such as the tandem dimer Tomato (Shaner et al., 2004).

The relative expression level of these fluorescent proteins may also drastically alter endocytic dynamics. This is especially true for monomeric proteins like Dab2 and ARH. Overexpression of ARH, for example, has dramatic consequences for LDL internalization (Mishra et al., 2005), so the protein expression level must be carefully modulated. This can be partially mitigated by the incorporation of an overexpressed subunit into a protein complex, as the cell has active mechanisms in place to degrade unincorporated, excess subunits. For example, β2-YFP forms large agglomerates only at very high expression levels. However, at moderate levels of expression, β2-YFP is also incorporated into AP-1. It is only at low expression levels that β2-YFP is incorporated solely into AP-2. Thus, careful examination of fluorescent protein dynamics is necessary to ensure that expressed proteins are behaving appropriately. Even at low expression levels, the system is likely dealing with an excess of the protein in question, as the system also contains an unlabeled, endogenous population. Overall, overexpressing proteins must be carefully done, as expression level alone can completely alter the behaviors and properties of a fluorescent protein.

A final complicating factor is the ability to detect fluorescent cargo in coated vesicles. As coated vesicles from the plasma membrane are generally 100 nm in diameter, they are going to be considerably dimmer than both the extensive surface lattices or the larger endosomes. These

intermediates will be more difficult to detect, especially when bright, fluorescently-labeled endosomes dock near static lattices. This is observed in endosomal dynamics, as it is estimated that the smallest detectable GFP-Rab5 structures contain ~300 molecules, and the smallest trackable structures contain at least 630, while most endosomes typically contained 2000-3000 molecules (Rink et al., 2005). Therefore, examination of endocytic dynamics is going to require a careful and thorough documentation of cargo, clathrin and CLASP dynamics, as begun here.

Given all of these complications in cultured mammalian cells, is there any hope to unravel endocytic dynamics? In *S. cerevisiae*, substantial progress has been made in delineating the temporal relationship of endocytic adaptors due to the power of yeast genetics (Kaksonen et al., 2003; Kaksonen et al., 2005). Although yeast are small, making imaging more difficult, endogenous genes can be deleted and fluorescent rescue proteins expressed using endogenous promoters. Reversal of any phenotype resulting from knockout of the endogenous protein upon expression of the fluorescent rescue protein assuages any concerns of functionality. Endocytosis in *S. cerevisiae* also proceeds from cortical actin patches, which are more easily defined and followed than the horde of clathrin-coated structures in a mammalian cell, although endosomes may still complicate analysis, as endosomal scavenging was first described in yeast (Toshima et al., 2006). Finally, *S. cerevisiae* is a simpler organism, lacking much of the redundancy present in mammals, making it easier to assign functions to the endocytic proteins present in the *S. cerevisiae* genome. Unfortunately, endocytosis in *S. cerevisiae* is mechanistically different from that in mammals, as AP-2 does not bind to clathrin, nor does it appear to mediate cargo selection (Boehm and Bonifacino, 2002). Investigations into the budding yeast *Pichia pastoris* and the fission yeast *Schizosaccharomyces pombe* will likely uncover more information directly relevant

to mammals, as the protein trafficking pathways more closely resemble mammalian cells than do

S. cerevisiae, while remaining genetically tractable organisms (Rossanese et al., 1999).

Elucidation of endocytic dynamics in the mammalian system will improve as cells stably

expressing inducible RNAi systems are generated to attenuate endogenous protein levels and

curb potentially high expression levels of rescue proteins. Also, usage of the tandem dimer

DsRed derivatives, most notably Tomato, will circumvent fluorescent protein-induced

oligomerization (Shaner et al., 2004). Finally, computational models and more careful

delineation of specific activities will aid in understanding endocytic adaptor protein dynamics.

Thus, the work presented here lays the foundation for future live cell studies. It also refutes the

dogma of a 110 nm penetration depth for TIR-FM, the designation of all clathrin structures

detectable by TIR-FM as plasma membrane associated, and the idea that overexpression of

fluorescently tagged proteins has no effects upon the protein dynamics, all basic, erroneous

assumptions still made in the field.

5.2   VALIDATION OF THE CLASP HYPOTHESIS

This dissertation represents the first work that formally validates the CLASP hypothesis.

Previous investigators have laid the groundwork, demonstrating that Dab2 and ARH contain the

necessary information to fulfill the role of a CLASP (He et al., 2002; Maurer and Cooper, 2005;

Mishra et al., 2005; Mishra et al., 2002a; Mishra et al., 2002b; Morris and Cooper, 2001). Work

with the poly/multiubiquitin-selective CLASPs has demonstrated that artificial receptor systems

are dependent on eps15, eps15R and epsin (Barriere et al., 2006; Duncan et al., 2006b; Hawryluk et al., 2006; Wang et al., 2006). However, my work formally demonstrates that an endogenous receptor, the LDL receptor, is sorted into coated pits and subsequently endocytosed in a Dab2 and ARH dependent manner (Figures 4-1 to 4-3, 4-6). My work also goes further to demonstrate that while AP-2 independent clathrin-mediated endocytosis can occur, in a normal cell, CLASPs and AP-2 work together to internalize cargo. Indeed, I find that CLASPs, AP-2 and various cargo classes reside together in the general population of coated pits, with no evidence of coated pit specialization.

The finding that ARH and Dab2 function redundantly in LDL receptor sorting and internalization has several important repercussions. First, it attests to the redundancies present in the mammalian endocytic system. Disruption of many endocytic proteins appears to have little or no obvious effect; likely it will be necessary to knock them out in tandem with other partially redundant proteins. This may be somewhat complicated when multiple isoforms are involved, or when a process is conserved between proteins that fulfill different functions. For example, two endocytic accessory proteins that can polymerize clathrin into cages are Dab2 and GAK/auxilin. These proteins have drastically different functions in endocytosis, as Dab2 assists with cargo selection while GAK/auxilin potentiates uncoating. Thus, determining the contribution of each factor to clathrin polymerization will be difficult, as perturbation of each component will carry other consequences for clathrin-mediated endocytosis. Likewise, ARH and eps15, which do not polymerize clathrin on their own, are redundant with proteins that can assemble clathrin. Thus, the mammalian cell has evolved a number of safeguards in the endocytic machinery to ensure that this vital process can occur even without a particular endocytic factor.

137

Like the lower organisms that may only possess one of multiple redundant proteins, some tissues in mammals appear to specialize in which CLASPs they express. This is likely the result of the multifunctional nature of many CLASPs, and may be a key to dissecting their role in each stage of coat assembly. Dab2 and epsin both possess very proline-rich C-termini; although the Dab2 PRD has been assigned a role in signaling, these proteins may also use this region to engage the SH3 domains present in many other endocytic accessory factors, especially those associated with the actin cytoskeleton. Dab2 also directly interfaces with CIN85 and myosin VI (Morris et al., 2002a). It may be that to fully support AP-2 independent endocytosis, CLASPs also need to recruit the actin cytoskeleton to the bud site. Alternatively, the TGF-β sensitivity that Dab2 expression confers (Hocevar et al., 2005) may explain why proliferative cells like hepatocytes and carcinomas downregulate Dab2. Determining the consequences of replacing ARH with Dab2 in the mouse liver will shed insight into the tissue specificity of CLASPs. If the presence of Dab2 impairs liver growth or regeneration, it would suggest that TGF-β sensitivity is the limiting factor. Conversely, replacement of Dab2 with ARH in the visceral endoderm will also explain the requirement for Dab2 there. This may demonstrate that Dab2 is required to coordinate signaling with internalization, or that interactions with the actin cytoskeleton are necessary. Possibly, swapping these CLASPs will not rescue cargo internalization, which will imply that different cell types possess distinct regulatory mechanisms for controlling CLASP/cargo/coated pit interactions. Thus, the tissue specificity of these CLASPs may aid in understanding the multiple roles they play.

Understanding the characteristics necessary for CLASP function will enable us to assign other CLASPs. Many of the endocytic accessory proteins could be CLASPs once cognate cargoes are identified. Although the YXXΦ, dileucine, FXNPXY and poly/multiubiquitin internalization signals are accounted for, SNAREs, and synaptotagmins have poorly defined internalization sequences. Recent work relying on overexpression systems suggests that the endocytic protein stonin2 might sort synaptotagmins in an AP-2 dependent fashion (Diril et al., 2006). Stonin2 contains a C-terminal μ2 homology domain that is proposed to interact with synaptotagmin and three α appendage binding WXXF motifs (Jha et al., 2004; Ritter et al., 2003; Walther et al., 2004; Walther et al., 2001). Overexpression of stonin2 generally blocks endocytosis by sequestering AP-2, attesting to the potency of its AP-2 binding (Jha et al., 2004; Martina et al., 2001). Finally, disruption of the *Drosophila* stonin2 ortholog, stoned B, is lethal, though overexpression of synaptotagmin restores viability, suggesting that this lethality is due to an inability to sort synaptotagmins (Fergestad and Broadie, 2001; Petrovich et al., 1993). However, formally assigning stonin2 as a CLASP must await RNAi knockdown and rescue.

RNAi will be a major asset in assigning CLASPs, and identifying the role of other endocytic accessory proteins. Using this technology, it has already been shown that the endocytic adaptor AP180/CALM appears to govern lattice shape (Meyerholz et al., 2005). Future work identifying new internalization motifs and pairing these motifs with CLASPs will permit a complete understanding of clathrin-mediated endocytic signals. Fully delineating how endocytosis is driven by CLASPs and other endocytic accessory proteins will bring us to understanding the minimum machinery required for endocytosis, and the development of a reliable cell-free endocytosis assay.

5.3   TWO-CLASP MODEL

Based upon the redundant sorting of the LDL receptor by Dab2 and ARH, a model for CLASP function may be proposed, termed the Two-CLASP model. In this model, two CLASPs, an usher CLASP and an independent CLASP, are dedicated to sorting each class of cargo. The usher CLASP is a CLASP that binds to a privileged site on AP-2 and uses this interaction to usher receptors through the endocytic pathway, ensuring their incorporation into coated pits. The independent CLASP is capable of sustaining endocytosis in the absence of AP-2, though it interfaces with AP-2 via a nonprivileged binding surface. The independent CLASP ensures endocytosis of a given cargo type and limits saturation by other cargo subtypes. Thus, in the case of LDL internalization, ARH is the usher CLASP, while Dab2 is the independent CLASP. The poly/multiubiquitin system also fits this model, as epsin bears the hallmarks of an independent CLASP, including the ability to polymerize clathrin, while eps15 and eps15R would be usher CLASPs (Barriere et al., 2006; Drake et al., 2000; Edeling et al., 2006; Hawryluk et al., 2006).

The usher CLASPs may be important for initially binding to receptors and subsequently tethering them to coated pits. For example, β-arrestins first bind activated GPCRs, and then encounter a coated pit, instead of residing in coated pits and binding cargo there. If this is a general property of usher CLASPs, ARH, eps15 and eps15R should similarly recognize receptors outside of coated pits *in vivo*, though independent CLASPs like epsin and Dab2 would not. In addition to recognizing cargo outside of the lattice and ensuring its clathrin-mediated uptake, the

usher CLASPs may play a second role in receptor trafficking. There is growing evidence that usher CLASPs are present on endosomes and direct the fate of cargo there. Eps15 is part of a complex responsible for sorting EGF receptors from endosomes into multivesicular bodies for subsequent degradation (Bache et al., 2003). β-arrestin interacts with certain GPCRs in endosomes, and these interactions slow GPCR recycling (Oakley et al., 1999). ARH has also been reported on endosomes, though the function of ARH there remains unclear (Nagai et al., 2003). Thus, usher CLASPs may play a second role in sorting cargo further along the endocytic route. However, this role in endosomal trafficking is likely secondary to the role usher CLASPs play at the surface, as seen by the steady state distribution of these CLASPs at the surface (Figures 4-11, 4-12). Furthermore, no LDL recycling defects are immediately apparent in ARH$^{-/-}$ fibroblasts (Figures 4-6, 4-7), though it is possible that there are other, redundant endosomal sorting proteins. Confirmation *in vivo* of ARH/endosome interactions, and identification of a role for endosomal ARH in LDL receptor trafficking would support the idea that usher CLASPs also act in endosomal trafficking. Determination of the mechanisms through which β-arrestin slows GPCR recycling will help us understand both how these CLASPs function on endosomes and how GPCRs are recycled. Finally, determination of endosomal receptor kinetics in the absence of usher CLASPs will determine what effect, if any, these CLASPs have on receptor trafficking.

The independent CLASPs, on the other hand, act only at the surface to ensure endocytosis by cooperating with AP-2 to drive lattice polymerization, invagination, actin recruitment and scission. These CLASPs tend to have a more stable association with coated pits, as seen in the Dab2/ARH system, where at steady state Dab2 is in 86% of surface LDL receptor positive coated pits (AP-2 is present in 89% of these structures), while ARH is present in only

63% of these structures. Positioned at the clathrin lattice, these CLASPs may help increase the retention time of cargo molecules within the coated pit, and prevent competition between cargo classes for incorporation into the coated vesicle. Furthermore, these CLASPs should have all of the information necessary to drive the construction of new coated vesicles. Thus, independent CLASPs should be capable of clathrin polymerization as well as recruitment of downstream factors that induce invagination, actin recruitment and scission. Although Dab2 interacts with myosin VI and CIN85, linking it to the actin machinery, it remains to be observed if epsin can also interact with the actin machinery, as predicted by this model. Future work should also examine the role of various Dab2 and epsin binding partners. Based upon this model, the majority of these proteins should be involved in invagination, actin recruitment or scission. As the role of these binding proteins is clarified, it may be possible to reconstitute AP-2 independent endocytosis.

As with identification of novel CLASPs in general, RNAi will be a tremendous asset in identifying usher and independent CLASPs. Functionally, usher CLASPs will likely be identified based on their requirement for AP-2 to sustain endocytosis, as may be the case in the stonin2-synaptotagmin system. Using AP-2 RNAi, Diril et al. show that stonin2-mediated internalization of overexpressed synaptotagmin is dependent on AP-2, yet they present no stonin2 RNAi results (Diril et al., 2006). It may be that stonin2 RNAi has no effect on synaptotagmin sorting. Given the Two-CLASP model presented here, this might be expected, as the independent CLASP that could drive synaptotagmin internalization would still be present. Indeed, in flies, selective expression of stoned B in neurons is sufficient to overcome the phenotype of stoned B disruption, despite the presence of synaptotagmins in all tissues, suggesting that another

synaptotagmin internalization determinant is present in non-neuronal tissues (Estes et al., 2003; Li et al., 1995). Identification of the independent CLASP in this system will enhance our understanding of synaptotagmin sorting, and strengthen the Two-CLASP model. In general, independent CLASPs will be most easily identified by RNAi screens for proteins that cause cargo internalization defects in AP-2 compromised cells.

The only two CLASPs that do not seem to fit the Two-CLASP model are AP-2 and β-arrestin. AP-2 is a special case, as it is the primary adaptor in cells. Any usher CLASP that is dependent on AP-2 will itself be susceptible to AP-2 knockdown, so it would have to be identified based on its ability to bind to either YXXΦ or dileucine motifs. This identification will be further complicated if the usher CLASP binding to cargo is regulated similar to the μ2 subunit, as there is a 25-fold difference between clathrin-coated pit associated, phosphorylated, cargo-binding competent μ2 and cytosolic, non-phosphorylated, cargo-binding incompetent conformations (Ricotta et al., 2002). Possibly the newly characterized TTP is the usher CLASP for AP-2, although TTP engages the TfR via a nonconventional SH3 binding site rather than via the YXXΦ motif (Tosoni et al., 2005). It is also possible that AP-2 is sufficiently abundant in a cell that an usher CLASP is unnecessary at the surface, and that AP-1 fulfills any roles usher CLASPs play in endosomes.

The other apparent exception to this model is the β-arrestin-mediated sorting of GPCRs. In this system, there are two, semi-redundant usher CLASPs that sort the entire cohort of 600+ GPCRs, though some GPCRs do have multiple internalization motifs. Elimination of both β-arrestins is lethal in mice, though fibroblasts can be generated (Kohout et al., 2001), suggesting

that like ARH, they are absolutely critical in at least one tissue type. There may still exist an independent CLASP for GPCRs, however. The independent CLASP may not have been identified due to the difficulty in identifying binding partners of multiply phosphorylated GPCR tails. Here an RNAi screen of proteins that inhibit GPCR endocytosis in the context of an AP-2 knockdown may turn up another GPCR-selective CLASP. Alternatively, immunoprecipitation of activated GPCRs coupled with mass spectroscopy could turn up a novel GPCR-selective CLASP. If this CLASP is found, it will immeasurably strengthen the Two-CLASP model. Thus, this model is consistent with the behavior of currently known CLASPs. Overall, this dissertation has validated the CLASP hypothesis, and I propose the Two-CLASP model as a general mechanism for cargo internalization in mammalian cells.

5.4   AP-2 BINDING DETERMINANTS

Closely related to the Two-CLASP model is the question of why different CLASPs engage AP-2 in very different manners. This dissertation has demonstrated that ARH is dependent upon its helical FXX[FL]XXXR β2-appendage binding motif for targeting to coated pits, and that disruption of this motif has consequences for LDL internalization. Dab2, on the other hand, preferentially binds to the α-appendage of AP-2 via multiple short motifs (Morris and Cooper, 2001). Epsin has 8 tandemly arrayed DPW motifs and the newly identified FXX[FL]XXXR motif enabling it to engage both α- and β2-appendages (Edeling et al., 2006; Traub et al., 1999),

while eps15 has 12 tandemly arrayed DPF motifs enabling it to similarly bind to both the α- and β2-appendages (Benmerah et al., 1996), and stonin2 has 3 WXXF motifs that engage the α-appendage (Jha et al., 2004; Ritter et al., 2003; Walther et al., 2004). Thus, there are considerable differences between the mode in which these CLASPs bind to AP-2. In the case of α appendage binding, these assorted binding determinants may be crucial for proper timing of these components (Mishra et al., 2004). The presence of Dab2 at the rims of coated pits may also be the result of its displacement from the lattice by a higher-affinity component after serving a role in lattice assembly (Figure 4-13). The helical FXX[FL]XXXR β2-appendage binding determinant may ensure that CLASPs using this motif can freely interact with AP-2 throughout the course of lattice assembly.

One method that may allow the elucidation of the differences in modes of AP-2 engagement is the generation of chimeric endocytic proteins that are blends of different CLASPs. However, it is interesting to note that a chimeric protein consisting of the Dab2 PTB domain followed by the ARH C-terminus does not rescue LDL internalization, despite targeting to punctate structures on the cell surface (data not shown). This suggests that certain combinations of domains may not be compatible for endocytosis, either because a given combination does not serve well as a CLASP, or because these proteins regulate their folded domain via their unstructured C-termini, and these interactions are not preserved in the chimera. Regulation of these CLASPs is likely, as a lack of regulation would lead to AP-2 engagement and clathrin polymerization in the cytosol, which would be deleterious to a cell. Unraveling the mechanism

through which these CLASPs are regulated is the next major task in understanding the molecular basis of clathrin-mediated endocytosis, and may uncover novel methods through which proteins are regulated.

Another method to unravel the differences of AP-2 engagement by CLASPs is the generation of a wholly synthetic CLASP that possesses all four known CLASP properties. First, this CLASP would need a lipid binding domain that targets $PtdIns(4,5)P_2$ that is not present in any known CLASPs, for example, a PH domain. Next, it would need a cargo recognition domain and a cognate cargo. This cargo recognition domain should be a folded domain that recognizes a cognate "cargo" peptide motif with a K_D similar to that of the PTB domain-FXNPXY or $\mu2$-YXXΦ interactions and not already present in mammalian cells. Bacterial cell wall proteins may have interactions that can be used for this purpose. To generate a receptor bearing the chosen "cargo" motif, the extracellular and transmembrane domains of Tac, also known as CD25 or the IL-2α receptor, could be fused to a linker followed by the "cargo" motif. Finally, the synthetic CLASP would need an unstructured C-terminus containing an array of clathrin and AP-2 binding determinants. Once it was validated that this synthetic CLASP bound $PtdIns(4,5)P_2$, the chosen bacterial "cargo" motif, clathrin and AP-2, it could be introduced into cells along with the chimeric Tac receptor, and rate of receptor endocytosis measured. The effect of varying the number of or distance between clathrin and AP-2 binding motifs on the receptor endocytosis could be determined, as could its ability to compete with AP-2 binding determinants in other CLASPs. Creation of a synthetic CLASP that could sort a synthetic cargo would also strengthen the CLASP hypothesis immensely, as it would be a proof of principle. The synthetic CLASP could be further modified to resemble an usher CLASP, and the Two-CLASP model further

146

tested with this system as well. If the synthetic CLASP fails to internalize the receptor, understanding why will help elucidate the requirements for receptor internalization. For example, it might require the introduction of regulatory sites, or binding sites to recruit the actin machinery. Even if the synthetic CLASP does not function in a cell-based assay, it could still be used in biochemical assays, and these would still determine the importance of number and positioning of AP-2 and clathrin-binding determinants. These experiments could lead to a complete understanding of clathrin and AP-2 binding determinants in a cell, along with testing both the CLASP hypothesis and Two-CLASP model. Thus, this system offers great promise for the future of CLASP-AP-2/clathrin interactions.

In conclusion, this dissertation has made a substantial contribution to the understanding of clathrin-mediated endocytosis. It has laid the foundations for future live cell studies through the demonstration that clathrin or cargo structures may not be coated pits, even when viewed by TIR-FM, and that the static structures are most likely surface associated, based on the dynamics of several CLASPs in conjunction with both cargo and clathrin. This dissertation also demonstrated that the novel FXX[FL]XXXR β2-appendage binding sequence is required for ARH function. Finally, this dissertation represents the first formal validation of the CLASP hypothesis, demonstrating that Dab2 and ARH redundantly sort the LDL receptor, and that they, like AP-2 and clathrin, are generally distributed into the cell's entire cohort of coated pits.

147

MATERIALS AND METHODS

A.1   REAGENTS

All reagents were from Fisher Biosciences unless otherwise noted. Polyacrylamide resolving gels containing 10% acrylamide, 375 mM Tris-HCl (pH 8.8), 0.1% SDS polymerized with 0.06% ammonium persulfate and 0.06% N,N,N',N'-tetramethylethylenediamine (TEMED), while the stacking gel was 4% acrylamide in 125 mM Tris-HCl (pH 6.8), 0.1% SDS polymerized with 0.15% ammonium persulfate and 0.25% TEMED. The acrylamide:bis-acrylamide ratio for the acrylamide stock solution was altered to 30:0.4. The decreased crosslinking generally improves resolution but also affects the relative mobility of several proteins, most noticeably AP180 and epsin 1. SDS-PAGE reservoir buffer was 25 mM Tris, 192 mM Glycine and 0.1% SDS, while transfer buffer was 15.6 mM Tris and 120 mM Glycine. Tris-buffered saline with Tween-20 (TBST) contained 10 mM Tris-HCl (pH 7.5), 150 mM NaCl and 0.1% Tween-20. Western blot stripping buffer was 31.25 mM Tris-HCl (pH 6.8), 2% SDS and 0.8% 2-mercaptoethanol. SDS-sample buffer was 62.5 mM Tris-HCl (pH 6.8), 2.3% SDS, 10% sucrose, 5% 2-mercaptoethanol and bromophenol blue, while non-reducing SDS sample buffer lacked the 2-mercaptoethanol and used phenol red instead of bromophenol blue. Enhanced chemiluminescent reagent was prepared

by mixing equal volumes of 0.0183% H_2O_2 in 100 mM Tris-HCl (pH 8.5) with 360 µM p-coumaric acid and 2.5 mM luminol in 100 mM Tris-HCl (pH 8.5). Homogenization buffer was 25 mM 4-(2-hydroxythyl)-1-piperazineethanesulfonic acid (HEPES)-KOH (pH 7.4) and 250 mM sucrose with 200 mM phenylmethanesulfonyl fluoride (PMSF) and 1/4 complete protease inhibitor cocktail tablet (Roche, Indianapolis, IN) per mL. Assay buffer was: 25 mM HEPES-KOH (pH 7.2), 125 mM potassium acetate, and 5 mM magnesium acetate. Starvation medium was either Dulbecco's modified Eagle's medium (DMEM) (for A431, CV-1 and HeLa cells) or Eagle's minimal essential medium (EMEM) (fibroblasts) supplemented with 25 mM HEPES-KOH (pH 7.2) and 0.5% BSA. KHMgE buffer was: 30 mM HEPES-KOH (PH 7.3), 70 mM potassium chloride, 5 mM magnesium chloride and 3 mM EGTA. Gelvatol mounting medium was 140 mM Tris-HCl (pH 8.5), 300 mM 1,4-diazabicyclo[2.2.2]-octane (Sigma, St. Louis, MO), 14% polyvinyl alcohol (average molecular weight 30,000-70,000) (Sigma), 28% glycerol and 0.05% sodium azide.

A.2   PLASMIDS

To label clathrin with the enhanced green fluorescent protein (GFP), a plasmid containing a human neuronal-specific clathrin light chain a (LCa) isoform ligated into the *BamH*I and *Xba*I sites of pEGFP-C3 (GFP-LCa) (BD Biosciences, Palo Alto, CA) was used. By inserting the brain LCa via the internal BamHI site, the four amino-terminal residues (MAEL) of the 248-amino acid light chain sequence are removed and replaced with residues (PRAR) encoded by the vector polylinker joining the carboxyl terminus of GFP to the amino-terminal end of LCa. The ARH-

149

GFP and ARH PTB-GFP constructs were prepared by ligating either full-length human ARH or the ARH PTB domain (residues 1-179) into the *Nhe*I and *Bgl*II sites of pEGFP-N1 (BD Biosciences) whereas GFP-ARHC1 was cloned into pEGFP-C1 (BD Biosciences) using the *EcoR*I and *BamH*I sites. The GFP-ARHM2 was constructed using a single annealed oligonucleotide pair containing residues 248–269 of human ARH ligated into pEGFP-C1 between the *EcoR*I and *BamH*I restriction sites. YFP-Dab2 was generated by first by cloning enhanced yellow fluorescent protein (YFP) into pECFP-N1 at the *Nhe*I and *Bgl*II sites, followed by replacing the in-frame CFP with full-length murine Dab2, inserted between the *Sal*I and *Not*I sites. The plasmid was made RNAi-resistant by introducing silent mutations (S249, L250 and R251) using QuikChange mutagenesis (Stratagene, La Jolla, CA). The GFP-epsin was created by cloning rat epsin 1 into pEGFP-C1 between the *Xho*I and *Kpn*I sites. The Dab2-GFP construct (Morris and Cooper, 2001) was kindly provided by Jonathan Cooper (Fred Hutchinson Cancer Center, Seattle, WA), while the Hip1R-GFP construct (Engqvist-Goldstein et al., 2001) was kindly provided by David Drubin (University of California Berkeley, San Francisco, CA), the plasmid encoding DsRed fused to the amino terminus of a non-neuronal LCa (DsRed-LCa) was kindly provided by Tomas Kirchhausen (Harvard Medical School, Boston, MA), the plasmid encoding the AP-2 α_C subunit fused via the carboxyl terminus to YFP (α_C-YFP) was a kind gift from James Keen (University of Pennsylvania, Philadelphia, PA), and the AP-2 β2 subunit fused via the carboxyl terminus to YFP (β2-YFP) was a kind gift from Alexander Sorkin (University of Colorado Denver, Denver CO) (Jiang et al., 2003); upon sequencing of this construct, a Y707C mutation was found within the hinge region that has no discernable functional effect (Jiang et al., 2003). The β2-YFP was made RNAi-resistant by introducing silent mutations (L465 and L466) using QuickChange mutagenesis. The β2 subunit trunk (residues 1-603) fused to YFP (β2-

YFP$_{TRUNK}$) was prepared from this plasmid by introduction of an in-frame *Eco*RI site immediately following Gly603, removal of the intervening *Eco*RI fragment by digestion, and religation. This procedure removes the β2 subunit hinge+appendage but leaves the contiguous, C-terminal YFP fusion. Other appropriate mutations were introduced into either YFP-Dab2, ARH-GFP or β2-YFP using QuikChange mutagenesis with the required primers, the sequences of which are available upon request. All plasmids and constructs were verified by automated dideoxynucleotide sequencing.

A.3   SIRNA DUPLEXES

The siRNA oligonucleotides used, which target base pair 1384-1402 of the AP-2 β2 subunit, base pair 472-490 of dynamin 2, base pair 1325-1343 of epsin 1 and base pair 3313-3331 of the clathrin heavy chain (HC) nucleotide sequence, have been described (Hinrichsen *et al.*, 2003; Huang *et al.*, 2004). The Dab2 siRNA selected targets base pair 745-763 of the Dab2 nucleotide sequence (UUCUUUAAGAGAAAAUCCA), the ARH siRNA targets base pair 633-651 of the ARH nucleotide sequence (CCUGCUGGACUUAGAGGAG) (Qiagen, Valencia, CA or Dharmacon, Lafayette, CO), and the AP-1 β1 subunit siRNA oligo targets base pair 1529-1547 of the β1 subunit nucleotide sequence (CCACUCAGGACUCAGAUAA) (Invitrogen, Carlsbad, CA or Dharmacon). The ARH-specific siGENOME SMARTpool (M-013025-00) was also obtained from Dharmacon, as was the AP-2 α subunit siRNA oligo that is essentially that previously described (Hinrichsen *et al.*, 2003) directed against base pair 1052-1070 of the α

subunit, but the final base pair of this sequence was omitted, yielding the sequence GCAUGUGCACGCUGGCCA (Dharmacon). All siRNA oligos were synthesized with dTdT overhangs and directed against human sequences, unless otherwise noted.

A.4   ANTIBODIES

The monoclonal antibodies (mAb) against the clathrin HC TD.1 (Nathke *et al.*, 1992) and X22 (Brodsky, 1985), the anti-AP-1/2 β1/β2 subunit mAb 100/1 (Ahle *et al.*, 1988) and affinity purified GD/1 and GD/2 antibodies (Traub *et al.*, 1995), the anti-AP-1 β1 subunit antibody RY/1 (Traub *et al.*, 1996), the anti-AP-1 γ subunit antibody AE/1 (Traub et al., 1995), the AP-2 α subunit mAb AP.6 (Chin *et al.*, 1989), affinity-purified anti-epsin 1 polyclonal (Drake *et al.*, 2000), and the anti-cation independent mannose 6-phosphate receptor antibody (Zhu et al., 1999) have been described. Affinity-purified anti-eps15 polyclonal and anti-clathrin light chain polyclonal R461 were generous gifts from Ernst Ungewickell (Medizinische Hochschule Hannover, Hannover, Germany) and rabbit anti-AP-2 μ2 subunit serum was kindly provided by Juan Bonifacino (NIH, Bethesda, MD). Affinity-purified anti-LRP1 antibodies were kindly provided by Guojun Bu (Washington University School of Medicine, St. Louis, MO), the rat-isoform specific anti-LDL receptor polyclonal antibody was a kind gift from Gene Ness (University of South Florida, Tampa, FL), the anti-lamp1 mAb G1/139 was kindly provided by K. Akasaki (Akasaki et al., 1995), the anti-GFP polyclonal antibody B5 was generously provided by Phyllis Hanson (Washington University School of Medicine, St. Louis, MO) (Dalal et al.,

2004), and the anti-α-mannosidase II antiserum was kindly provided by Kelley Moremen (University of Georgia, Athens, GA). A second mAb (clone 8) against the AP-2 α subunit was purchased from BD Transduction Laboratories (San Jose, CA), and a third mAb (clone C-8) from Santa Cruz Laboratories (Santa Cruz, CA). The anti-CD71/transferrin receptor mAb RVS-10 was from Chemicon (Temecula, CA), while the anti-AP-1 γ subunit mAb was purchased from BD Transduction Laboratories. A goat anti-Dab2 polyclonal antibody was purchased from Santa Cruz Biotechnology. The hybridoma secreting the anti-LDL receptor mAb IgG-C7 was obtained from the ATCC (Manassas, VA). The rodent-specific anti-asialoglycoprotein receptor mAb 8D7 was from HyCult Biotechnologies (Uden, The Netherlands). The anti-tubulin mAb E7 was purchased from the Developmental Studies Hybridoma Bank (Iowa City, IA). The affinity-purified ARH antibody (Mishra *et al.*, 2002b) was further cross-adsorbed with fixed and permeabilized ARH$^{-/-}$ fibroblasts, followed by removal of Hsc70 cross-reactivity by incubation with GST-DnaK bound to glutathione-Sepharose. The affinity-purified Dab2 (Mishra *et al.*, 2002a) antibody was similarly cross-adsorbed with immobilized GST-DnaK. Goat anti-mouse or anti-rabbit secondary antibodies conjugated to either AlexaFluor488 or AlexaFluor568 were purchased from Invitrogen, while goat anti-mouse or anti-rabbit antibodies conjugated to Cy5, HRP-conjugated donkey anti-mouse and anti-rabbit secondary antibodies, and colloidal gold-conjugated goat anti-rabbit secondary antibodies were purchased from Jackson ImmunoResearch (West Grove, PA). HRP-conjugated donkey anti-goat secondary antibody was from Santa Cruz.

A.5   ELECTROPHORESIS AND IMMUNOBLOTTING

Samples were resolved by SDS-PAGE, and then proteins were either stained with Coomassie blue or transferred to nitrocellulose in ice-cold transfer buffer. Blots were usually blocked overnight in 5% skim milk in TBST and then portions incubated with primary antibodies as indicated in the individual figure legends. After incubation with HRP-conjugated anti-mouse or anti-rabbit IgG, immunoreactive bands were visualized with enhanced chemiluminescence. Alternatively, donkey anti-rabbit IgG was iodinated with ICl utilizing an established method (Breitfeld *et al.*, 1989), and used at 200,000 cpm/mL to detect the bands. For stripping, blots were incubated at 50˚C in stripping buffer for 20 min, washed extensively in TBST, and blocked in 5% skim milk in TBST and reprobed with primary and secondary antibodies. Quantitation of the signal from blots was performed using a Phosphor-Imager (Bio-Rad, Hercules, CA).

A.6   LIPOSOME BINDING ASSAYS

Sedimentation binding assays utilizing either multilamellar control liposomes composed of 40% phosphatidylcholine, 40% phosphatidylethanolamine, 10% phosphatidylserine and 10% cholesterol or PtdIns(4,5)P$_2$-containing liposomes composed of 35% phosphatidylcholine, 35% phosphatidylethanolamine, 10% phosphatidylserine, 10% cholesterol and 10% PtdIns(4,5)P$_2$ were performed as described previously (Mishra *et al.*, 2002a; Mishra *et al.*, 2002b).

A.7   CELL CULTURE

All cell lines were cultured at 37° C in a humidified atmosphere containing 5% CO_2. MCF-7 and MDA-MB-231 cells were grown in RPMI supplemented with 10% fetal calf serum (FCS) (Hyclone, Logan UT) and 2 mM L-glutamine (Invitrogen), while primary control (GM01386, Human Genetic Cell Repository at the Coriell Institute) and $ARH^{-/-}$ (GM06697) fibroblasts and BS-C-1 cells were cultured in EMEM supplemented with 10% FCS, 2 mM L-glutamine and 1X nonessential amino acids (Mediatech, Herndon, VA). HeLa SS6, CV-1 (CCL-70, ATCC), A431 (CRL-1555, ATCC) and HepG2 cells were cultured in DMEM supplemented with 10% FCS and 2 mM L-glutamine. BS-C-1 cells stably transfected with either the σ2-GFP or clathrin LCa-GFP were a generous gift from Tomas Kirchhausen (Harvard Medical School, Boston, MA) and cultured in DMEM supplemented with 10% FCS, 2 mM L-glutamine and 0.4 mg/mL G418 (Sigma).

A.8   TISSUE AND CELL PREPARATION

Rat liver Golgi membranes (Tabas and Kornfeld, 1979) and plasma membrane sheets (Hubbard *et al.*, 1983) were prepared using published protocols. Freshly isolated rat hepatocyte and total rat liver non-hepatocyte cell fractions were kind gifts from William Bowen, Jr. For western blots, cells were trypsinized, washed in PBS, lysed directly in boiling SDS-sample buffer, heated to 95° C for 5 min, sonicated to shear DNA, and centrifuged at 12,000 Xg_{max} for 2 min to pellet insoluble material. Protein levels were standardized using a Coomassie blue-based filter paper binding assay (Minamide and Bamburg, 1990); 25 μg was loaded per lane. Rat liver samples

were prepared by finely mincing the tissue with a razor blade at 0° C, homogenizing in a small volume of homogenization buffer with a Teflon homogenizer, and solubilization directly in boiling SDS-sample buffer or in non-reducing SDS-sample buffer at 37° C. After incubation at either 95° C or 37° C respectively for 5 min, the samples were sonicated and centrifuged at 12,000xg_{max} for 2 min to pellet insoluble material.

A.9   IMMUNOPRECIPITATION

HeLa cells grown in 6-well plates, treated or untreated with siRNA against β2 subunit as described above, were trypsinized, washed in PBS and lysed in homgenization buffer supplemented with 1% triton X-100 for 30 min on ice. Cell debris was removed by centrifugation at 18,000xg_{max} for 10 min at 4° C, and the supernatants frozen in dry ice and stored at -80° C until use. The samples were thawed and incubated with 2 μg of anti-α subunit mAb AP.6 for 1 h at 4° C with gentle shaking, followed by the addition of protein G-coupled beads (Sigma), an additional 1 h at 4° C with gentle shaking, and then centrifugation to separate supernatant from pellet. The pellets were washed extensively in PBS, 1% Triton X-100 and then mixed with SDS sample buffer such that 1/8 of the pellet and about 1/25 of the supernatant were analyzed by SDS-PAGE.

A.10 TRANSFECTIONS

For transient transfections in a 35-mm dish, 6 µL of Lipofectamine 2000 (Invitrogen) was mixed with 375 µL of Opti-MEM (Invitrogen) and 500 ng of DNA and incubated at room temperature for 45 min before adding the mixture to the dish containing cells and the appropriate culture medium. The cells were 40-60% confluent at the time of transfection, and processed 18-24 h after transfection. For immunofluorescence, the cells were plated onto 12 mm glass coverslips prior to transfection, while for TIR-FM experiments cells were plated onto glass-bottom 35-mm tissue culture dishes (MatTek, Ashland, MA).

For HeLa SS6 cell RNAi, the cells were passaged to yield 50%-70% confluence in 24-well plates on the day of transfection. Transfections were performed with Transit-TKO reagent (Mirus Bio Corporation, Madison, WI) according to manufacturer's protocol using 100 nM of each siRNA. The culture media was replaced with fresh medium the following day, and cells were prepared for analysis 48-50 h after transfection with siRNA duplexes. For rescue experiments, 100 ng of rescue plasmid DNA was included along with the siRNA duplexes at the time of transfection, and did not block RNAi-mediated knockdown of the proteins (Figure 3-6). Transfection of primary fibroblasts was performed by electroporating 2×10^6 cells using a Nucleofector II (Amaxa, Gathersburg, MD), primary fibroblast electroporation solution (Amaxa), and 1 µM siRNA duplexes according to the manufacturer's protocol with program U-023. Cells were passaged the following day and harvested ~72 h after electroporation.

A.11   IMMUNOFLUORESCENCE

Cells were fixed for 20 min in 2% paraformaldehyde, washed in PBS, blocked with 10% goat serum, 0.2% saponin in PBS for 30 min, and incubated sequentially with primary and secondary antibodies diluted with 10% goat serum and 0.05% saponin in PBS each for 1 h prior to mounting in gelvatol. To eliminate the cytosolic pool of clathrin, ARH or Dab2, an additional 1 min incubation in 0.3% saponin in assay buffer on ice was performed prior to fixation. To visualize only the plasma membrane associated clathrin, or only AP-2 with the anti-$\beta1/\beta2$ antibody GD/1, cells were treated with 10 μg/mL brefeldin A (Epicentre, Madison, WI) for 15 min, followed by permeabilization in 0.3% saponin in assay buffer for 1 min on ice prior to fixation to remove cytosolic and ARF-dependent clathrin and AP-1.

A.12   LIGAND BINDING AND INTERNALIZATION

For the transferrin or EGF uptake experiments by TIR-FM, cells were serum starved by incubation in starvation medium for 1 h at 37 °C prior to placement on the microscope stage. Once cells were ready for imaging, transferrin conjugated to Alexa 488 (Tfn488) (Invitrogen), or EGF conjugated to Alexa 488 (EGF488) (Invitrogen) was added to a final concentration of 50 μg/mL or 10 ng/mL, respectively, and the cells were imaged immediately. For LDL uptake experiments, cells were cultured in DMEM containing 10% lipoprotein-deficient fetal calf serum (LPDS) (Cocalico, Reamstown, PA) and 2 mM L-glutamine for 24 h prior to imaging to up-regulate endogenous LDL receptors. Cells were given 20 μg/mL DiO-LDL (Biomedical

158

Technologies) and imaged immediately. For transferrin pulse experiments, cells transfected with DsRed-LCa were serum starved as above, incubated with 50 µg/mL Tfn488 for 30 min, washed, and imaged in starvation medium.

To measure surface levels of receptors (Chapters 3 and 4), cells were incubated with either the anti-LDL receptor mAb IgG-C7, anti-transferrin receptor mAb RVS-10, 4 µg/mL DiI-LDL (Biomedical Technologies, Stoughton, MA), 25 µg/mL transferrin conjugated to AlexaFluor488 (Tfn488) (Invitrogen), or 50 µg/mL transferrin conjugated to AlexaFluor633 (Tfn633) (Invitrogen) in starvation medium for 1 h on ice at 4° C, fixed and processed for immunofluorescence as follows. To measure the LDL and transferrin receptor internalization for RNAi and rescue experiments, after the 1 h in starvation medium, cells were incubated in the continuous presence of either 4 µg/mL DiI-LDL alone, 4 µg/mL DiI-LDL with 50 µg/mL Tfn633, or 25 µg/mL Tfn conjugated to AlexaFluor568 (Tfn568) with mAb IgG-C7 for 15 min at 37° C prior to fixation and processing for immunofluorescence. Alternatively, cells were incubated on ice as described above and then washed and warmed to 37° C for 15 min prior to fixation. To measure LDL receptor colocalization simultaneously with Dab2 and ARH, HeLa cells were transfected with YFP-Dab2, cultured in DMEM containing 10% LPDS and 2 mM L-glutamine for ~24 h, incubated with mAb IgG-C7 for 1 or 5 min at 37º C, permeabilized on ice with 0.3% saponin in assay buffer for 1 min, fixed, and processed for immunofluorescence.

A.13 MICROSCOPY AND ANALYSIS

For TIR-FM imaging, cells grown on glass-bottom dishes were transfected as described with 500 ng DNA. Cells were imaged either in DMEM supplemented with 10% FCS and 2 mM L-glutamine or phenol-free starvation medium, neither of which affected the dynamics or the imaging of the cells, although 0.45 M sucrose had a higher refractive index than normal medium, so the evanescent wave penetrated deeper. Cells were imaged on a Nikon 2000E inverted microscope (Melville, NY) with a 1.45 NA oil immersion objective capable of both epifluorescence and TIR-FM illumination through the objective. GFP, YFP, Alexa 488, and DiO were excited with a 488 nm line of an argon laser, whereas DsRed was excited with a 567 nm line of a krypton laser (laser bench provided by Prairie Technologies, Madison, WI). All laser lines were selectively blocked within the laser bench and illumination (both intensity and blanking) was controlled by acousto-optical tunable filters. To image both green and red fluorophores simultaneously, an Optical Insights image splitter was used. Images were collected using a water-cooled Orca II ER (Hamamatsu, Tokyo, Japan). Data sets were acquired using SimplePCI (C-imaging systems, Cranberry, PA) software. In all TIR-FM experiments images were collected at ~1 frame/s. The only post-processing performed was to ensure appropriate registration (using fiduciary points) of two color images, and image scaling such that labeled structures are clearly visible. No other filters or enhancements were applied to the data sets.

For sucrose treatments, the culture medium in the dish was replaced after acquiring several images of a single cell by TIR-FM with 0.45 M sucrose in starvation medium. The cell was located and imaging resumed ~30 s after addition of the sucrose solution. Cells were then imaged for up to 1 h after treatment, during which they remained the same in appearance. To

160

depolymerize the microtubule cytoskeleton, cells were incubated with 10 µM nocodazole (Sigma) for 30 min at 37 °C in starvation medium prior to imaging, and then imaged in the continued presence of the nocodazole.

Visualization of subtle motion is difficult in monochromatic image sequences. However, using color superposition of these monochrome stacks, it is possible to see quite small changes in object position. Thus, by sequencing temporal imaging sets in the red, green, and blue color channels of a color image, non-motile structures will appear as white structures, whereas motile structures will show a green-red-blue trail. For image motion over time, an *XY* time image can be generated such that the position is visualized in the *x* axis, and time visualized in the *y* axis, which is similar to a classical kymograph, and used extensively here. On the kymographs, a solid, vertical line represents a non-moving vesicle, whereas breaks in an individual line represent the appearance/disappearance of the object from the region, and slanted lines represent lateral particle motion. Even breaks across the entire projection represent a temporary adjustment of focus. Two-color TIR-FM images were processed similarly, except they were not time colored.

Epifluorescent images were acquired using a 63x objective lens on a Nikon Microphot-FXL, while confocal microscopy was performed using an Olympus Fluoview 500 or Olympus 1000 confocal microscope by sequentially scanning by line with an argon laser for 488 nm excitation, and two helium-neon lasers for 543 and 633 nm excitation through a PlanApomat 60X 1.40 NA objective with a 488/543/633 dichroic. Emitted light was separated with beam splitters SDM560 and SDM640, and passed through either band pass filters BA505-525 (green), BA560-600 (red) and long pass filter BA660IF (cy5) on the Fluoview 500 or diffraction gratings

161

that pass 500-530 nm (green) or 555-625 nm (red) light or a BA650IF filter (cy5) on the Fluoview 1000 prior to detection. Linescan analysis of Dab2 and surface LDL receptor fluorescence along arbitrary 76 pixel lines using the average integrated intensity of 3 perpendicular pixels for each point along the line was measured in Metamorph (Molecular Devices, Downingtown, PA). Quantitation of the colocalization between various clathrin coat components was performed as described (Hawryluk et al., 2006). Quantitation of ARH coated pit localization (Chapter 3) was performed using Metamorph software by measuring the integrated intensity of ARH staining in cell surface confocal sections that were either control (normal Tfn internalization), knocked down (blocked Tfn internalization) or rescued (YFP expression) and subtracting the intensity of knockdown cells from that of either mock transfected or neighboring rescued cells. Quantitation of the rescue of the Dab2+ARH RNAi phenotype (Chapter 4) was measured by counting the number of transfected cells showing either normal, impaired, or no LDL receptor internalization, and displaying each as a percentage of the total cells counted. A small portion of plasmid transfected cells displayed an overexpression phenotype (Mishra et al., 2005); these were excluded from this analysis.

For fluorescence recovery after photobleaching (FRAP) experiments, HeLa cells grown on chambered glass cover slips (Nalge Nunc International, Rochester, NY) were transfected with either YFP-Dab2 or ARH-GFP and imaged every 5.2 s with the argon 488 nm laser line on the Fluoview 1000. A 405 nm laser diode was used at maximum intensity for 5 s to bleach YFP-Dab2 or ARH-GFP fluorescence during the acquisition. The intensity of each bleached region was measured using Metamorph, corrected for background, each plane normalized to the intensity of an unbleached cell to account for any fluctuations in focus or intensity, and then

normalized to the average intensity of the frames prior to the bleach. To follow LDL and transferrin internalization in the context of the knockdown, RNAi-treated, serum-starved HeLa cells were incubated with 25 µg/mL Tfn488 and 4 µg/mL DiI-LDL and imaged every 3-6 s. To visualize LDL internalization in real time, HeLa cells in chambered glass cover slips transfected with YFP-Dab2 were imaged every 3-4 s in starvation medium. During image acquisition, starvation medium containing DiI-LDL was added such that the final concentration of DiI-LDL was 4 µg/mL. Measurement of DiI-LDL and YFP-Dab2 intensity in Dab2 structures that accumulated LDL within 250 s of LDL addition was performed using Metamorph; 17 such structures were measured and averaged.

A.14   ELECTRON MICROSCOPY

Cells cultured in LPDS were surface labeled with 50 µg/ml LDL (Biomedical Technologies) or not, before preparing 'unroofed' cell cortices for rapid-freeze deep-etch EM essentially as previously described (Edeling et al., 2006; Heuser, 2000). Briefly, cells grown on small oriented, carbon-coated cover slips were disrupted by sonication directly in 2% paraformaldehyde, 0.025% glutaraldehyde in KHMgE buffer. After washing, preparations were quenched with 50 mM ammonium chloride, 50 mM L-lysine in KHMgE, and blocked with 1% BSA in KHMgE, followed by incubation with affinity-purified anti-Dab2 or anti-ARH antibodies and then 15-nm colloidal gold-conjugated anti-rabbit antibody. Finally, the membranes were fixed in 2%

glutaraldehyde before freezing. For surface labeling, washed cells were fixed directly in 2% glutaraldehyde without sonication. Platinum casts were examined on a transmission electron microscope.

A.15   MOVIES

Movie 2-1 is live cell TIR-FM corresponding to experiments shown in Figure 2-1 (GFP-LCa), Movie 4-1 is live cell confocal following DiI-LDL and Tfn488 internalization in control and Dab2+ARH siRNA treated HeLa cells, while Movie 4-2 follows DiI-LDL internalization in YFP-Dab2 transfected HeLa cells corresponding to Figure 4-14E are shown. Additional movies can be found at www.cbi.pitt.edu/movies/keyel/keyel.html

BIBLIOGRAPHY

Ahle, S., Mann, A., Eichelsbacher, U. and Ungewickell, U. (1988) Structural relationships between clathrin assembly proteins from the Golgi and the plasma membrane. *EMBO J.*, **7**, 919-929.

Ahle, S. and Ungewickell, E. (1986) Purification and properties of a new clathrin assembly protein. *EMBO J.*, **5**, 3143-3149.

Ajioka, R.S. and Kaplan, J. (1987) Characterization of endocytic compartments using the horseradish peroxidase-diaminobenzidine density shift technique. *J. Cell Biol.*, **104**, 77-85.

Akasaki, K., Michihara, A., Mikuba, K., Fujiwara, Y. and Tsuji, H. (1995) Biosynthetic transport of a major lysosomal membrane glycoprotein, lamp-1: convergence of biosynthetic and endocytic pathways occurs at three distinctive points. *Exp. Cell Res.*, **220**, 464-473.

Anderson, R.G., Vasile, E., Mello, R.J., Brown, M.S. and Goldstein, J.L. (1978) Immunocytochemical visualization of coated pits and vesicles in human fibroblasts: relation to low density lipoprotein receptor distribution. *Cell*, **15**, 919-933.

Arca, M., Zuliani, G., Wilund, K., Campagna, F., Fellin, R., Bertolini, S., Calandra, S., Ricci, G., Glorioso, N., Maioli, M., Pintus, P., Carru, C., Cossu, F., Cohen, J. and Hobbs, H.H. (2002) Autosomal recessive hypercholesterolaemia in Sardinia, Italy, and mutations in ARH: a clinical and molecular genetic analysis. *Lancet*, **359**, 841-847.

Augustin, R., Riley, J. and Moley, K.H. (2005) GLUT8 contains a [DE]XXXL[LI] sorting motif and localizes to a late endosomal/lysosomal compartment. *Traffic*, **6**, 1196-1212.

Axelrod, D. (1981) Cell-substrate contacts illuminated by total internal reflection fluorescence. *J. Cell Biol.*, **89**, 141-145.

Axelrod, D. (1989) Total internal reflection fluorescence microscopy. *Methods Cell Biol.*, **30**, 245-270.

Bache, K.G., Raiborg, C., Mehlum, A. and Stenmark, H. (2003) STAM and Hrs are subunits of a multivalent ubiquitin-binding complex on early endosomes. *J. Biol. Chem.*, **278**, 12513-12521.

Barriere, H., Nemes, C., Lechardeur, D., Khan-Mohammad, M., Fruh, K. and Lukacs, G.L. (2006) Molecular basis of oligoubiquitin-dependent internalization of membrane proteins in Mammalian cells. *Traffic*, **7**, 282-297.

Bartee, E., Mansouri, M., Hovey Nerenberg, B.T., Gouveia, K. and Fruh, K. (2004) Downregulation of major histocompatibility complex class I by human ubiquitin ligases related to viral immune evasion proteins. *J. Virol.*, **78**, 1109-1120.

Basu, S.K., Goldstein, J.L., Anderson, R.G. and Brown, M.S. (1981) Monensin interrupts the recycling of low density lipoprotein receptors in human fibroblasts. *Cell*, **24**, 493-502.

Bauerfeind, R., Takei, K. and De Camilli, P. (1997) Amphiphysin I is associated with coated endocytic intermediates and undergoes stimulation-dependent dephosphorylation in nerve terminals. *J. Biol. Chem.*, **272**, 30984-30992.

Bazinet, C., Katzen, A.L., Morgan, M., Mahowald, A.P. and Lemmon, S.K. (1993) The Drosophila clathrin heavy chain gene: clathrin function is essential in a multicellular organism. *Genetics*, **134**, 1119-1134.

Bellve, K.D., Leonard, D., Standley, C., Lifshitz, L.M., Tuft, R.A., Hayakawa, A., Corvera, S. and Fogarty, K.E. (2006) Plasma membrane domains specialized for clathrin-mediated endocytosis in primary cells. *J. Biol. Chem.*, **in press**.

Belouzard, S. and Rouille, Y. (2006) Ubiquitylation of leptin receptor OB-Ra regulates its clathrin-mediated endocytosis. *EMBO J.*, **25**, 932-942.

Benmerah, A., Begue, B., Dautry-Varsat, A. and Cerf-Bensussan, N. (1996) The ear of alpha-adaptin interacts with the COOH-terminal domain of the eps15 protein. *J. Biol. Chem.*, **271**, 12111-12116.

Benmerah, A., Gagnon, J., Begue, B., Megarbane, B., Dautry-Varsat, A. and Cerf-Bensussan, N. (1995) The tyrosine kinase substrate eps15 is constitutively associated with the plasma membrane adaptor AP-2. *J. Cell Biol.*, **131**, 1831-1838.

Bennett, E.M., Lin, S.X., Towler, M.C., Maxfield, F.R. and Brodsky, F.M. (2001) Clathrin hub expression affects early endosome distribution with minimal impact on receptor sorting and recycling. *Mol. Biol. Cell*, **12**, 2790-2799.

Berdnik, D., Torok, T., Gonzalez-Gaitan, M. and Knoblich, J. (2002) The endocytic protein α-Adaptin is required for Numb-mediated asymmetric cell division in Drosophila. *Dev. Cell*, **3**, 221-231.

Blanchard, E., Belouzard, S., Goueslain, L., Wakita, T., Dubuisson, J., Wychowski, C. and Rouille, Y. (2006) Hepatitis C virus entry depends on clathrin-mediated endocytosis. *J. Virol.*, **80**, 6964-6972.

Blanpied, T.A., Scott, D.B. and Ehlers, M.D. (2002) Dynamics and regulation of clathrin coats at specialized endocytic zones of dendrites and spines. *Neuron*, **36**, 435-449.

Blanpied, T.A., Scott, D.B. and Ehlers, M.D. (2003) Age-related regulation of dendritic endocytosis associated with altered clathrin dynamics. *Neurobiol. Aging*, **24**, 1095-1104.

Blondeau, F., Ritter, B., Allaire, P.D., Wasiak, S., Girard, M., Hussain, N.K., Angers, A., Legendre-Guillemin, V., Roy, L., Boismenu, D., Kearney, R.E., Bell, A.W., Bergeron, J.J. and McPherson, P.S. (2004) Tandem MS analysis of brain clathrin-coated vesicles reveals their critical involvement in synaptic vesicle recycling. *Proc. Natl. Acad. Sci. U S A*, **101**, 3833-3838.

Bloom, W.S., Fields, K.L., Yen, S.H., Haver, K., Schook, W. and Puszkin, S. (1980) Brain clathrin: immunofluorescent patterns in cultured cells and tissues. *Proc. Natl. Acad. Sci. U. S. A.*, **77**, 5520-5524.

Boehm, M. and Bonifacino, J.S. (2002) Genetic analyses of adaptin function from yeast to mammals. *Gene*, **286**, 175-186.

Boll, W., Rapoport, I., Brunner, C., Modis, Y., Prehn, S. and Kirchhausen, T. (2002) The μ2 subunit of the clathrin adaptor AP-2 binds to FDNPVY and YppΦ sorting signals at distinct sites. *Traffic*, **3**, 590-600.

Bonifacino, J.S. and Traub, L.M. (2003) Signals for sorting of transmembrane proteins to endosomes and lysosomes. *Annu. Rev. Biochem.*, **72**, 395-447.

Bousarghin, L., Touze, A., Sizaret, P.Y. and Coursaget, P. (2003) Human papillomavirus types 16, 31, and 58 use different endocytosis pathways to enter cells. *J. Virol.*, **77**, 3846-3850.

Breitfeld, P.P., Casanova, J.E., Harris, J.M., Simister, N.E. and Mostov, K.E. (1989) Expression and analysis of the polymeric immunoglobulin receptor in Madin-Darby canine kidney cells using retroviral vectors. *Methods Cell Biol.*, **32**, 329-337.

Brett, T.J., Traub, L.M. and Fremont, D.H. (2002) Accessory protein recruitment motifs in clathrin-mediated endocytosis. *Structure*, **10**, 797-809.

Brodsky, F.M. (1985) Clathrin structure characterized with monoclonal antibodies. II. Identification of in vivo forms of clathrin. *J. Cell Biol.*, **101**, 2055-2062.

Brodsky, F.M., Chen, C.Y., Knuehl, C., Towler, M.C. and Wakeham, D.E. (2001) Biological basket weaving: formation and function of clathrin-coated vesicles. *Annu. Rev. Cell Dev. Biol.*, **17**, 517-568.

Brown, M.S. and Goldstein, J.L. (1986) A receptor-mediated pathway for cholesterol homeostasis. *Science*, **232**, 34-47.

Bruck, S., Huber, T.B., Ingham, R.J., Kim, K., Niederstrasser, H., Allen, P.M., Pawson, T., Cooper, J.A. and Shaw, A.S. (2006) Identification of a novel inhibitory actin-capping protein binding motif in CD2-associated protein. *J. Biol. Chem.*, **281**, 19196-19203.

Buss, F., Arden, S.D., Lindsay, M., Luzio, J.P. and Kendrick-Jones, J. (2001) Myosin VI isoform localized to clathrin-coated vesicles with a role in clathrin-mediated endocytosis. *EMBO J.*, **20**, 3676-3684.

Camidge, D.R. and Pearse, B.M. (1994) Cloning of Drosophila beta-adaptin and its localization on expression in mammalian cells. *J. Cell Sci.*, **107 (Pt 3)**, 709-718.

Cao, T.T., Mays, R.W. and von Zastrow, M. (1998) Regulated endocytosis of G-protein-coupled receptors by a biochemically and functionally distinct subpopulation of clathrin-coated pits. *J. Biol. Chem.*, **273**, 24592-24602.

Carbone, R., Fre, S., Iannolo, G., Belleudi, F., Mancini, P., Pelicci, P.G., Torrisi, M.R. and Di Fiore, P.P. (1997) eps15 and eps15R are essential components of the endocytic pathway. *Cancer Res.*, **57**, 5498-5504.

Carpentier, J.L., Gorden, P., Anderson, R.G., Goldstein, J.L., Brown, M.S., Cohen, S. and Orci, L. (1982) Co-localization of ^{125}I-epidermal growth factor and ferritin-low density lipoprotein in coated pits: a quantitative electron microscopic study in normal and mutant human fibroblasts. *J. Cell Biol.*, **95**, 73-77.

Chen, H., Fre, S., Slepnev, V.I., Capua, M.R., Takei, K., Butler, M.H., Di Fiore, P.P. and De Camilli, P. (1998) Epsin is an EH-domain-binding protein implicated in clathrin-mediated endocytosis. *Nature*, **394**, 793-797.

Chen, W.J., Goldstein, J.L. and Brown, M.S. (1990) NPXY, a sequence often found in cytoplasmic tails, is required for coated pit-mediated internalization of the low density lipoprotein receptor. *J. Biol. Chem.*, **265**, 3116-3123.

Cheng, S.Y., Maxfield, F.R., Robbins, J., Willingham, M.C. and Pastan, I.H. (1980) Receptor-mediated uptake of 3,3',5-triiodo-L-thyronine by cultured fibroblasts. *Proc. Natl. Acad. Sci. U. S. A.*, **77**, 3425-3429.

Chin, D.J., Straubinger, R.M., Acton, S., Nathke, I. and Brodsky, F.M. (1989) 100-kDa polypeptides in peripheral clathrin-coated vesicles are required for receptor-mediated endocytosis. *Proc. Natl. Acad. Sci. USA*, **86**, 9289-9293.

Chinkers, M., McKanna, J.A. and Cohen, S. (1979) Rapid induction of morphological changes in human carcinoma cells A-431 by epidermal growth factors. *J. Cell Biol.*, **83**, 260-265.

Chu, J.J. and Ng, M.L. (2004) Infectious entry of West Nile virus occurs through a clathrin-mediated endocytic pathway. *J. Virol.*, **78**, 10543-10555.

Codran, A., Royer, C., Jaeck, D., Bastien-Valle, M., Baumert, T.F., Kieny, M.P., Pereira, C.A. and Martin, J.P. (2006) Entry of hepatitis C virus pseudotypes into primary human hepatocytes by clathrin-dependent endocytosis. *J. Gen. Virol.*, **87**, 2583-2593.

Collins, B.M., McCoy, A.J., Kent, H.M., Evans, P.R. and Owen, D.J. (2002) Molecular architecture and functional model of the endocytic AP2 complex. *Cell*, **109**, 523-535.

Conner, S.D. and Schmid, S.L. (2003a) Differential requirements for AP-2 in clathrin-mediated endocytosis. *J. Cell Biol.*, **162**, 773-780.

Conner, S.D. and Schmid, S.L. (2003b) Regulated portals of entry into the cell. *Nature*, **422**, 37-44.

Conner, S.D., Schroter, T. and Schmid, S.L. (2003) AAK1 mediated μ2 phosphorylation is stimulated by assembled clathrin. *Traffic*, **4**, in press.

Coscoy, L., Sanchez, D.J. and Ganem, D. (2001) A novel class of herpesvirus-encoded membrane-bound E3 ubiquitin ligases regulates endocytosis of proteins involved in immune recognition. *J. Cell Biol.*, **155**, 1265-1273.

Cuitino, L., Matute, R., Retamal, C., Bu, G., Inestrosa, N.C. and Marzolo, M.P. (2005) ApoER2 is endocytosed by a clathrin-mediated process involving the adaptor protein Dab2 independent of its rafts' association. *Traffic*, **6**, 820-838.

Cupers, P., Jadhav, A.P. and Kirchhausen, T. (1998) Assembly of clathrin coats disrupts the association between Eps15 and AP-2 adaptors. *J. Biol. Chem.*, **273**, 1847-1850.

Dafforn, T.R. and Smith, C.J. (2004) Natively unfolded domains in endocytosis: hooks, lines and linkers. *EMBO Rep.*, **5**, 1046-1052.

Dahms, N.M. and Hancock, M.K. (2002) P-type lectins. *Biochim. Biophys. Acta.*, **1572**, 317-340.

Dalal, S., Rosser, M.F., Cyr, D.M. and Hanson, P.I. (2004) Distinct roles for the AAA ATPases NSF and p97 in the secretory pathway. *Mol. Biol. Cell*, **15**, 637-648.

Damke, H., Baba, T., Warnock, D.E. and Schmid, S.L. (1994) Induction of mytant dynamin specifically blocks endocytic coated vesicle formation. *J. Cell Biol.*, **127**, 915-934.

David, C., McPherson, P.S., Mundigl, O. and De Camilli, P. (1996) A role of amphiphysin in synaptic vesicle endocytosis suggested by its binding to dynamin in nerve terminals. *Proc. Natl. Acad. Sci. USA*, **93**, 331-335.

Davis, C.G., Lehrman, M.A., Russell, D.W., Anderson, R.G., Brown, M.S. and Goldstein, J.L. (1986) The J.D. mutation in familial hypercholesterolemia: amino acid substitution in cytoplasmic domain impedes internalization of LDL receptors. *Cell*, **45**, 15-24.

Davis, C.G., van Driel, I.R., Russell, D.W., Brown, M.S. and Goldstein, J.L. (1987) The low density lipoprotein receptor. Identification of amino acids in cytoplasmic domain required for rapid endocytosis. *J. Biol. Chem.*, **262**, 4075-4082.

Day, P.M., Lowy, D.R. and Schiller, J.T. (2003) Papillomaviruses infect cells via a clathrin-dependent pathway. *Virology*, **307**, 1-11.

Di Paolo, G., Sankaranarayanan, S., Wenk, M.R., Daniell, L., Perucco, E., Caldarone, B.J., Flavell, R., Picciotto, M.R., Ryan, T.A., Cremona, O. and De Camilli, P. (2002) Decreased synaptic vesicle recycling efficiency and cognitive deficits in amphiphysin 1 knockout mice. *Neuron*, **33**, 789-804.

Diril, M.K., Wienisch, M., Jung, N., Klingauf, J. and Haucke, V. (2006) Stonin 2 is an AP-2-dependent endocytic sorting adaptor for synaptotagmin internalization and recycling. *Dev. Cell*, **10**, 233-244.

Doray, B., Ghosh, P., Griffith, J., Geuze, H.J. and Kornfeld, S. (2002) Cooperation of GGAs and AP-1 in packaging Man-6-P receptors at the trans-Golgi network. *Science*, **297**, 1700-1703.

Drake, M.T., Downs, M.A. and Traub, L.M. (2000) Epsin binds to clathrin by associating directly with the clathrin-terminal domain: evidence for cooperative binding through two discrete sites. *J. Biol. Chem.*, **275**, 6479-6489.

Drake, M.T. and Traub, L.M. (2001) Interaction of two structurally-distinct sequence types with the clathrin terminal domain β-propeller. *J. Biol. Chem.*, **276**, 28700-28709.

Duncan, L.M., Piper, S., Dodd, R.B., Saville, M.K., Sanderson, C.M., Luzio, J.P. and Lehner, P.J. (2006a) Lysine-63 linked ubiquitination is required for endolysosomal degradation of class I molecules. *EMBO J.*, **25**, 1635-1645.

Duncan, L.M., Piper, S., Dodd, R.B., Saville, M.K., Sanderson, C.M., Luzio, J.P. and Lehner, P.J. (2006b) Lysine-63-linked ubiquitination is required for endolysosomal degradation of class I molecules. *EMBO J.*, **25**, 1635-1645.

Dunn, K.W. and Maxfield, F.R. (1992) Delivery of ligands from sorting endosomes to late endosomes occurs by maturation of sorting endosomes. *J. Cell Biol.*, **117**, 301-310.

Dunn, K.W., McGraw, T.E. and Maxfield, F.R. (1989) Iterative fractionation of recycling receptors from lysosomally destined ligands in an early sorting endosome. *J. Cell Biol.*, **109**, 3303-3314.

Edeling, M.A., Mishra, S.K., Keyel, P.A., Steinhauser, A.L., Collins, B.M., Roth, R., Heuser, J.E., Owen, D.J. and Traub, L.M. (2006) Molecular switches involving the AP-2 beta2 appendage regulate endocytic cargo selection and clathrin coat assembly. *Dev. Cell*, **10**, 329-342.

Eden, E.R., Naoumova, R.P., Burden, J.J., McCarthy, M.I. and Soutar, A.K. (2001) Use of homozygosity mapping to identify a region on chromosome 1 bearing a defective gene that causes autosomal recessive homozygous hypercholesterolemia in two unrelated families. *Am. J. Hum. Genet.*, **68**, 653-660.

Eden, E.R., Patel, D.D., Sun, X., Burden, J.J., Themis, M., Edwards, M., Lee, P., Neuwirth, C., Naoumova, R.P. and Soutar, A.K. (2002) Restoration of LDL-receptor function in cells from patients with autosomal recessive hypercholesterolemia by retroviral expression of *ARH1*. *J. Clin. Invest.*, **110**, 1695-1702.

Egner, R. and Kuchler, K. (1996) The yeast multidrug transporter Pdr5 of the plasma membrane is ubiquitinated prior to endocytosis and degradation in the vacuole. *FEBS Lett.*, **378**, 177-181.

Ehrlich, M., Boll, W., Van Oijen, A., Hariharan, R., Chandran, K., Nibert, M.L. and Kirchhausen, T. (2004) Endocytosis by random initiation and stabilization of clathrin-coated pits. *Cell*, **118**, 591-605.

Engqvist-Goldstein, A.E. and Drubin, D.G. (2003) Actin assembly and endocytosi: from yeast to mammals. *Annu. Rev. Cell Dev. Biol.*, **19**, 287-332.

Engqvist-Goldstein, A.E., Warren, R.A., Kessels, M.M., Keen, J.H., Heuser, J. and Drubin, D.G. (2001) The actin-binding protein Hip1R associates with clathrin during early stages of endocytosis and promotes clathrin assembly in vitro. *J. Cell Biol.*, **154**, 1209-1224.

Estes, P.S., Jackson, T.C., Stimson, D.T., Sanyal, S., Kelly, L.E. and Ramaswami, M. (2003) Functional dissection of a eukaryotic dicistronic gene: transgenic stonedB, but not stonedA, restores normal synaptic properties to Drosophila stoned mutants. *Genetics*, **165**, 185-196.

Fazili, Z., Sun, W., Mittelstaedt, S., Cohen, C. and Xu, X.X. (1999) Disabled-2 inactivation is an early step in ovarian tumorigenicity. *Oncogene*, **18**, 3104-3113.

Fazioli, F., Minichiello, L., Matoskova, B., Wong, W.T. and Di Fiore, P.P. (1993) eps15, a novel tyrosine kinase substrate, exhibits transforming activity. *Mol. Cell Biol.*, **13**, 5814-5828.

Fergestad, T. and Broadie, K. (2001) Interaction of stoned and synaptotagmin in synaptic vesicle endocytosis. *J. Neurosci.*, **21**, 1218-1227.

Ford, M.G., Pearse, B.M., Higgins, M.K., Vallis, Y., Owen, D.J., Gibson, A., Hopkins, C.R., Evans, P.R. and McMahon, H.T. (2001) Simultaneous binding of PtdIns(4,5)P$_2$ and clathrin by AP180 in the nucleation of clathrin lattices on membranes. *Science*, **291**, 1051-1055.

Fotin, A., Cheng, Y., Sliz, P., Grigorieff, N., Harrison, S.C., Kirchhausen, T. and Walz, T. (2004) Molecular model for a complete clathrin lattice from electron cryomicroscopy. *Nature*, **432**, 573-579.

Fujimoto, L.M., Roth, R., Heuser, J.E. and Schmid, S.L. (2000) Actin assembly plays a variable, but not obligatory role in receptor- mediated endocytosis in mammalian cells. *Traffic*, **1**, 161-171.

Futter, C.E., Gibson, A., Allchin, E.H., Maxwell, S., Ruddock, L.J., Odorizzi, G., Domingo, D., Trowbridge, I. and Hopkins, C.R. (1998) In polarized MDCK cells basolateral vesicles arise from clathrin-γ-adaptin-coated domains on endosomal tubules. *J. Cell Biol.*, **141**, 611-624.

Gaidarov, I., Chen, Q., Falck, J.R., Reddy, K.K. and Keen, J.H. (1996) A functional phosphatidylinositol 3,4,5-trisphosphate/phosphoinositide binding domain in the clathrin adaptor AP-2 α subunit. *J. Biol. Chem.*, **271**, 20922-20929.

Gaidarov, I., Krupnick, J.G., Falck, J.R., Benovic, J.L. and Keen, J.H. (1999a) Arrestin function in G protein-coupled receptor endocytosis requires phosphoinositide binding. *EMBO J.*, **18**, 871-881.

Gaidarov, I., Santini, F., Warren, R.A. and Keen, J.H. (1999b) Spatial control of coated-pit dynamics in living cells. *Nat. Cell Biol.*, **1**, 1-7.

Galan, J.M., Moreau, V., Andre, B., Volland, C. and Haguenauer-Tsapis, R. (1996) Ubiquitination mediated by the Npi1p/Rsp5p ubiquitin-protein ligase is required for endocytosis of the yeast uracil permease. *J. Biol. Chem.*, **271**, 10946-10952.

Garcia, C.K., Wilund, K., Arca, M., Zuliani, G., Fellin, R., Maioli, M., Calandra, S., Bertolini, S., Cossu, F., Grishin, N., Barnes, R., Cohen, J.C. and Hobbs, H.H. (2001) Autosomal recessive hypercholesterolemia caused by mutations in a putative LDL receptor adaptor protein. *Science*, **292**, 1394-1398.

Garuti, R., Jones, C., Li, W.P., Michaely, P., Herz, J., Gerard, R.D., Cohen, J.C. and Hobbs, H.H. (2005) The modular adaptor protein autosomal recessive hypercholesterolemia (ARH) promotes low density lipoprotein receptor clustering into clathrin-coated pits. *J. Biol. Chem.*, **280**, 40996-41004.

Ghosh, R.N., Gelman, D.L. and Maxfield, F.R. (1994) Quantification of low density lipoprotein and transferrin endocytic sorting HEp2 cells using confocal microscopy. *J. Cell Sci.*, **107 (Pt 8)**, 2177-2189.

Gonzalez-Gaitan, M. and Jackle, H. (1997) Role of Drosophila alpha-adaptin in presynaptic vesicle recycling. *Cell*, **88**, 767-776.

Grant, B. and Hirsh, D. (1999) Receptor-mediated endocytosis in the Caenorhabditis elegans oocyte. *Mol. Biol. Cell.*, **10**, 4311-4326.

Greene, B., Liu, S.-H., Wilde, A. and Brodsky, F.M. (2000) Complete reconstitution of clathrin basket formation with recombinant protein fragments: Adaptor control of clathrin self-assembly. *Traffic*, **1**, 69-75.

Gurevich, V.V. and Gurevich, E.V. (2004) The molecular acrobatics of arrestin activation. *Trends Pharmacol. Sci.*, **25**, 105-111.

Hammes, A., Andreassen, T.K., Spoelgen, R., Raila, J., Hubner, N., Schulz, H., Metzger, J., Schweigert, F.J., Luppa, P.B., Nykjaer, A. and Willnow, T.E. (2005) Role of endocytosis in cellular uptake of sex steroids. *Cell*, **122**, 751-762.

Han, M., Gurevich, V.V., Vishnivetskiy, S.A., Sigler, P.B. and Schubert, C. (2001) Crystal structure of beta-arrestin at 1.9 A: possible mechanism of receptor binding and membrane Translocation. *Structure*, **9**, 869-880.

Han, W., Ng, Y.K., Axelrod, D. and Levitan, E.S. (1999) Neuropeptide release by efficient recruitment of diffusing cytoplasmic secretory vesicles. *Proc. Natl. Acad. Sci. U S A*, **96**, 14577-14582.

Handley, D.A., Arbeeny, C.M., Witte, L.D. and Chien, S. (1981) Colloidal gold—low density lipoprotein conjugates as membrane receptor probes. *Proc. Natl. Acad. Sci. U S A*, **78**, 368-371.

Hanover, J.A., Willingham, M.C. and Pastan, I. (1984) Kinetics of transit of transferrin and epidermal growth factor through clathrin-coated membranes. *Cell*, **39**, 283-293.

Harada-Shiba, M., Takagi, A., Marutsuka, K., Moriguchi, S., Yagyu, H., Ishibashi, S., Asada, Y. and Yokoyama, S. (2004) Disruption of autosomal recessive hypercholesterolemia gene shows different phenotype in vitro and in vivo. *Circ. Res.*, **95**, 945-952.

Harasaki, K., Lubben, N.B., Harbour, M., Taylor, M.J. and Robinson, M.S. (2005) Sorting of major cargo glycoproteins into clathrin-coated vesicles. *Traffic*, **6**, 1014-1026.

Hausdorff, W.P., Caron, M.G. and Lefkowitz, R.J. (1990) Turning off the signal: desensitization of beta-adrenergic receptor function. *FASEB J.*, **4**, 2881-2889.

Hawryluk, M.J., Keyel, P.A., Mishra, S.K., Watkins, S.C., Heuser, J.E. and Traub, L.M. (2006) Epsin 1 is a polyubiquitin-selective clathrin-associated sorting protein. *Traffic*, **7**, 262-281.

He, G., Gupta, S., Michaely, P., Hobbs, H.H. and Cohen, J.C. (2002) ARH is a modular adaptor protein that interacts with the LDL receptor, clathrin and AP-2. *J. Biol. Chem.*, **277**, 44044-44049.

Heuser, J. (1980) Three-dimensional visualization of coated vesicle formation in fibroblasts. *J. Cell Biol.*, **84**, 560-583.

Heuser, J.E. (2000) Membrane traffic in anaglyph stereo. *Traffic*, **1**, 35-37.

Heuser, J.E. and Anderson, R.G.W. (1989) Hypertonic media inhibit receptor-mediated endocytosis by blocking clathrin-coated pit formation. *J. Cell Biol.*, **108**, 389-400.

Hewitt, E.W., Duncan, L., Mufti, D., Baker, J., Stevenson, P.G. and Lehner, P.J. (2002) Ubiquitylation of MHC class I by the K3 viral protein signals internalization and TSG101-dependent degradation. *EMBO J.*, **21**, 2418-2429.

Hicke, L. (1999) Gettin' down with ubiquitin: turning off cell-surface receptors, transporters and channels. *Trends Cell Biol.*, **9**, 107-112.

Hicke, L. and Riezman, H. (1996) Ubiquitination of a yeast plasma membrane receptor signals its ligand-stimulated endocytosis. *Cell*, **84**, 277-287.

Hilgard, P. and Stockert, R. (2000) Heparan sulfate proteoglycans initiate dengue virus infection of hepatocytes. *Hepatology*, **32**, 1069-1077.

Hinrichsen, L., Harborth, J., Andrees, L., Weber, K. and Ungewickell, E.J. (2003) Effect of clathrin heavy chain- and α-adaptin specific small interfering RNAs on endocytic accessory proteins and receptor trafficking in HeLa cells. *J. Biol. Chem.*, **278**.

Hinrichsen, L., Meyerholz, A., Groos, S. and Ungewickell, E.J. (2006) Bending a membrane: How clathrin affects budding. *Proc. Nat. Acad. Sci. U S A*, **103**, 8715-8720.

Hocevar, B.A., Mou, F., Rennolds, J.L., Morris, S.M., Cooper, J.A. and Howe, P.H. (2003) Regulation of the Wnt signaling pathway by disabled-2 (Dab2). *EMBO J.*, **22**, 3084-3094.

Hocevar, B.A., Prunier, C. and Howe, P.H. (2005) Disabled-2 (Dab2) mediates transforming growth factor beta (TGFbeta)-stimulated fibronectin synthesis through TGFbeta-activated kinase 1 and activation of the JNK pathway. *J. Biol. Chem.*, **280**, 25920-25927.

Hocevar, B.A., Smine, A., Xu, X.X. and Howe, P.H. (2001) The adaptor molecule Disabled-2 links the transforming growth factor beta receptors to the Smad pathway. *EMBO J.*, **20**, 2789-2801.

Hofmann, K. and Falquet, L. (2001) A ubiquitin-interacting motif conserved in components of the proteasomal and lysosomal protein degradation systems. *Trends Biochem. Sci.*, **26**, 347-350.

Honing, S., Ricotta, D., Krauss, M., Spate, K., Spolaore, B., Motley, A., Robinson, M., Robinson, C., Haucke, V. and Owen, D.J. (2005) Phosphatidylinositol-(4,5)-bisphosphate regulates sorting signal recognition by the clathrin-associated adaptor complex AP2. *Mol. Cell*, **18**, 519-531.

Hopkins, C.R. and Trowbridge, I.S. (1983) Internalization and processing of transferrin and the transferrin receptor in human carcinoma A431 cells. *J. Cell Biol.*, **97**, 508-521.

Horak, J. and Wolf, D.H. (1997) Catabolite inactivation of the galactose transporter in the yeast Saccharomyces cerevisiae: ubiquitination, endocytosis, and degradation in the vacuole. *J. Bacteriol.*, **179**, 1541-1549.

Howell, B.W., Lanier, L.M., Frank, R., Gertler, F.B. and Cooper, J.A. (1999) The disabled 1 phosphotyrosine-binding domain binds to the internalization signals of transmembrane glycoproteins and to phospholipids. *Mol. Cell Biol.*, **19**, 5179-5188.

Huang, F., Khvorova, A., Marshall, W. and Sorkin, A. (2004) Analysis of clathrin-mediated endocytosis of epidermal growth factor receptor by RNA interference. *J. Biol. Chem.*, **279**, 16657-16661.

Huang, F., Nesterov, A., Carter, R.E. and Sorkin, A. (2001) Trafficking of yellow-fluorescent-protein-tagged μ1 subunit of clathrin adaptor AP-1 complex in living cells. *Traffic*, **2**, 345-357.

Hubbard, A.L., Wall, D.A. and Ma, A. (1983) Isolation of rat hepatocyte plasma membranes. I. Presence of the three major domains. *J. Cell Biol.*, **96**, 217-229.

Husebye, H., Halaas, O., Stenmark, H., Tunheim, G., Sandanger, O., Bogen, B., Brech, A., Latz, E. and Espevik, T. (2006) Endocytic pathways regulate Toll-like receptor 4 signaling and link innate and adaptive immunity. *EMBO J.*, **25**, 683-692.

Hussain, M.M. (2001) Structural, biochemical and signaling properties of the low-density lipoprotein receptor gene family. *Front. Biosci.*, **6**, D417-D428.

Jackson, A.P., Flett, A., Smythe, C., Hufton, L., Wettey, F.R. and Smythe, E. (2003) Clathrin promotes incorpotration of cargo into coated pits by activation of the AP2 adaptor μ2 kinase. *J. Cell Biol.*, **163**, 231-236.

Jackson, A.P., Seow, H.F., Holmes, N., Drickamer, K. and Parham, P. (1987) Clathrin light chains contain brain-specific insertion sequences and a region of homology with intermediate filaments. *Nature*, **326**, 154-159.

Jaiswal, J.K., Andrews, N.W. and Simon, S.M. (2002) Membrane proximal lysosomes are the major vesicles responsible for calcium-dependent exocytosis in nonsecretory cells. *J. Cell Biol.*, **159**, 625-635.

Janvier, K. and Bonifacino, J.S. (2005) Role of the endocytic machinery in the sorting of lysosome-associated membrane proteins. *Mol. Biol. Cell*, **16**, 4231-4242.

Janvier, K., Kato, Y., Boehm, M., Rose, J.R., Martina, J.A., Kim, B.Y., Venkatesan, S. and Bonifacino, J.S. (2003) Recognition of dileucine-based sorting signals from HIV-1 Nef and LIMP-II by the AP-1 gamma-sigma1 and AP-3 delta-sigma3 hemicomplexes. *J. Cell Biol.*, **163**, 1281-1290.

Jha, A., Agostinelli, N.R., Mishra, S.K., Keyel, P.A., Hawryluk, M.J. and Traub, L.M. (2004) A novel AP-2 adaptor interaction motif initially identified in the long-splice isoform of synaptojanin 1, SJ170. *J. Biol. Chem.*, **279**, 2281-2290.

Jiang, X., Huang, F., Marusyk, A. and Sorkin, A. (2003) Grb2 regulates internalization of EGF receptors through clathrin-coated pits. *Mol. Biol. Cell*, **14**, 858-870.

Jones, C., Hammer, R.E., Li, W.P., Cohen, J.C., Hobbs, H.H. and Herz, J. (2003) Normal sorting, but defective endocytosis of the LDL receptor in mice with autosomal recessive hypercholesterolemia. *J. Biol. Chem.*, **278**, 29024-29030.

Kaksonen, M., Sun, Y. and Drubin, D.G. (2003) A pathway for association of receptors, adaptors, and actin during endocytic internalization. *Cell*, **115**, 475-487.

Kaksonen, M., Toret, C.P. and Drubin, D.G. (2005) A modular design for the clathrin- and actin-mediated endocytosis machinery. *Cell*, **123**, 305-320.

Kaksonen, M., Toret, C.P. and Drubin, D.G. (2006) Harnessing actin dynamics for clathrin-mediated endocytosis. *Nat. Rev. Mol. Cell Biol.*, **7**, 404-414.

Kaneko, T., Maeda, A., Takefuji, M., Aoyama, H., Nakayama, M., Kawabata, S., Kawano, Y., Iwamatsu, A., Amano, M. and Kaibuchi, K. (2005) Rho mediates endocytosis of epidermal growth factor receptor through phosphorylation of endophilin A1 by Rho-kinase. *Genes Cells*, **10**, 973-987.

Keen, J.H. (1987) Clathrin assembly proteins: affinity purification and a model for coat assembly. *J. Cell Biol.*, **105**, 1989-1998.

Keen, J.H., Willingham, M.C. and Pastan, I.H. (1979) Clathrin-coated vesicles: isolation, dissociation and factor-dependent reassociation of clathrin baskets. *Cell*, **16**, 303-312.

Keyel, P.A., Watkins, S.C. and Traub, L.M. (2004) Endocytic adaptor molecules reveal an endosomal population of clathrin by total internal reflection fluorescence microscopy. *J. Biol. Chem.*, **279**, 13190-13204.

Kim, Y.M. and Benovic, J.L. (2002) Differential roles of arrestin-2 interaction with clathrin and adaptor protein 2 in G protein-coupled receptor trafficking. *J. Biol. Chem.*, **277**, 30760-30768.

Kirchhausen, T. (2000) Clathrin. *Annu. Rev. Biochem.*, **69**, 699-727.

Koenig, J.H. and Ikeda, K. (1983) Evidence for a presynaptic blockage of transmission in a temperature-sensitive mutant of Drosophila. *J. Neurobiol.*, **14**, 411-419.

Kohout, T.A., Lin, F.S., Perry, S.J., Conner, D.A. and Lefkowitz, R.J. (2001) beta-Arrestin 1 and 2 differentially regulate heptahelical receptor signaling and trafficking. *Proc. Natl. Acad. Sci. U. S. A.*, **98**, 1601-1606.

Kolling, R. and Hollenberg, C.P. (1994) The ABC-transporter Ste6 accumulates in the plasma membrane in a ubiquitinated form in endocytosis mutants. *EMBO J.*, **13**, 3261-3271.

Konopka, C.A., Schleede, J.B., Skop, A.R. and Bednarek, S.Y. (2006) Dynamin and cytokinesis. *Traffic*, **7**, 239-247.

Kowanetz, K., Husnjak, K., Holler, D., Kowanetz, M., Soubeyran, P., Hirsch, D., Schmidt, M.H., Pavelic, K., De Camilli, P., Randazzo, P.A. and Dikic, I. (2004) CIN85 associates with multiple effectors controlling intracellular trafficking of epidermal growth factor receptors. *Mol. Biol. Cell*, **15**, 3155-3166.

Kowanetz, K., Terzic, J. and Dikic, I. (2003) Dab2 links CIN85 with clathrin-mediated receptor internalization. *FEBS Lett.*, **554**, 81-87.

Kreitzer, G., Schmoranzer, J., Low, S.H., Li, X., Gan, Y., Weimbs, T., Simon, S.M. and Rodriguez-Boulan, E. (2003) Three-dimensional analysis of post-Golgi carrier exocytosis in epithelial cells. *Nat. Cell. Biol.*, **5**, 126-136.

Lafer, E.M. (2002) Clathrin-protein interactions. *Traffic*, **3**, 513-520.

Lakadamyali, M., Rust, M.J., Babcock, H.P. and Zhuang, X. (2003) Visualizing infection of individual influenza viruses. *Proc. Natl. Acad. Sci. U S A*, **100**, 9280-9285.

Lakadamyali, M., Rust, M.J. and Zhuang, X. (2006) Ligands for clathrin-mediated endocytosis are differentially sorted into distinct populations of early endosomes. *Cell*, **124**, 997-1009.

Lampson, M.A., Schmoranzer, J., Zeigerer, A., Simon, S.M. and McGraw, T.E. (2001) Insulin-regulated release from the endosomal recycling compartment is regulated by budding of specialized vesicles. *Mol. Biol. Cell*, **12**, 3489-3501.

Laporte, S.A., Miller, W.E., Kim, K.M. and Caron, M.G. (2002) β-arrestin/AP-2 interaction in G protein-coupled receptor internalization. Identification of a β-arrestin binding site in β2-adaptin. *J. Biol. Chem.*, **277**, 9247-9254.

Laporte, S.A., Oakley, R.H., Holt, J.A., Barak, L.S. and Caron, M.G. (2000) The interaction of β-arrestin with the AP-2 adaptor is required for the clustering of β$_2$-adrenergic receptor into clathrin-coated pits. *J. Biol. Chem.*, **275**, 23120-23126.

Laporte, S.A., Oakley, R.H., Zhang, J., Holt, J.A., Ferguson, S.S., Caron, M.G. and Barak, L.S. (1999) The β2-adrenergic receptor/βarrestin complex recruits the clathrin adaptor AP-2 during endocytosis. *Proc. Natl. Acad. Sci. U. S. A.*, **96**, 3712-3717.

Le Roy, C. and Wrana, J.L. (2005) Clathrin- and non-clathrin-mediated endocytic regulation of cell signalling. *Nat. Rev. Mol. Cell Biol.*, **6**, 112-126.

Lee, T.H. and Linstedt, A.D. (1999) Osmotically induced cell volume changes alter anterograde and retrograde transport, Golgi structure, and COPI dissociation. *Mol. Biol. Cell*, **10**, 1445-1462.

Letourneur, F. and Klausner, R.D. (1992) A novel di-leucine motif and a tyrosine-based motif independently mediate lysosomal targeting and endocytosis of CD3 chains. *Cell*, **69**, 1143-1157.

Li, C., Ullrich, B., Zhang, J.Z., Anderson, R.G., Brose, N. and Sudhof, T.C. (1995) Ca(2+)-dependent and -independent activities of neural and non-neural synaptotagmins. *Nature*, **375**, 594-599.

Li, S.C., Zwahlen, C., Vincent, S.J., McGlade, C.J., Kay, L.E., Pawson, T. and Forman-Kay, J.D. (1998) Structure of a Numb PTB domain-peptide complex suggests a basis for diverse binding specificity. *Nat. Struct. Biol.*, **5**, 1075-1083.

Lippincott-Schwartz, J. and Fambrough, D.M. (1986) Lysosomal membrane dynamics: structure and interorganellar movement of a major lysosomal membrane glycoprotein. *J. Cell Biol.*, **102**, 1593-1605.

Liu, S.-H., Wong, M.L., Craik, C.S. and Brodsky, F.M. (1995) Regulation of clathrin assembly and trimerization defined using recombinant triskelion hubs. *Cell*, **83**, 257-267.

Lundmark, R. and Carlsson, S.R. (2002) The β-appendages of the four adaptor-protein (AP) complexes: structure and binding properties, and identification of sorting nexin 9 as an accessory protein to AP-2. *Biochem. J.*, **362**, 597-607.

Marchese, A., Raiborg, C., Santini, F., Keen, J.H., Stenmark, H. and Benovic, J.L. (2003) The E3 ubiquitin ligase AIP4 mediates ubiquitination and sorting of the G protein-coupled receptor CXCR4. *Dev. Cell*, **5**, 709-722.

Marks, M.S., L., W., Ohno, H. and Bonifacino, J.S. (1996) Protein targeting by tyrosine- and di-leucine-based signals: evidence for distinct saturable components. *J. Cell Biol.*, **135**, 341-354.

Marsh, M. and Helenius, A. (2006) Virus entry: open sesame. *Cell*, **124**, 729-740.

Martina, J.A., Bonangelino, C.J., Aguilar, R.C. and Bonifacino, J.S. (2001) Stonin 2: an adaptor-like protein that interacts with components of the endocytic machinery. *J. Cell Biol.*, **153**, 1111-1120.

Maurer, M.E. and Cooper, J.A. (2005) Endocytosis of megalin by visceral endoderm cells requires the Dab2 adaptor protein. *J. Cell. Sci.*, **118**, 5345-5355.

Maurer, M.E. and Cooper, J.A. (2006) The adaptor protein Dab2 sorts LDL receptors into coated pits independently of AP-2 and ARH. *J. Cell Sci.*, *in press*.

Maxfield, F.R. and McGraw, T.E. (2004) Endocytic recycling. *Nat. Rev. Mol. Cell Biol.*, **5**, 121-132.

Maxfield, F.R., Schlessinger, J., Shechter, Y., Pastan, I. and Willingham, M.C. (1978) Collection of insulin, EGF and alpha2-macroglobulin in the same patches on the surface of cultured fibroblasts and common internalization. *Cell*, **14**, 805-810.

Mayor, S., Presley, J.F. and Maxfield, F.R. (1993) Sorting of membrane components from endosomes and subsequent recycling to the cell surface occurs by a bulk flow process. *J. Cell Biol.*, **121**, 1257-1269.

Medintz, I., Jiang, H. and Michels, C.A. (1998) The role of ubiquitin conjugation in glucose-induced proteolysis of Saccharomyces maltose permease. *J. Biol. Chem.*, **273**, 34454-34462.

Merrifield, C.J., Feldman, M.E., Wan, L. and Almers, W. (2002) Imaging actin and dynamin recruitment during invagination of single clathrin-coated pits. *Nat. Cell Biol.*, **4**, 691-698.

Merrifield, C.J., Moss, S.E., Ballestrem, C., Imhof, B.A., Giese, G., Wunderlich, I. and Almers, W. (1999) Endocytic vesicles move at the tips of actin tails in cultured mast cells. *Nat. Cell Biol.*, **1**, 72-74.

Merrifield, C.J., Perrais, D. and Zenisek, D. (2005) Coupling between clathrin-coated-pit invagination, cortactin recruitment, and membrane scission observed in live cells. *Cell*, **121**, 593-606.

Metzler, M., Legendre-Guillemin, V., Gan, L., Chopra, V., Kwok, A., McPherson, P.S. and Hayden, M.R. (2001) HIP1 functions in clathrin-mediated endocytosis through binding to clathrin and AP2. *J. Biol. Chem.*, **21**, 21.

Meyer, C., Zizioli, D., Lausmann, S., Eskelinen, E.L., Hamann, J., Saftig, P., von Figura, K. and Schu, P. (2000) µ1A-adaptin-deficient mice: lethality, loss of AP-1 binding and rerouting of mannose 6-phosphate receptors. *EMBO J.*, **19**, 2193-2203.

Meyerholz, A., Hinrichsen, L., Groos, S., Esk, P.C., Brandes, G. and Ungewickell, E.J. (2005) Effect of clathrin assembly lymphoid myeloid leukemia protein depletion on clathrin coat formation. *Traffic*, **6**, 1225-1234.

Miele, A.E., Watson, P.J., Evans, P.R., Traub, L.M. and Owen, D.J. (2004) Two distinct interaction motifs in amphiphysin bind two independent sites on the clathrin terminal domain beta-propeller. *Nat. Struct. Mol. Biol.*, **11**, 242-248.

Milano, S.K., Pace, H.C., Kim, Y.M., Brenner, C. and Benovic, J.L. (2002) Scaffolding functions of arrestin-2 revealed by crystal structure and mutagenesis. *Biochemistry*, **41**, 3321-3328.

Minamide, L.S. and Bamburg, J.R. (1990) A filter paper dye-binding assay for quantitative determination of protein without interference from reducing agents or detergents. *Anal. Biochem.*, **190**, 66-70.

Mishra, S.K., Agostinelli, N.R., Brett, T.J., Mizukami, I., Ross, T.S. and Traub, L.M. (2001) Clathrin- and AP-2-binding sites in HIP1 uncover a general assembly role for endocytic accessory proteins. *J. Biol. Chem.*, **276**, 46230-46236.

Mishra, S.K., Hawryluk, M.J., Brett, T.J., Keyel, P.A., Dupin, A.L., Jha, A., Heuser, J.E., Fremont, D.H. and Traub, L.M. (2004) Dual engagement regulation of protein interactions with the AP-2 adaptor alpha appendage. *J. Biol. Chem.*, **279**, 46191-46203.

Mishra, S.K., Keyel, P.A., Edeling, M.A., Dupin, A.L., Owen, D.J. and Traub, L.M. (2005) Functional dissection of an AP-2 beta2 appendage-binding sequence within the autosomal recessive hypercholesterolemia protein. *J. Biol. Chem.*, **280**, 19270-19280.

Mishra, S.K., Keyel, P.A., Hawryluk, M.J., Agostinelli, N.R., Watkins, S.C. and Traub, L.M. (2002a) Disabled-2 exhibits the properties of a cargo-selective endocytic clathrin adaptor. *EMBO J.*, **21**, 4915-4926.

Mishra, S.K., Watkins, S.C. and Traub, L.M. (2002b) The autosomal recessive hypercholesterolemia (ARH) protein interfaces directly with the clathrin-coat machinery. *Proc. Natl. Acad. Sci. U S A*, **99**, 16099-16104.

Mitsunari, T., Nakatsu, F., Shioda, N., Love, P.E., Grinberg, A., Bonifacino, J.S. and Ohno, H. (2005) Clathrin adaptor AP-2 is essential for early embryonal development. *Mol. Cell. Biol.*, **25**, 9318-9323.

Mok, S.C., Chan, W.Y., Wong, K.K., Cheung, K.K., Lau, C.C., Ng, S.W., Baldini, A., Colitti, C.V., Rock, C.O. and Berkowitz, R.S. (1998) DOC-2, a candidate tumor suppressor gene in human epithelial ovarian cancer. *Oncogene*, **16**, 2381-2387.

Monjas, A., Alcover, A. and Alarcon, B. (2004) Engaged and bystander T cell receptors are down-modulated by different endocytotic pathways. *J. Biol. Chem.*, **279**, 55376-55384.

Morris, S.M., Arden, S.D., Roberts, R.C., Kendrick-Jones, J., Cooper, J.A., Luzio, J.P. and Buss, F. (2002a) Myosin VI Binds to and Localises with Dab2, Potentially Linking Receptor-Mediated Endocytosis and the Actin Cytoskeleton. *Traffic*, **3**, 331-341.

Morris, S.M. and Cooper, J.A. (2001) Disabled-2 colocalizes with the LDLR in clathrin-coated pits and interacts with AP-2. *Traffic*, **2**, 111-123.

Morris, S.M., Tallquist, M.D., Rock, C.O. and Cooper, J.A. (2002b) Dual roles for the Dab2 adaptor protein in embryonic development and kidney transport. *EMBO J.*, **21**, 1555-1564.

Motley, A., Bright, N.A., Seaman, M.N. and Robinson, M.S. (2003) Clathrin-mediated endocytosis in AP-2-depleted cells. *J. Cell Biol.*, **162**, 909-918.

Mukherjee, S., Tessema, M. and Wandinger-Ness, A. (2006) Vesicular trafficking of tyrosine kinase receptors and associated proteins in the regulation of signaling and vascular function. *Circ. Res.*, **98**, 743-756.

Nagai, M., Meerloo, T., Takeda, T. and Farquhar, M.G. (2003) The Adaptor Protein ARH Escorts Megalin to and through Endosomes. *Mol. Biol. Cell*.

Nakagawa, T., Setou, M., Seog, D., Ogasawara, K., Dohmae, N., Takio, K. and Hirokawa, N. (2000) A novel motor, KIF13A, transports mannose-6-phosphate receptor to plasma membrane through direct interaction with AP-1 complex. *Cell*, **103**, 569-581.

Naoumova, R.P., Neuwirth, C., Lee, P., Miller, J.P., Taylor, K.G. and Soutar, A.K. (2004) Autosomal recessive hypercholesterolaemia: long-term follow up and response to treatment. *Atherosclerosis*, **174**, 165-172.

Nathke, I.S., Heuser, J., Lupas, A., Stock, J., Turck, C.W. and Brodsky, F.M. (1992) Folding and trimerization of clathrin subunits at the triskelion hub. *Cell*, **68**, 899-910.

Neutra, M.R., Ciechanover, A., Owen, L.S. and Lodish, H.F. (1985) Intracellular transport of transferrin- and asialoorosomucoid-colloidal gold conjugates to lysosomes after receptor-mediated endocytosis. *J. Histochem. Cytochem.*, **33**, 1134-1144.

Oakley, R.H., Laporte, S.A., Holt, J.A., Barak, L.S. and Caron, M.G. (1999) Association of beta-arrestin with G protein-coupled receptors during clathrin-mediated endocytosis dictates the profile of receptor resensitization. *J. Biol. Chem.*, **274**, 32248-32257.

Ohno, H., J., S., Fournier, M.-C., Bosshart, H., Rhee, I., Miyatake, S., Saito, T., Galluser, A., Kirchhausen, T. and Bonifacino, J.S. (1995) Interaction of tyrosine-based sorting signals with clathrin-associated proteins. *Science*, **269**, 1872-1875.

Oleinikov, A.V., Zhao, J. and Makker, S.P. (2000) Cytosolic adaptor protein Dab2 is an intracellular ligand of endocytic receptor gp600/megalin. *Biochem. J.*, **347 Pt 3**, 613-621.

Olusanya, O., Andrews, P.D., Swedlow, J.R. and Smythe, E. (2001) Phosphorylation of threonine 156 of the μ2 subunit of the AP2 complex is essential for endocytosis in vitro and in vivo. *Curr. Biol.*, **11**, 896-900.

Orci, L., Carpentier, J.L., Perrelet, A., Anderson, R.G., Goldstein, J.L. and Brown, M.S. (1978) Occurrence of low density lipoprotein receptors within large pits on the surface of human fibroblasts as demonstrated by freeze-etching. *Exp. Cell Res.*, **113**, 1-13.

Osono, Y., Woollett, L.A., Herz, J. and Dietschy, J.M. (1995) Role of the low density lipoprotein receptor in the flux of cholesterol through the plasma and across the tissues of the mouse. *J. Clin. Invest.*, **95**, 1124-1132.

Owen, D.J., Collins, B.M. and Evans, P.R. (2004) Adaptors for clathrin coats: structure and function. *Annu. Rev. Cell Dev. Biol.*, **20**, 153-191.

Owen, D.J. and Evans, P.R. (1998) A structural explanation for the recognition of tyrosine-based endocytotic signals. *Science*, **282**, 1327-1332.

Owen, D.J. and Luzio, J.P. (2000) Structural insights into clathrin-mediated endocytosis. *Curr. Opin. Cell Biol.*, **12**, 467-474.

Owen, D.J., Vallis, Y., Noble, M.E., Hunter, J.B., Dafforn, T.R., Evans, P.R. and McMahon, H.T. (1999) A structural explanation for the binding of multiple ligands by the α-adaptin appendage domain. *Cell*, **97**, 805-815.

Owen, D.J., Vallis, Y., Pearse, B.M., McMahon, H.T. and Evans, P.R. (2000) The structure and function of the β2-adaptin appendage domain. *EMBO J.*, **19**, 4216-4227.

Paavola, L.G., Strauss, J.F., 3rd, Boyd, C.O. and Nestler, J.E. (1985) Uptake of gold- and [^{3}H]cholesteryl linoleate-labeled human low density lipoprotein by cultured rat granulosa cells: cellular mechanisms involved in lipoprotein metabolism and their importance to steroidogenesis. *J. Cell Biol.*, **100**, 1235-1247.

Page, L. and Robinson, M. (1995) Targeting signals and subunit interactions in coated vesicle adaptor complexes. *J. Cell Biol.*, **131**, 619-630.

Panakova, D., Sprong, H., Marois, E., Thiele, C. and Eaton, S. (2005) Lipoprotein particles are required for Hedgehog and Wingless signalling. *Nature*, **435**, 58-65.

Pasieka, T.J., Maresova, L. and Grose, C. (2003) A functional YNKI motif in the short cytoplasmic tail of varicella-zoster virus glycoprotein gH mediates clathrin-dependent and antibody-independent endocytosis. *J. Virol.*, **77**, 4191-4204.

Pearse, B.M. (1975) Coated vesicles from pig brain: purification and biochemical characterization. *J. Mol. Biol.*, **97**, 93-98.

Petrovich, T.Z., Merakovsky, J. and Kelly, L.E. (1993) A genetic analysis of the stoned locus and its interaction with dunce, shibire and Suppressor of stoned variants of Drosophila melanogaster. *Genetics*, **133**, 955-965.

Poodry, C.A. and Edgar, L. (1979) Reversible alteration in the neuromuscular junctions of Drosophila melanogaster bearing a temperature-sensitive mutation, shibire. *J. Cell Biol.*, **81**, 520-527.

Praefcke, G.J., Ford, M.G., Schmid, E.M., Olesen, L.E., Gallop, J.L., Peak-Chew, S.Y., Vallis, Y., Babu, M.M., Mills, I.G. and McMahon, H.T. (2004) Evolving nature of the AP2 alpha-appendage hub during clathrin-coated vesicle endocytosis. *EMBO J.*, **23**, 4371-4383.

Presley, J.F., Ward, T.H., Pfeifer, A.C., Siggia, E.D., Phair, R.D. and Lippincott-Schwartz, J. (2002) Dissection of COPI and Arf1 dynamics in vivo and role in Golgi membrane transport. *Nature*, **417**, 187-193.

Qualmann, B., Kessels, M.M. and Kelly, R.B. (2000) Molecular links between endocytosis and the actin cytoskeleton. *J. Cell Biol.*, **150**, F111-F116.

Raiborg, C., Gronvold Bache, K., Mehlum, A., Stang, E. and Stenmark, H. (2001) Hrs recruits clathrin to early endosomes. *EMBO J.*, **20**, 5008-5021.

Ramjaun, A.R. and McPherson, P.S. (1998) Multiple amphiphysin II splice variants display differential clathrin binding: identification of two distinct clathrin-binding sites. *J. Neurochem.*, **70**, 2369-2376.

Rapoport, I., Chen, Y.C., Cupers, P., Shoelson, S.E. and Kirchhausen, T. (1998) Dileucine-based sorting signals bind to the beta chain of AP-1 at a site distinct and regulated differently from the tyrosine-based motif-binding site. *EMBO J.*, **17**, 2148-2155.

Rappoport, J.Z. and Simon, S.M. (2003) Real-time analysis of clathrin-mediated endocytosis during cell migration. *J. Cell Sci.*, **116**, 847-855.

Rappoport, J.Z., Taha, B.W., Lemeer, S., Benmerah, A. and Simon, S.M. (2003a) The AP-2 complex is excluded from the dynamic population of plasma membrane-associated clathrin. *J. Biol. Chem.*, **278**, 47357-47360.

Rappoport, J.Z., Taha, B.W. and Simon, S.M. (2003b) Movement of plasma-membrane-associated clathrin spots along the microtubule cytoskeleton. *Traffic*, **4**, 460-467.

Ren, G., Vajjhala, P., Lee, J.S., Winsor, B. and Munn, A.L. (2006) The BAR domain proteins: molding membranes in fission, fusion, and phagy. *Microbiol. Mol. Biol. Rev.*, **70**, 37-120.

Ricotta, D., Conner, S.D., Schmid, S.L., von Figura, K. and Honing, S. (2002) Phosphorylation of the AP2 µ subunit by AAK1 mediates high affinity binding to membrane protein sorting signals. *J. Cell Biol.*, **156**, 791-795.

Rink, J., Ghigo, E., Kalaidzidis, Y. and Zerial, M. (2005) Rab conversion as a mechanism of progression from early to late endosomes. *Cell*, **122**, 735-749.

Ritter, B., Denisov, A.Y., Philie, J., Deprez, C., Tung, E.C., Gehring, K. and McPherson, P.S. (2004) Two WXXF-based motifs in NECAPs define the specificity of accessory protein binding to AP-1 and AP-2. *EMBO J.*, **23**, 3701-3710.

Ritter, B., Philie, J., Girard, M., Tung, E.C., Blondeau, F. and McPherson, P.S. (2003) Identification of a family of endocytic proteins that define a new α-adaptin ear-binding motif. *EMBO Rep.*

Robinson, M.S. (2004) Adaptable adaptors for coated vesicles. *Trends Cell Biol.*, **14**, 167-174.

Robinson, M.S. and Pearse, B.M. (1986) Immunofluorescent localization of 100K coated vesicle proteins. *J. Cell Biol.*, **102**, 48-54.

Rosenthal, J.A., Chen, H., Slepnev, V.I., Pellegrini, L., Salcini, A.E., Di Fiore, P.P. and De Camilli, P. (1999) The epsins define a family of proteins that interact with components of the clathrin coat and contain a new protein module. *J. Biol. Chem.*, **274**, 33959-33965.

Rossanese, O.W., Soderholm, J., Bevis, B.J., Sears, I.B., O'Connor, J., Williamson, E.K. and Glick, B.S. (1999) Golgi structure correlates with transitional endoplasmic reticulum organization in Pichia pastoris and Saccharomyces cerevisiae. *J. Cell Biol.*, **145**, 69-81.

Roth, A.F. and Davis, N.G. (1996) Ubiquitination of the yeast **a**-factor receptor. *J. Cell Biol.*, **134**, 661-574.

Roth, T.F. and Porter, K.R. (1964) Yolk Protein Uptake in the Oocyte of the Mosquito Aedes Aegypti. L. *J. Cell. Biol.*, **20**, 313-332.

Royle, S.J. and Lagnado, L. (2003) Endocytosis at the synaptic terminal. *J. Physiol.*, **553**, 345-355.

Sachse, M., Urbe, S., Oorschot, V., Strous, G.J. and Klumperman, J. (2002) Bilayered Clathrin Coats on Endosomal Vacuoles Are Involved in Protein Sorting toward Lysosomes. *Mol. Biol. Cell*, **13**, 1313-1328.

Sakai, T., Yamashina, S. and Ohnishi, S. (1991) Microtubule-disrupting drugs blocked delivery of endocytosed transferrin to the cytocenter, but did not affect return of transferrin to plasma membrane. *J. Biochem (Tokyo)*, **109**, 528-533.

Salzman, N.H. and Maxfield, F.R. (1989) Fusion accessibility of endocytic compartments along the recycling and lysosomal endocytic pathways in intact cells. *J. Cell Biol.*, **109**, 2097-2104.

Sanan, D.A. and Anderson, R.G. (1991) Simultaneous visualization of LDL receptor distribution and clathrin lattices on membranes torn from the upper surface of cultured cells. *J. Histochem. Cytochem.*, **39**, 1017-1024.

Sanan, D.A., Van der Westhuyzen, D.R., Gevers, W. and Coetzee, G.A. (1987) The surface distribution of low density lipoprotein receptors on cultured fibroblasts and endothelial cells. Ultrastructural evidence for dispersed receptors. *Histochemistry*, **86**, 517-523.

Santini, F., Gaidarov, I. and Keen, J.H. (2002) G protein-coupled receptor/arrestin3 modulation of the endocytic machinery. *J. Cell Biol.*, **156**, 665-676.

Santini, F. and Keen, J.H. (2002) A glimpse of coated vesicle creation? Well almost! *Nat. Cell Biol.*, **4**, E230-E232.

Santini, F., Marks, M.S. and Keen, J.H. (1998) Endocytic clathrin-coated pit formation is independent of receptor internalization signal levels. *Mol. Biol. Cell*, **9**, 1177-1194.

Santini, F., Penn, R.B., Gagnon, A.W., Benovic, J.L. and Keen, J.H. (2000) Selective recruitment of arrestin-3 to clathrin coated pits upon stimulation of G protein-coupled receptors. *J. Cell Sci.*, **113 (Pt 13)**, 2463-2470.

Schmid, E.M., Ford, M.G., Burtey, A., Praefcke, G.J., Peak Chew, S.Y., Mills, I.G., Benmerah, A. and Mcmahon, H.T. (2006) Role of the AP2 β-appendage hub in recruiting partners for clathrin coated vesicle assembly. *PLoS Biol.*, **4**, in press.

Schmidt, U., Briese, S., Leicht, K., Schurmann, A., Joost, H.G. and Al-Hasani, H. (2006) Endocytosis of the glucose transporter GLUT8 is mediated by interaction of a dileucine motif with the beta2-adaptin subunit of the AP-2 adaptor complex. *J. Cell Sci.*, **119**, 2321-3231.

Schmoranzer, J. and Simon, S.M. (2003) Role of microtubules in fusion of post-Golgi vesicles to the plasma membrane. *Mol. Biol. Cell*, **14**, 1558-1569.

Scott, M.G., Benmerah, A., Muntaner, O. and Marullo, S. (2002) Recruitment of activated G protein-coupled receptors to pre-existing clathrin-coated pits in living cells. *J. Biol. Chem.*, **277**, 3552-3559.

Sever, S., Damke, H. and Schmid, S.L. (2000) Garrotes, springs, ratchets, and whips: putting dynamin models to the test. *Traffic*, **1**, 385-392.

Shaner, N.C., Campbell, R.E., Steinbach, P.A., Giepmans, B.N., Palmer, A.E. and Tsien, R.Y. (2004) Improved monomeric red, orange and yellow fluorescent proteins derived from Discosoma sp. red fluorescent protein. *Nat. Biotechnol.*, **22**, 1567-1572.

Shim, J. and Lee, J. (2000) Molecular genetic analysis of apm-2 and aps-2, genes encoding the medium and small chains of the AP-2 clathrin-associated protein complex in the nematode Caenorhabditis elegans. *Mol. Cells*, **10**, 309-316.

Shupliakov, O., Low, P., Grabs, D., Gad, H., Chen, H., David, C., Takei, K., De Camilli, P. and Brodin, L. (1997) Synaptic vesicle endocytosis impaired by disruption of dynamin-SH3 domain interactions. *Science*, **276**, 259-263.

Slepnev, V.I. and De Camilli, P. (2000) Accessory factors in clathrin-dependent synaptic vesicle endocytosis. *Nat. Rev. Neurosci.*, **1**, 161-172.

Smith, C.J., Grigorieff, N. and Pearse, B.M. (1998) Clathrin coats at 21 A resolution: a cellular assembly designed to recycle multiple membrane receptors. *EMBO J.*, **17**, 4943-4953.

Snyers, L., Zwickl, H. and Blaas, D. (2003) Human rhinovirus type 2 is internalized by clathrin-mediated endocytosis. *J. Virol.*, **77**, 5360-5369.

Sorkin, A. (2004) Cargo recognition during clathrin-mediated endocytosis: a team effort. *Curr. Opin. Cell Biol.*, **16**, 392-399.

Sorkin, A., Krolenko, S., Kudrjavtceva, N., Lazebnik, J., Teslenko, L., Soderquist, A.M. and Nikolsky, N. (1991) Recycling of epidermal growth factor-receptor complexes in A431 cells: identification of dual pathways. *J. Cell Biol.*, **112**, 55-63.

Sorkin, A., McKinsey, T., Shih, W., Kirchhausen, T. and Carpenter, G. (1995) Stoichiometric interaction of the epidermal growth factor receptor with the clathrin-associated protein complex AP-2. *J. Biol. Chem.*, **270**, 619-625.

Sorkina, T., Huang, F., Beguinot, L. and Sorkin, A. (2002) Effect of tyrosine kinase inhibitors on clathrin-coated pit recruitment and internalization of epidermal growth factor receptor. *J. Biol. Chem.*, **277**, 27433-27441.

Soutar, A.K., Naoumova, R.P. and Traub, L.M. (2003) Genetics, clinical phenotype, and molecular cell biology of autosomal recessive hypercholesterolemia. *Arterioscler. Thromb. Vasc. Biol.*

Springael, J.Y. and Andre, B. (1998) Nitrogen-regulated ubiquitination of the Gap1 permease of Saccharomyces cerevisiae. *Mol. Biol. Cell.*, **9**, 1253-1263.

Steyer, J.A., Horstmann, H. and Almers, W. (1997) Transport, docking and exocytosis of single secretory granules in live chromaffin cells. *Nature*, **388**, 474-478.

Stoddart, A., Dykstra, M.L., Brown, B.K., Song, W., Pierce, S.K. and Brodsky, F.M. (2002) Lipid rafts unite signaling cascades with clathrin to regulate BCR internalization. *Immunity*, **17**, 451-462.

Stolt, P.C., Jeon, H., Song, H.K., Herz, J., Eck, M.J. and Blacklow, S.C. (2003) Origins of peptide selectivity and phosphoinositide binding revealed by structures of Disabled-1 PTB domain complexes. *Structure (Camb)*, **11**, 569-579.

Stolt, P.C., Vardar, D. and Blacklow, S.C. (2004) The dual-function disabled-1 PTB domain exhibits site independence in binding phosphoinositide and peptide ligands. *Biochemistry*, **43**, 10979-10987.

Stoorvogel, W., Geuze, H.J. and Strous, G.J. (1987) Sorting of endocytosed transferrin and asialoglycoprotein occurs immediately after internalization in HepG2 cells. *J, Cell Biol*,, **104**, 1261-1268.

Stoorvogel, W., Oorschot, V. and Geuze, H.J. (1996) A novel class of clathrin-coated vesicles budding from endosomes. *J. Cell Biol.*, **132**, 21-33.

Sweitzer, S.M. and Hinshaw, J.E. (1998) Dynamin undergoes a GTP-dependent conformational change causing vesiculation. *Cell*, **93**, 1021-1029.

Tabas, I. and Kornfeld, S. (1979) Purification and characterization of a rat liver Golgi alpha-mannosidase capable of processing asparagine-linked oligosaccharides. *J. Biol. Chem.*, **254**, 11655-11663.

Tabas, I., Lim, S., Xu, X.X. and Maxfield, F.R. (1990) Endocytosed beta-VLDL and LDL are delivered to different intracellular vesicles in mouse peritoneal macrophages. *J. Cell Biol.*, **111**, 929-940.

Takei, K., Haucke, V., Slepnev, V., Farsad, K., Salazar, M., Chen, H. and De Camilli, P. (1998) Generation of coated intermediates of clathrin-mediated endocytosis on protein-free liposomes. *Cell*, **94**, 131-141.

Takei, K., Slepnev, V.I., Haucke, V. and De Camilli, P. (1999) Functional partnership between amphiphysin and dynamin in clathrin-mediated endocytosis. *Nat. Cell Biol.*, **1**, 33-39.

Tebar, F., Sorkina, T., Sorkin, A., Ericsson, M. and Kirchhausen, T. (1996) eps15 is a component of clathrin-coated pits and vesicles and is located at the rim of clathrin-coated pits. *J. Biol. Chem.*, **271**, 28727-28730.

ter Haar, E., Harrison, S.C. and Kirchhausen, T. (2000) Peptide-in-groove interactions link target proteins to the beta-propeller of clathrin. *Proc. Natl. Acad. Sci. U S A*, **97**, 1096-1100.

ter Haar, E., Musacchio, A., Harrison, S.C. and Kirchhausen, T. (1998) Atomic structure of clathrin: a β propeller terminal domain joins an α zigzag linker. *Cell*, **95**, 563-573.

Toomre, D., Steyer, J.A., Keller, P., Almers, W. and Simons, K. (2000) Fusion of constitutive membrane traffic with the cell surface observed by evanescent wave microscopy. *J. Cell Biol.*, **149**, 33-40.

Toshima, J.Y., Toshima, J., Kaksonen, M., Martin, A.C., King, D.S. and Drubin, D.G. (2006) Spatial dynamics of receptor-mediated endocytic trafficking in budding yeast revealed by

using fluorescent alpha-factor derivatives. *Proc. Natl. Acad. Sci. U. S. A.*, **103**, 5793-5798.

Tosoni, D., Puri, C., Confalonieri, S., Salcini, A.E., De Camilli, P., Tacchetti, C. and Di Fiore, P.P. (2005) TTP specifically regulates the internalization of the transferrin receptor. *Cell*, **123**, 875-888.

Traub, L.M. (2003) Sorting it out: AP-2 and alternate clathrin adaptors in endocytic cargo selection. *J. Cell Biol.*, **163**, 203-208.

Traub, L.M. (2005) Common principles in clathrin-mediated sorting at the Golgi and the plasma membrane. *Biochim. Biophys. Acta.*, **1744**, 415-437.

Traub, L.M., Bannykh, S.I., Rodel, J.E., Aridor, M., Balch, W.E. and Kornfeld, S. (1996) AP-2–containing clathrin coats assemble on mature lysosomes. *J. Cell Biol.*, **135**, 1801-1804.

Traub, L.M., Downs, M.A., Westrich, J.L. and Fremont, D.H. (1999) Crystal structure of the α appendage of AP-2 reveals a recruitment platform for clathrin-coat assembly. *Proc. Natl. Acad. Sci. USA*, **96**, 8907-8912.

Traub, L.M., Kornfeld, S. and Ungewickell, E. (1995) Different domains of the AP-1 adaptor complex are required for Golgi membrane binding and clathrin recruitment. *J. Biol. Chem.*, **270**, 4933-4942.

Tuma, P.L. and Collins, C.A. (1995) Dynamin forms polymeric complexes in the presence of lipid vesicles. Characterization of chemically cross-linked dynamin molecules. *J. Biol. Chem.*, **270**, 26707-26714.

Tycko, B., Keith, C.H. and Maxfield, F.R. (1983) Rapid acidification of endocytic vesicles containing asialoglycoprotein in cells of a human hepatoma line. *J. Cell Biol.*, **97**, 1762-1776.

Tycko, B. and Maxfield, F.R. (1982) Rapid acidification of endocytic vesicles containing alpha 2-macroglobulin. *Cell*, **28**, 643-651.

Ungewickell, E. and Branton, D. (1981) Assembly units of clathrin coats. *Nature (Lond.)*, **289**, 420-422.

Ungewickell, E. and Ungewickell, H. (1991) Bovine Brain Clathrin Light Chains Impede Heavy Chain Assembly *in Vitro*. *J. Biol. Chem.*, **266**, 12710-12714.

Ungewickell, E., Ungewickell, H., Holstein, S.E.H., Lindner, R., Prasad, K., Barouch, W., Martin, B., Greene, L.E. and Eisenberg, E. (1995) Role of auxilin in uncoating clathrin-coated vesicles. *Nature*, **378**, 632-635.

van Dam, E.M. and Stoorvogel, W. (2002) Dynamin-dependent transferrin receptor recycling by endosome-derived clathrin-coated vesicles. *Mol. Biol. Cell*, **13**, 169-182.

Veiga, E. and Cossart, P. (2005) Listeria hijacks the clathrin-dependent endocytic machinery to invade mammalian cells. *Nat. Cell Biol.*, **7**, 894-900.

Via, D.P., Willingham, M.C., Pastan, I., Gotto, A.M., Jr. and Smith, L.C. (1982) Co-clustering and internalization of low-density lipoproteins and α_2-macroglobulin in human skin fibroblasts. *Exp. Cell Res.*, **141**, 15-22.

Waguri, S., Dewitte, F., Le Borgne, R., Rouille, Y., Uchiyama, Y., Dubremetz, J.F. and Hoflack, B. (2003) Visualization of TGN to endosome trafficking through fluorescently labeled MPR and AP-1 in living cells. *Mol. Biol. Cell*, **14**, 142-155.

Walther, K., Diril, M.K., Jung, N. and Haucke, V. (2004) Functional dissection of the interactions of stonin 2 with the adaptor complex AP-2 and synaptotagmin. *Proc. Natl. Acad. Sci. U. S. A.*, **101**, 964-969.

Walther, K., Krauss, M., Diril, M.K., Lemke, S., Ricotta, D., Honing, S., Kaiser, S. and Haucke, V. (2001) Human stoned B interacts with AP-2 and synaptotagmin and facilitates clathrin-coated vesicle uncoating. *EMBO Rep.*, **2**, 634-640.

Wang, H., Traub, L.M., Weixel, K.M., Hawryluk, M.J., Shah, N., Edinger, R.S., Perry, C.J., Kester, L., Butterworth, M.B., Peters, K.W., Kleyman, T.R., Frizzell, R.A. and Johnson, J.P. (2006) Clathrin-mediated endocytosis of the epithelial sodium channel. Role of epsin. *J. Biol. Chem.*, **281**, 14129-14135.

Warren, R.A., Green, F.A. and Enns, C.A. (1997) Saturation of the endocytic pathway for the transferrin receptor does not affect the endocytosis of the epidermal growth factor receptor. *J. Biol. Chem.*, **272**, 2116-2121.

Warren, R.A., Green, F.A., Stenberg, P.E. and Enns, C.A. (1998) Distinct saturable pathways for the endocytosis of different tyrosine motifs. *J. Biol. Chem.*, **273**, 17056-17063.

Wigge, P., Vallis, Y. and Mcmahon, H.T. (1997) Inhibition of receptor-mediated endocytosis by the amphiphysin SH3 domain. *Curr. Biol.*, **7**, 554-560.

Willingham, M.C., Haigler, H.T., Fitzgerald, D.J., Gallo, M.G., Rutherford, A.V. and Pastan, I.H. (1983) The morphologic pathway of binding and internalization of epidermal growth factor in cultured cells. Studies on A431, KB, and 3T3 cells, using multiple methods of labelling. *Exp. Cell Res.*, **146**, 163-175.

Willingham, M.C., Pastan, I.H., Sahagian, G.G., Jourdian, G.W. and Neufeld, E.F. (1981) Morphologic study of the internalization of a lysosomal enzyme by the mannose 6-phosphate receptor in cultured Chinese hamster ovary cells. *Proc. Natl. Acad. Sci. U S A*, **78**, 6967-6971.

Wollenberg, G.K., Semple, E., Quinn, B.A. and Hayes, M.A. (1987) Inhibition of proliferation of normal, preneoplastic, and neoplastic rat hepatocytes by transforming growth factor-β. *Cancer Res.*, **47**, 6595-6599.

Wong, W.T., Schumacher, C., Salcini, A.E., Romano, A., Castagnino, P., Pelicci, P.G. and Di Fiore, P. (1995) A protein-binding domain, EH, identified in the receptor tyrosine kinase substrate Eps15 and conserved in evolution. *Proc. Natl. Acad. Sci. U S A*, **92**, 9530-9534.

Wu, X., Zhao, X., Baylor, L., Kaushal, S., Eisenberg, E. and Greene, L.E. (2001) Clathrin exchange during clathrin-mediated endocytosis. *J.Cell Biol.*, **155**, 291-300.

Wu, X., Zhao, X., Puertollano, R., Bonifacino, J.S., Eisenberg, E. and Greene, L.E. (2003) Adaptor and clathrin exchange at the plasma membrane and trans-Golgi network. *Mol. Biol. Cell*, **14**, 516-528.

Wu, Z. and Simister, N.E. (2001) Tryptophan- and dileucine-based endocytosis signals in the neonatal Fc receptor. *J. Biol. Chem.*, **276**, 5240-5247.

Xu, X.X., Yang, W., Jackowski, S. and Rock, C.O. (1995) Cloning of a novel phosphoprotein regulated by colony-stimulating factor 1 shares a domain with the Drosophila disabled gene product. *J. Biol. Chem.*, **270**, 14184-14191.

Xu, X.X., Yi, T., Tang, B. and Lambeth, J.D. (1998) Disabled-2 (Dab2) is an SH3 domain-binding partner of Grb2. *Oncogene*, **16**, 1561-1569.

Yamashiro, D.J., Tycko, B., Fluss, S.R. and Maxfield, F.R. (1984) Segregation of transferrin to a mildly acidic (pH 6.5) para-Golgi compartment in the recycling pathway. *Cell*, **37**, 789-800.

Yarar, D., Waterman-Storer, C.M. and Schmid, S.L. (2005) A dynamic actin cytoskeleton functions at multiple stages of clathrin-mediated endocytosis. *Mol. Biol. Cell*, **16**, 964-975.

Yarbrough, D., Wachter, R.M., Kallio, K., Matz, M.V. and Remington, S.J. (2001) Refined crystal structure of DsRed, a red fluorescent protein from coral, at 2.0-A resolution. *Proc. Natl. Acad. Sci. U. S. A.*, **98**, 462-467.

Ybe, J.A., Brodsky, F.M., Hofmann, K., Lin, K., Liu, S.H., Chen, L., Earnest, T.N., Fletterick, R.J. and Hwang, P.K. (1999) Clathrin self-assembly is mediated by a tandemly repeated superhelix. *Nature*, **399**, 371-375.

Yim, Y.I., Scarselletta, S., Zang, F., Wu, X., Lee, D.W., Kang, Y.S., Eisenberg, E. and Greene, L.E. (2005) Exchange of clathrin, AP2 and epsin on clathrin-coated pits in permeabilized tissue culture cells. *J. Cell. Sci.*, **118**, 2405-2413.

Yun, M., Keshvara, L., Park, C.G., Zhang, Y.M., Dickerson, J.B., Zheng, J., Rock, C.O., Curran, T. and Park, H.W. (2003) Crystal structures of the dab homology domains of mouse disabled 1 and 2. *J. Biol. Chem.*, **278**, 36572-36581.

Zhou, J. and Hsieh, J.T. (2001) The inhibitory role of DOC-2/DAB2 in growth factor receptor-mediated signal cascade. DOC-2/DAB2-mediated inhibition of ERK phosphorylation via binding to Grb2. *J. Biol. Chem.*, **276**, 27793-27798.

Zhou, M.M., Ravichandran, K.S., Olejniczak, E.F., Petros, A.M., Meadows, R.P., Sattler, M., Harlan, J.E., Wade, W.S., Burakoff, S.J. and Fesik, S.W. (1995) Structure and ligand recognition of the phosphotyrosine binding domain of Shc. *Nature*, **378**, 584-592.

Zhou, Y., Zhang, J. and King, M.L. (2003) Xenopus autosomal recessive hypercholesterolemia protein couples lipoprotein receptors with the AP-2 complex in oocytes and embryos and is required for vitellogenesis. *J. Biol. Chem.*, **278**, 44584-44592.

Zhu, Y., Traub, L.M. and Kornfeld, S. (1999) High-affinity binding of the AP-1 adaptor complex to trans-Golgi network membranes devoid of mannose 6-phosphate receptors. *Mol. Biol. Cell*, **10**, 537-549.

Zuliani, G., Arca, M., Signore, A., Bader, G., Fazio, S., Chianelli, M., Bellosta, S., Campagna, F., Montali, A., Maioli, M., Pacifico, A., Ricci, G. and Fellin, R. (1999) Characterization of a new form of inherited hypercholesterolemia: familial recessive hypercholesterolemia. *Arterioscler. Thromb. Vasc. Biol.*, **19**, 802-809.